Anaerobic Electrospray Ionization Mass Spectrometry of Methylalumoxane and Zirconium complexes

by

Anuj Joshi
M.Sc. from Indian Institute of Technology Madras, 2016
B. Sc (Honours) from University of Delhi, 2013

A Dissertation Submitted in Partial Fulfillment
of the Requirements for the Degree of

DOCTOR OF PHILOSOPHY

in the Department of Chemistry

Supervisory Committee

Anaerobic Electrospray Ionization Mass Spectrometry of Methylalumoxane and Zirconium complexes

by

Anuj Joshi
M.Sc. from Indian Institute of Technology Madras, 2016
B. Sc (Honours) from University of Delhi, 2013

Supervisory Committee

Dr. Scott McIndoe, Department of Chemistry
Supervisor

Dr. Neil Burford, Department of Chemistry
Departmental Member

Dr. Heather Buckley, Department of Chemistry
Departmental Member

Dr. Dean Karlen, Department of Physics and Astronomy
Outside Member

Abstract

In this thesis, the reactivity and synthesis of methylalumoxane (MAO) via electrospray ionization mass spectrometry (ESI-MS) was investigated. The olefin polymerization catalyst $[Cp_2Zr(\mu\text{-}Me)_2AlMe_2]^+$ $[B(C_6F_5)_4]^-$ was also used to evaluate the efficacy of a nitrogen generator as a source for desolvation gas for ESI-MS analysis. The same catalyst was then used to study catalyst deactivation after 1-hexene addition.

MAO ionizes very selectively in the presence of octamethyltrisiloxane (OMTS) to generate $[Me_2Al{\cdot}OMTS]^+$ $[(MeAlO)_{16}(Me_3Al)_6Me]^-$. The advantage of this transformation was used to examine the reactivity and synthesis of MAO. The reactivity of this ion pair with other trialkyl aluminum (R_3Al) components was studied both offline and in real-time. The exchanges are fast and reversible, and the methyl groups on the cation are also observed to exchange with the added R_3Al species. MAO is also famously intractable to structural elucidation, consisting as it does of a complex mixture of oligomers generated from hydrolysis of pyrophoric trimethylaluminum (TMA). Synthesis of MAO was probed in real-time by ESI-MS, and the principal activated product of the benchtop synthesis was found to be the same as that observed in industrial samples, namely $[(MeAlO)_{16}(Me_3Al)_6Me]^-$. Computationally, a new sheet structure for this ion was proposed.

The increasing competitiveness of nitrogen generators, which provide gas purity levels that vary inversely with flow rate, prompted an investigation of the effect of gas-phase oxygen on the speciation of ions by ESI-MS. The most reactive species studied, the reduced titanium complex $[Cp_2Ti(NCMe)_2]^+[ZnCl_3]^-$ and the olefin polymerization pre-catalyst $[Cp_2Zr(\mu\text{-}Me)_2AlMe_2]^+[B(C_6F_5)_4]^-$, only exhibited detectable oxidation when they were

rendered coordinatively unsaturated through in-source fragmentation. The catalyst $[Cp_2Zr(\mu\text{-}Me)_2AlMe_2]^+[B(C_6F_5)_4]^-$ was further studied by ESI-MS to understand better the complexities of catalyst deactivation in the polymerization of 1-hexene.

I also contributed to other projects, namely the interaction of neutral donors with MAO, saturation problems in ESI-MS, and ligand substitution reaction in ruthenium complexes, and my work on all these projects are summarized in this thesis.

Table of Contents

List of Figures

List of Equations

List of Schemes

Acknowledgments

I want to thank my supervisor Prof Scott McIndoe for his help and support throughout my PhD. He has been a constant source of encouragement, and his patience and help with challenging projects are incredible. Many thanks to Dr. Scott Collins, Dr. Harmen Zijlstra, and Prof Mikko Linnolahti, who have helped me finishing this work and worked with me closely on most of my projects. I got to learn so much working with them, and I am grateful to each one of them for sharing their expertise.

I wish to acknowledge Bibhuti Bhusan Rath and the entire CHEM 600 crew; they supported me through the writing of my thesis during the initial days of lockdown. I would also like to thank Isaac Omari; his knowledge in analytical chemistry helped me a lot in the initial struggle days of PhD, and I thank him for all the wonderful memories we have in this lab. I also want to thank Dr. Ori Granot for troubleshooting the 16-year-old QToF micro, which, as expected, broke down a lot. Ori has been very helpful and has been a great teacher throughout these four years.

Lastly, I want to thank Kaitlyn Ramsay, and her family in Markham, for all their support during this PhD. They supported me through the ups and downs of my degree. Many thanks to our pets Monty and Balok, whose constant love made the work from home this year bearable. Lastly, I want to thank my mom, dad, and my sister. I could not have come to Canada without their support. They are a constant source of motivation, and I thank them for their understanding and patience with being away from home so long.

Dedication

To my late grandmother Mrs. Laxmi Joshi and late grandfather Mr. Bhola Dutt Joshi.

Chapter 1 Analysis of air and moisture sensitive compounds.

Parts of this chapter will be submitted as a tutorial review to Journal of Mass spectrometry: "Handling considerations for the mass spectrometry of organometallic compounds" A Joshi, HS Zijlstra and JS McIndoe, *Journal of Mass Spectrometry*, to be submitted.

1.1 Overview

Anaerobic mass spectrometry is used for samples that degrade in the presence of either air or moisture. A reliable spectrum without any decomposition can then be collected though it requires certain modifications. The McIndoe group has used electrospray ionization mass spectrometry (ESI-MS) to study air and moisture sensitive compounds.[1–8] The instrument used in this work has an ESI source, hybrid quadrupole-time of flight mass analyzers, and a multichannel plate detector. The following chapter begins with a brief introduction to these components. There have also been various strategies employed by researchers to avoid decomposition of samples during analysis; this chapter highlights these strategies based on different ionization types.

1.2 Electrospray ionization

Dole and co-workers in the late 1960s were the first to report the use of electrospray as an ionization source by electrospraying a dilute polymer solution into an evaporation chamber.[9] This technique was improved later in 1984 by Yamashita and Fenn, who coupled the electrospray source to a quadrupole mass analyzer.[10–12] Fenn also reported the use of ESI to analyze large molecules such as proteins,[13] and due to his pioneering work in this field, he was awarded the 2002 Noble Prize in Chemistry.

In ESI, the analyte of interest is passed through a charged capillary (2-5 kV) into a chamber, maintained at atmospheric pressure. Due to the presence of an electric field, the solution that comes out of the capillary forms a Taylor cone, and from the end of it, a very fine spray of charged droplet appears.[9] This process is called nebulization. The warm counter flow of N_2 gas helps in the evaporation of the solvent, and droplets shrink in size gradually. This leads to the increase in the charge density in the droplet, and the gaseous analyte ions evaporate from the surface of the droplet. These ions can then be drawn into the inlet of the mass spectrometer.[14–16] Another mechanism for ESI involves the formation of droplet fragments due to increased charge density. This process is called a Coulombic explosion and is more applicable to larger ions such as proteins.

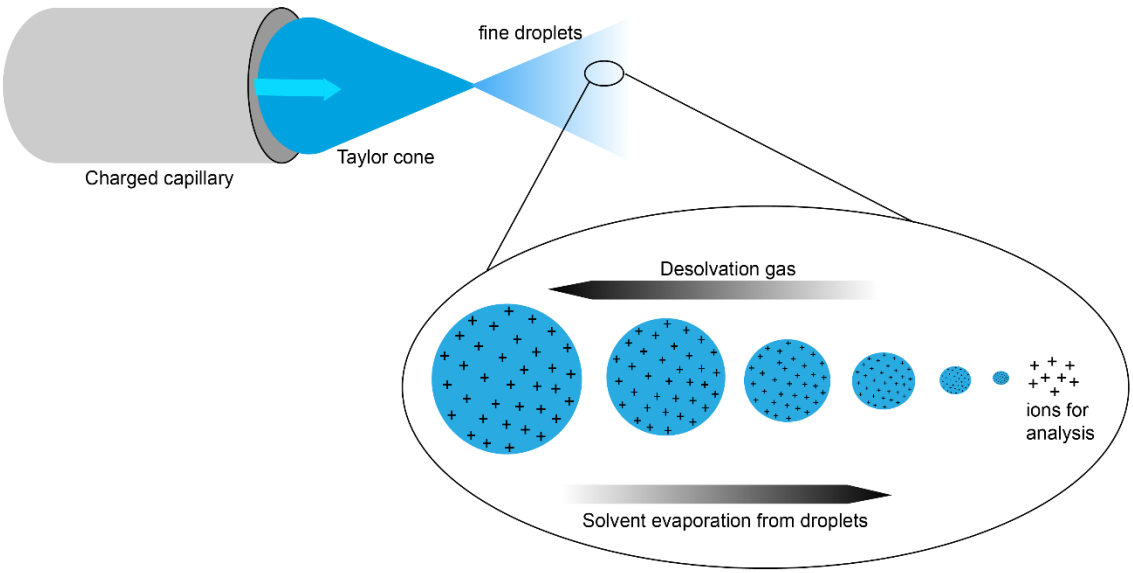

Figure 1.1 An illustration of the electron ionization process.

ESI is referred to as a soft ionization technique meaning that there is very little or no fragment of the sample. For this reason, it is a very popular technique among organometallic chemists and is used widely over the years. One of the drawbacks of ESI is

that it can only analyze charged compounds. The McIndoe group over the years have used charge tagging to introduce a charge in a neutral analyte compound for analysis.[17–22]

1.3 Mass analyzers

The electrospray process discussed above happens at high pressure (atmospheric). The ions after this enter a low-pressure region of the mass spectrometer. The mass analyzer requires the low pressure for ion separation. As shown in Figure 1.2, the sampling cone and skimmer cone acts as small orifices between the two regions at different pressure. The capillary points orthogonal and not directly to the mass analyzer to limit contamination to the mass spectrometer.[15]

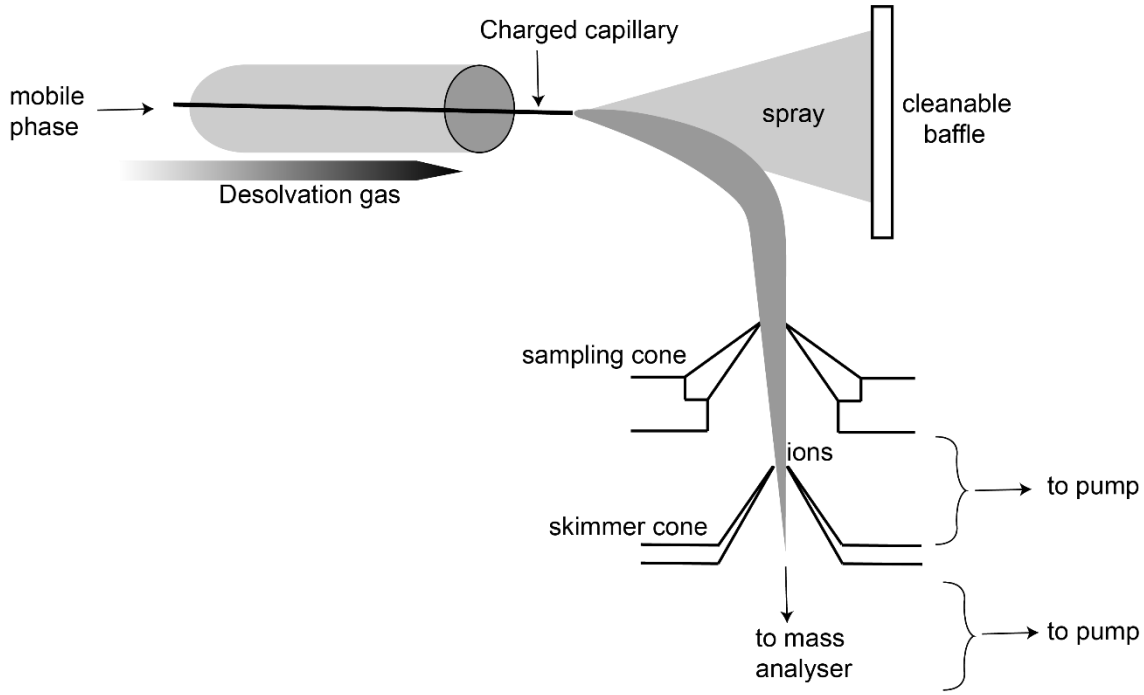

Figure 1.2 Series of skimmer cones to enable the entry of the analyte ions into the mass analyzer.

The purpose of the mass analyzer to separate ions based on the mass to charge ratio. For this work, the instrument used has a hybrid mass analyzer, i.e., a combination of a quadrupole and time of flight mass analyzer. They are together abbreviated as a QToF mass analyzer.

The quadrupole mass analyzer consists of four parallel rods with opposite pairs of poles connected electrically and charged by a DC voltage and a superimposed radio frequency potential.[15,23] The trajectory of ions depends on the combination of these two fields. For example, if the positive ion comes to the mass analyzer, it is attracted to the poles that are charged negatively, but the polarity of the poles changes quickly, and the direction of the ion will change again. If the ion hits the rod due to an unstable trajectory, it will be discharged and not make it to the detector. Ions with selected *m/z* proceed to the detector.

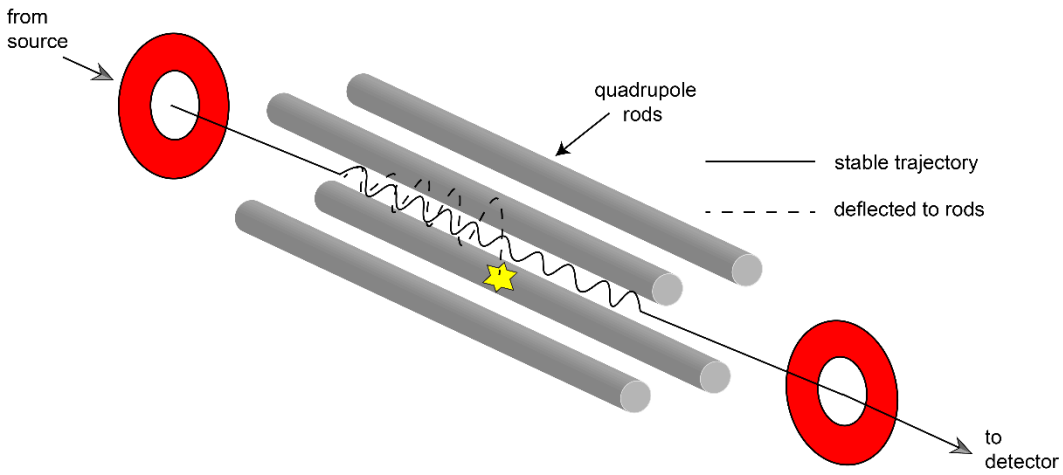

Figure 1.3 A schematic of a quadrupole mass analyzer.

In the instrument used in this work, the quadrupole acts as an ion guide in MS mode, and all ions, regardless of the *m/z* value, pass through (the quadrupole is used when performing tandem mass spectrometry). The quadrupole is combined with a time of flight (ToF) mass analyzer. A ToF separates ions based on the speed at which they reach the detector.[24–26] In ToF, the ions are pushed by a pulsing electrode, which provides the same kinetic energy to all the ions. Since the velocity is inversely proportional to the square root of mass, the lighter ion is faster than, the heavier ion, and there is a difference in speeds as they pass through a drift tube (Figure 1.4). The ions reach the detector at different times, and the arrival times of ions can be transformed into a mass spectrum. The *m/z* value of the ion can be calculated if we know the time it takes for the ion to travel in the drift tube, the length of the drift tube, and the kinetic energy applied to the ion.

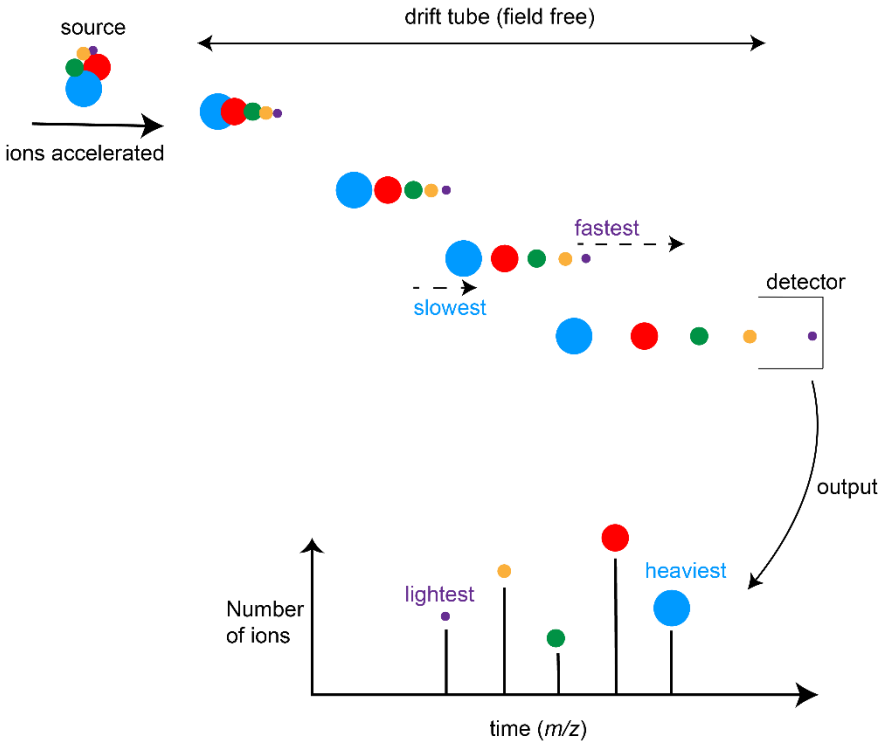

Figure 1.4 An illustration of the ToF mass analyzer.

The ion leaving the ion source for the ToF instrument has different starting times and different kinetic energies.[15] Ions with the same *m/z* can also have a range of kinetic energies depending on their formation conditions. In such cases, a reflectron is used to normalize the speed of the ions such that they reach the detector at the same time.[27,28] A reflectron is an electronic ion mirror in which electrons can penetrate, and their paths are reversed. The ion with greater kinetic energy will penetrate the reflectron deeper than the one with less kinetic energy. As a result, the ion traveling faster spends more time in the reflectron and exits the reflectron later than the one traveling slower.

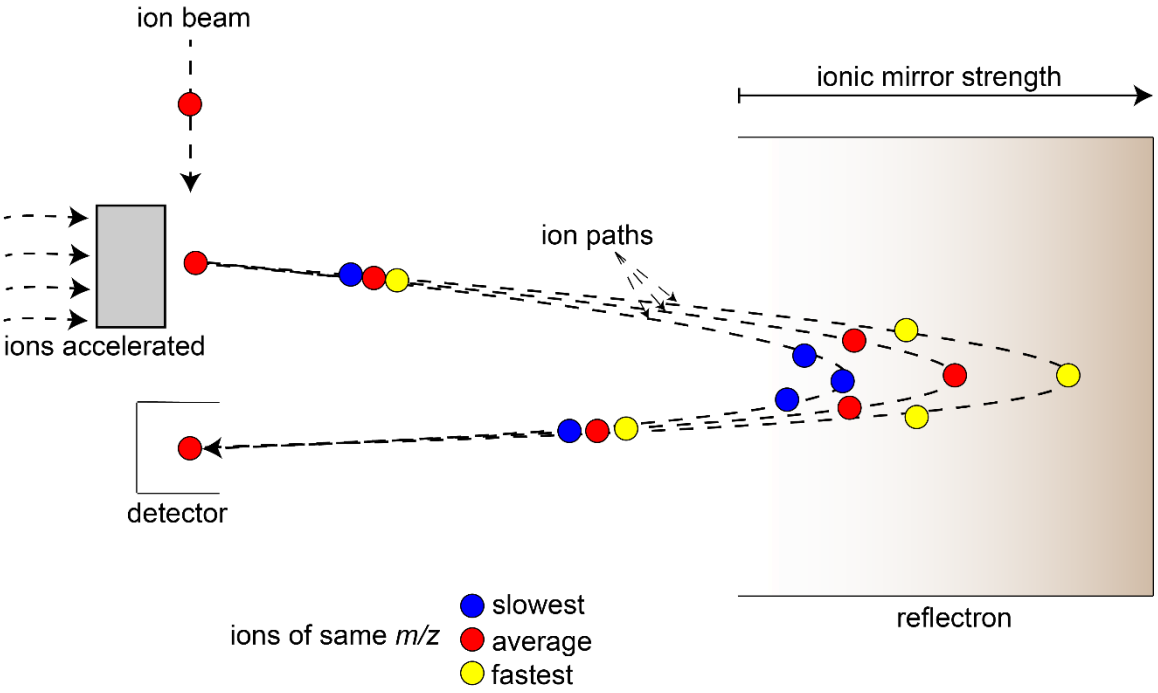

Figure 1.5 An illustration of normalization of travel speeds of ions with the same *m/z*.

1.4 Detector

The ion beam is perpendicular to the pulsing electrode, and this avoids the detection of ions that have not been pushed; and the arrangement is called orthogonal ToF. In this

arrangement, it is important to use an array detector called a microchannel plate (MCP).[29,30] Since a whole section of the beam is pulsed away at once; the MCP detector ensures that all the ions are collected. An MCP detector consists of an array of individual electron multipliers, and each of them can register one ion with a short delay before it registers another. One can saturate the detector if the samples are run at higher concentration and the counts observed in the mass spectra will not be representative of the number of ions that reach the detector. A variety of strategies to avoid saturation are discussed in Chapter 6.

1.5 Tandem mass spectrometry (MS/MS)[31]

The ions observed in mass spectrometry experiments are fragmented to aid with the assignment of the ion. These fragments provide insight into functional groups, or ligands, which are attached to the ion. For example, methylalumoxane anions have the general formula $[(MeAlO)_x(Me_3Al)_yMe]^-$, and by fragmenting these anions, one can observe losses of 72 Da that corresponds to the loss of Me_3Al group. The collision cell in the instrument used in this study is a hexapole (Figure 1.6). The ion for fragmentation is selected in the quadrupole mass analyzer and enters the collision cell filled with argon gas. The ion collides with argon in the collision cell and results in the fragmentation of the ion. The second mass analyzer, ToF, is then used to collect the daughter ion spectrum.

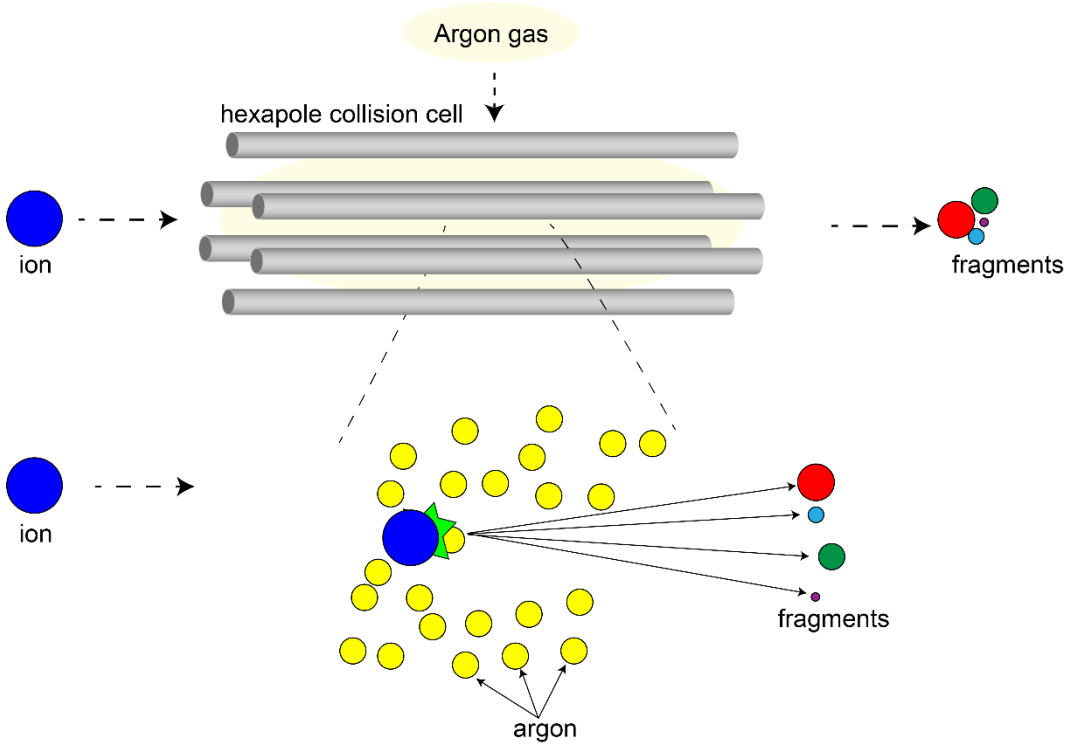

Figure 1.6 An illustration of the collision cell.

1.6 Handling considerations for air and moisture sensitive samples

Mass spectrometry is a powerful tool in disparate areas of chemistry, but its strength of extreme sensitivity can be an Achilles heel in the context of studying highly reactive compounds. A quantity of material suitable for mass spectrometric analysis often represents a tiny grain or a very dilute solution. Both are highly susceptible to decomposition due to ambient oxygen or moisture. This complexity can be hugely frustrating to chemists and analysts alike: the former being unable to get spectra free of decomposition products, and the latter often being poorly equipped to handle reactive samples. Fortunately, many creative solutions to such problems have been developed over the years, and this section summarizes some key methods for handling reactive samples.

1.6.1 Electron Ionization

Electron ionization (EI) (a.k.a. electron impact ionization) generates radical cations using high energy electrons that interact with gas-phase molecules. Removing an electron imparts considerable internal energy to the ion and results in unimolecular decomposition of the ion.[32,33]

EI is a widely used technique for volatile compounds. The sample introduction in EI can be directly in the source or as effluent from a GC column.[34] EI has been used to study metal carbonyls, main group organometallics, and metallocenes, provided their masses are less than 1000 Da.[35,36] In particular, metal carbonyls and metallocenes are widely characterized by EI due to its high volatility and thermostability (e.g., ferrocene, which forms a highly abundant molecular ion).[37,38]

The sample introduction step in EI for air-sensitive compounds is problematic as the sample is exposed to air for a short time. There are a variety of different strategies for the analysis of such sensitive compounds.[39,40] These include injection of an analyte via a gas-tight syringe, working under a stream of inert gas, using a glovebag or doing the sample introduction fast (taking less time to transfer samples) to limit the exposure to air.[41–43] Other modifications, such as a small purgeable glove chamber affixed to the front end of the mass spectrometer, can also analyze reactive organometallic species by direct probe methods.[44] This modification is more robust than a glovebag and does not need the requirement of a full glovebox dedicated to analysis (Figure 1.7).

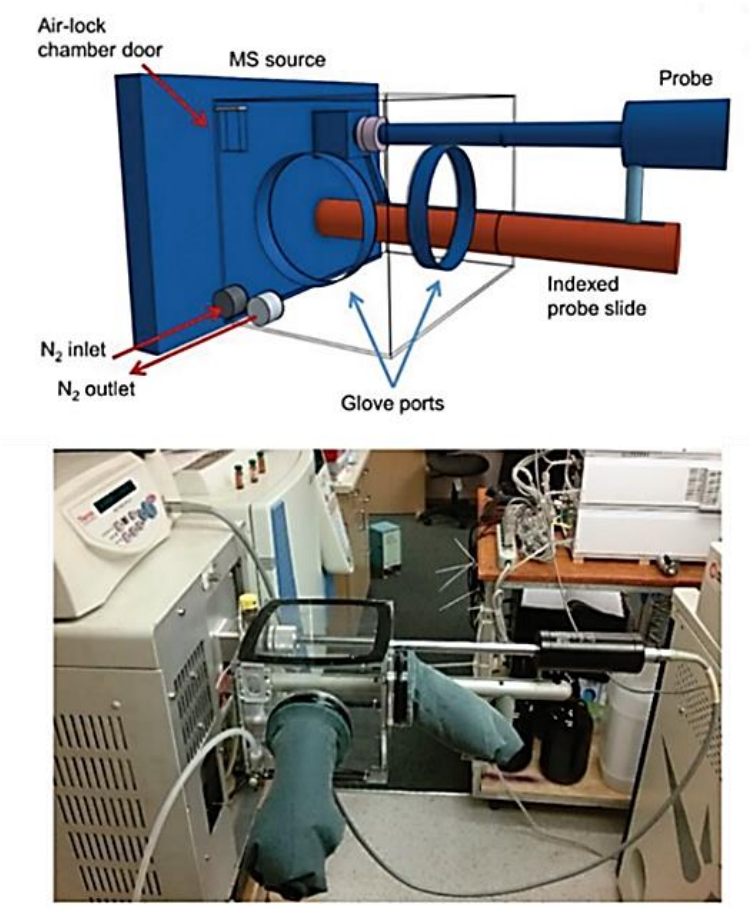

Figure 1.7 Top: Schematic of the glove chamber. Bottom: Glove chamber in place on direct probe EI-MS. Adapted with permission from Penafiel *et al.*[44] Copyright (2016) Royal Society of Chemistry.

Excellent EI spectra of air and moisture sensitive compounds such as $ZrCp_2Cl_2$, $ZrCp_2Me_2$, $TiCp_2Cl_2$, and $TiCp_2Cl$ were recorded using the glove chamber (Figure 1.8).

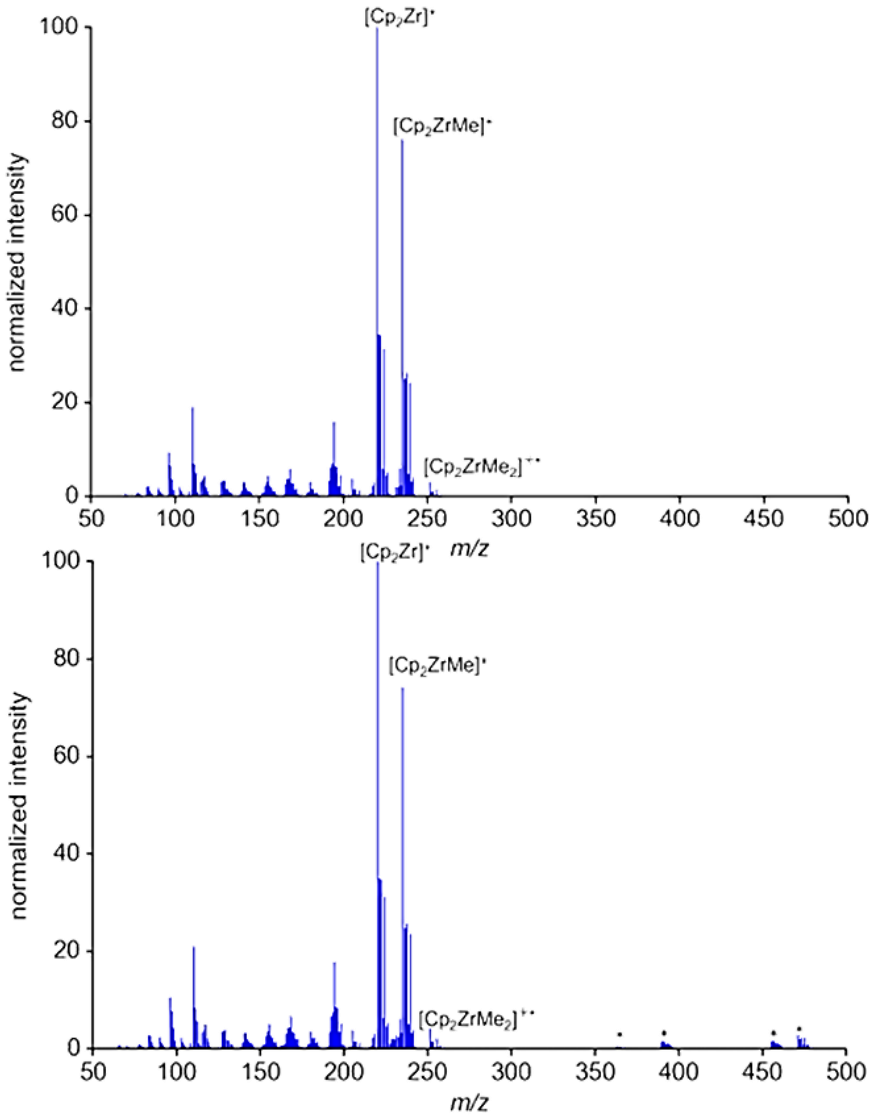

Figure 1.8 EI-MS spectrum of $ZrCp_2Me_2$ (*m/z* 250). Top: Spectrum obtained using the glove chamber. Bottom: The measurement was performed under air (no glove chamber). Peaks marked * are unassigned decomposition products. Adapted with permission from Penafiel *et al.*[44]

Volatile samples can also be analyzed by headspace analysis.[45,46] Here, the sample vial is heated, and a volatile sample ends up in the headspace leaving the denser matrix at the bottom. The sample is injected into a GC without exposure to air using an autosampler. In EI, the sample is heated in an oxygen-free chamber (or tube) and the gaseous analyte is

introduced into the ion source. However, many air-sensitive compounds can decompose at elevated temperatures, limiting the use of EI to thermally stable compounds.

1.6.2 Direct analysis in real-time (DART)

Direct analysis in real-time (DART) is an ionization technique that uses high energy metastable He* atoms and molecules, e.g., N_2* to analyze samples of interest.[47] As discussed previously, the sample is placed under vacuum in EI, but for DART analysis, the sample is brought to the source in the open air. This feature makes it appealing for various applications but makes the analysis of air and moisture sensitive compounds very challenging by DART.[33,48] However, DART requires minimum sample preparation as the analyte is simply held next to the source of excited atoms and using this simple setup, analysis of organogallium and organoaluminium compound is reported in literature.[49]

Borges *et al.* reported the use of DART in the detection of organometallic compounds.[50] The orifice of the DART ion source was positioned so that the stream of helium or nitrogen exiting the source was in line with the inlet orifice of the mass spectrometer (Figure 1.9). Samples were loaded as pure compounds or as a solution in toluene or methanol in the glass vial and sealed by a silicone septum. N_2 was used as a purge gas, and the headspace vapors are directed to the inlet of the mass spectrometer. Several organometallic compounds of As, Fe, Hg, Pb, Se, and Sn were analyzed using this simple setup. Mazzotta

et al. also reported the analysis of fused ring heterocyclic organometallic compounds using DART.[51]

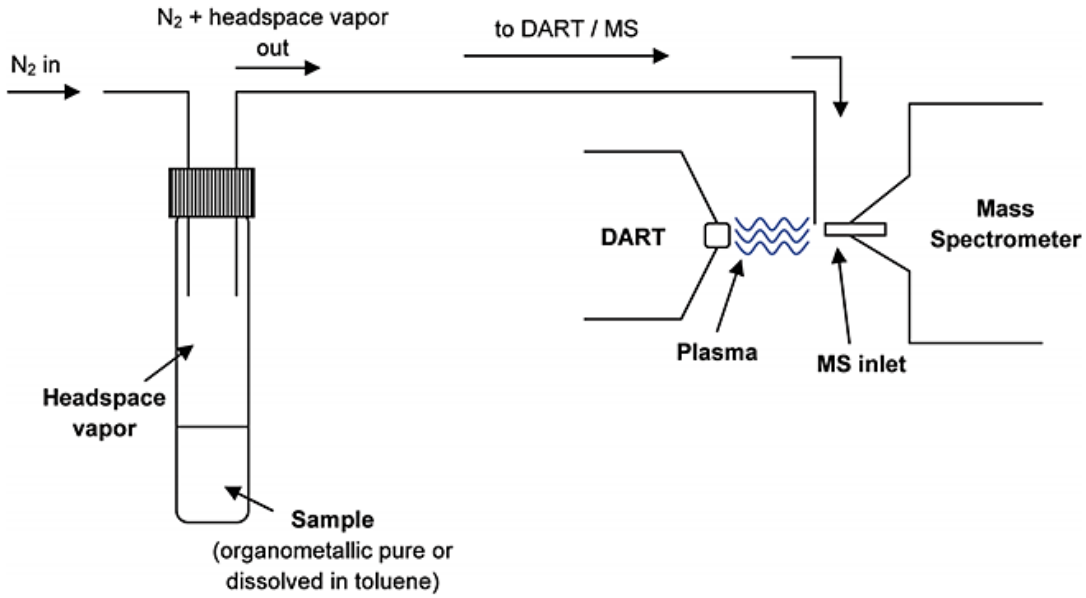

Figure 1.9 Schematic representation of the setup for the gas-phase sampling of organometallic compounds for detection by DART-MS. Adapted with permission from Borges *et al.*[50] Copyright (2009) American Chemical Society.

1.6.3 Field Ionization (FI)

In field ionization (FI), the neutral sample is heated under vacuum and driven into the gas phase near a high surface area emitter. If the molecule gets sufficiently close, an electron tunnels to the anode, and the molecule is repelled and drawn into the mass spectrometer. It is called field desorption (FD) if the sample is adsorbed on the surface of the emitter.[52]

The main advantage of FD is the ability to form singly charged molecular ions for a variety of compounds and is used widely for organometallic compounds.[53–56] Non-polar compounds, which are generally difficult to study by ESI or MALDI due to bad ionization, can be explored by FD. The main drawback of FD is the sample preparation, as the sample

must be introduced to the emitter. Two methods (both under open-air) are used to do this. One involves dipping the emitter quickly in the analyte, and the other involves dropping a small amount of analyte via a microsyringe in the emitter.[57] These sample preparation steps make it very difficult to study air and moisture sensitive compounds by FD.

The development of liquid injection field desorption ionization (LIFDI)[58] benefited the analysis of air-sensitive compounds.[59–64] The only difference between FD and LIFDI is the fused silica tubing, which connects the emitter to the sample vial outside and thus allows for easy analysis without breaking the vacuum and eliminating sample preparation under air.[65]

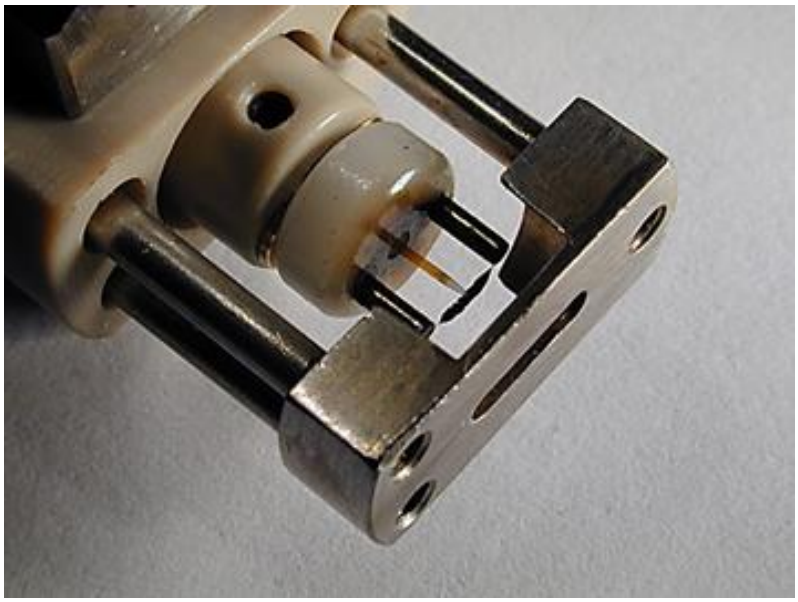

Figure 1.10 Liquid Introduction Field Desorption Ionization (LIFDI) showing the capillary which carries the analyte and the emitter. Image provided courtesy of Prof H. Bernhard Linden.

Analysis of air sensitive compounds is done by rinsing the capillary with the inert gas from the headspace of the vial, and then it is immersed in the sample solution. Even after injection of the sample, the capillary continues to draw inert gas in the headspace into the capillary. This ensures an inert atmosphere throughout the analysis. Shown below is the LIFDI spectrum of some air-sensitive Ru complexes.

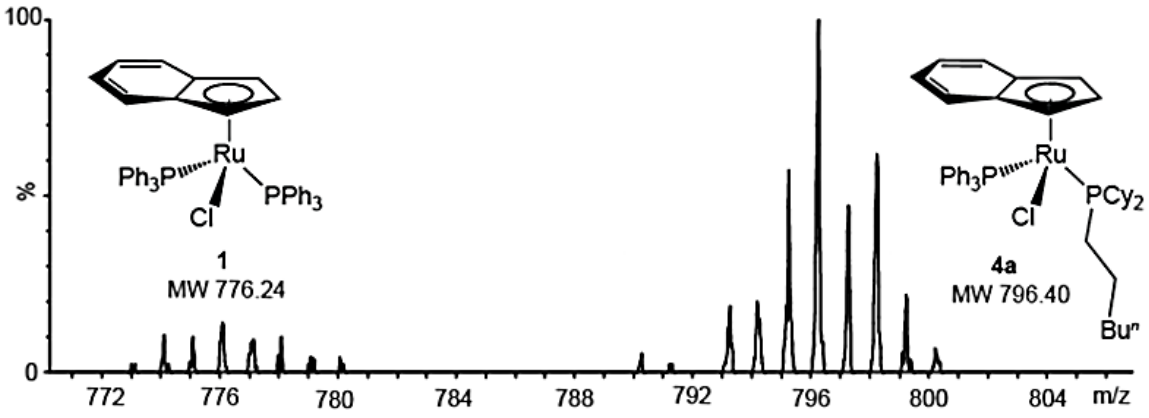

Figure 1.11 Liquid Introduction Field Desorption Ionization (LIFDI) MS data for a mixture of Ru complexes. Adapted with permission from Belli *et al.*[59] Copyright (2015) American Chemical Society.

1.6.4 Fast Atom Bombardment and Liquid secondary ion mass spectrometry

Techniques such as fast atom bombardment (FAB) and liquid secondary ion mass spectrometry (LSIMS) have also been used to characterize organometallic compounds.[66–69] Both ionization techniques involve bombarding a sample dissolved in a liquid matrix with fast-moving particles: atoms such as Xe for FAB and ions such as Cs^+ for LSIMS.[70,71] Air-sensitive alkyllithium compounds were analyzed by FAB by making a solution in Nujol[72] or Schlenk techniques.[73] Using organic solvents as matrixes, it was possible to analyze air-sensitive compounds by low-temperature secondary ion mass spectrometry (LT-SIMS).[74] In this technique, the sample solution is frozen by applying it on the tip of the insertion probe maintained at -120 °C under a cold N_2 stream. $(Me_2AlNEt_2)_2$, a highly

air-sensitive compound, was analyzed using LT-SIMS. The highest mass ion observed was $[M-Me]^+$, and the fragmentation pattern is similar in different solvents. The analyte's polarity was too low to allow dissolution in any viscous matrixes used in LSIMS. Therefore, no signal could be obtained by using LSIMS to analyze this compound at room temperature.

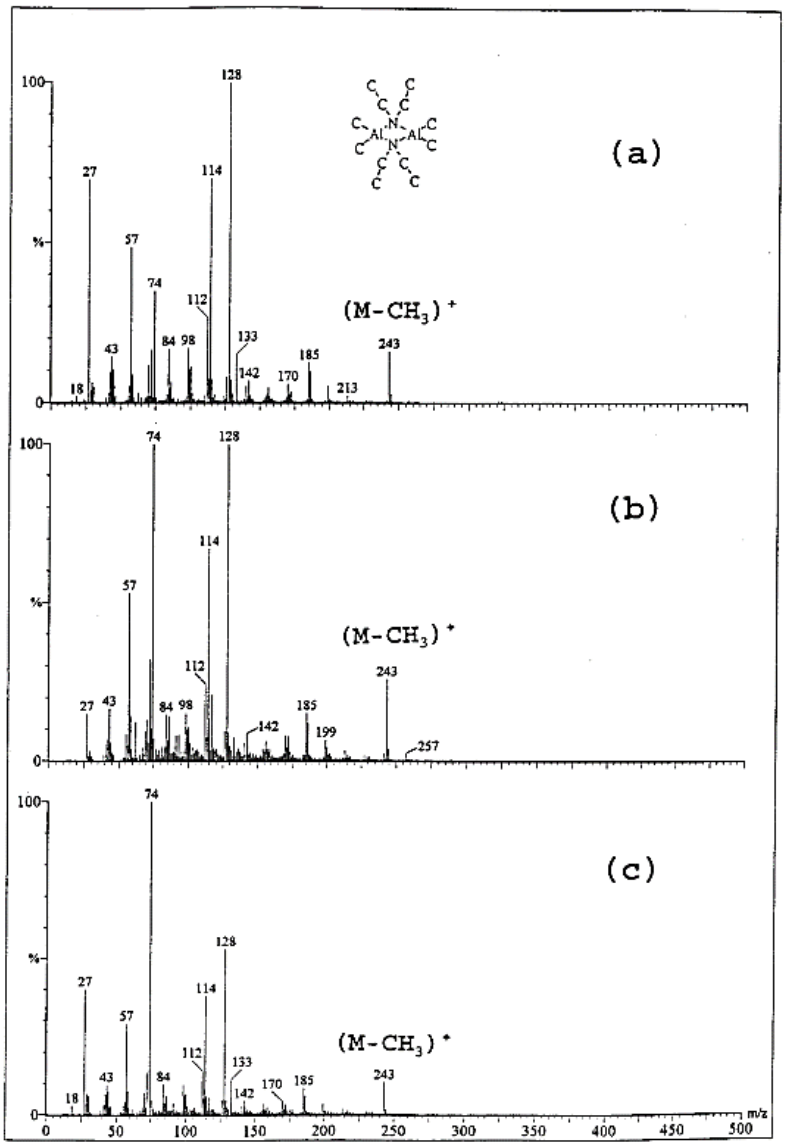

Figure 1.12 Positive-ion LT-SIMS mass spectra of $(Me_2AlNEt_2)_2$ (258 g/mol) dissolved in (a) benzene, (b) hexane, and (c) diethyl ether. Adapted with permission from Huang *et al.*[74] Copyright (1999) American Chemical Society.

1.6.5 Matrix-Assisted Laser Desorption Ionization (MALDI)

In MALDI, the neutral sample is generally prepared by co-crystallizing the analyte with a matrix compound with a suitable chromophore to allow absorption of laser irradiation.[75,76] The matrix molecules absorb most of the photons and are ablated into the gas phase, carrying the analyte molecules with them and ionizing them through protonation and oxidation.[33]

Finding appropriate matrixes for analysis of organometallic compounds is challenging, and therefore the use of MALDI in the characterization of organometallic compounds has been rare. However, Fogg and coworkers showed that unfunctionalized polyarenes, such as anthracene and pyrene, perform well as matrixes for fragile metal complexes. They also interfaced an inert atmosphere glove box with a MALDI-TOF to overcome problems regarding decomposition during sample transfer to the source.[77,78]

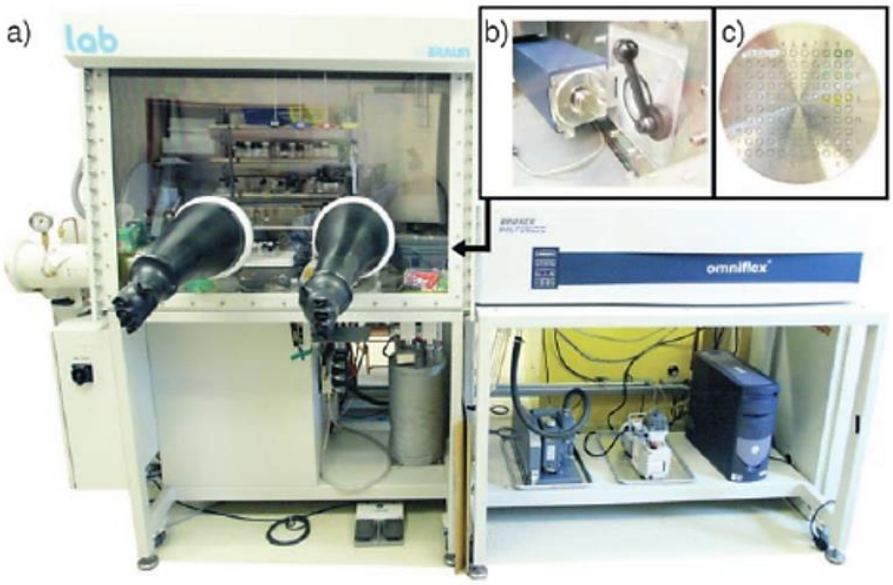

Figure 1.13 a) Inert-atmosphere MALDI-TOF mass spectrometer; b) open loading chamber projecting into the glovebox; c) target plate. Adapted with permission from Eelman *et al.*[77] Copyright (2008) Wiley-VCH.

Using the above-mentioned MALDI setup, an oxygen-sensitive titanium (III) complex (catalyst for ethylene polymerization)[79] was analyzed. The MALDI sample of the compound was made by co-crystallizing the analyte by dissolving it with pyrene in a volatile solvent (CH_2Cl_2 or C_6H_6). After this, microliter aliquots were spotted onto the MALDI target plate. A thin film of the sample with the matrix is left after solvent evaporation, and on that, MALDI-TOF was recorded.

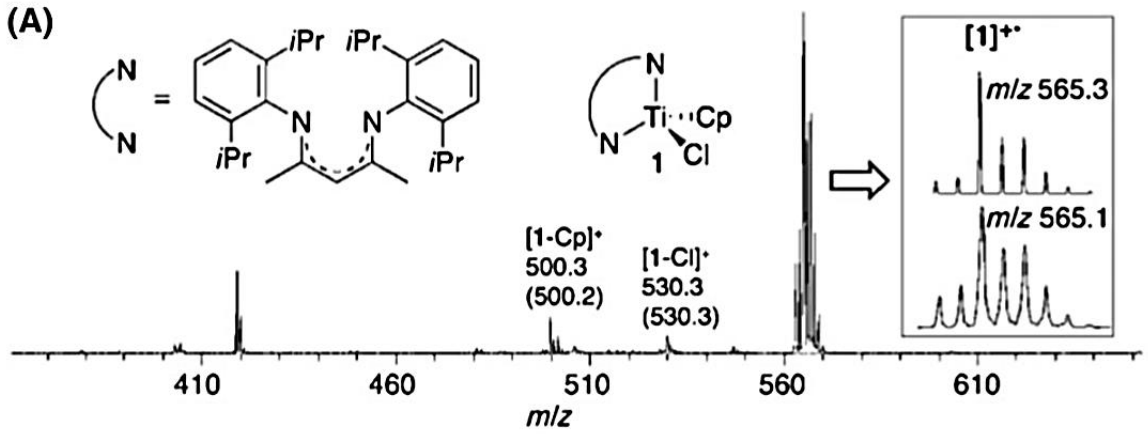

Figure 1.14 MALDI mass spectra of an oxophilic Ti (III) complex in a pyrene matrix. Adapted with permission from Eelman *et al.*[77] Copyright (2008) Wiley-VCH.

Laser desorption mass spectrometry uses a laser to ionize the analyte directly. The only difficulty is to transfer the sample to the mass spectrometer without any decomposition.[80] The solid sample could be pressed between cellophane tape or pressed in a KBr pellet. An inert gas purge box[80] for laser desorption/ionization mass spectrometry of air-sensitive solids is done if the user is worried about contamination from the matrix such as tape, KBr, or Nujol. When a purge box is used, the air-reactive sample is always under inert gas while transferring the sample to the source. Using the inert purge box laser desorption/ionization mass spectra of sensitive compounds $NbCl_2(C_5H_5)_2$ and $Zr(CH_3)_2(C_5H_5)_2$ are reported.

1.6.6 Electrospray Ionization (ESI)

ESI is a popular technique to characterize and study organometallic compounds.[81–83] Pioneering work by Lipshutz *et al.*[84] on the detection of organocuprates and by the Koszinowski group[85] on the detection of highly reactive intact Grignard reagents by ESIMS are reported in literature. Analysis of air-sensitive compounds can be achieved using a gas-tight syringe,[86] pressurized sample infusion[87], or a more permanent solution of having a glovebox close to the mass spectrometer.[88] A small hole on the side of the glovebox allows a feedthrough tubing (PTFE or PEEK) to pass, and samples for analysis can then be injected directly from inside the glovebox to the mass spectrometer without exposure to air.

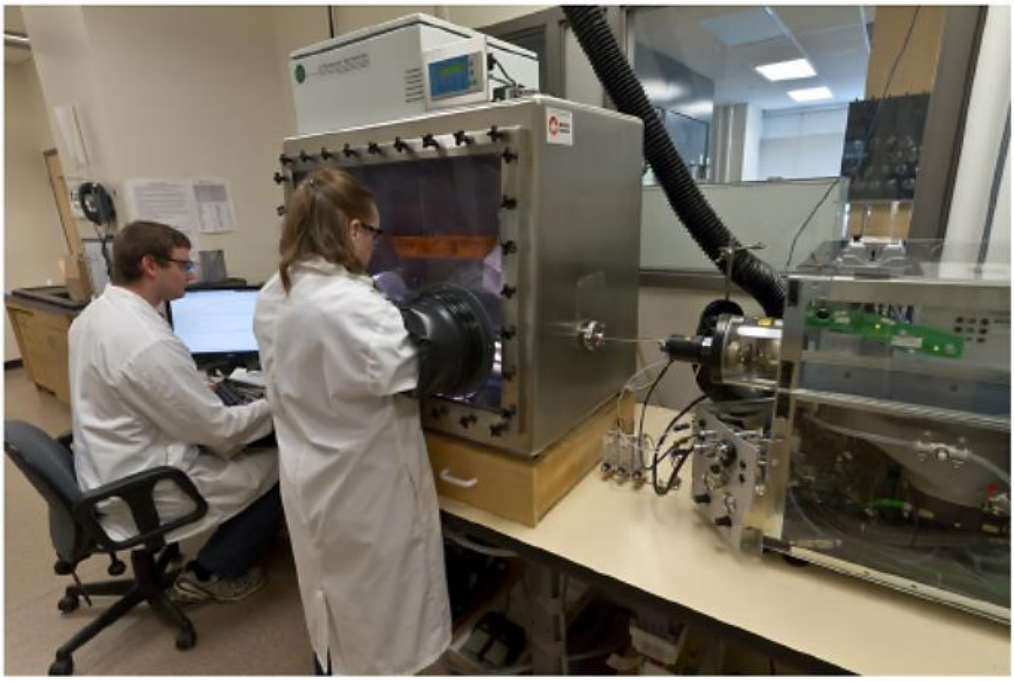

Figure 1.15 Glovebox adjacent to the ESI-MS. The syringe pump in use is located inside the glovebox. Adapted with permission from Yunker *et al.*[43] Copyright (2014) John Wiley & Sons.

The ESI-MS spectrum of a highly moisture-sensitive iron borylene complex [(η^5-C_5H_5)Fe(CO)$_2$BNCy$_2$][BArF$_4$] was reported with and without using the glovebox. When the iron complex is injected from outside the glovebox, decomposition of the iron complex by hydrolysis to [NH_2Cy_2]$^+$ at *m/z* 182 was reported. When the same sample was injected using a glovebox, the decomposition product was minimal in the same time frame, and an intense peak for the iron complex at *m/z* 368 was observed. Further advantages of using a glovebox are that sealed samples (in ampules, Schlenk flask, screw cap vials) can be brought to the glovebox sealed and stored indefinitely. The sample can be opened securely at leisure without fear of mishandling.

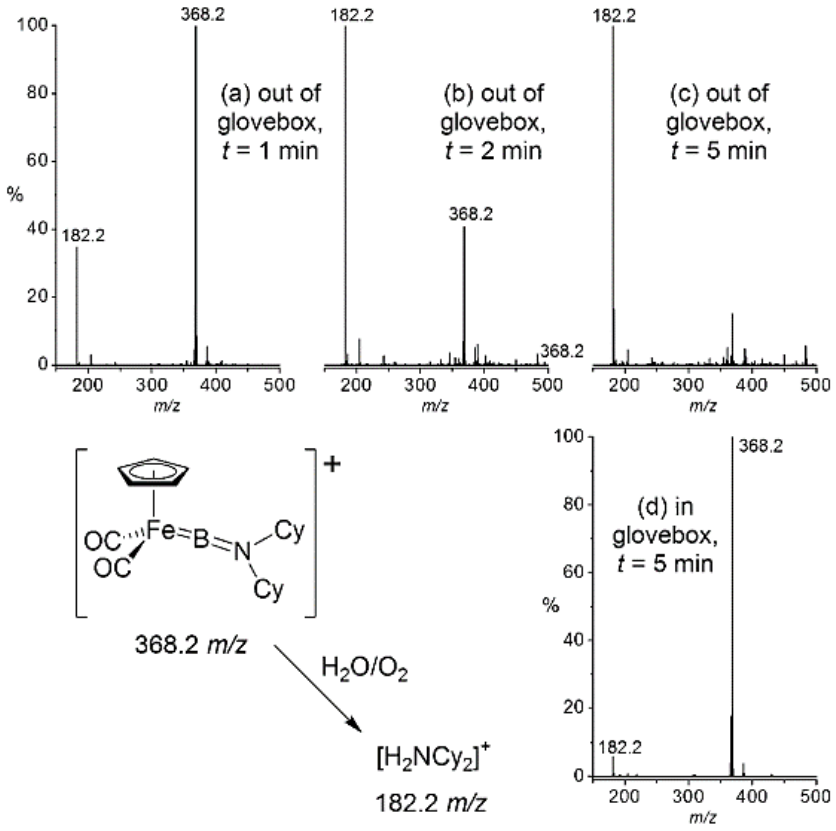

Figure 1.16 Handling the iron complex [(η^5 -C_5H_5)Fe(CO)$_2$BNCy$_2$][BArF$_4$] (inset, *m/z* 368.2) outside of the glovebox (a-c). Inside the glovebox, minimal decomposition is observed within the same time frame (d). Adapted with permission from Lubben *et al.*[88] Copyright (2008) American Chemical Society.

Reactions can be performed in syringes if stirring and temperature control are not critical.[89] Pressurized sample infusion (PSI) is used to analyze air-sensitive compounds undergoing reactions.[87] This technique can be thought of as a cannula transfer from a Schlenk flask directly to the mass spectrometer. The PSI flask is designed to have an inlet where inert gas (Ar or N_2) could be introduced, and this positive pressure allows the solution on the Schlenk flask to be introduced to the mass spectrum via a PEEK/PTFE tubing. Reactions can be conducted at temperatures up to the boiling point of the solvent, and the PSI flask is designed in a way that contamination from the rubber septa leaching from the solvent can be avoided entirely.[90] PSI is straightforward to implement in any laboratory and allows continuous monitoring of the reaction. PSI experiments can also be under the positive pressure of an inert gas from a rubber balloon.[91]

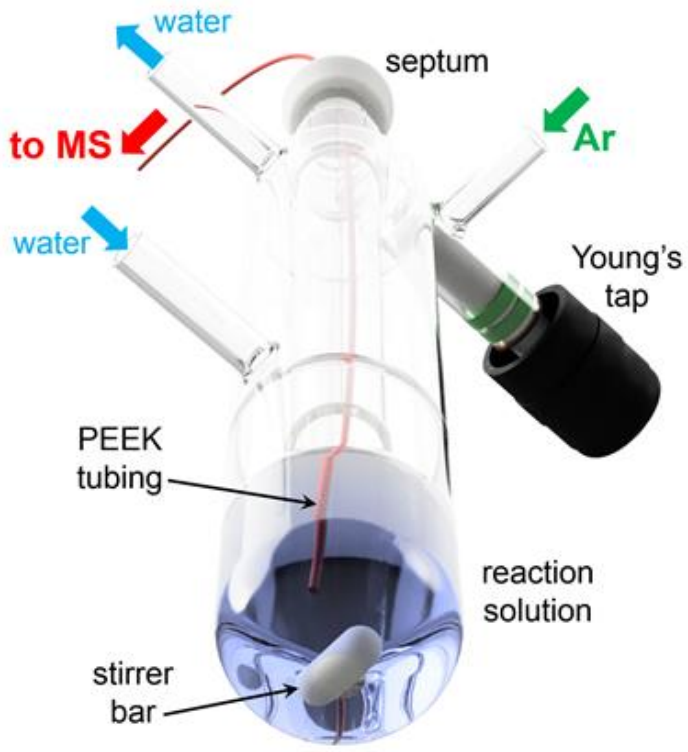

Figure 1.17 Pressurized sample infusion (PSI) flask.

Zare and co-workers have demonstrated the use of a glass slide for droplet spray ionization of a highly air and moisture sensitive sample.[92]

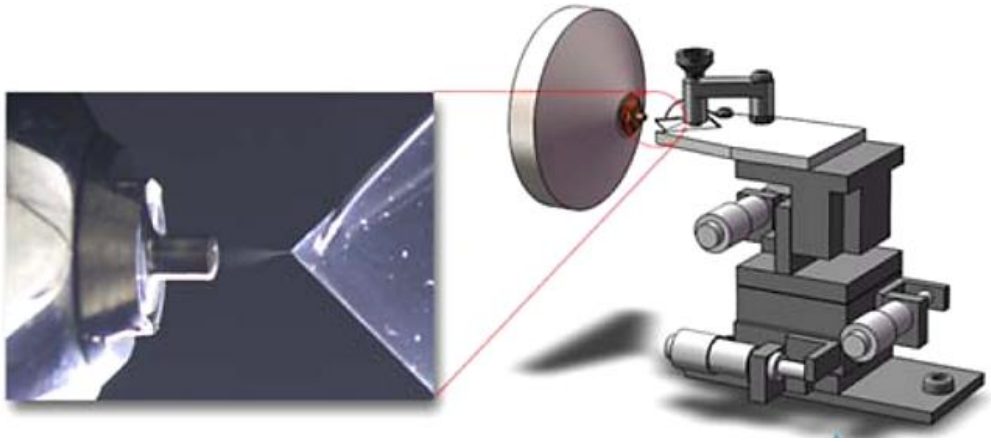

Figure 1.18 Illustration of the droplet spray. The angle between the MS inlet and the tip-end is 10°. Adapted with permission from Jiang *et al.*[92] Copyright (2015) American Chemical Society.

The experimental setup uses a glass slide which can hold sample volumes up to 60 µL. The corner of the glass slide is positioned so that the distance of the end of the tip to the MS inlet is 10 mm for acetonitrile and 5 mm for THF and PhF. Using this simple setup, Zare and co-workers reported ethylene polymerization by Cp_2ZrCl_2/MAO system and observed vital intermediates. Figure 1.19 shows the catalytically active species analyzed by droplet spray ionization. The Zr species, as well as methylalumoxane, are both susceptible to air and water and decomposes very quickly.[8,93–96] The fact that the authors observe these sensitive cations by this open-air technique is astonishing. Possible reasons for this could be the proximity of the corner of the glass side to the MS inlet, the decomposition products are deposited on the glass slide and not make it to the MS, or most importantly, quenching by acetonitrile or THF makes the adduct which is less sensitive to air or moisture.

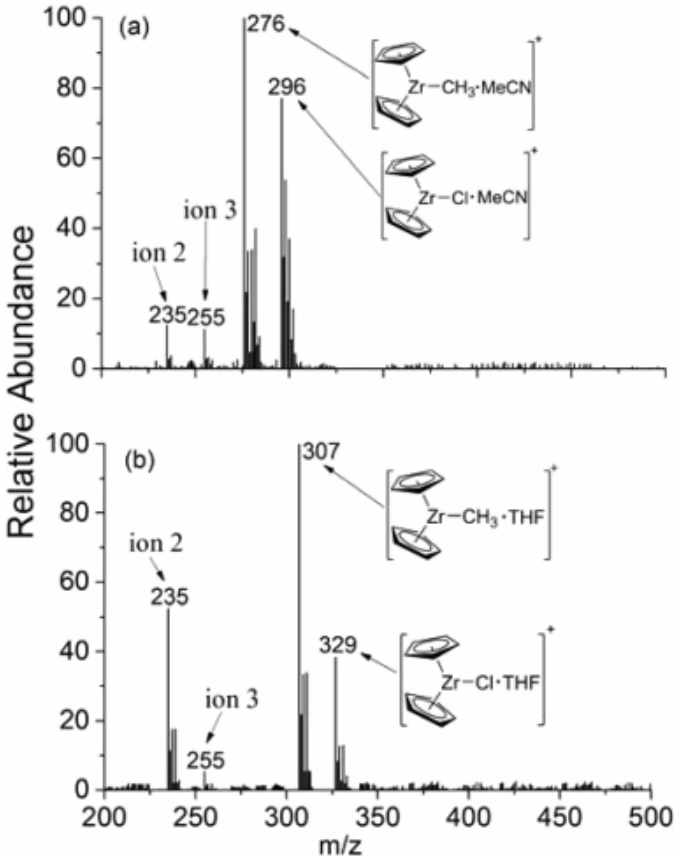

Figure 1.19 Full-scan positive-mode droplet spray mass spectra of catalytically active species in different solvents:(a) acetonitrile/toluene and (b) THF. Ion 2 is $[Cp_2ZrMe]^+$ and ion 3 is $[Cp_2ZrCl]^+$. Adapted with permission from Jiang *et al.*[92] Copyright (2015) American Chemical Society.

The analyte studied by mass spectrometry sometimes requires running at a higher concentration (>10 μM). This is due to the high reactivity of the analyte with trace amounts of water and oxygen in the solvent, and therefore running it in dilute conditions increases the chances of decomposition. There is a range of strategies that can be employed to mitigate the inevitable saturation effects in these mass spectrometric experiments and can be achieved by detuning the instrument.[97] In the case of methylalumoxane and zirconium

ions, the probe tip is kept adjusted close to the sample inlet of the mass spectrometer such that any reactions with air/moisture are minimized.

Analysis of highly reactive compounds also requires the use of exhaustively purified solvents. Solvents employed for ESI-MS of sensitive compounds are distilled and stored over activated molecular sieves for three days inside the glovebox before analysis.[98] Using samples with water before or even sometimes months before analyzing air-sensitive compounds interferes in the spectra. A good example is $[Cp_2ZrMe]^+$ cation, which readily reacts with any residual water and gives M+2 species $[M+H_2O-CH_4]^+$ to give $[Cp_2ZrOH]^+$. For methylalumoxane anions, trace amounts of water could complicate the analysis as these anions can have dozens of Al-Me bonds, and multiple hydrolysis reactions could lead to very complicated spectra.

The collision gas plays a significant role in getting reliable MS/MS spectrum.[99] When the system being studied is very sensitive to air and moisture, such as $[Cp_2Zr(\mu\text{-}Me)_2AlMe_2]^+$ $[B(C_6F_5)_4]^-$, often collision gas employed is passed through a gas drying unit. When active, indicating DRIERITE is a distinct blue color. When exhausted, it turns pink. However, the moisture could also be in the collision chamber inside the mass spectrometer and is very difficult to remove. Getting reliable MS/MS in such cases could be achieved by lowering the collision gas pressure.[99] Trace amounts of water (background water) in quadrupole ion traps (QIT) also complicates the analysis of moisture-sensitive compounds.[100,101]

1.6.7 Atmospheric solids analysis probe (ASAP)

The atmospheric solids analysis probe (ASAP) was first reported in 2005 by McEwen.[102] By using this technique, mass spectra could be acquired very quickly as both vaporization and ionization occur at atmospheric pressure. The ASAP technique utilizes the heated nitrogen desolvation gas to vaporize the sample and a corona discharge for sample ionization. In 2019, Giusti and co-workers reported the analysis of air-sensitive solids or liquids by paraffin inert atmospheric solids analysis probe (piASAP).[103] This method allows the study of air-sensitive compounds using a glass capillary filled with a sample and then sealed by a paraffin plug to maintain the inert sample until the ionization process. The sample can then be taken out of the glovebox and inserted in the ASAP probe as long as the paraffin is intact. Since paraffin is a mixture of alkanes, it does not interfere in the mass spectra as alkanes do not ionize readily compared to the analyte, and it also melts quickly.

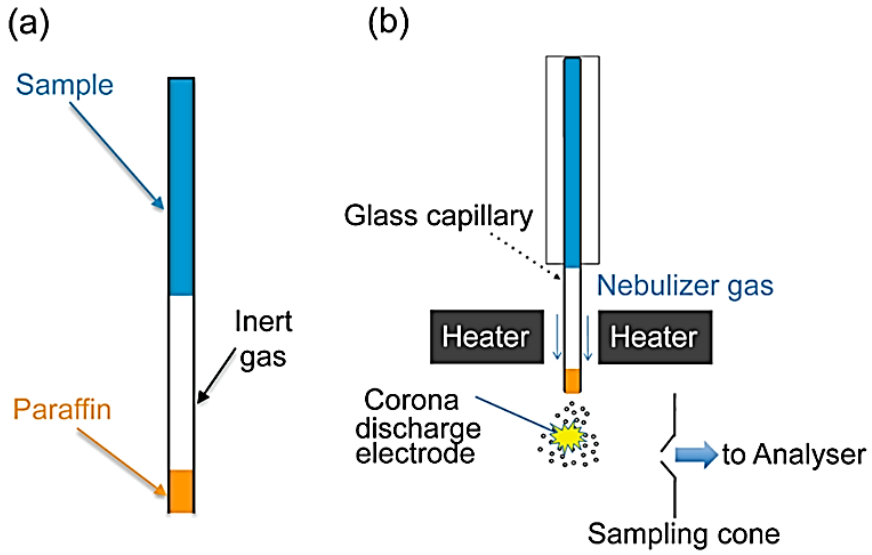

Figure 1.20 (a) Paraffin-inert ASAP glass capillary. (b) Paraffin-inert atmospheric solids analysis probe (piASAP) principle. Adapted with permission from Naim *et al.*[103] Copyright (2019) American Chemical Society.

Using the piASAP technique the air-sensitive dinuclear zirconium complex {BisInd}($Zr(NMe_2)_3)_2$ [**1**] was characterized. As shown in Figure 1.21, when ASAP is done of the same compound in air, the spectra show a lack of any $[M+H]^+$ or any related ions.

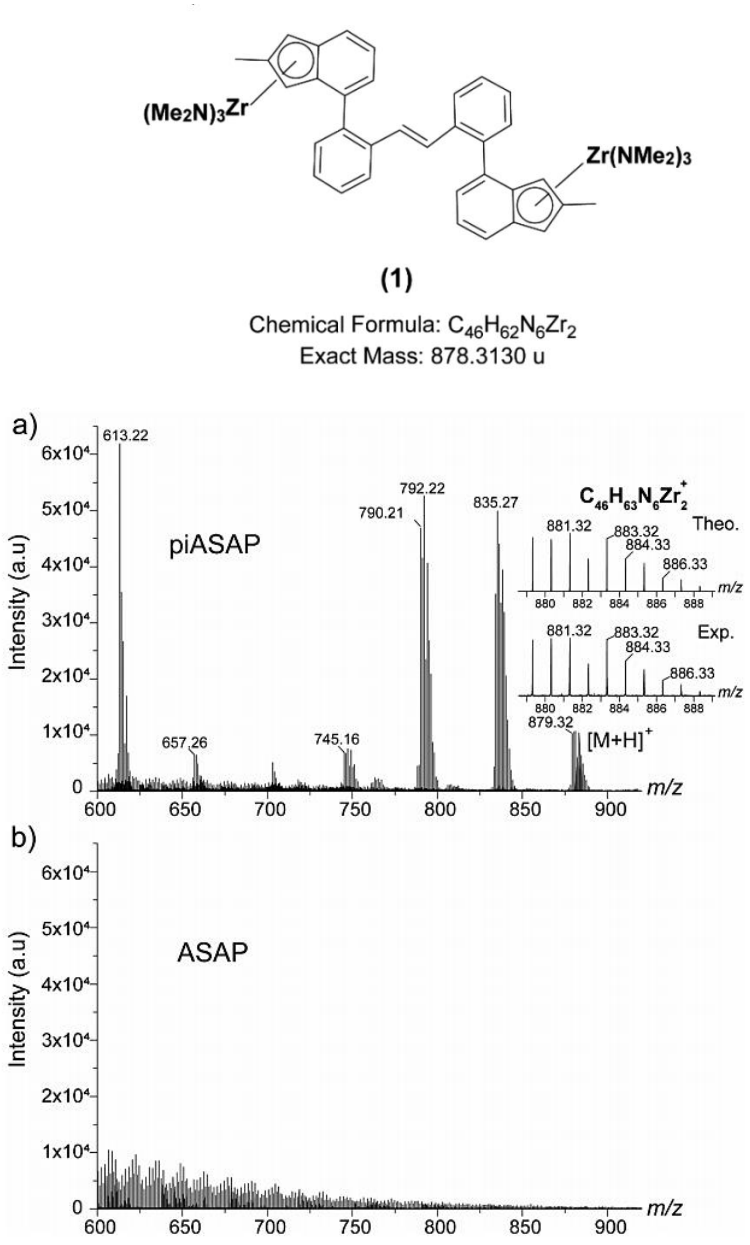

Figure 1.21 Analysis of E-Zr dimer (**1**) by piASAP and ASAP techniques. (a) and (b) are mass spectra of piASAP and ASAP conducted under inert and aerobic conditions, respectively. The zoomed areas showcase the theoretical and experimental isotopic patterns of complex **1**. Adapted with permission from Naim *et al.*[103] Copyright (2019) American Chemical Society.

Another technique that uses the ASAP probe to analyze air-sensitive compounds is called inert atmospheric solids analysis probe (iASAP). There were two reports in the literature on iASAP by two different research groups. The first is a patent by Krossing *et al.,* and the analysis is done commercially by Advion using iASAP.[104] In this technique, a probe vessel is engaged with an atmospheric solids analysis probe. The probe vessel is configured so that the sample is introduced into an ionization system under inert gas. Figure 1.22 shows a probe assembly engaging with an ASAP probe and the capillary, which contains the sample. The whole assembly is then connected to an ionization system. The iASAP probe is designed to provide analysis in less than 30 seconds without sample decomposition.

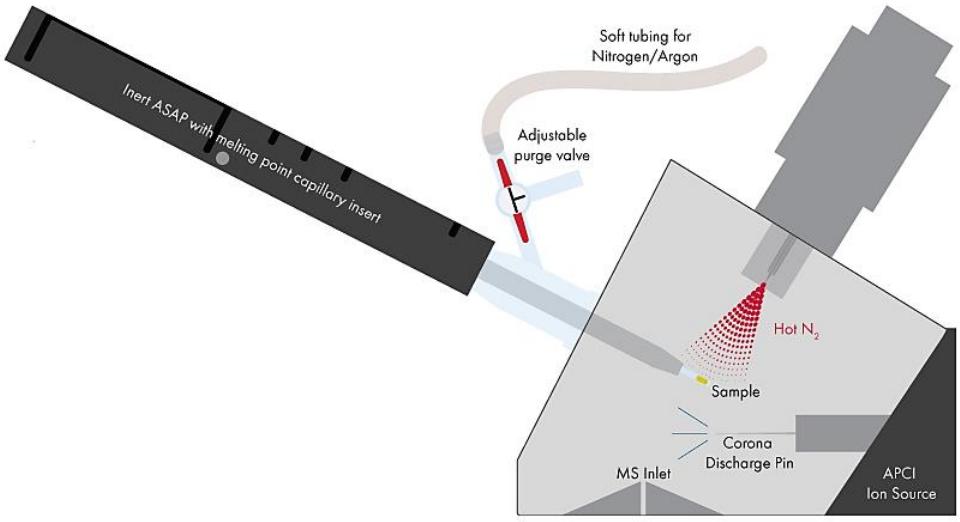

Figure 1.22 The inert atmospheric solids analysis probe. Figure used with permission from Advion Inc.

Mosely *et al.*[105] reported using a melting point tube (MPT) in which they loaded the air-sensitive sample for analysis in a glovebox. The melting point tube was enclosed in plasticine and then sealed with a flame after taking it out of the glovebox. The MPT is heated and stretched (2-3 cm away from the sample) and carefully broken to give a shorter

length MPT. This is then inserted in an ASAP holder, which is modified slightly to incorporate shorter length MPT. The MPT is then broken inside the inert atmosphere API source housing with a baffle, and the sample is ionized by hot N_2. Using this technique, two highly air and moisture sensitive compounds were analyzed and compared with the standard ASAP procedure. The tungsten cluster was only observed by iASAP, and only decomposition products were observed with the ASAP technique.[105]

1.6.8 Probe electrospray ionization (PESI)

Mass spectrometry efforts are being made to develop "solvent-free" MS for green chemistry applications. This approach has advantages as solvent-free ionization enables easy handling of the sample, and a wide variety of compounds can be analyzed, including moisture-sensitive samples and samples which are not soluble in traditional MS solvents. Probe electrospray ionization (PESI) is an ionization technique that relies on "solvent-free" MS. Hiraoka and co-workers first reported probe electrospray ionization (PESI).[106] It employs a conductive solid probe in which a small amount of analyte can be deposited. Chen and co-workers later reported solvent-free PESI ionization, and this technique was used to analyze moisture/air-sensitive compounds.[107] The technique involves heating the needle probe to convert the solid sample into a liquid, followed by applying a high voltage to the probe for spray ionization.

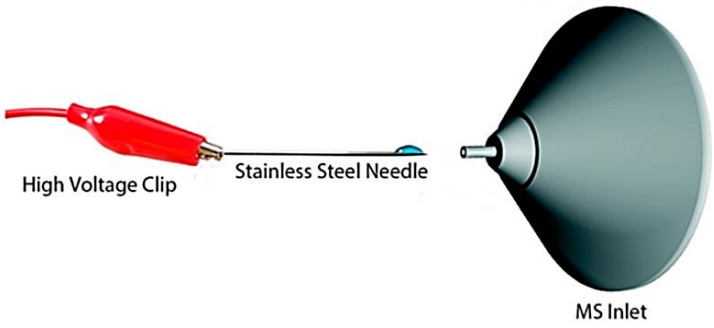

Figure 1.23 PESI-MS apparatus using stainless steel as the probe. Adapted with permission from Liu *et al.* [107] Copyright (2014) American Chemical Society.

A highly moisture-sensitive sample [bmim][$AlCl_4$]) was analyzed by this approach, and the results were compared against ESI. It was reported that the negative ion $[AlCl_4]^-$ remains intact in PESI analysis and appears as a dominant peak, whereas in ESI measurements, the sample is hydrolyzed, and ions resulting from $[AlCl_4]^-$ hydrolysis could be seen. It is to be noted that ESI measurements in the paper are done in MeOH/ H_2O, so it is not at all surprising that the authors see a hydrolyzed spectrum (MeCN would have been a much better option). Analysis of the organometallic complex Cp_2ZrCl_2 was also reported. In this case, a solid complex was melted around 240 °C on the probe and then sprayed with 5 kV applied to the probe. The desired peak of the cation $[Cp_2ZrCl]^+$ was observed, but a peak at +18 Da (water adduct) was also seen and reported.

The authors also reported the analysis of a ruthenium complex [Rh-MeDuPHOS][OTf], which is used as a catalyst for asymmetric hydrogenation. This catalyst is extremely air-sensitive, and it was analyzed in ionic liquids like [bmim][PF_6]. The ionic liquid stabilized the catalyst by protecting it from oxygen, and PESI-MS was recorded after the catalyst was weighed in a glovebox, dissolved in [bmim][PF_6], and diluted to 1 mM. The spectra below show the peak for the ionic liquid cation and cation cluster ions (*m/z* 139 and 423) and a peak for intact catalyst cation [Rh-MeDuPHOS]$^+$, observed at *m/z* 517.

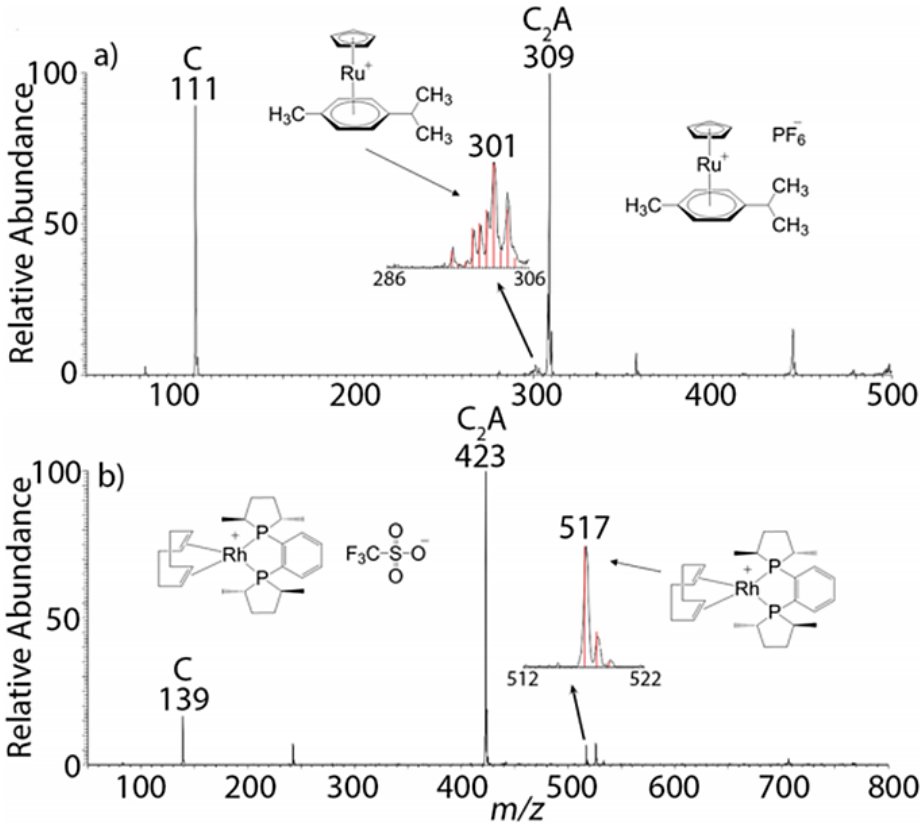

Figure 1.24 PESI-MS spectra of extremely air-sensitive Ru complexes. Adapted with permission from Liu *et al.*[107] Copyright (2014) American Chemical Society.

1.7 Conclusion

Mass spectrometry analysis of air and moisture sensitive compounds can be extremely challenging, and this chapter mentions some of the problem-solving approaches taken by various research groups in this regard. Meaningful data could be obtained by taking the necessary precautions while running such samples. The work in this thesis drew upon and extended many of these ideas.

Chapter 2 Modifying Methylalumoxane via Alkyl Exchange

Portions from this chapter have been previously published and are reproduced with permission from "Modifying Methylalumoxane via Alkyl Exchange" HS Zijlstra, A Joshi, M Linnolahti, S Collins, J.S McIndoe, *Dalton Transactions*, 2018**,** 47**,** 17291-17298.

A Joshi recorded all the MS spectra that are provided in this Chapter with the exception of two (Figure 2.1 and Figure 2.2 which were recorded by Dr. Scott Collins and mentioned in the caption). Dr. HS Zijlstra did all the preliminary experiments and started the project. He also co-wrote the paper along with A Joshi, and Prof Scott McIndoe. Prof M Linnolahti did computational studies included in this chapter. Supplementary spectra from this chapter are presented in Appendix A.

2.1 Introduction

Methylalumoxane (MAO) is an important activator for single-site, olefin polymerization catalysts.[62,108] Its utility as a cocatalyst arises from its multiple functions: it transforms the precatalyst by alkylation and ionization, forming a weakly coordinating anion that stabilizes the active catalyst, and is an effective scavenger of trace impurities such as water and oxygen.[109–111] Despite extensive use and decades of study, MAO remains incompletely understood, and its exact functioning and structure remain subject to ongoing investigations.[112–115] The exact characteristics of this mixture vary with time and temperature, making it hard to obtain concrete structural information. Its average composition $(Me_{1.4\text{-}1.5}AlO_{0.75\text{-}0.80})_n$,[116] molecular weight (MW ~ 1200-2000)[117] have been established and, in combination with computational studies[118–122] and structurally characterized aluminoxanes[123–125] it is generally thought that MAO is made up of cage-like structures that have the general formula $(MeAlO)_n(Me_3Al)_m$.

MAO is supplied as a solution in toluene containing a variable amount of free trimethylaluminum (Me_3Al) arising from incomplete hydrolysis. The amount of excess Me_3Al is known to influence polymerization catalysis and often dramatically so.[126,127] Me_3Al will reversibly bind to metallocenium ions leading to both stabilization of the active species but inhibiting direct insertion into the M-C bond,[128] while efficiently participating in chain transfer reactions.[129] This latter feature is undesirable for many applications, requiring physical or chemical removal of excess Me_3Al.[126,127] Moreover, the use of MAO for catalyst activation requires the use of toluene due to its low solubility and stability in pure hydrocarbons.[130]

In attempts to develop more economical activator/scavenger combinations, higher trialkylaluminums (R_3Al) have been used, with reduced amounts of MAO, in propene polymerization.[131] In a very detailed kinetic study involving 1-hexene polymerization in hexane media, MAO, which had been previously depleted of free Me_3Al, was used in combination with either Me_3Al, *i*Bu_3Al, or *n*Oct_3Al for catalyst activation and polymerization.[132] In this case, there was no effect on polymerization rates (at constant total Al:Zr) but rather reduced rates of chain transfer to Al in the order *i*Bu_3Al ~ *n*Oct_3Al < Me_3Al.

Modified MAO (MMAO) prepared via non-hydrolytic routes from Me_3Al and R_3Al is widely used for activation and scavenging in pure hydrocarbon media.[130] In comparison to MAO, the activation of metallocene or other catalysts using MMAO is not as well studied.[62,108] MMAO or MAO that has been modified by *i*Bu_3Al is a more effective reducing agent than MAO and leads to the production of Zr-hydrides or Zr(III) complexes, which are less active resting states or inactive, respectively.[108] In the kinetic study just

discussed, it was noted that extended activation times using MAO, modified by *n*Oct_3Al, resulted in a polymer featuring a bimodal MWD, resulting from more than one type of active species.[132]

Modification of MAO by R_3Al involves alkyl exchange, forming MMAO and R_nAlMe_{3-n} type structures. Alkyl exchange between aluminum alkyls such as Me_3Al and *i*Bu_3Al is known to be rapid.[133] Studies of alkyl exchange in alumoxanes are rare, but it has been shown that strained *t*Bu alumoxanes undergo facile ring-opening and alkyl exchange with Me_3Al.[134]

There are no reports on attempts to establish the rate of Me exchange between Me_3Al and MAO, though separate signals for Me_3Al are seen at low temperatures in the toluene solution by NMR spectroscopy.[135] Labeled compounds such as $Cp_2Zr(^{13}CH_3)_2$ undergo low energy scrambling reactions with both Me_3Al and MAO.[136] NMR PFG-SE diffusion experiments on MAO, and Me_3Al suggest that the exchange of free and bound Me_3Al is more rapid than the time scale (< 50 msec) of those experiments.[137]

Electrospray ionization mass spectrometry (ESI-MS) can be used to study the activation of metallocene catalysts by MAO in both positive and negative ionization mode, and the data obtained can be related to polymerization experiments.[138–140] This technique gives information about individual MAO oligomers and their reactions.[3,4] When MAO is exposed to a chelating Lewis base such as octamethyltrisiloxane (OMTS), a surprisingly clean spectrum is obtained.[3] Negative ion spectra of MAO and this additive show almost exclusively a species with *m/z* 1375 which is readily assignable as $[(MeAlO)_{16}(Me_3Al)_6Me]^-$ (henceforth [**16,6**]$^-$ and containing 35 Me groups) partnered

with a $[Me_2Al{\cdot}OMTS]^+$ cation as seen in the positive ion spectrum. These findings support the idea that MAO acts as a source of $[Me_2Al]^+$ during catalyst activation.[141]

We wondered what happens when MAO is combined with simple R_3Al and whether this technique could characterize commercial MMAO. This chapter summarizes the previously developed, anaerobic real-time ESI-MS technique[43,142,143] to probe the effect of higher R_3Al species on MAO anions and new insights into the alkyl exchange process.

2.2 MMAO-12 analysis via ESI-MS

MMAO is sold under different trade names depending on the alkyl group (3A = *i*Bu, 7 and 12 = *n*Oct) and composition (3A ca. 85:15 Me:*i*Bu, 7 ca. 85:15 Me:*n*Oct, 12 ca. 95:5 Me:*n*Oct).[130] We investigated MMAO-12 using 5 mol % OMTS and obtained a reasonable total ion current with [Al] = 0.01 M in fluorobenzene (PhF). However, the negative ion mass spectrum (Figure 2.1) consisted of a broad continuum of ions from ~1000 to >3000 Da. Expansion of the negative ion mass spectrum shows many signals separated in mass by 58 Da, which can be tentatively assigned based on their nominal mass. The major peaks are “normal” MAO anions, while others contain one octyl group (and one less Me group). There is also evidence of anion oxidation, containing one less MAO unit than their parent anion with the composition $[(MeAlO)_{n-1}(Me_3Al)_{m-1}(Me_2AlOMe)Me]$.[4]

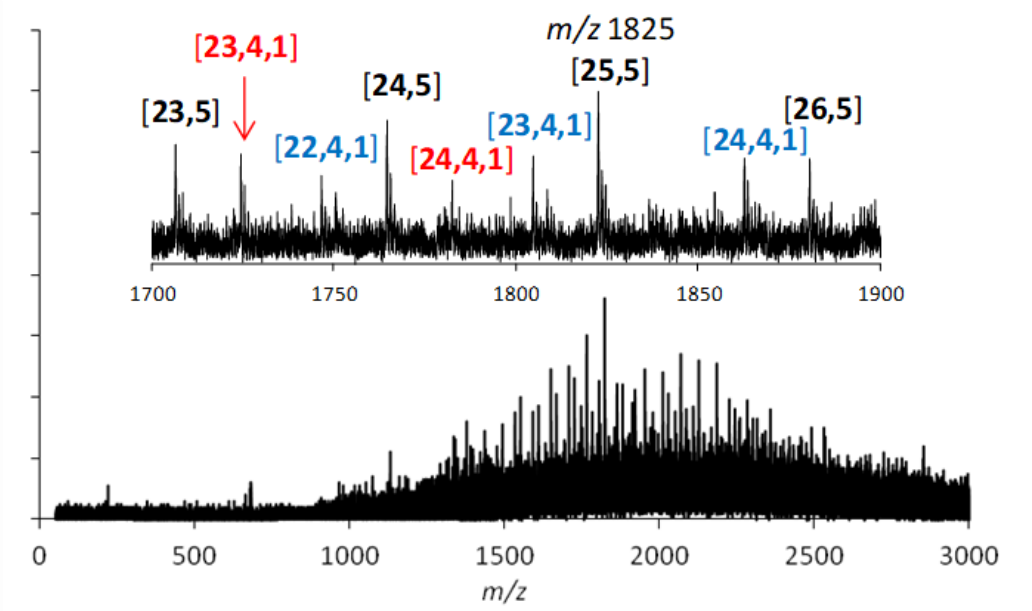

Figure 2.1 Negative ion spectrum of MMAO-12 + 5 mol % OMTS in PhF with [Al] = 0.01 M. MAO anions shown in black, and oxidized anions in red and those containing 1 *n*Oct group in blue (assignments are tentative as MS/MS analyses were not possible due to extremely low intensities). This spectrum was recorded by Dr. Scott Collins and reproduced with his permission.

The complex mixture of anions vs. that present in hydrolytic MAO likely reflects differences in their method of synthesis, along with random permutations of Me for *n*Oct, possibly coupled with physical aging and oxidation upon prolonged storage or repackaging. On the other hand, the corresponding positive ion mass spectrum consisted of only two species $[Me_2Al{\cdot}OMTS]^+$ (*m/z* 293) and $[Me(nOct)Al{\cdot}OMTS]^+$ (*m/z* 391) in about a 98:2 ratio (Figure 2.2). Thus, the mode of action of MMAO-12 is identical to that of MAO, though the anion distributions are different.

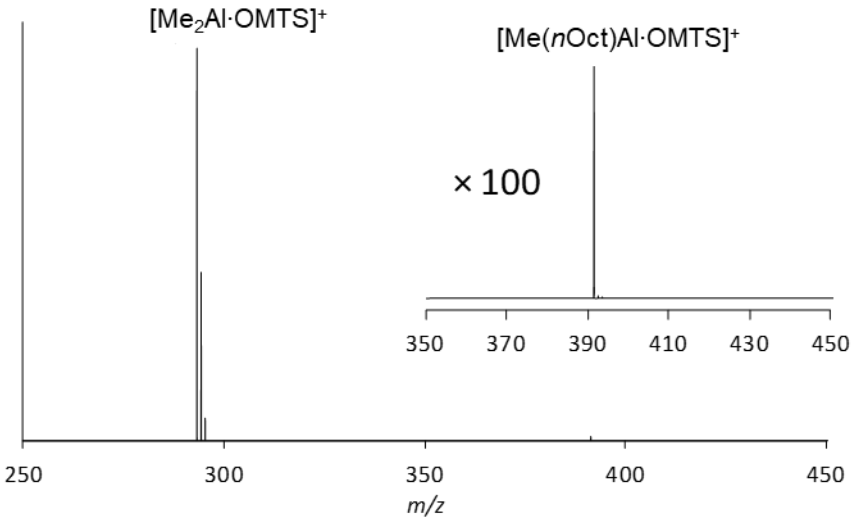

Figure 2.2 Positive ion mass spectrum of MMAO-12 + 5 mol % OMTS in PhF. This spectrum was recorded by Dr. Scott Collins and reproduced with his permission**.**

2.3 Addition of *i*Bu$_3$Al to MAO

As the quality of the negative ion spectrum in MMAO is marginal, the rest of this chapter is focused on the modification of MAO by the direct addition of R_3Al. The addition of *i*Bu$_3$Al to MAO, either before or after ionization with OMTS, cleanly led to multiple substitutions of Me for *i*Bu on the MAO anions. Depending on the amount added, the extent of *i*Bu/Me substitution on [**16,6**]$^-$ could be controlled (Figure 2.3). Before the addition of *i*Bu$_3$Al, the expected spectrum, dominated by [**16,6**]$^-$ is obtained (Figure 2.3 a). The addition of 1 mol % *i*Bu$_3$Al resulted in Me/*i*Bu exchange as indicated by the appearance of peaks 42 Da (the mass difference between *i*Bu and Me) higher than the parent ion (Figure 2.3 b). An equilibrium was quickly reached, and the distribution remained unchanged for the remainder of the measurement.

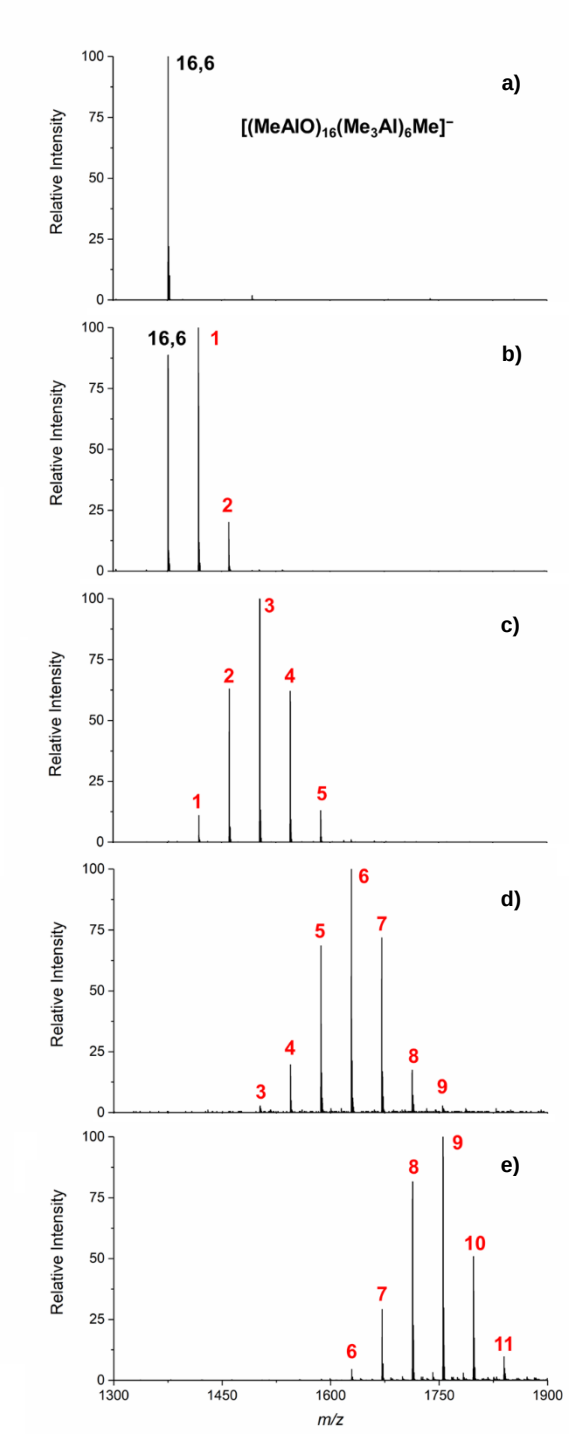

Figure 2.3 Room temperature negative ion ESI-MS spectra in PhF of (a) 30 wt. % MAO at equilibrium (5 minutes after mixing), (b) modified with 1 mol % *i*Bu_3Al, (c) 5 mol % *i*Bu_3Al (d) 10 mol % *i*Bu_3Al (e) 20 mol % *i*Bu_3Al . All at an OMTS:Al ratio of 1:100. Number of Me/*i*Bu substitutions on **[16,6]**$^-$ is shown in red.

The distribution after adding 1 mol % *i*Bu_3Al is essentially statistical; it reaches a maximum at one *i*Bu substituent and has a weighted average of 0.63 *i*Bu groups. Since the 30 wt. % MAO used in this study features 1.64 moles of Me groups per mole of Al, the use of 1.0 mol % of *i*Bu_3Al with respect to Al corresponds to a ratio of *i*Bu/Me groups of 0.03/1.64 = 0.0183 or 1.83 mol %. As previously mentioned, [**16,6**]$^-$ has 35 Me groups, so upon addition of 1.0 mol % *i*Bu_3Al, 0.21 Me substitutions would be expected on a statistical basis if only one *i*Bu group is exchanged per mole of *i*Bu_3Al to a maximum of 0.64 if all three *i*Bu groups are equilibrated.

The addition of 5 mol % *i*Bu_3Al leads to a more extensive substitution, with a weighted average of 2.90 substituted Me groups (1.07-3.20 expected, Figure 2.3 c). The addition of more *i*Bu_3Al leads to a maximal replacement of 11 Me groups (Figure 2.3 d and 2.3 e). The substitution process is reversible, and upon addition of excess Me_3Al to the mixture, the equilibrium is pushed backward to give a spectrum that consists principally of [**16,6**]$^-$ with a low level of residual mono-substituted product (Figure 2.4).

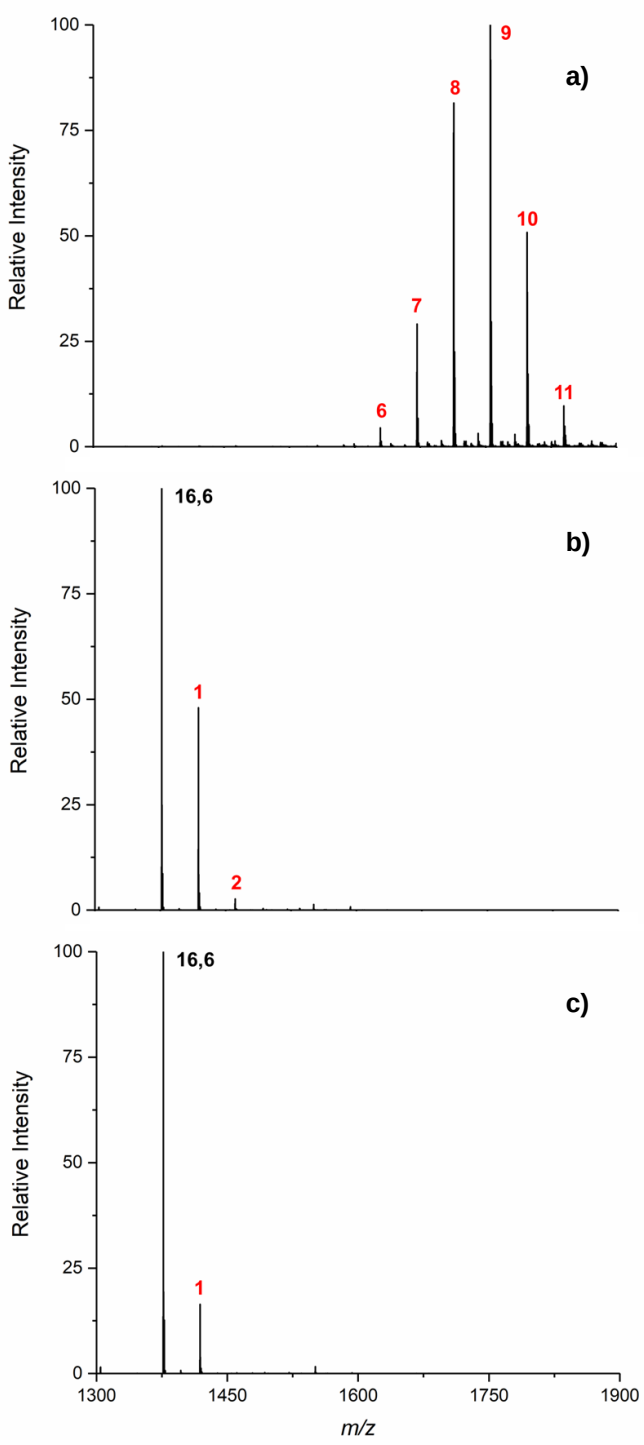

Figure 2.4 Negative ion ESI-MS spectra in PhF of (a) 30 wt. % MAO modified with 20 mol % *i*Bu$_3$Al (b) 20 mol % *i*Bu$_3$Al and 0.1 mL Me$_3$Al (2 M) and (c) 20 mol % *i*Bu$_3$Al and 0.2 mL Me$_3$Al (2 M). Number of Me/*i*Bu substitutions in [**16,6**]$^-$ shown in red.

The mechanism of alkyl exchange in simple R_3Al involves dissociation into monomeric R_3Al, followed by the formation of mixed dimers.[133] In the case of *i*Bu_3Al, which is largely dissociated, especially under these dilute conditions, exchange with MAO or the anions derived from MAO might involve dissociation of Me_3Al from the latter, followed by association of *i*Bu_3Al. On the other hand, anions with three *i*Bu groups are not prominent at low extents of substitution, suggesting that a mixed alkyl such as Me_2Al*i*Bu is involved in the exchange process, having been formed by rapid scrambling between *i*Bu_3Al and excess Me_3Al (Equation 2.1).

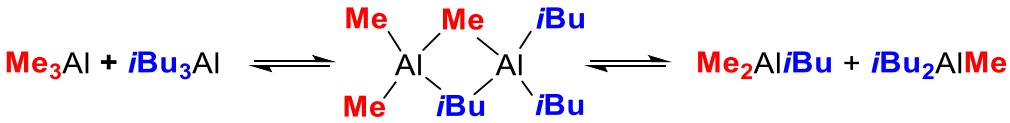

Equation 2.1 Scrambling between Me_3Al and *i*Bu_3Al

This expectation is borne out in the MS/MS fragmentation pattern, which shows an over-represented amount of Me_2Al*i*Bu loss as compared to Me_3Al when the ion with *m/z* 1501 (three *i*Bu groups) undergoes collision-induced dissociation with argon (Figure 2.5). The MS/MS spectrum shows that the first R_3Al loss has a ~45% chance of *i*$BuAlMe_2$, but with only 3 of 35 R groups being *i*Bu, we would expect the ratio to be ~ 26% (chance of an *i*Bu loss in the first R_3Al loss is 3/35 + 3/34 + 3/33 = ~26%). This indicates that bound *i*$BuAlMe_2$ is especially labile compared with bound Me_3Al. There are no direct losses of either *i*Bu_3Al or *i*Bu_2AlMe from the parent ion, suggesting that if those compounds are involved in the exchange, they do so with the incorporation of *i*Bu groups into less labile sites of the MAO oligomer.

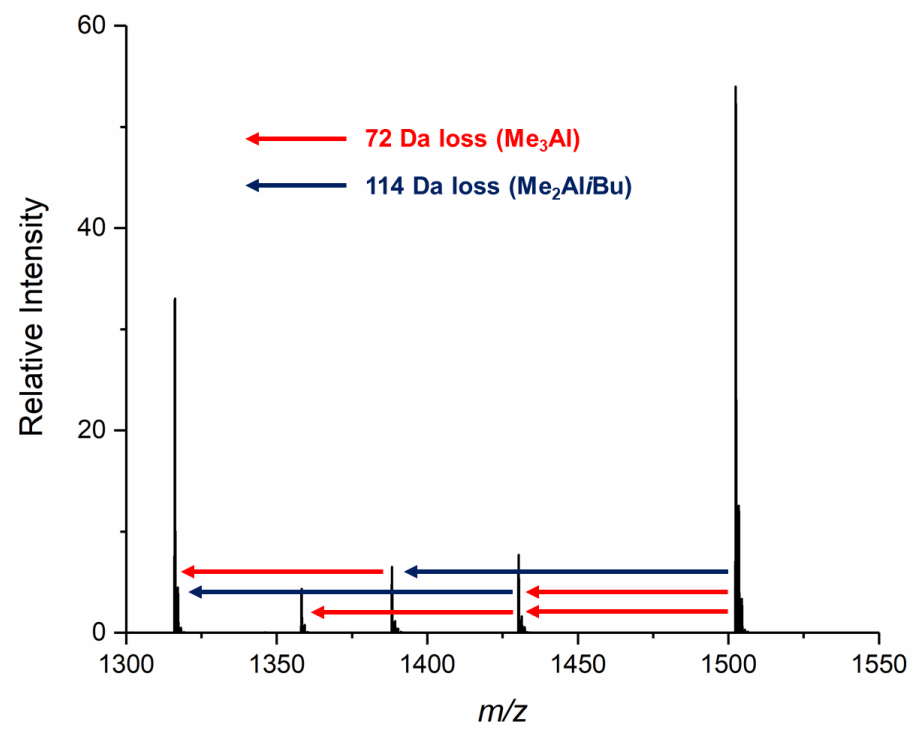

Figure 2.5 Partial MS/MS spectrum of the $[Me_{32}iBu_3Al_{22}O_{16}]^-$ species (i.e., [**16,6**]$^-$ after three Me for Bu exchanges) at *m/z* 1501. Initial two losses are shown only to illustrate the preference for *i*Bu loss of Me.

The positive ion mode spectra show a mixture of $[Me_n(iBu_{(2-n)})Al{\cdot}OMTS]^+$ cations upon the addition of the iBu_3Al. However, unlike the corresponding negative ion spectra, the order of addition of OMTS vs. iBu_3Al has a pronounced effect on the positive ion spectra (Figure 2.6).

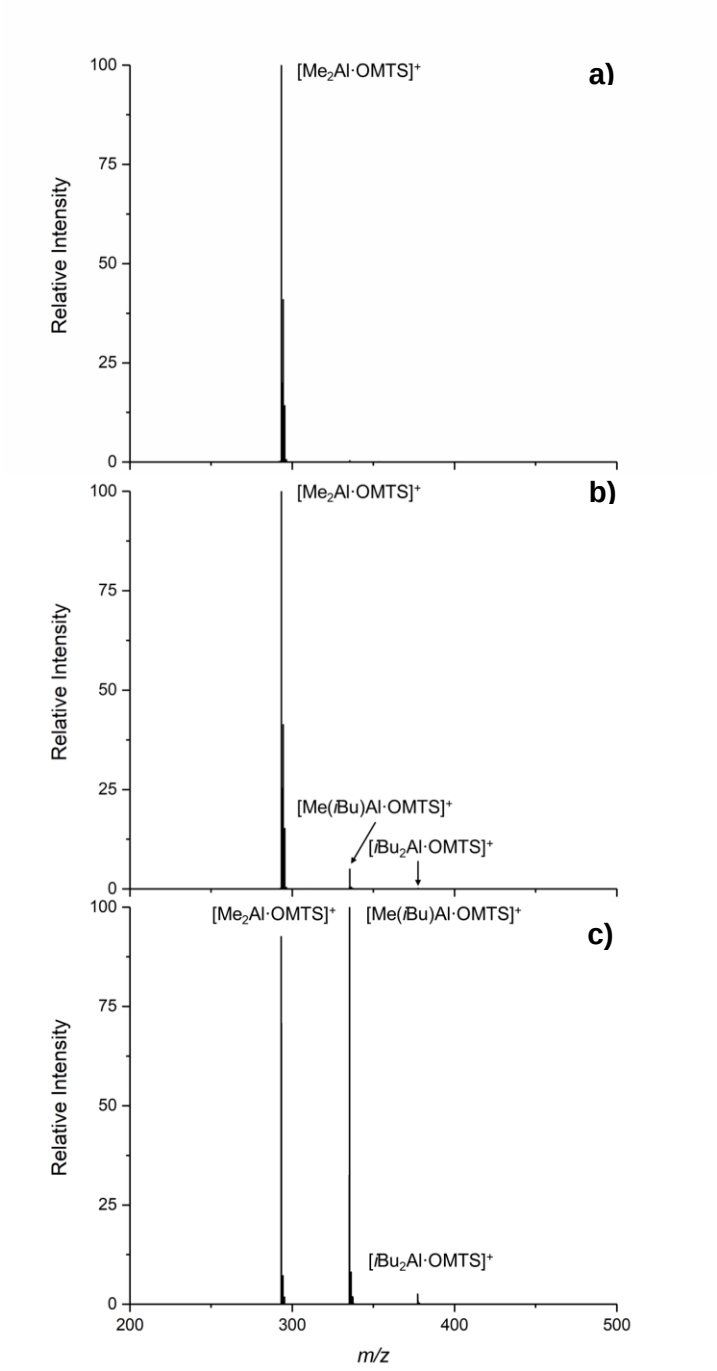

Figure 2.6 Positive ion spectra in PhF of (a) 30 wt. % MAO (b) 30 wt. % MAO with 15% *i*Bu_3Al added after ionization and (c) 30 wt. % MAO with 15% *i*Bu_3Al added before ionization. All at an OMTS:MAO ratio of 1:100.

When 15 mol % *i*Bu_3Al is added before ionization with OMTS, the main cation present is $[Me(iBu)Al{\cdot}OMTS]^+$ (Figure 2.6 c). In contrast, when the *i*Bu_3Al is added after ionization, the spectrum is dominated by $[Me_2Al{\cdot}OMTS]^+$ (Figure 2.6 b). In the latter case, it is somewhat unanticipated to see *any* mixed alkyl cations given the chelating nature of the OMTS ligand. However, it is known that the alkyl exchange process involving R_3Al does proceed in the presence of strong donors like pyridine, where rate-limiting dissociation of the donor adduct is involved.[133] Perhaps, a similar process is operative in the corresponding $[R_2Al]^+$ cations. It is also possible that the ionization of MAO is reversible, though one never observes a spectrum resembling Figure 2.6 c. The order of OMTS addition does not change the equilibrium distribution of the anions, suggesting that alkyl exchange is equally facile between both neutral MAO and their ionized analogs.

When *i*Bu_3Al is added first to MAO, all labile $AlMe_n$ (n = 1-3) sites are involved in the scrambling process, including those that are reactive to ion-pair formation via $[R_2Al]^+$ abstraction when OMTS is added. In fact, at 15 mol % *i*Bu_3Al, an *i*Bu:Me ratio of 0.45/1.64 = 0.274 in the corresponding cations is expected if there is no difference in reactivity between sites substituted by Me vs. *i*Bu. Figure 2.6 c suggests a slightly higher ratio of ca. 0.35, indicating a preferential exchange at the active sites or that those active sites bearing an *i*Bu group are more reactive towards $[R_2Al]^+$ abstraction.

Linnolahti *et al.*[3] have identified two types of sites that are reactive towards $[Me_2Al]^+$ abstraction in structures identified as stable aluminoxane products arising from the hydrolysis of Me_3Al.[119] One of those sites is shown generically in Scheme 2.1, and it is obvious from its structure that it should also be prone to exchange with R_3Al through the loss of Me_3Al.[133]

Three isomeric structures (**2-4**) will result in binding of Me_2Al*i*Bu, though the one with *i*Bu in the bridging position is expected to be unstable with respect to the other two. All three will interconvert through the process of alkyl exchange between bridging and terminal positions. In looking at structures **1-4**, only one of these will react with OMTS to produce $[Me(i\text{Bu})Al{\cdot}OMTS]^+$. Thus, on a statistical basis (which seems probable given that exchange is essentially complete at 20 mol % $i\text{Bu}_3Al$, and 15 mol % $i\text{Bu}_3Al$, one expects average labeling of 9.6 Me groups - cf. Figure 2.3 e) one would expect a ratio of $[Me_2Al{\cdot}OMTS]$:$[Me(i\text{Bu})Al{\cdot}OMTS]^+$ of ca. 1:1 assuming all reactive sites are substituted by at least one *i*Bu group. The ratio of these two cations in Figure 2.6 c is close to that predicted.

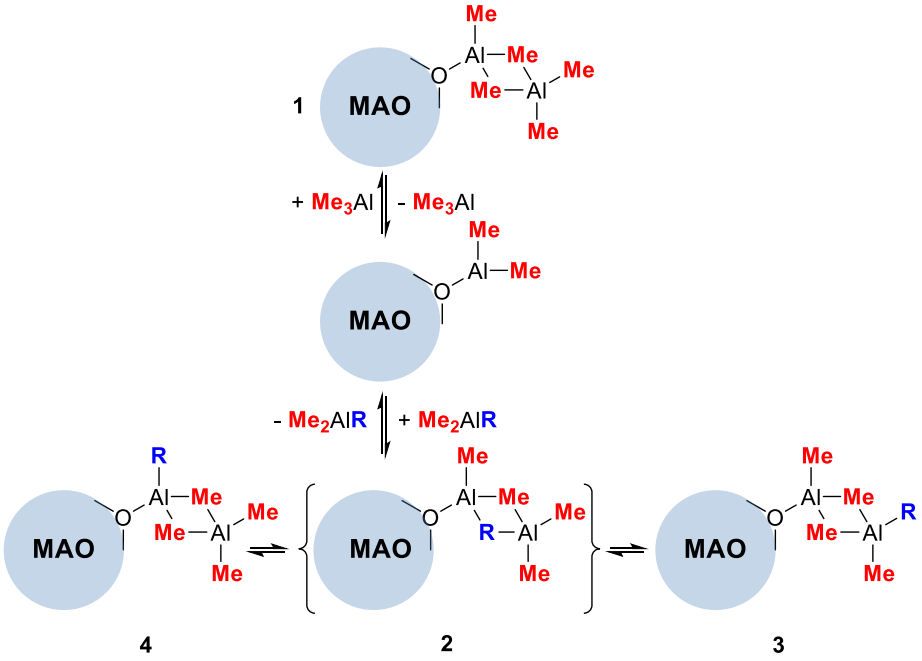

Scheme 2.1 Alkyl exchange between MAO and Me_2AlR.

Analogous structures are possible for reaction with $MeAli\text{Bu}_2$, but in this case, only two feature bridging Me groups, while of these, only one can react to form $[Me(i\text{Bu})Al{\cdot}OMTS]^+$, with the other forming $[i\text{Bu}_2Al{\cdot}OMTS]^+$. The latter cation is

drastically under-represented on a statistical basis in Figure 2.6 c. This suggests, as already mentioned, that *i*Bu_2AlMe may not be involved in the exchange process or that an O-(Me)$AlMe_2$Al*i*Bu_2 site is much less reactive towards ionization.

2.4 Addition of Et_3Al to MAO

The results with *i*Bu_3Al suggest that only limited substitution can occur (up to 11 exchanges), but the isobutyl group is significantly bulkier than the methyl group. Substitution by Et_3Al is expected to be much more like the self-exchange process involving Me_3Al. The Et/Me exchange is extremely fast and depending on the amount of Et_3Al that was added, [**16,6**]$^-$ derivatives with over 24 Et groups could be observed (Figure 2.7). At the 30 mol % level used, the Et/Me ratio is 0.90/1.64 = 0.55 and thus the average level of substitution should be 19.2 vs. ~ 20 observed, suggesting statistical labeling of the MAO and the resulting anions.

However, at lower amounts of Et_3Al, the distribution is far from statistical – for example, at 1 mol % Et_3Al the average degree of substitution is between 2-3 Me groups vs. 0.64 Me groups for a statistical process (Figure 2.7). The ion-pairs may be more reactive towards exchange than the neutrals in the case of Et_3Al at low levels of substitution. Some evidence for this is seen in the exchange of MAO vs. the ion-pairs with Me_2AlCl, admittedly where there is a strong driving force for substitution.[140] On the other hand, MS/MS spectra reveal that loss of Me_3Al is significantly more favorable than the loss of $EtAlMe_2$ from the parent ions (see Appendix A), while the direct loss of, e.g., Et_3Al is still not observed, suggesting that binding of $EtAlMe_2$ to labile sites on MAO is favored over that of Me_3Al, or more likely, that the Et group is rapidly scrambled into less labile sites on the MAO anions, as in structure 4, Scheme 2.1.

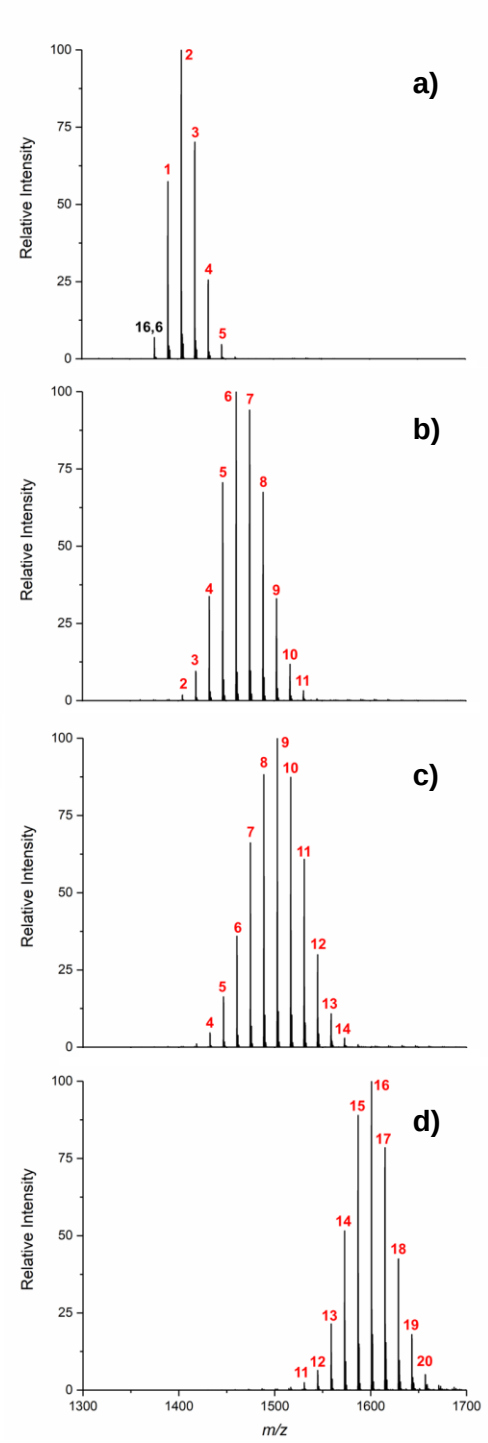

Figure 2.7 Negative ion ESI-MS spectra in PhF of 30 wt. % MAO modified with (a) 1 mol % Et_3Al (b) 5 mol % Et_3Al (c) 10 mol % Et_3Al (d) 20 mol % Et_3Al. All at an OMTS:Al ratio of 1:100. The number of Me/Et substitutions in [**16,6**]$^-$ shown in red.

These results point to R groups scrambling over the entire oligomer, meaning that the oligomer is highly dynamic with respect to exchange. The fact that the *i*Bu exchanges are more limited is probably a function of steric effects because fitting the larger R groups into the oligomer becomes increasingly difficult.

2.5 Addition of *n*Octyl$_3$Al to MAO

The most surprising results are obtained using *n*Oct$_3$Al. Despite being intermediate in steric hindrance (i.e., Et < *n*Oct < *i*Bu)[144], no more than seven positions are substituted at the same 30 mol % loading (Figure 2.8 b). Moreover, the rate of substitution is Et > *i*Bu > *n*Oct (*vide infra*).

In comparing Figure 2.8 b with, e.g., Figure 2.3 c where the anion substitution level is similar, it is obvious that the signal:noise ratio for *n*Oct anions is very much reduced compared with *i*Bu. Total ion counts decrease when the MAO anions are substituted by R groups in the order Et < *i*Bu < *n*Oct at similar extents of substitution. Additionally, when monitoring substitution by pressurized sample infusion (*vide infra*), the more highly substituted ions are significantly less sensitively detected that those featuring lower degrees of substitution when R = *n*Oct vs. Et (see Figure 2.10 vs. 2.11). Ions containing flexible alkyl chains exhibit lower ESI-MS response than rigid ions due to aggregation,[145,146] and this effect may be in play here. If so, the distribution observed with *n*Oct (Figure 2.8 b) is not representative of the actual degree of substitution.

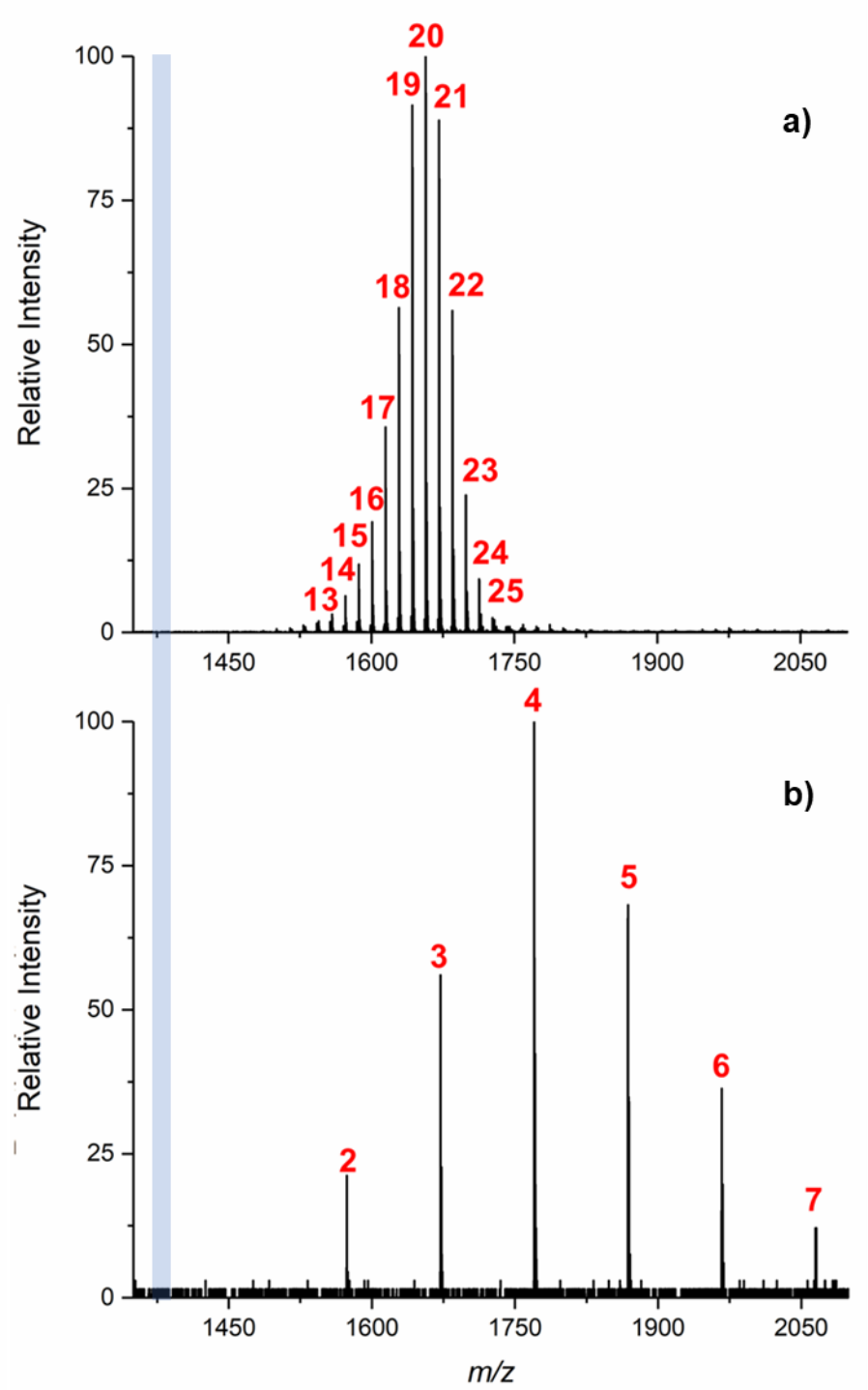

Figure 2.8 Negative ion ESI-MS spectra in PhF of 30 wt. % MAO modified with (a) 30 mol % Et_3Al and (b) 30 mol % nOct$_3$Al. Number of Me/R substitutions in [**16,6**]$^-$ shown in the red, blue box indicates the original *m/z* value of **[16,6]**$^-$.

2.6 Pressurized sample infusion to study alkyl exchange process

To better understand the R_3Al/MAO-Me exchange process, the reaction was conducted in real-time using pressurized sample infusion (continuous injection of a solution into the mass spectrometer using a variant of cannula transfer).[43,142,143] Upon addition of 1% *i*Bu_3Al to MAO, the rapid exchange is observed, resulting in the formation of the one, two, and three *i*Bu/Me substituted [**16,6**]$^-$ derivatives (see Appendix). These species equilibrate within a minute, and their ion counts thenceforth remain stable. Further insight into the alkyl exchange can be obtained upon the addition of excess (10 mol % with respect to total Al) of *i*Bu_3Al to the MAO/OMTS mixture (Figure 2.9). Now a series of consecutive *i*Bu/Me exchanges can be observed for 8 minutes.

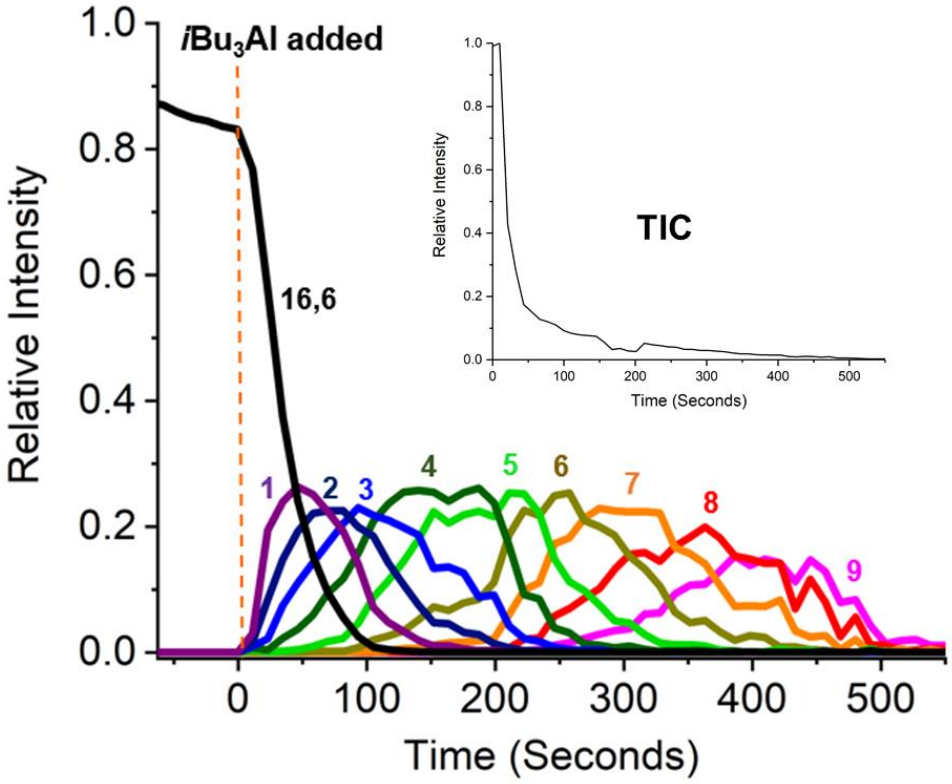

Figure 2.9 Pressurized sample infusion (PSI) of 10 mol % *i*Bu_3Al modified MAO/OMTS with Al:OMTS 100:1 in PhF. Inset: total ion counts over time (TIC). Numbers on top of traces corresponds to the number of *i*Bu groups exchanged.

During this period, the total ion chronogram (i.e., the sum of the intensities of all ions in the spectrum) shows a large decrease in intensity (see Figure 2.9 inset). Real-time data of the addition of Et_3Al and nOct$_3$Al to MAO/OMTS mixtures show similar trends as the iBu$_3$Al data (Figure 2.10 and Figure 2.11). The speed at which the exchange takes place varies with the individual exchanges being on the second-time scale for Et ($t_{½}$ ~ 2 sec for the disappearance of [**16,6**]$^-$), on the minute time scale for iBu ($t_{½}$ ~ 40 sec), and on the multi-minute time scale for nOct ($t_{½}$ ~ 200 sec).

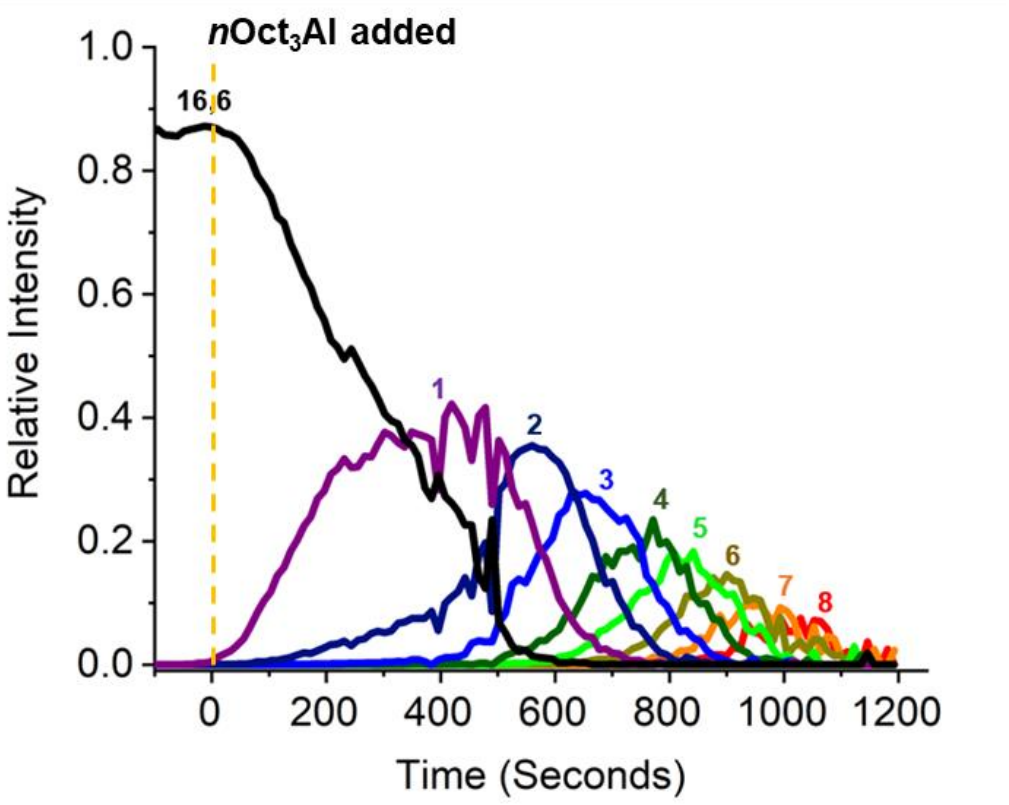

Figure 2.10 Pressurized sample infusion (PSI) of 10 mol % nOct$_3$Al modified MAO/OMTS with Al:OMTS 100:1 in PhF. Numbers on top of traces corresponds to the number of octyl groups exchanged.

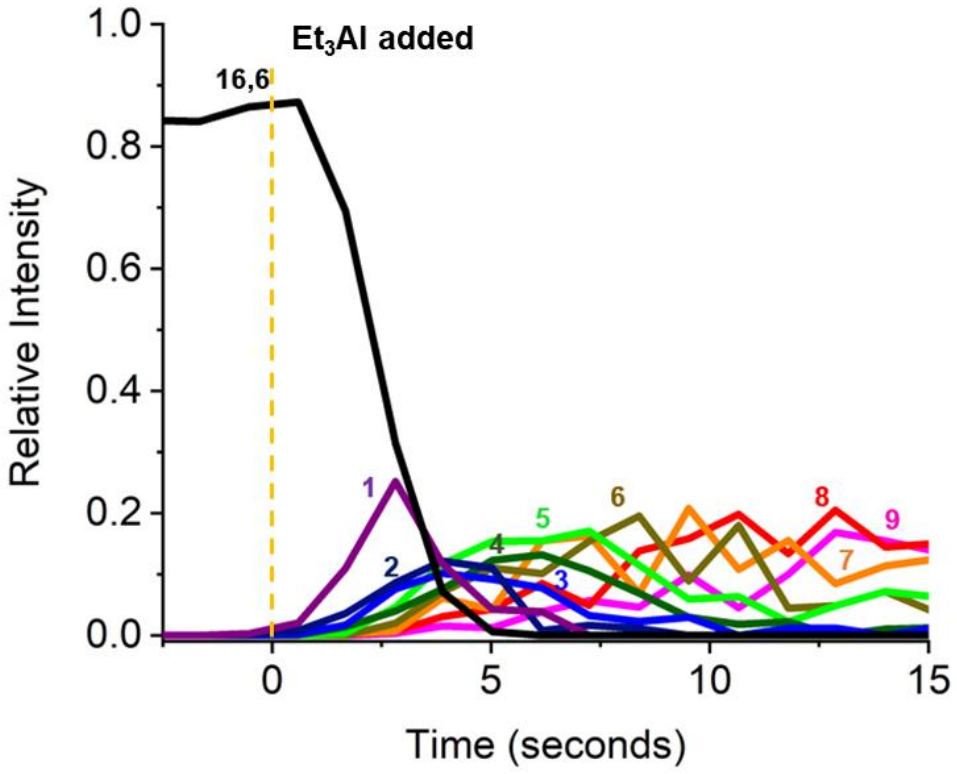

Figure 2.11 Pressurized sample infusion (PSI) of 10 mol % Et_3Al modified MAO/OMTS with Al:OMTS 100:1 in PhF. Numbers on top of traces corresponds to the number of ethyl groups exchanged.

The differential rates are likely a function of at least two different factors: the extent to which the R_6Al_2 dimer is dissociated (K_d = 6.0 M, 1.7×10^{-3} M, and 2.2×10^{-5} M for *i*Bu, *n*Oct, and Et at 25 °C in benzene),[129,147–149] where low dissociation will lead to lower rates of exchange; and the relative rates at which monomeric R_3Al can compete with monomeric Me_3Al ($K_d = 9.0\times10^{-8}$ M) for the occupation of a vacant site on the "unsaturated" MAO (i.e., **16,5**; this rate will be slower for sterically encumbered R_3Al). Unfortunately, we are unable to quantitatively account for the observed differences in rate using these simple arguments. This suggests that the mechanism for exchange may well differ depending on R_3Al, or at least the rate-determining step in the substitution process is different for Et and *n*Oct vs. *i*Bu to account for the strange order in the observed rates.

2.7 Computational studies on alkyl exchange

In earlier theoretical work, Linnolahti *et al.* adopted a model for the precursor to this ion-pair that was especially stable relative to other aluminoxane structures located during a systematic but targeted grid search of the reactions between Me_3Al and H_2O.[5b] This model and the corresponding anion formed by methide abstraction share structural features that are associated with the reactivity of MAO but are common to many other cage structures that were located during this process. As shown in Figure 2.12, the model for $(MeAlO)_{16}(Me_3Al)_6$ has a total of 18 methyl groups that could be considered labile, in the sense that only Al-C bonds would be broken during the exchange (they are highlighted in blue). While this might account for the results seen with *i*Bu_3Al (6 of these positions are bridging rather than terminal and thus disfavored), it falls short of the 24 low energy substitution reactions observed for Et_3Al.

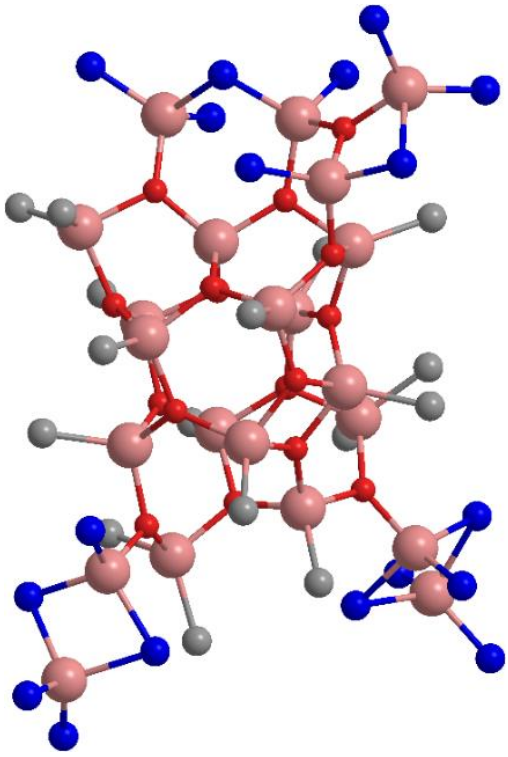

Figure 2.12 Optimized structure for neutral $(MeAlO)_{16}(Me_3Al)_6$ (Al pink, O red, and C grey). Modeling studies are done by Prof. Mikko Linnolahti and reproduced with his permission.

To accommodate this number of substitutions, one would have to break Al-O bonds during the dynamic processes that interconvert R groups on the oligomer. There is only one Al_2O_2 ring in this structure, with the rest being six-membered, Al_3O_3 rings and thus relatively strain-free. A similar interconverting process involving strained Al_2O_2 rings has been used by Barron *et al.* to explain the different isomers observed during the reaction of $(t\text{BuAlO})_6$ with one equivalent of Me_3Al.[134]

Given the number of alkyl substitutions and their selectivity for a minor component of the mixture in the case of Et_3Al, the MAO activator(s) must have unusual structures that depart significantly from the cage-like motifs or even nanotubes that have been considered in the past. A new structure of sheet structure [**16,6**]$^-$ is proposed in Chapter 3.

2.8 Conclusions

The selective ionization of MAO provided a unique opportunity to investigate a hitherto intractable problem: the modification of MAO with R_3Al species. Rapid reactivity followed by statistical equilibration was observed in the case of $i\text{Bu}_3\text{Al}$, and the sequential reactivity suggested that the scrambling of the R_3Al species with Me_3Al was faster than an exchange with the MAO oligomer. The extent of substitution was very high with Et_3Al, pointing towards exchange being facile not just for the most exposed methyl groups on the oligomer but possibly also for Me groups, which are less labile by incorporation into the aluminoxane structure. These observations will spur further examination of MAO's structure by computational approaches and encourage that real-time kinetic analysis of MAO reactivity is possible.

2.9 Experimental

MAO (10 and 30 wt. % in toluene) was obtained from Albemarle and stored in the glovebox freezer upon receiving. The samples were warmed to room temperature and thoroughly swirled to dissolve any precipitated content before use. OMTS (98%), Me_3Al (2 M in toluene), Et_3Al (1.9 M in toluene), *i*Bu_3Al (1 M in toluene) and *n*Oct_3Al (0.48 M in toluene) were purchased from Sigma-Aldrich and used as received. Fluorobenzene (Oakwood) was refluxed over CaH_2, distilled under N_2, and dried over molecular sieves inside a glovebox for at least three days prior to use.

2.9.1 ESI-MS Details

In a typical procedure, a stock solution (3 mL) was prepared by dilution of MAO (0.5 mL of 1.5 M (10 wt. %) or 0.15 mL of 4.6 M (30 wt. %) and 0.5 mL of a premade PhF solution of OMTS (0.015 M) to give a mixture with an Al:OMTS ratio of 100:1. After this, 0.2 mL of this solution was further diluted to 3 mL to give a mixture with the final [Al] of 0.0167 M. To this mixture, varying amounts of R_3Al (R = Et, *i*Bu, or octyl; for exact details, see section 2.9.2) were added to give the desired MAO-Al:R_3Al ratios. The resulting solution was injected from the glove box to a Micromass QTOF micro spectrometer via PTFE tubing (1/16” o.d., 0.005” i.d.). The capillary voltage was set at 3000 V with source and desolvation gas temperature at 85 °C and 185 °C, respectively, with the desolvation gas flow at 400 L/hr. MS/MS data were obtained using argon as the collision gas and a voltage range of 2-100 V.

For PSI experiments, 0.4 mL of an MAO-OMTS solution was diluted with 6 mL of PhF and placed in a glass vial (0.0167 M). The vial was attached to a rubber septum, and a 178 μm ID PTFE tubing was immersed in the MAO-OMTS solution, and the other end of the

tubing was connected to the MS source. PSI experiments were carried out by the addition of the R_3Al to give the desired MAO-Al:R_3Al ratio.

2.9.2 Additional Experimental Details

iBu_3Al addition: A stock solution of 0.00167 M *i*Bu_3Al was prepared by dilution of 10 μL of *i*Bu_3Al (1 M in toluene) to 6 mL with PhF. The following amounts of this solution were added to the 0.0167 M solution of MAO/OMTS (Al:OMTS 100:1) to give the desired Al:R_3Al ratios. All mixtures were allowed to equilibrate for 5 minutes before being analyzed by ESI-MS in negative ion mode (see Figure 2.3 for spectra).

100:1 - 0.3 mL of 0.00167 M *i*Bu_3Al stock solution (final MAO [Al] = 0.015 M)

100:5 - 1.5 mL of 0.00167 M *i*Bu_3Al stock solution (final MAO [Al] = 0.011 M)

100:10 - 3 mL of 0.00167 M *i*Bu_3Al stock solution (final MAO [Al] = 8.4×10^{-3} M)

100:15 - 4.5 mL of 0.00167 M *i*Bu_3Al stock solution (final MAO [Al] = 6.7×10^{-3} M)

100:20 - 6.0 mL of 0.00167 M *i*Bu_3Al stock solution (final MAO [Al] = $5.6\ 10^{-3}$ M)

For the reverse reaction Me_3Al (2 M in toluene) was added to the 100:20 Al:R_3Al mixture in 0.1 mL increments (2x) and the speciation was subsequently analyzed in negative ion mode (see Figure 2.4 for spectra).

Positive ion spectra comparison: A stock solution of 0.033 M *i*Bu_3Al was prepared by diluting 0.1 mL *i*Bu_3Al (1 M in toluene) to 3 mL using PhF. Then 0.1 mL of this stock solution was added to the 0.0167 M MAO/OMTS (Al:OMTS 100:1) stock solution to give a solution with Al:*i*Bu_3Al of 100:15 (final MAO [Al] = 0.016 M). The mixture was equilibrated for 5 min. and then the positive ion ESI-MS spectrum was taken. To observe the speciation when *i*Bu_3Al was added before ionization, a stock solution of 0.0167 M MAO was prepared. To 3 mL of this solution were added 0.1 mL of the 0.033 M *i*Bu_3Al

solution. The mixture was allowed to equilibrate for 5 min. before 0.2 mL of a 0.000167 M stock solution of OMTS was added. The mixture was again allowed to equilibrate for 5 min. after which the positive ion ESI-MS spectrum was collected (see Figure 2.6 for spectra).

nOct_3Al addition: A stock solution of 0.0050 M *n*Oct_3Al was prepared by dilution of 63 μL of *n*Oct_3Al (0.48 M in hexane) to 6 mL with PhF. Then 3.0 mL of this solution was added to 3 mL of a 0.0167 M stock solution of MAO/OMTS (Al:OMTS 100:1) to give an *n*Oct_3Al to MAO-Al ratio of 100:30. The mixture was allowed to equilibrate for 30 minutes before being analyzed by ESI-MS in negative ion mode (See Figure 2.8 for spectrum).

100:30 - 3.0 mL of 0.0050 M *n*Oct_3Al stock solution (final MAO [Al] = 8.4×10^{-3} M)

Et_3Al addition: Stock solutions 0.00167 M and 0.0050 M Et_3Al were prepared by dilution of 5 μL and 15 μL of Et_3Al (1.9 M in toluene) to 6 mL with PhF. The following amounts of the solutions were added to the 0.0167 M solution of MAO/OMTS (Al:OMTS 100:1) to give the desired Al:R_3Al ratios. All mixtures were allowed to equilibrate for 5 minutes before being analyzed by ESI-MS in negative ion mode (see Figure 2.7 for spectra).

100:1 - 0.3 mL of 0.00167 M *n*Oct_3Al stock solution (final MAO [Al] = 0.015 M)

100:5 - 1.5 mL of 0.00167 M *n*Oct_3Al stock solution (final MAO [Al] = 0.011 M)

100:10 - 3.0 mL of 0.00167 M *n*Oct_3Al stock solution (final MAO [Al] = 8.4×10^{-3} M)

100:20 - 2.0 mL of 0.0050 M *n*Oct_3Al stock solution (final MAO [Al] = $1.0\ 10^{-2}$ M)

100:30 - 3.0 mL of 0.0050 M *n*Oct_3Al stock solution (final MAO [Al] = 8.4×10^{-3} M)

PSI experiments: All glassware was oven-dried overnight before use. Reagents were stored and manipulated in a glovebox under an inert atmosphere. Then 0.4 mL of a 0.25 M Al MAO/OMTS (100:1) stock solution was diluted with 6 mL of PhF and placed in a glass

vial ([Al] = 0.0167 M). The vial was attached to a rubber septum, and a 178 μm ID PTFE tubing was immersed in the MAO/OMTS solution, and the other end of the tubing was connected to the ESI-MS source. A UHMWPE (10 μm) frit was installed at the beginning of the PTFE tubing to prevent blocking of the capillary, which hinders consistent data recording. This way, the solution was filtered before injection into the ESI-MS, thus preventing the blocking of the capillary. The experiment was started, and as soon as a stable ion count of [**16,6**]$^-$ was observed, the R_3Al solutions described below were added at once

iBu_3Al aluminum addition: A stock solution of *i*Bu_3Al was prepared by dilution of 0.1 mL of *i*Bu_3Al (1M in toluene) to 4 mL solution with PhF ([*i*Bu_3Al] = 0.025 M). Then 0.4 mL of this solution was added to the MAO/OMTS solution as soon as a stable count of [**16,6**]$^-$ was observed to give an Al:*i*Bu_3Al ratio of 100:10, and the spectrum was recorded until no further ions were observed (see Figure 2.9 for spectrum).

For the Al:*i*Bu_3Al ratio of 100:1 experiment, a stock solution of *i*Bu_3Al was prepared by dilution of 0.25 mL of *i*Bu_3Al (1 M in toluene) to 4 mL solution with PhF ([*i*Bu_3Al] = 0.062 M). 0.1 mL of this solution was added to the MAO/OMTS solution as soon as a stable count of [**16,6**]$^-$ was observed to give an Al:*i*Bu_3Al ratio of 100:1, and the spectrum was recorded until no further ions were observed (see Appendix for spectrum).

nOct_3Al addition: A stock solution of *n*Oct_3Al was prepared by dilution of 0.21 mL of 0.48 M *n*Oct_3Al solution to 4 mL with of PhF ([*n*Oct_3Al] = 0.025 M). 0.4 mL of this solution was added to the MAO/OMTS solution as soon as a stable count of [**16,6**]$^-$ was observed to give an Al:*n*Oct_3Al ratio of 100:10, and the spectrum was recorded until no further ions were observed (see 2.10 for spectrum).

Et_3Al addition: A stock solution of Et_3Al was prepared by dilution of 0.053 mL of Et_3Al (1.9 M in toluene) to 4 mL solution with PhF ([Et_3Al] = 0.025 M). 0.4 mL of this solution was added to the MAO/OMTS solution as soon as a stable count of [**16,6**]$^-$ was observed to give an Al:Et_3Al ratio of 100:10, and the spectrum was recorded until no further ions were observed (see Figure 2.11 for spectrum).

Chapter 3 Real-time analysis of methylalumoxane formation

Portions from this chapter have been previously published and reproduced with permission from "Real-Time Analysis of Methylalumoxane Formation" A Joshi, H S Zijlstra, E Liles, C Concepcion, M Linnolahti and J S McIndoe, *Chemical Science*, **2020**. Prof. Mikko Linnolahti did computational studies included in this chapter

3.1 Introduction

Methylalumoxane (MAO) is an oligomeric activator for single-site olefin polymerization precatalysts, prepared by the reaction of trimethylaluminum (TMA) with water.[150–156] MAO is a complete activator[62,108,110] through playing multiple roles: it acts as a scavenger of oxygen and water; it can alkylate the precatalyst; and it can ionize the precatalyst via abstraction of a methyl group.[109,157] TMA is a capable scavenger on its own,[158] and will also methylate metal-halogen bonds,[159,160] but it is not able to ionize the precatalyst.[122] MAO is however expensive due to the high aluminum to metal ratios required to achieve high productivities, with ratios of 10^4 being typical.[110] A limited understanding of the structure of MAO has hampered efforts to improve its efficiency. Different grades of MAO are available commercially containing varying amounts of unreacted TMA arising from incomplete hydrolysis.[109,111] The TMA in MAO can be divided into two kinds: "bound TMA" which is incorporated in the MAO and "free TMA" which can be removed under vacuum to form TMA-depleted MAO (DMAO).[161] Free TMA can be effectively trapped by adding a sterically hindered phenol such as 2,6-di-tert-butyl-4-methylphenol(BHT).[127,162] The catalytic productivity and polymer molecular weight depends on the amount of free TMA in MAO and its synthesis history.[126–128,163–167] Replacing the methyl group in MAO by bulkier alkyl groups such as isobutyl or octyl leads

to the formation of modified MAO (MMAO), which have increased solubility and stability.[109,130,163,168]

Ionization comes about via neutral MAO generating the reactive Lewis acidic species $[Me_2Al]^+$, with the resulting bulky MAO anions being sufficiently weakly coordinating to allow high reactivity towards alkenes at the cationic metal center.[169–173] The McIndoe group have previously shown through mass spectrometric means that the anionic products of the activation process are dominated by a single ion, $[(MeAlO)_{16}(Me_3Al)_6Me]^-$ henceforth [**16,6**]$^-$.[1] The three-dimensional structure of this anion has not been elucidated, but its mysteriously high abundance in the spectra of post-activation commercial MAO does raise all sorts of questions about why it is so prominent since the synthesis of MAO does not on the face of it appear to be particularly selective, being the controlled mixing of water and pyrophoric trimethylaluminum.[174] Laboratory scale syntheses of hydrolytic MAO use hydrated salts[175-176] to slowly release the water such that controlled hydrolysis of TMA is possible. Direct hydrolysis of TMA by the use of ice [177] or wet solvent [178,179] has also been reported. Alternative methods for preparation of MAO from reaction of benzoic acid, CO_2 with TMA or from the reaction of TMA with Me_3SnOH have been reported.[180–182]

The appearance of a “magic” ion that dominates a mixture with a broad distribution of possible products has always attracted attention from curious chemists. For example, the time-of-flight mass spectra of laser-vaporized graphite reveal a range of $(C_2)_n$ ions, of which C_{60} was the most abundant component thanks to the exceptional stability of the truncated icosahedral structure of that molecule.[183] Protonated water droplets $[H(H_2O)_n]^+$, feature $[H(H_2O)_{21}]^+$ as an especially prominent ion, thanks to the stability of a water

molecule surrounded by 20 others in an icosahedral array.[184] Understanding the special stability of [**16,6**]$^-$ is challenging due to the pyrophoric nature of the matrix itself, so separation of this component is exceptionally challenging. We resolved to discover what we could by the generation of this ion by real-time monitoring of the synthesis process itself and to delve deeper computationally into its structure.

ESI-MS reveals predominantly [**16,6**]$^-$ ion in MAO solutions in the presence of any additive that reacts readily with $[Me_2Al]^+$. Cp_2ZrMe_2 generates [Cp_2ZrMe] [**16,6**]$^-$, [NBu_4]Cl generates [NBu_4] [**16,6**]$^-$, but the most convenient way to make the ion is via addition of octamethyltrisiloxane ($Me_3SiOSiMe_2OSiMe_3$, OMTS). OMTS chelates available $[Me_2Al]^+$ to generate $[Me_2Al(OMTS)]^+$ (Figure 3.1).[1,185]

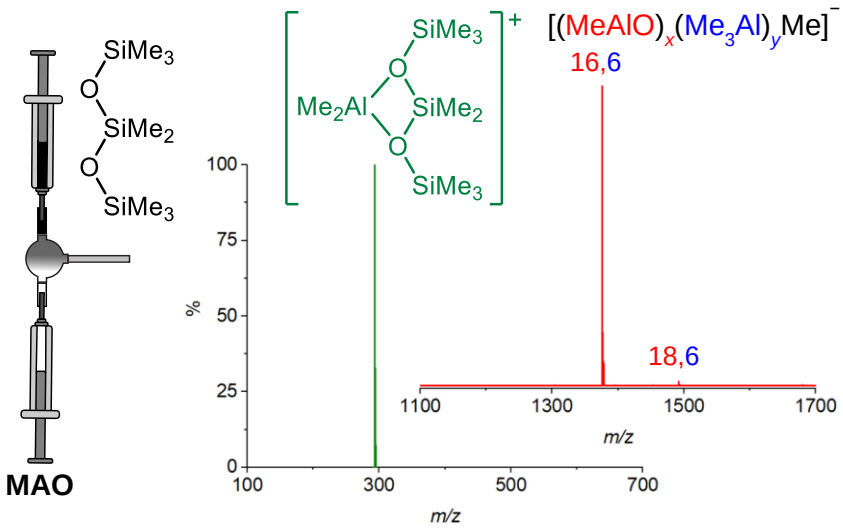

Figure 3.1 Ionization of MAO to generate $[Me_2Al(OMTS)]^+$ (green) and predominantly [**16,6**]$^-$ (red).

The resulting anions can be characterized in negative mode ESI-MS. The McIndoe group has used this technique to study alkyl exchange,[168] aging,[3] and oxidation[186] of MAO, where

the anion distribution changes in response to these processes. In this chapter, the dynamic behavior of MAO anions formed via the reaction of TMA and water is discussed.

3.2 Monitoring experiments in 1,2-Difluorobenzene(DFB)

When water and TMA are combined, a fast exothermic reaction generates MAO with methane as a byproduct.[187] Severe methodological challenges were faced in studying this system mass spectrometrically, because of the evolution of methane, the exothermicity of the reaction, the low polarity of the toluene solvent[188] generally used in synthesis, the propensity of the reacting solution to cause capillary blockages during analysis, the complexity of the mixture, and the inapplicability of normalization in the context of a system whose total ion count is changing. These factors conspired together to give extremely noisy time course data (Figure 3.2), though with consistent trends in speciation. Figure 3.2 shows the Total Ion Count (TIC) as a function of time for a typical ESI-MS run of MAO synthesis for seven different runs. The TIC was often highly erratic as it is

extremely challenging to run and analyze MAO mixtures. The most common problems are inconsistent spray/clogging while running these experiments.

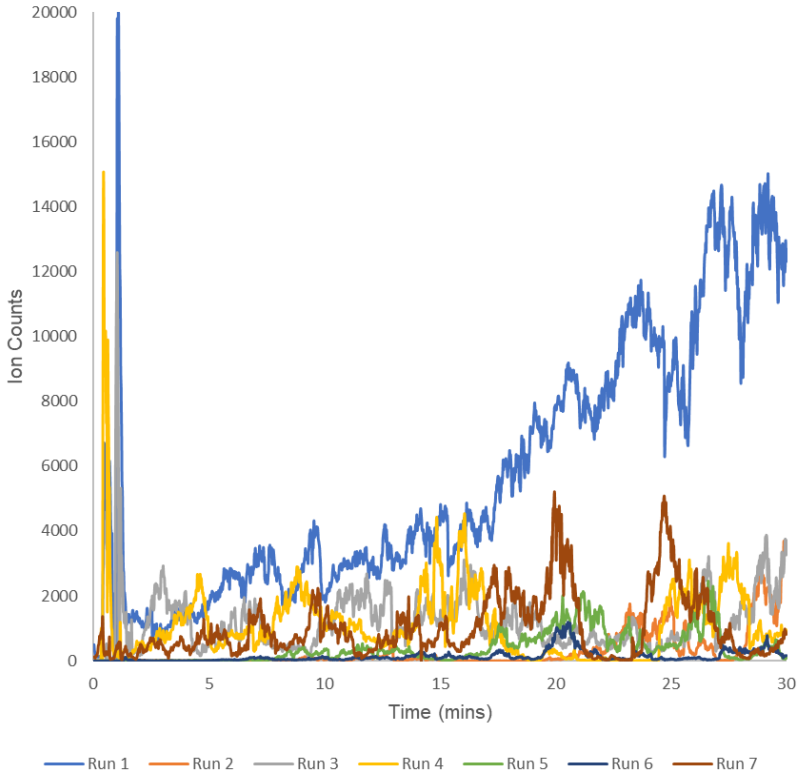

Figure 3.2 Total Ion Counts (TIC) as a function of time for seven different ESI-MS run of monitoring MAO synthesis.

The rate of reaction was significantly affected by the amount of water present, and the reaction could be slowed considerably by reducing the concentration of water used. The water concentration in the solvent was measured after the addition of Cp_2ZrMe_2 by ^1H NMR.[189] None of the reaction components (TMA, H_2O, OMTS, DFB) on their own provide significant quantities of ions, but their combination generates aluminoxane species capable of ionizing via capture of $[Me_2Al]^+$ by OMTS. More than 99% of the ion current during the hydrolysis experiments could be assigned to ions of the form $[(MeAlO)_x(Me_3Al)_yMe]^-$

(Figure 3.3); hence the general formula $(MeAlO)_x(Me_3Al)_{y+1}$ for the neutral precursors applies for those aluminoxanes competent to act as activators.

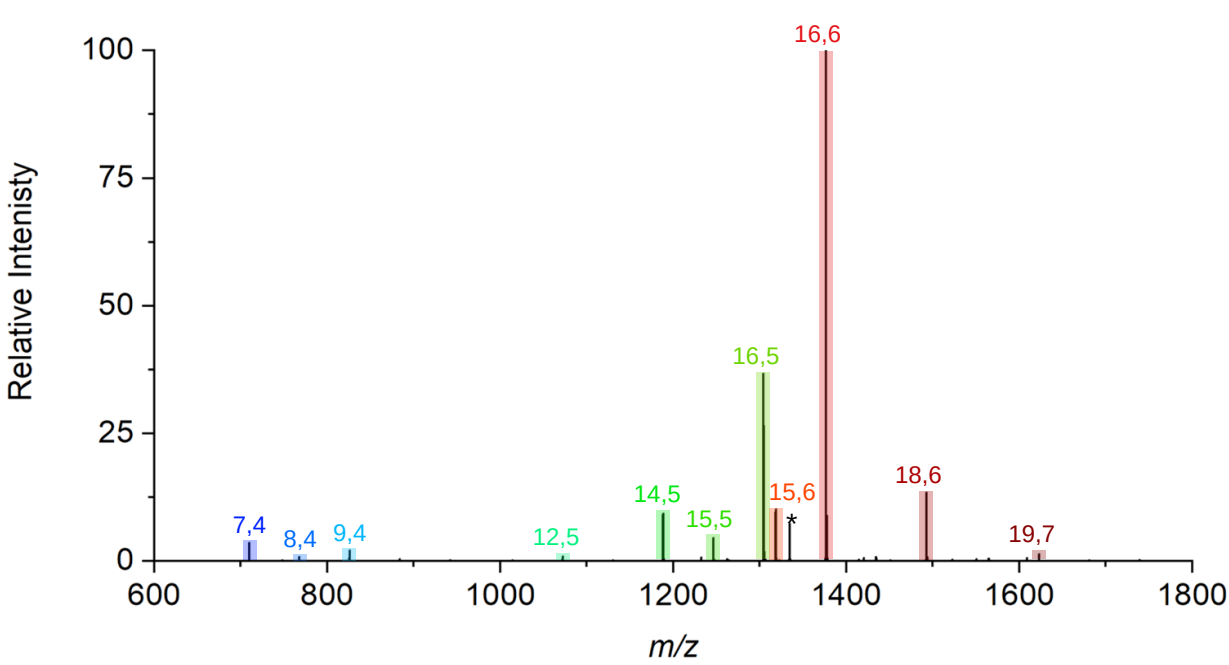

Figure 3.3 Summation of all negative ion ESI mass spectra collected for 30 minutes after mixing of Me_3Al, wet (0.055 M H_2O) degassed DFB and OMTS.

The error in the TIC is huge, but the speciation remains the same irrespective of the TIC appearance. When the spectra are plotted at 10 mins for all the seven different experiments, we observe the anion $[(MeAlO)_{16}(Me_3Al)_6Me]^-$ henceforth **[16,6]** $^-$ as the dominant ion in each case (Figure 3.4). The anion **[16,6]** $^-$ is observed when we run a commercial sample of MAO with the additive OMTS. The similarity in the spectra is remarkable considering the differences in reaction conditions between a small syringe and an industrial-scale reactor.

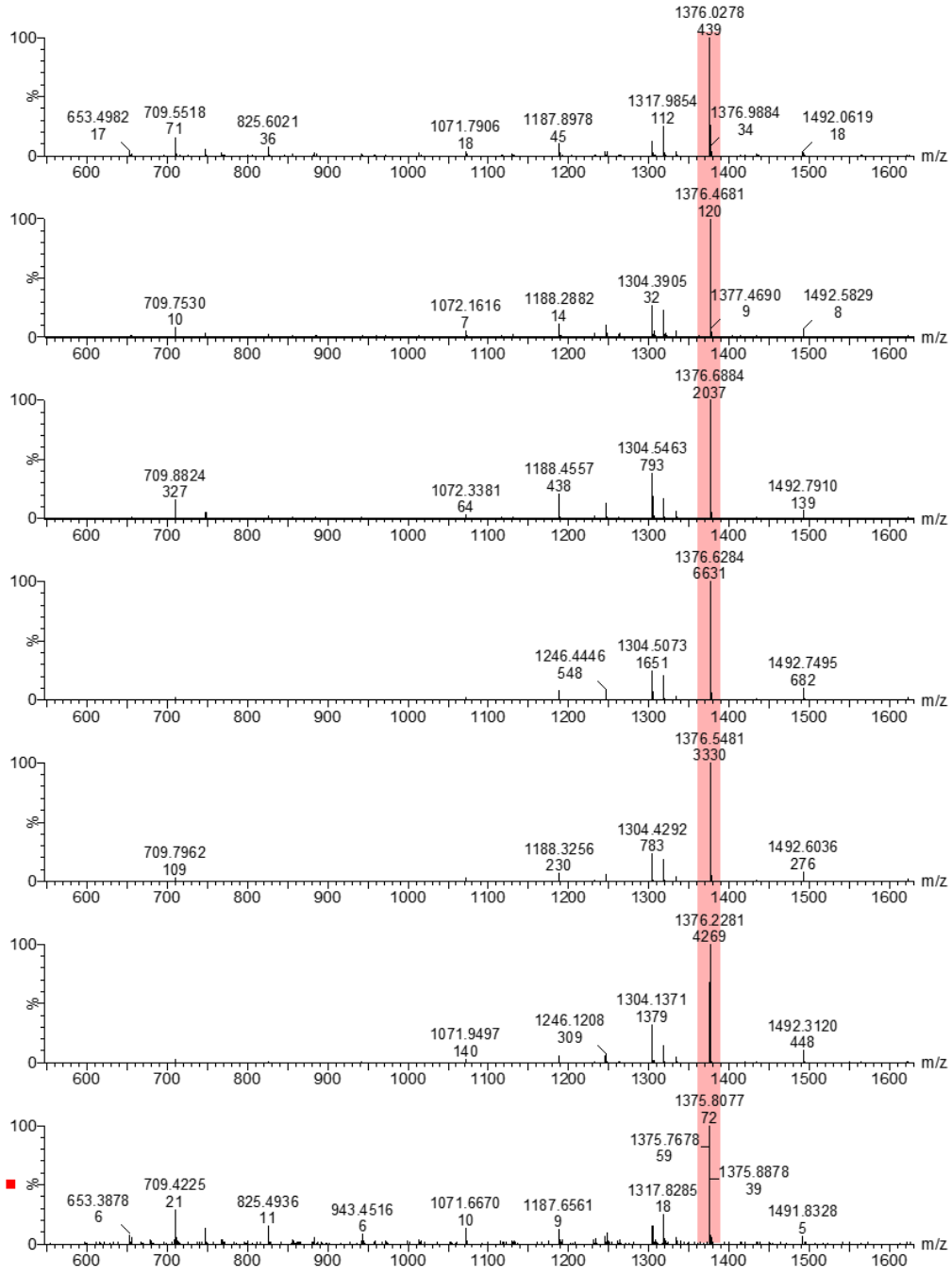

Figure 3.4 The anion distribution upon addition of TMA to wet (0.055 M H_2O) degassed DFB and OMTS after 10 mins for seven different experiments. The red line shows the dominant [**16,6**]$^-$ anion observed in commercial MAO samples.

3.3 Reaction of TMA and water in Fluorobenzene (PhF)

Toluene, fluorobenzene, and difluorobenzene provided essentially the same collection of ions but with increasingly better ion intensity as the solvent polarity increased. The rate of reaction was significantly affected by the amount of water present, and the reaction could be slowed considerably by reducing the concentration of water used or by releasing it slowly using hydrated salts as the water source. The reaction of TMA and water in PhF is slower than the reaction in DFB solvent. The formation of [**16,6**]$^-$ in PhF happens over a span of 4 hours compared to 10 mins in DFB. Heating the mixture after 4 hours in PhF leads to a spectrum dominated by [**16,6**]$^-$ (Figure 3.5). The reaction of TMA and water in PhF was also done at elevated temperatures, i.e., 60 °C, and the formation of [**16,6**]$^-$ was observed in 20 mins but not as a single dominant ion (Figure 3.6). The spectra recorded for analysis at higher temperatures was complicated compared to that recorded in room temperature due to oxidation of the anions. Since reactions in PhF at room temperature take such a long time, it is not suited for reaction monitoring as the MAO system is very prone to clogging/spray problems, and longer reaction means chances for capillary blockages are high. The reaction at a higher temperature in PhF is faster, but heating also increases the rate of oxidation, and therefore the spectra observed is not clean and is accompanied by ions that are oxidized. The oxidized anions are seen by the presence of species 42 Da lower-than-normal MAO anions.[4] The 42 Da mass difference is explained by the addition of oxygen and removal of one MeAlO unit (16 Da − 58Da = −42Da). The anion [**16,6**]$^-$ is also not a dominant anion when the reactions are done at higher temperatures. Considering all these factors, DFB was used as a solvent for monitoring the process of MAO synthesis.

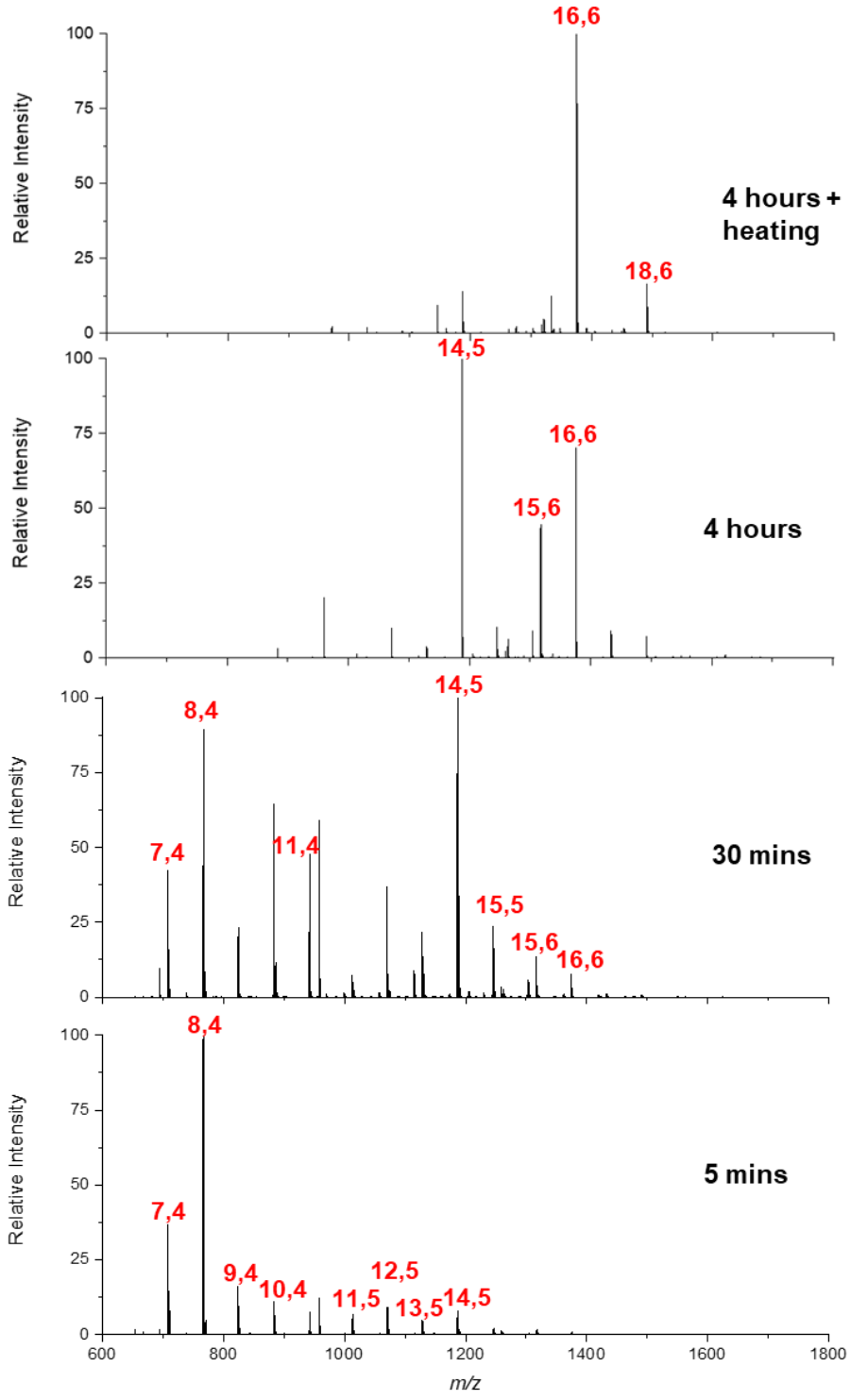

Figure 3.5 Reaction of TMA in PhF with [H_2O] = 0.009 M at 100:1 OMTS ratio. The lower amount of water slows down the reaction as compared to the reaction in DFB. The anion [**16,6**]$^-$ is observed as a dominant anion upon heating the reaction mixture after 4 hours.

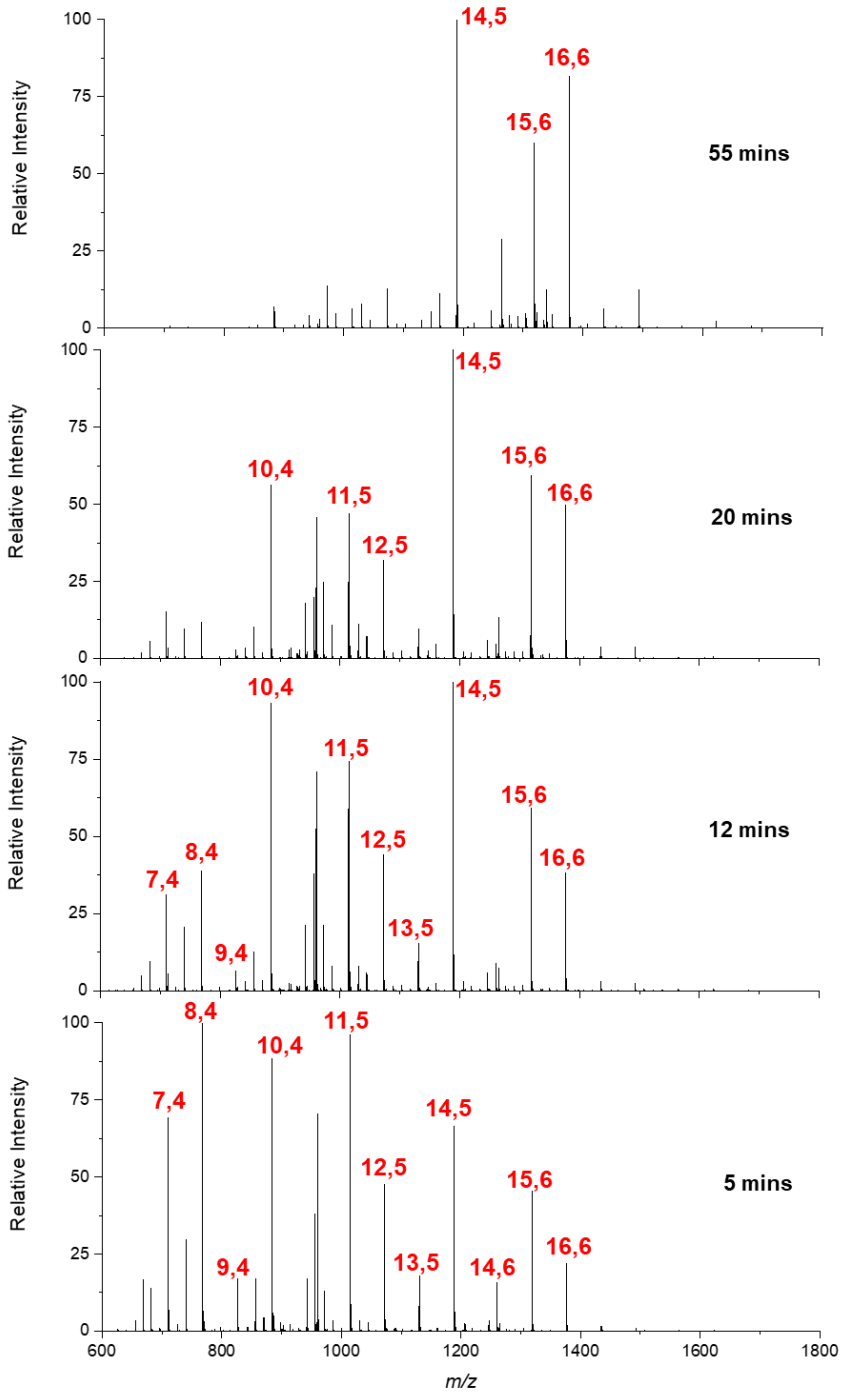

Figure 3.6 Reaction Monitoring at 60 degree in PhF with [H_2O] = 0.009 M at 100:1 OMTS ratio. The reaction is faster than room temperature, but the spectrum is not as clean as the spectrum at room temperature. Also, [**16,6**]$^-$ is not observed as a single dominant ion under these conditions.

3.4 Order of addition of OMTS

Speciation was also largely unaffected by whether OMTS was added at the start of the reaction or at the time of analysis (Figure 3.7). This meant that we did not have to add the additive OMTS in-situ, and it could be added at the start of the reaction. The offline experiments were performed with the additive OMTS present from the start but for monitoring experiments, since a dual syringe pump was used, the OMTS solution was added in-situ to the reaction mixture (TMA and water).

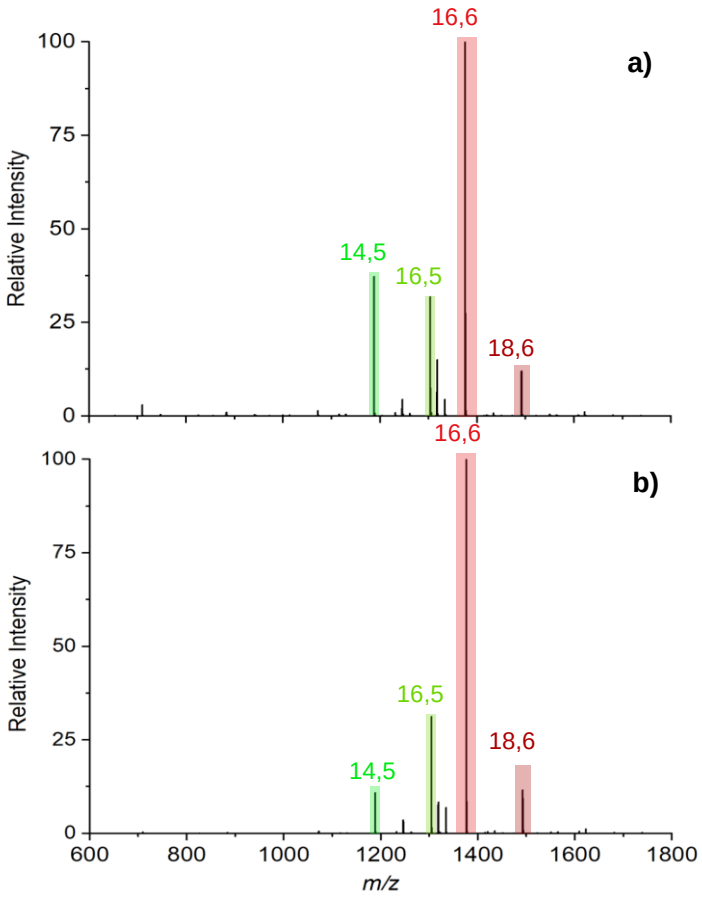

Figure 3.7 MS spectra after 20 mins of reaction monitoring of MAO synthesis in DFB when (a) additive (OMTS) is added from the start (offline) and (b) when OMTS is added through a mixing tee (on-line).

3.5 Change in anion distribution with time

As stated earlier, when experiments were monitored in DFB, the anion distribution changes rapidly, and the anion $[(MeAlO)_{16}(Me_3Al)_6Me]^-$ is observed as the most intense peak within 10 minutes of mixing TMA and water (Figure 3.8). At earlier times, i.e., around 1 min after mixing three ions with *m/z* 709, *m/z* 767 and *m/z* 825 are most intense. All these species are separated by 58 Da, which corresponds to one MeAlO unit. The ions fit in the general MAO formula and can be formulated as $[(MeAlO)_7(Me_3Al)_4Me]^-$ (*m/z* 709), $[(MeAlO)_8(Me_3Al)_4Me]^-$ (*m/z* 767), $[(MeAlO)_9(Me_3Al)_4Me]^-$ (*m/z* 825). These three ions are very short-lived, and the intensity of these species goes away after an initial spike at 1 min (vide infra). Anion distribution at different times for all seven separate experiments is shown in Appendix B.

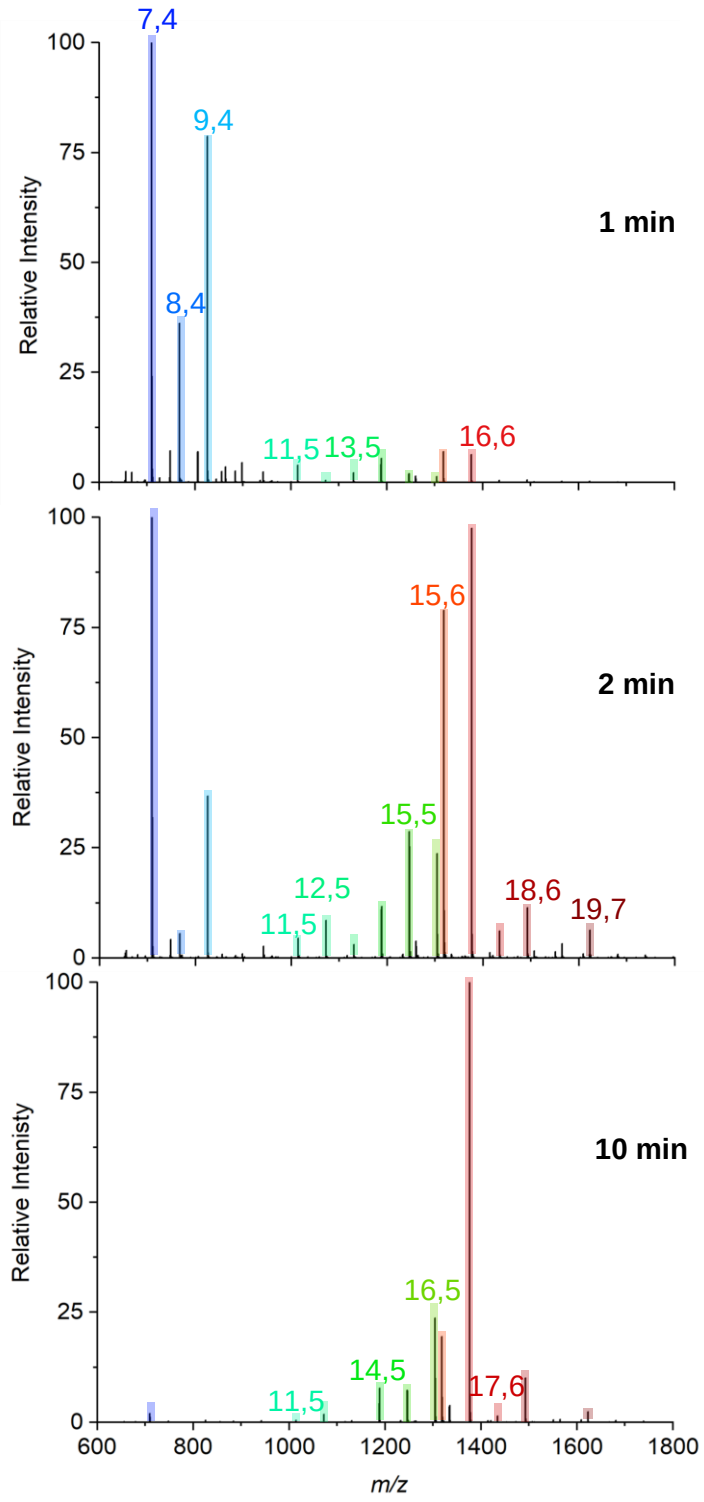

Figure 3.8 ESI-MS spectrum at different times showing the change in the anion distribution during the synthesis of MAO in wet (0.055 M H_2O) degassed DFB for one run.

The empirical formula of bulk MAO has been established by NMR[116] to fall in the range $Me_{1.3\text{-}1.5}AlO_{0.75\text{-}0.85}$. Nearly all the activator species we observe are comparatively rich in Me_3Al (all of them having higher Me and lower O content, in the range $Me_{1.5\text{-}1.8}AlO_{0.58\text{-}0.73}$).

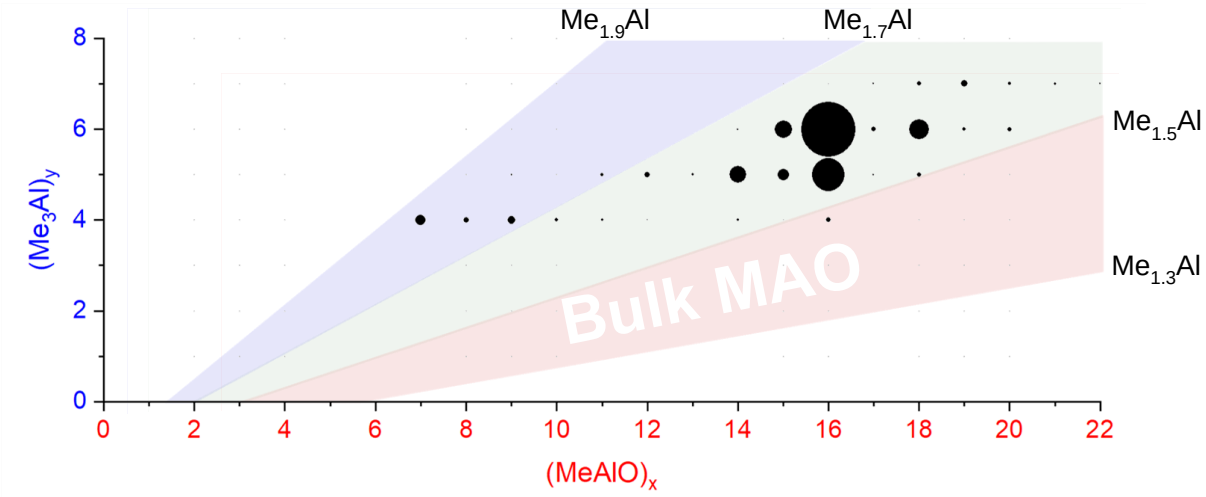

Figure 3.9 Plot of mass spectrometric intensities (proportional to circle area) from Figure 3.3 against x and y. The pink area shows Me:Al ratios between 1.3 to 1.5, the proportions reported for bulk MAO.

The mass spectrometric results must be interpreted carefully because they encapsulate two separate processes: increase in molecular weight through oligomerization, and the propensity for species to ionize via $[Me_2Al]^+$ loss. As a result, the mass spectrometric abundance of a particular alumoxane is proportional to both its concentration and its extent of ionization (complicated further somewhat by the fact that not all ions have the same response even at the same concentration due to variations in surface activity,[146] but given these ions are closely related these differences are likely to be comparatively minor). While the selectivity for ionized species complicates the analysis, it is nonetheless invaluable because it allows for molecular identification of only those species responsible for catalyst activation.

Out of a monitoring run, three collective data sets can be extracted: the total ion count, the average Me:Al ratio, and the average *m/z*. The ion intensity is high when the reacting solution first reaches the mass spectrometer, but rapidly drops away, and subsequently climbs again slowly. The average *m/z* value starts at ~800, climbs rapidly to ~1300, and very slowly climbs to approximately *m/z* 1350. The average Me:Al ratio starts at ~1.75 and drops to ~1.6, slowly decreasing to ~1.58.

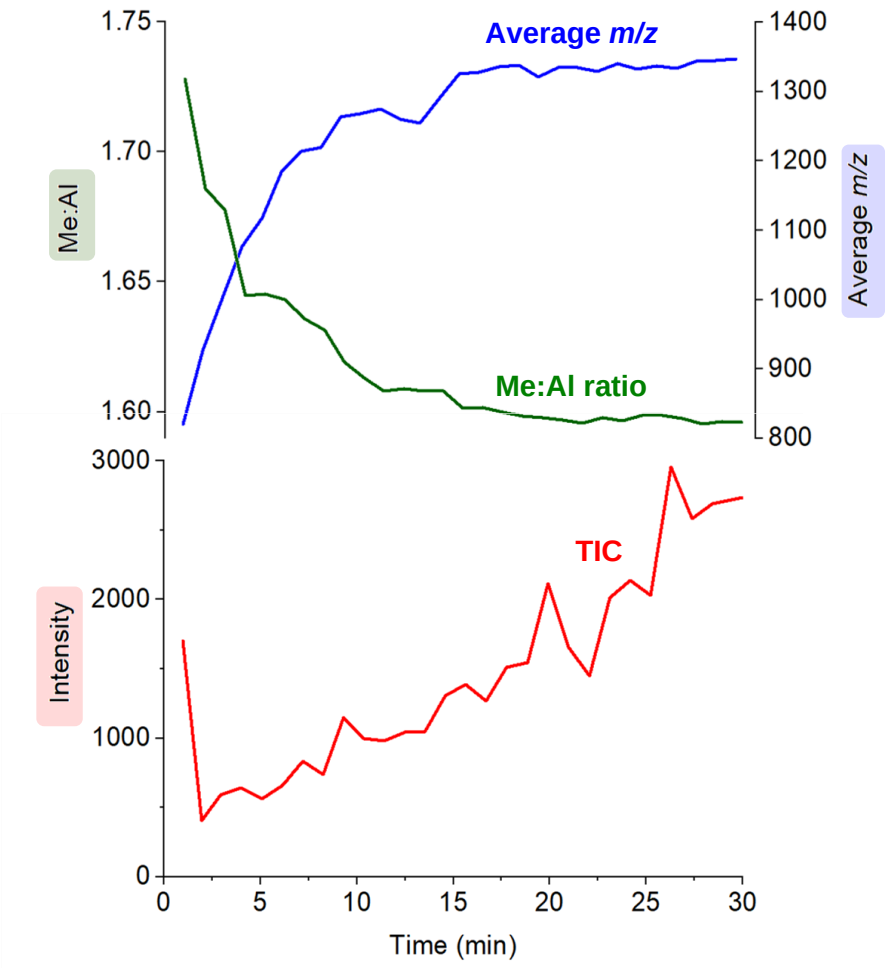

Figure 3.10 Plot of total ion current (TIC, red), Me:Al ratio (green), and average *m/z* (blue) as a function of time for the reaction of TMA with water followed by ionization using OMTS.

MAO oligomers are produced extremely rapidly (in the few seconds before the reaction solution even reaches the mass spectrometer), commensurate with the high reactivity of Me_3Al with water. The initial stages of reaction probably involve a cascade of hydrolysis, oligomerization, and isomerization reactions.[190–193] Species of *m/z* +2 (ions with -OH in place of -Me) were observed only in trace amounts, suggesting that these components of the mixture are short-lived in solution. Computationally it is possible to predict the lowest energy structures for a given *x,y* combination[119,121] but the solution is evolving extremely quickly and we expect it to be a complex mixture of kinetic products, with the linear, ring, and ladder-type structures all present and prone to reaction with each other, any proximal -OH groups on other MAO oligomers, and with Me_3Al.[194–197]

3.6 Real-time monitoring of MAO synthesis in DFB

Examining the ions contributing to the total ion current provides a complete picture of what is going on (Figure 3.11). Early on in the reaction, the initial high intensity is produced almost entirely by three ions:[**7,4**]$^-$, [**8,4**]$^-$ and [**9,4**]$^-$, suggesting that these ions are generated by the lowest mass precursors capable of acting as activators. Previous computations indicate that sheet structures dominate in this size domain, and beginning from $(MeAlO)_8(Me_3Al)_5$, i.e., the neutral precursor for [**8,4**]$^-$ via $[Me_2Al]^+$ loss, the sheets undergo the transition from Al five-coordinate to Al four-coordinate structures.[169] Slower reactions were also performed using lower concentrations of H_2O, and these three ions were still the lowest mass ions observed (Figure 3.5). The three ions have relatively high Me:Al ratios and are short-lived, declining to baseline levels within a couple of minutes. Despite their effectiveness at ionization, they are unlikely to contribute to the performance of MAO because their time in solution is so short-lived.

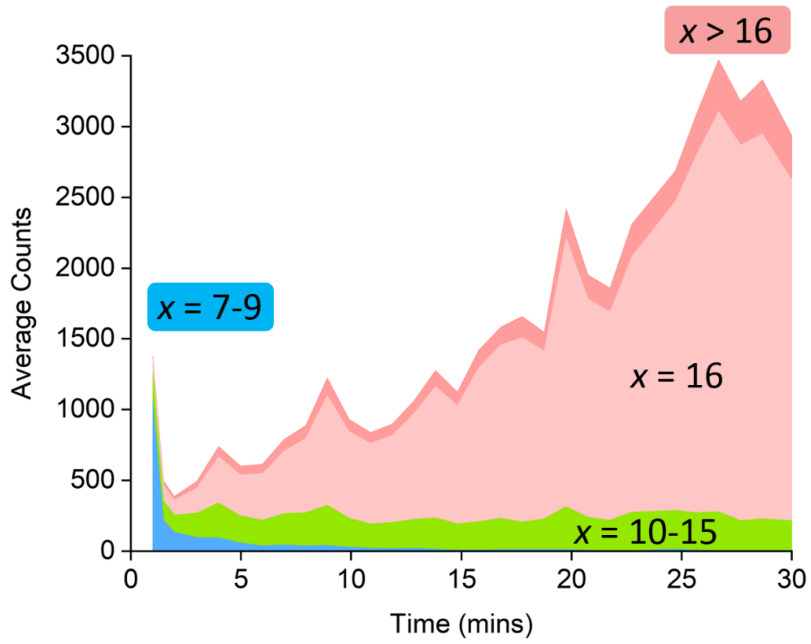

Figure 3.11 Ion intensity by x value, classified into different groups: blue (x = 7-9), green (x = 10-15), pink (x = 16) and red (x >16). x refers to the number of (MeAlO) units as the general formula for the anion is $[(MeAlO)_x(Me_3Al)_yMe]^-$.

Following the brief appearance of $[\mathbf{x,4}]^-$ (x = 7, 8, 9), the total ion current dips, and the three intense ions are not correspondingly replaced by incrementally larger oligomers. Instead, we see ions mostly of much higher molecular weight, prominent amongst which is the "magic" $[\mathbf{16,6}]^-$ ion, whose abundance steadily climbs over the 30 minutes of reaction time. Of the many potential ions of intermediate composition, we see only a limited subset: small amounts of $\mathbf{[11,4]}^-$, $[\mathbf{12,5}]^-$, $[\mathbf{14,5}]^-$ and $[\mathbf{15,5}]^-$. At long reaction times, we observe $[\mathbf{18,6}]^-$ and $[\mathbf{19,7}]^-$, ions previously observed in aged MAO solutions.[3]

The very fast production of the $[\mathbf{x,4}]^-$ (x = 7, 8, 9) species and the gradual emergence of higher mass species suggests that the oligomerization process involves multiple processes with very different rates. Given the high reactivity of water and TMA, free water will not survive for an appreciable duration. The early stages of oligomerization are probably

dominated by reactions involving methane loss (i.e., reactions between Al-OH and Al-Me) and incorporation of trimethylaluminum. The slower production of higher molecular weight species is likely the result of the aggregation of smaller methylalumoxane fragments (Scheme 3.1).[198]

The progressive reduction in Me:Al ratio as the reaction proceeds points towards aggregation processes accompanied by loss of Me_3Al. A possible explanation for the drop in ion current after the initial surge is due to aggregation processes forming open, high molecular weight, Me-rich structures that are ineffective activators until Me_3Al attrition and subsequent rearrangement renders them capable of activation (ionization) through efficiently delocalizing the resulting negative charge.

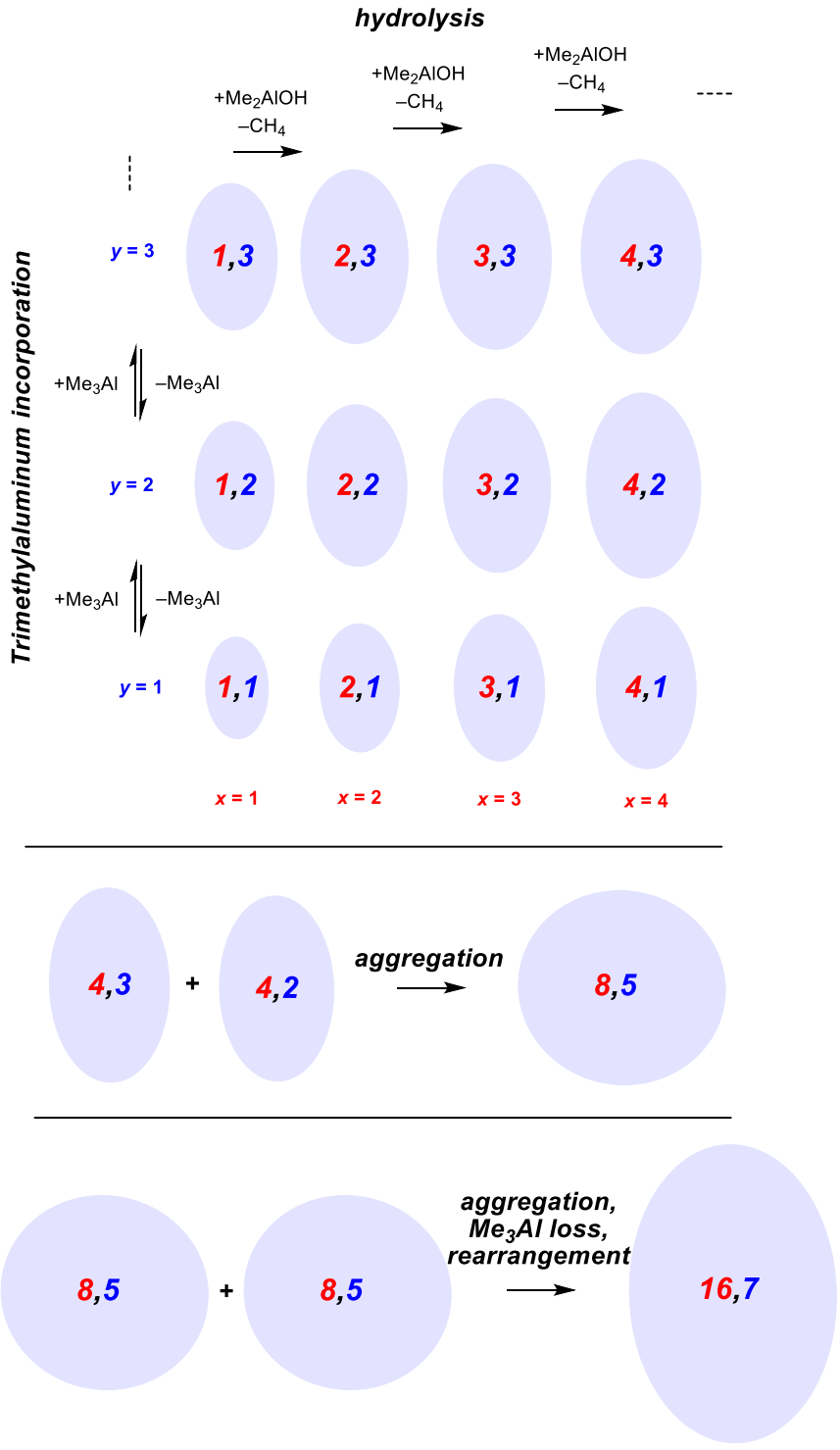

Scheme 3.1 Plausible processes contributing to oligomerization: top, fast processes, bottom, slower aggregation. Structures shown are systematic examples; many isomers exist for each x,y combination.

3.7 Computational studies

Combining the experimental results to ongoing computational studies by our collaborator Dr. Mikko Linnolahti on MAO using Gaussian 16 software[199] with M06-2X[200] DFT functional of the Minnesota series (as recommended for systems with dispersive interactions due to bridging Al-Me bonds)[166] in combination with the def-TZVP basis set,[201] allows us to propose a new structural model for the dominant [**16,6**]$^-$ anion. This new model, shown in Figure 3.12, has a hexagonal Al 4-coordinate sheet structure, and it could form via aggregation of smaller sheet structures (see above). Comparison to its previously reported cage isomers, preferably forming from the most stable neutral (**16,6**) cage located by DFT calculations[119] by Me^- abstraction,[139] rather than from the higher energy (**16,7**) cage by Me_2Al^+ cleavage[3], is eye-opening: The sheet anion is as much as 66 kJ mol^{-1} lower in total energy, 94 kJ mol^{-1} lower in gas phase Gibbs free energy (T = 298 K, p = 1 atm), and 86 kJ mol^{-1} lower in Gibbs free energy after corrections for condensed phase[119,165,202–204]. Each of the anions feature a Me_3Al end group, as illustrated by the blue circles in Figure 3.12.

The remarkable stabilization of the sheet anion in comparison to the cages arises from chelation of one of the methyl groups of Me_3Al with the adjacent Me_2Al end group, thus forming a six-membered ring in resemblance of bulk of the sheet.

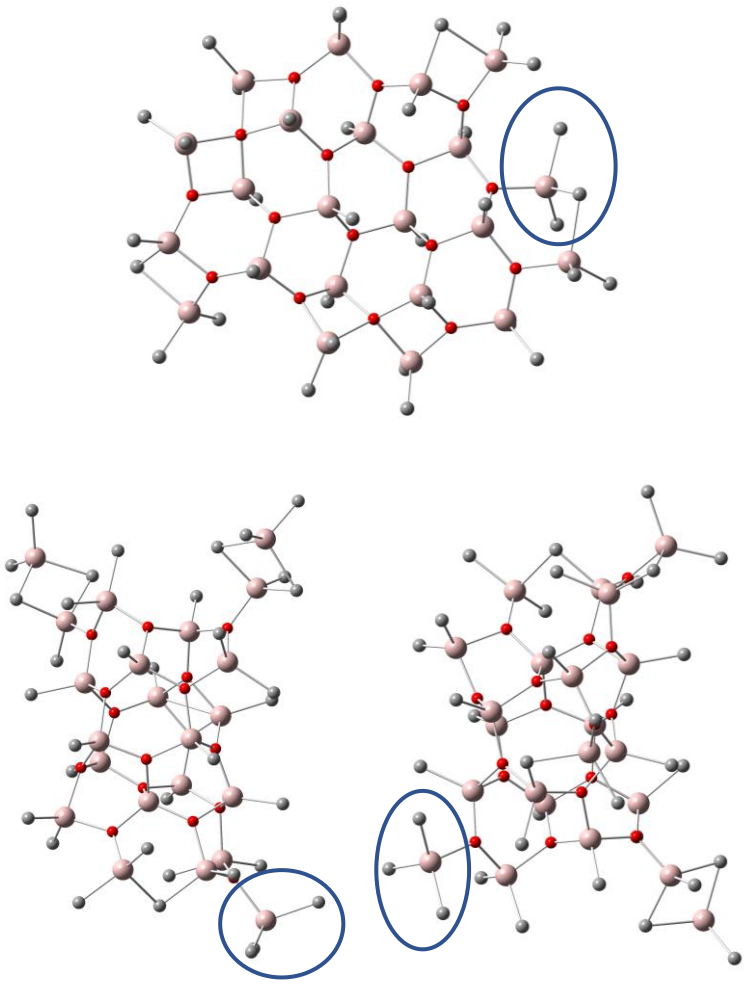

Figure 3.12 Calculated structure of $[16,6]^-$ sheet (top) with comparisons to previously reported cage anions. Bottom left: $[16,6]^-$ cage formed from (16,6) by Me^- abstraction.[139] Bottom right: $[16,6]^-$ cage formed from (16,7) by Me_2Al^+ cleavage.[3] Me_3Al end groups, characteristic for the anions, are indicated by the blue circle. Hydrogens are omitted for clarity. The energies and Gibbs free energies (T=298K, p=1atm) of the cage anions are given relative to the sheet anion. DG-c = estimate for condensed phase Gibbs free energy.

It is also worth noting that the sheet anion features 24 potentially labile edge methyl groups, which is the number of low energy substitutions observed for methyl to ethyl exchanges in our previous alkyl scrambling study.[168] With only 19 potentially labile methyl groups, the cage anions were in mismatch with those experiments, guiding us toward a more detailed investigation of alternative structural motifs.

As such, rearrangement would be required after an aggregation event, explaining the slow appearance of [**16,6**]$^-$ following the rapid disappearance of the lower molecular weight species. Given the relatively low ion intensities observed even at the half-hour mark compared to analyses of mature commercial samples, it is likely that only a fraction of the mixture has undergone all of the reactions (hydrolysis, aggregation, rearrangement) required for the formation of competent activators.

3.8 Conclusions

While special precautions are required to successfully study the growth of MAO oligomers mass spectrometrically (conditioning the instrument with a solution of TMA as a drying agent is a far from the routine procedure), a considerable pay-off is obtained in the form of the only meaningful data, thus far collected on this process. The ability to examine the dynamics of individual oligomers having undergone activation is a considerable advance in characterization capability, and the production of a solution dominated by the same ion ([**16**,**6**]$^-$) observed in commercial samples is a remarkable observation considering the differences in reaction conditions between a small syringe and an industrial-scale reactor. The time course information suggests that the formation of higher oligomers does not involve incremental additions of Al_1 species. Instead, it arises via aggregation of oligomers

of intermediate size followed by rearrangement processes that decrease the overall Me:Al ratio. The approach and results described here are a revealing first step towards understanding and optimizing the formation of those components of MAO most capable of behaving as activators.

3.9 Experimental section

All experiments were performed under an inert atmosphere using standard Schlenk and glovebox techniques. Fluorobenzene and 1,2-Difluorobenzene were obtained from Oakwood Chemicals Ltd. They were refluxed over CaH_2, distilled under N_2, and stored over activated molecular sieves 4Å inside a glovebox for a minimum of 3 days prior to use. Me_3Al (2 M in toluene) and OMTS (98%) were purchased from Sigma-Aldrich and were used as received. Cp_2ZrMe_2 was purchased from Strem Chemicals.

All mass spectra were collected on a Micromass Q-ToF micro mass spectrometer in the positive or negative ion mode using electrospray ionization. The capillary voltage was set at 3000 V with source and desolvation gas temperature at 85 °C and 185 °C, respectively. The desolvation gas flow was set to 400 L h^{-1}. All MS/MS data was obtained as product ion spectra using 5.0-grade argon as the collision gas, and a voltage range of 2–100 V. The ESI-MS spectra was recorded by injecting the solution from the glove box to the spectrometer via PTFE tubing (1/16″ o.d., 0.005″ i.d.) at a rate of 40 μL/min.

All experimental supplies, such as glass vial, syringes, gas-tight syringes, and PTFE tubings, were placed in a vacuum oven for 3 hours. Before the MS analysis, the materials were brought and stored inside a glovebox. Conditioning of the instrument was also done prior. A fresh capillary was used for each experiment to avoid unnecessary clogging issues.

The baffle and sample cone were rinsed with dilute HCl/MeOH mixture between runs to ensure that they were free of Al_2O_3 film formation (Figure 3.13).

Figure 3.13 Baffle cone (left) before and (right) after running MAO.

Before analyzing these moisture and air-sensitive samples, the PTFE tubing and attached instrument were conditioned by running a dilute solution (ca. 0.01 M) of Me_3Al. This precaution ensures the PTFE tubing, and the MS are free of trace amounts of moisture and oxygen. The probe tip was also adjusted for these experiments so that it was close (approximately 1 mm) to the sample cone.

3.9.1 Solvent water estimation

Cp_2ZrMe_2 (18.4 mg) was collected in a 10 mL glass vial with 0.5 mL of difluorobenzene and 0.2 mL of dry benzene-d_6. A ^1H proton NMR was recorded, and the amount of water in the solvent was calculated. The water concentration in the solvent DFB after enrichment with water was 0.055 M.

3.9.2 Monitoring experiments

A stainless-steel union tee was fitted with three lengths of PTFE tubing using PEEK ZDV low-pressure nuts and ferrules. The two short and equal lengths were fitted with Idex PEEK/PTFE syringe inlets using a PEEK union and ZDV nut/ferrule. The entire apparatus

was then dried in a vacuum oven before being transferred to an LC Technology Solutions LCB-120 glovebox. After flushing the entire apparatus with dry PhF via syringe, the measured, long-length PTFE tubing was connected to the QTOF Micro spectrometer. The dead time of this system was about 40 sec at a combined flow rate of 50 mL/min.

Syringe 1: 0.16 mL of 2 M Me_3Al was added to 5 mL of degassed DFB in a vial and quickly loaded into a 1 mL gas-tight syringe. *Syringe 2*: 16.8 mg of OMTS was dissolved in 5 mL of dry DFB. 0.4 mL of this solution was diluted with 10 mL DFB, degassed, and quickly loaded into a 1 mL gas-tight syringe. The two syringes were inserted into a dual syringe pump with PTFE tubing connected to the syringes. The tubing was connected to a mixing tee to combine the two solutions, and PTFE outlet tubing was attached to the mass spectrometer for analysis. The flow rates were set at 25 µL /min, and ESI-MS data were collected continuously.

Chapter 4 Reactive Metallocene Cations as Sensitive Indicators of Gas-Phase Oxygen and Water

Portions from this chapter have been previously published and reproduced with permission from "Reactive Metallocene Cations as Sensitive Indicators of Gas-Phase Oxygen and water" A Joshi, S Donnecke, O Granot, D Shin, S Collins, I Paci and J. S McIndoe, *Dalton Transactions*, 2020,49, 7028-7036. Sofia Donnecke and Prof. Irina Paci did computational studies included in this chapter. Supplementary spectra from this chapter are presented in Appendix C.

4.1 Introduction

Electrospray ionization mass spectrometry (ESI-MS) is a useful tool to study reactions involving transition metal complexes.[43,205–211] As this technique is very sensitive and operates best at low (charged) analyte concentrations (< μM), the air- and moisture sensitivity of many transition metal complexes requires rigorous precautions to remove air and moisture dissolved in solvents or other reagents to obtain meaningful results.[2] An inert atmosphere glove-box, when interfaced to the mass spectrometer, using flexible PEEK or PTFE tubing and an airtight seal, protects analyte solutions from atmospheric contamination during transit to the source compartment of the mass spectrometer.[88]

During the electrospray ionization process, charged droplets form and rapidly evaporate under the influence of an inert desolvation gas (nitrogen is typically used) to produce gas-phase ions within a source compartment operated typically at atmospheric pressure and elevated temperature. The electrospray process can involve chemical reactions prior to droplet evaporation,[212,213] even in the absence of charging effects.[214] The ions are deflected

towards the mass spectrometer and accelerated using a modest voltage bias (cone voltage) through the low vacuum (ca. 0.01 – 0.13 kPa) region of the mass spectrometer.[15]

During this transit, the ions encounter desolvation gas and other volatile materials such as solvent or contaminants like water and oxygen. The desolvation gas is rarely completely pure: 99.999% (5.0) nitrogen still contains as much as three ppm oxygen and five ppm water, and those contaminants are continually introduced into the mass spectrometer. If the source compartment and source are significantly contaminated, undesired ion-molecule reactions may occur during transit to the high vacuum regions of the instrument. Ion-molecule reactions can also occur in the collision cell of a tandem mass spectrometer, as this relatively high-pressure region can accumulate neutral molecules (especially water) during MS/MS experiments.

This chapter focusses on whether the reactive ions found in transition metal chemistry might be used to advantage to gauge experimental conditions within the mass spectrometer, and whether changes in desolvation or collision gas purity had demonstrable effects on the mass spectra of these species.

In previous years, the McIndoe group has shown evidence of impurity (mainly oxygen and water) problems during ESI-MS analysis. Examples in the case of oxygen include phosphine oxidation during Rh(I)- or Pd(0)-mediated catalysis.[91,215] In the case of Pd(0) triphenylphosphine complexes,[91] it was established that oxygen dissolved in solution, or deliberately introduced during pressurized sample infusion,[87] was responsible for the oxidation of excess phosphine, mediated by $L_2Pd(O_2)$ complexes.[216–219]

The McIndoe group has also mentioned the sensitivity of aluminoxane anions[1,186,220] and zirconocene methyl cations[2,94] towards both oxygen and water, obviously in solution, and

in the gas phase with reactive ions generated through in-source CID.[2] Earlier gas-phase EI MS[221–224] and recent solution ESI MS[225] work had also revealed the high reactivity of zirconocene cations towards *inter alia* water. The group has also studied the reaction of a reduced titanocene complex, which is used as a colored indicator for atmospheric oxygen,[226] with O_2.[227]

This chemistry might form the basis for sensitively detecting impurity problems associated with the operation of the mass spectrometer, as opposed to solution contamination, where rigorous drying and deoxygenation protocols usually suffice. In this chapter, the focus is on the use of reactive titanium and zirconium complexes as indicators for both gas-phase oxygen, and in the latter case, also water.

Nitrogen generators are becoming increasingly popular as a gas source for mass spectrometric applications.[228] Nitrogen generators supply nitrogen on demand and save a significant amount of money in labs that require continuous N_2 supply. Those advantages aside, an important query remains as to whether this source of N_2 is of high enough purity for air-sensitive chemistry.[229] As we had recently installed a factory-refurbished N_2 generator, supplied by Peak Scientific, we decided to investigate this issue using the transition metal complexes discussed above.

4.2 Phosphine oxidation

Exploratory studies using $Pd(PPh_3)_4$ and the charge tag $[PPN][Ph_2P(C_6H_4SO_3)]$ salt (**1**)[91] revealed that phosphine oxidation was not observed using either 99.99% cylinder or generator N_2 as desolvation gas. However, differences in the relative amounts of $[Pd(L)(\mathbf{1})]^-$ and $[(\mu\text{-}O_2)Pd(L)(\mathbf{1})]^-$ were seen in the ESI MS spectra (Figure 4.1). The very

low intensity of these ions (at mM concentrations of salt **1** in methanol) argued against the use of this system for analytical purposes.

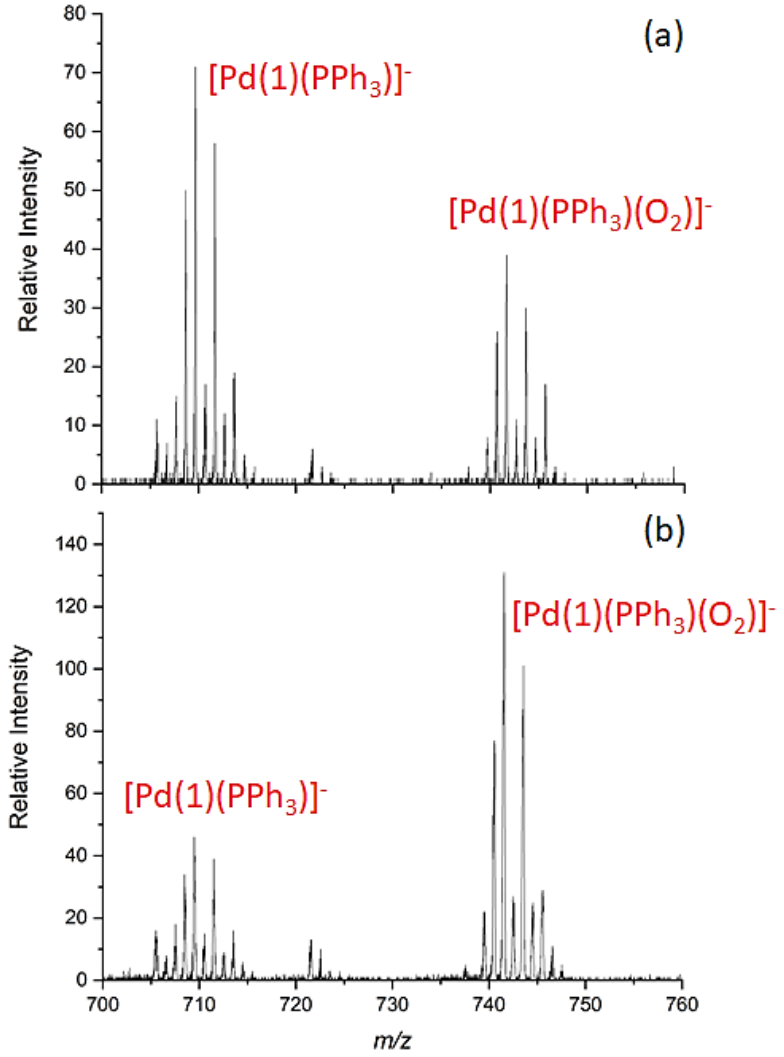

Figure 4.1 ESI MS of $[Pd(0)(1)(PPh_3)]^-$ complexes in MeOH solution [Pd] = 0.4 mM with desolvation gas supply from (a) 4.0 N_2 cylinder or (b) N_2 generator.

From this and prior work[91] it was clear that any solution-phase reaction would have to be effectively diffusion-controlled and irreversible for the reaction to be of use to monitor conditions within the mass spectrometer. The rest of the chapter is thus focused on the use

of reduced titanocene(III) complexes and cationic zirconocene(IV) alkyls as indicators for oxygen and water.

4.3 Oxidation of reduced titanium complex $[Cp_2Ti(NCMe)_2]^+[ZnCl_3]^-$

The ESI-MS of $[Cp_2Ti(NCMe)_2]^+[ZnCl_3]^-$ prepared from Cp_2TiCl_2 with Zn in acetonitrile under "normal" (using 99.999% purity N_2 from a cylinder as a source of the cone and desolvation gas) conditions results in a spectrum that is dominated by $[Cp_2Ti(NCMe)_n]^+$ (*n* = 1 or 2, *m/z* 219 and 260) ions (Figure 4.2 a).

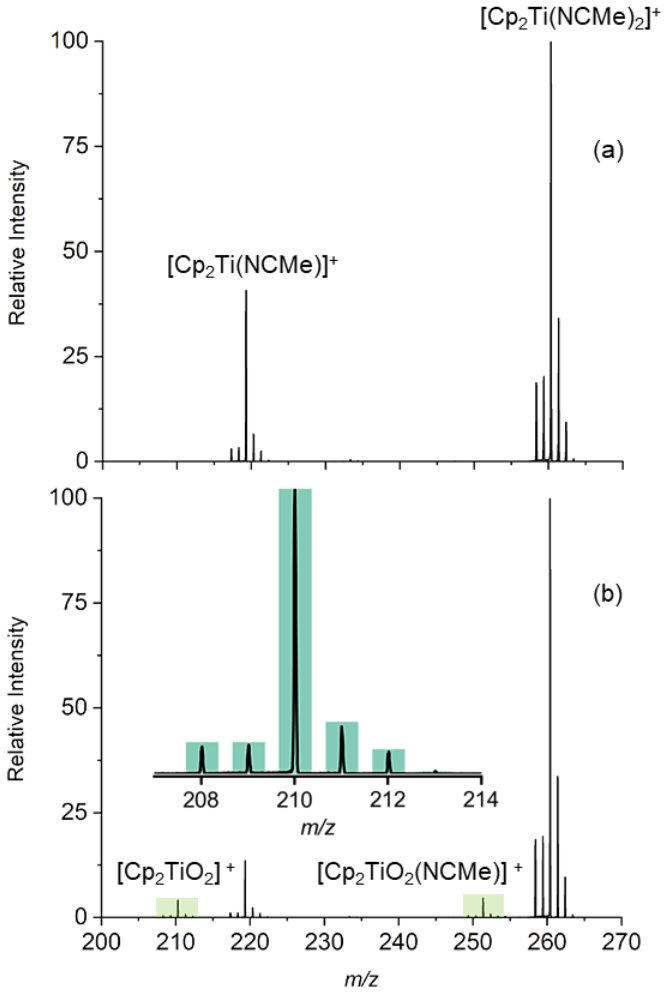

Figure 4.2 The $[Cp_2Ti(NCMe)_2]^+$ system with N_2 supply from (a) 5.0 purity N_2 cylinder and (b) Generator. Inset in 4.2 b shows the expected (highlighted) and experimental isotopic pattern of the *m/z* 210 species**.**

When the source of N_2 was changed to generator N_2, we saw two additional low abundance species (Figure 4.2 b), readily assigned to $[Cp_2TiO_2]^+$ (*m/z* 210) and $[Cp_2Ti(O_2)(NCMe)]^+$ (*m/z* 251) based on isotope pattern, *m/z* ratio and MS/MS behavior.

The MS/MS spectrum of $[Cp_2Ti(O_2)(NCMe)]^+$ shows acetonitrile ligand loss to form $[Cp_2TiO_2]^+$ (Figure 4.3 a). In the same vein, the MS/MS of $[Cp_2TiO_2]^+$ shows the loss of O_2 to form $[Cp_2Ti]^+$ (Figure 4.3 b).

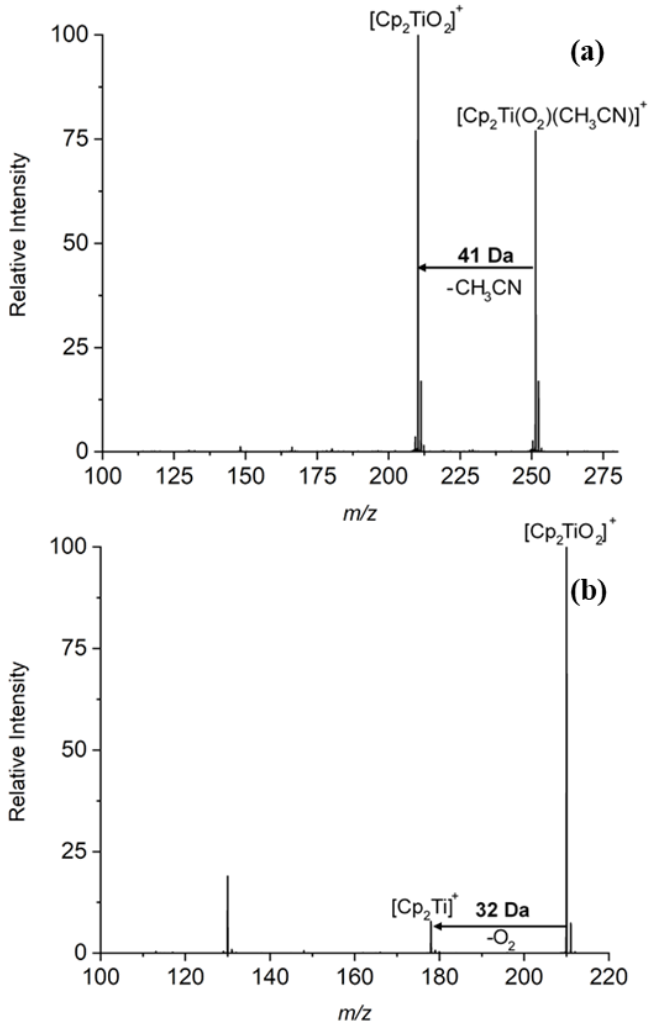

Figure 4.3 (a) MS-MS of *m/z* 251 species showing loss of acetonitrile ligand and (b) MS-MS of $[Cp_2TiO_2]^+$ (*m/z* 210) species showing loss of oxygen A prominent fragment ion with *m/z* 130 could correspond to loss of cyclopentadienone from the parent ion (vide infra)

The $[Cp_2TiO_2]^+$ species is proposed to be formed *via* the substitution of neutral acetonitrile ligands with O_2. This process may or may not be accompanied by oxidation of the metal center, i.e. $[Cp_2TiO_2]^+$ can be formulated either as $[Cp_2Ti(III)(\eta^2\text{-}O_2)]^+$ or as $[Cp_2Ti(IV)(\eta^2\text{-}O_2^{\bullet-})]^+$ wherein the latter ion, oxygen has been reduced to the superoxide radical anion.

To further support the claim that trace amounts of O_2 present in the generator N_2 reacts with the Ti species, the purity of N_2 produced was changed. Since the nitrogen purity of these generators is flow rate dependent[230,231] we changed the total rate of N_2 produced at the generator while maintaining constant cone and desolvation gas flow rates at the instrument (see Experimental Section for details). The ratio of the oxidized to un-oxidized species was plotted against the total flow rate of N_2 gas (Figure 4.4). It was observed that this ratio increases as the flow rate increases (as the purity of N_2 decreases).

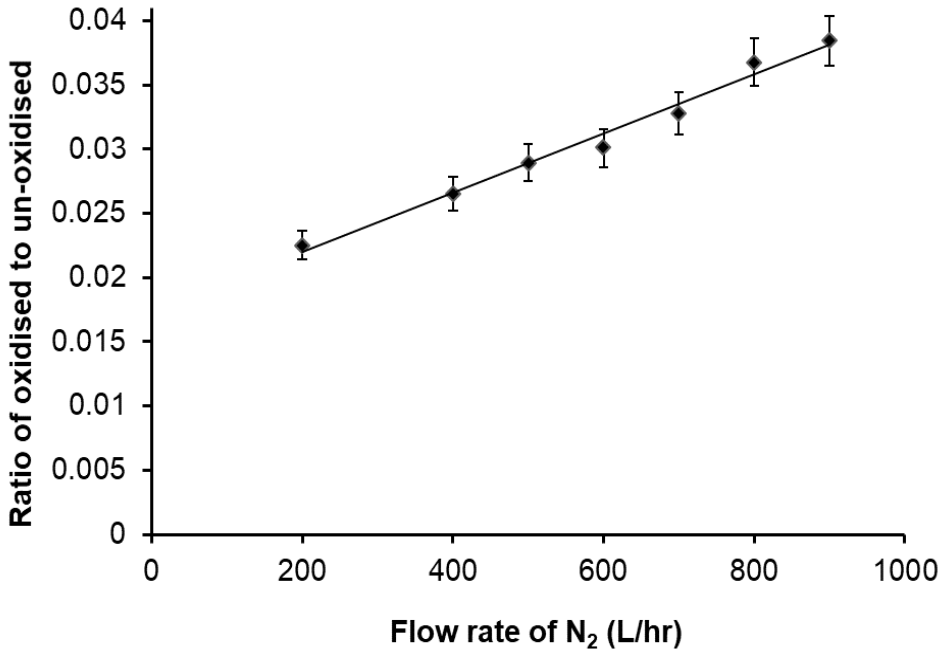

Figure 4.4 The ratio of oxidized species to unoxidized species plotted against flow rate with the error bars showing 95 percent confidence level in the measurements.

4.4 Computational studies on the oxidation of titanium complex

To better understand the observed oxidation reaction, we studied it computationally. Mass spectrometric results (Figure 4.2) suggest that $[Cp_2Ti(NCMe)]^+$ is the primary source of the oxygen-containing complex $[Cp_2TiO_2]^+$, given its reduced presence in Figure 4.2 b and its status as the only unsaturated species present. *Ab initio* molecular dynamics (AIMD) simulations[232] at 300 K of $[Cp_2Ti(NCMe)]^+ + O_2$ and $[Cp_2Ti(NCMe)_2]^+ + O_2$ support this hypothesis, as the titanium in the $[Cp_2Ti(NCMe)_2]^+$ complex is inert to O_2 while the Ti of $[Cp_2Ti(NCMe)]^+$ readily binds to O_2 .

As the concerted pathway from $[Cp_2Ti(NCMe)_2]^+$ to $[Cp_2TiO_2(NCMe)]^+$ or $[Cp_2TiO_2]^+$ is not likely, energy diagrams for two possible mechanisms are calculated, both involving the initial dissociation of $[Cp_2Ti(NCMe)_2]^+$ to $[Cp_2Ti(NCMe)]^+$: a concerted mechanism wherein O_2 replaces CH_3CN as a ligand, and a stepwise mechanism where the O_2 binds in a monodentate fashion before the loss of the second CH_3CN and O_2 reorientation to η^2-O_2 (Figure 4.5).

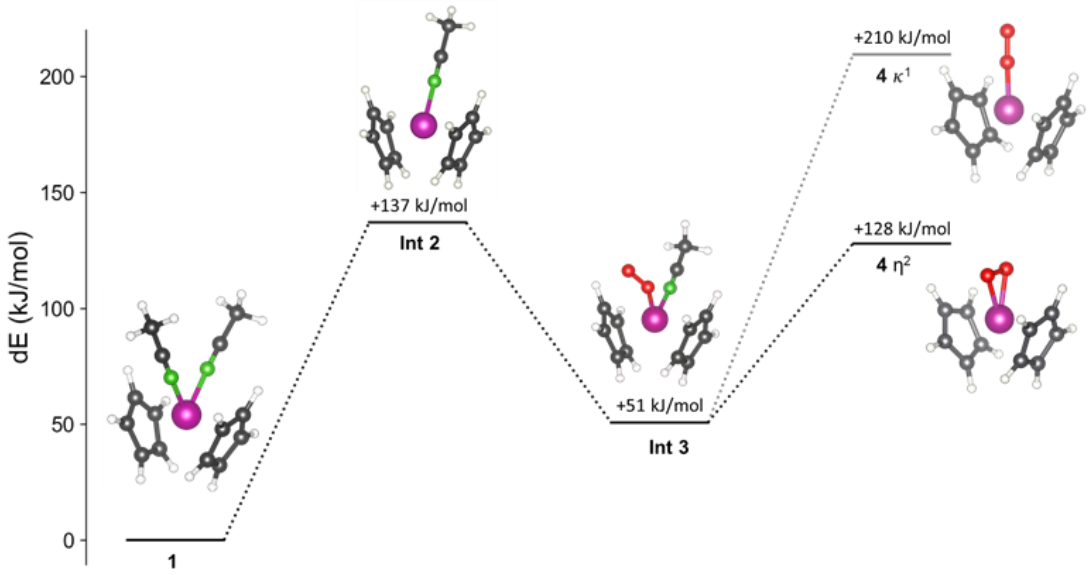

Figure 4.5 The $[Cp_2Ti(NCMe)_2]^+ + O_2$ reaction pathway calculated with SIESTA (UPBE-D2). In the stepwise mechanism for Ti ligand exchange, the reaction pathway can be modelled as a series of bond association/dissociation steps **1** → **2** → **3** → **4**. Complex **1** is $[Cp_2Ti(NCMe)_2]^+$, Complex **2** is $[Cp_2Ti(NCMe)]^+$, Complex **3** is $[Cp_2Ti(NCMe)(O_2)]^+$ and Complex **4** is $[Cp_2TiO_2]^+$ where O_2 can bind in a monodentate or a bidentate fashion. Calculations were done by Sofia Donnecke.

Loss of the first acetonitrile ligand in the first step destabilizes the complex, creating the opportunity for attack from the O_2 molecules present in the gas phase. Species **2**, **3**, and **4** were all observed in the mass spectrometry experiments. The most stable structure of **4** had O_2 in an η^2 configuration, replacing both monodentate CH_3CN ligands (see Figure 4.5). The **2** → **3** → **4** pathway is a sequence of bond dissociation and association steps, thus barrier-less, and the lowest energy pathway in the computational model. However, higher-energy species are accessible in the ESI-MS setup, making a concerted mechanism for the **2** → **4** pathway viable.

4.5 Oxidation and hydrolysis of olefin polymerization pre-catalyst $[Cp_2Zr(\mu\text{-}Me)_2AlMe_2]^+ [B(C_6F_5)_4]^-$

The final reactive system that was studied involved the ion $[Cp_2Zr(\mu\text{-}Me)_2AlMe_2]^+$ (*m/z* 307), which can be conveniently generated in situ from Cp_2ZrMe_2, excess $AlMe_3$, and $[Ph_3C][B(C_6F_5)_4]$ in fluorobenzene solution.[233,234] As discussed elsewhere, the appearance of the mass spectrum of this ion is sensitive to cone voltage (in-source fragmentation via collision-induced dissociation), and loss of 72 Da (Me_3Al) in the gas phase via CID, either in source or the collision cell is facile.[2,94] The resulting (gas-phase) 14 electron-ion $[Cp_2ZrMe]^+$ (*m/z* 235) is known to be exceptionally reactive towards a variety of gaseous species[221–224], but its reaction with O_2 or water has not been systematically studied.

When these studies were initiated, the mass spectra obtained were unexpectedly complicated. Instead of a spectrum consisting of just $[Cp_2Zr(\mu\text{-}Me)_2AlMe_2]^+$ and $[Cp_2ZrMe]^+$,[9] only trace amounts of the latter ion were present, while new ions with *m/z* 237 and 255 were detected using 5.0 N_2 (Figure 4.6 a). A spectrum at the same cone voltage (8 V) using generator N_2 revealed additional ions at *m/z* 252 and 270 (Figure 4.6 b).

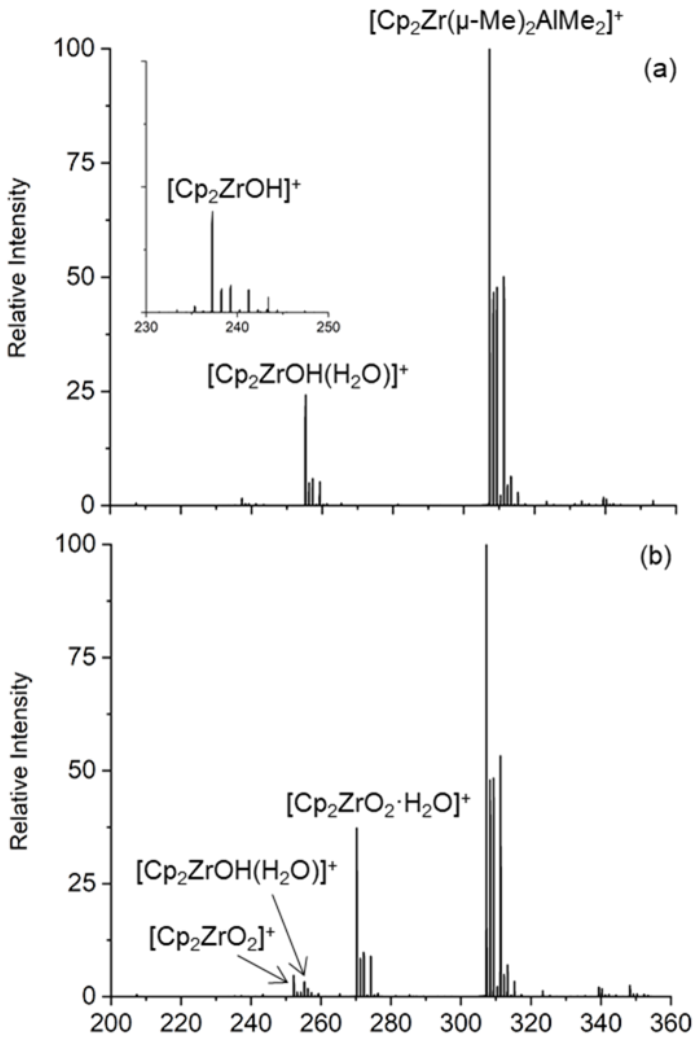

Figure 4.6 Positive ion mass spectrum of $[Cp_2ZrMe_2AlMe_2][B(C_6F_5)_4]$ (0.25 mM in PhF, cone voltage 8 V) generated using a) 99.999% N_2 from a cylinder b) N_2 from the generator. Inset in Figure 4.6 a show that the ion is actually $[Cp_2ZrOH]^+$ instead of $[Cp_2ZrMe]^+$

In earlier work, Trefz *et al.* invoked the hydrolysis of $[Cp_2ZrMe]^+$ to account for the enhanced intensity of the M+2 peak at *m/z* 237, corresponding to the formation of $[Cp_2ZrOH]^+$.[9] Since *m/z* 235 is generated via in source CID of $[Cp_2Zr(\mu\text{-}Me)_2AlMe_2]^+$, the results depicted in Figure 4.6 suggest the source or source compartment was contaminated with water vapor, rather than either N_2 gas supply.

After venting the spectrometer (which results in thorough flushing of the interior with N_2), re-establishing vacuum, and conditioning the MCP detector, subsequent spectra obtained using 5.0 N_2 showed no signs of oxidation or hydrolysis (Figure 4.7 a), indicating that the source of water was the instrument itself.

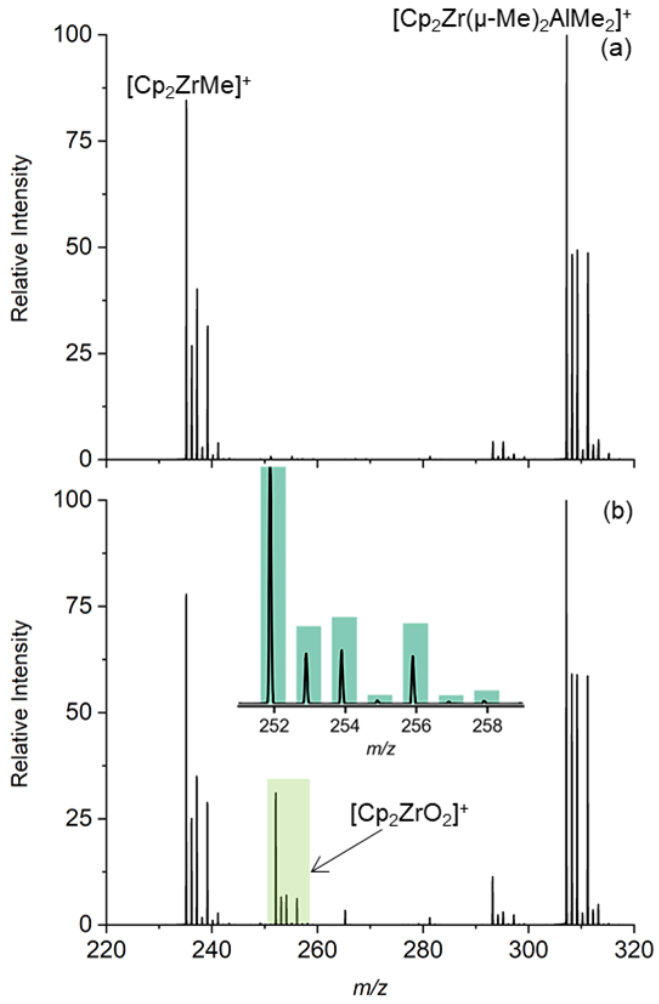

Figure 4.7 The ($[Cp_2Zr(\mu\text{-}Me)_2AlMe_2]^+$) system with N_2 supply from (a) 5.0 purity N_2 cylinder and (b) generator N_2. Inset in 4.7 b shows the expected (bars) and experimental (line) isotope pattern of $[Cp_2ZrO_2]^+$.

The remaining ions in Figure 4.6 b have *m/z* 252 and 270. Since the difference in mass between these two ions is also 18 Da, it is reasonable to assign the latter as the aqua complex of the former. In agreement with this hypothesis, *m/z* 270 was not observed

following venting and flushing of the instrument with N_2 on subsequent start-up (Figure 4.7 b). It was, however, quite prominent while conducting MS/MS experiments on *m/z* 252 (*vide infra*).

The ion with *m/z* 252 persisted as long as generator gas was supplied to the instrument (Figure 4.7 b; the exact amount of product was dependent on the age of the generator, with less oxidation observed when using a brand new nitrogen generator, see Appendix C. This ion was assigned to $[Cp_2ZrO_2]^+$ by analogy to the results obtained using the reduced titanocene complex with oxygen (*vide supra*). The ion has the expected isotope pattern (Figure 4.7 b), correct *m/z* ratio, and a similar MS/MS product ion spectrum compared with $[Cp_2TiO_2]^+$ (see Appendix C).

However, $[Cp_2ZrO_2]^+$ is not the expected product of oxidation of $[Cp_2Zr(\mu\text{-}Me)_2AlMe_2]^+$ nor $[Cp_2ZrMe]^+$ in solution; rather, Zr alkoxides are invariably produced, at least with neutral zirconocene dialkyls.[235] The stereochemistry of this oxidation process proceeded with 50% racemization and 50% retention of stereochemistry. The authors invoked the homolytic cleavage of a Zr-R bond as the first step in this process to account for the racemization (Equation 4.1). The second step involved the recombination of these radicals to form a metal peroxide intermediate. In the gas phase, such recombination is much less plausible, and so one might expect to form $[Cp_2ZrO_2]^+$ via the initial reaction of a cationic alkyl with O_2.

$$Cp_2ZrR_2 + O_2 \longrightarrow Cp_2Zr(R)O_2\cdot \quad + \quad R\cdot$$

Equation 4.1 Oxidation of Cp_2ZrR_2.

The hydrolytic sensitivity of $[Cp_2ZrMe]^+$ has been mentioned in several previous papers.[222,225] As shown above, when the instrument is contaminated with both water and oxygen, ions formed by both processes are observed. Normally such ions are characterized by MS^n studies, and our instrument is capable of both MS^2 and *pseudo*-MS^3 experiments (the latter requires in-source fragmentation of the precursor ion). Attempts to characterize $[Cp_2ZrO_2]^+$ via this process resulted in both the expected ion and one 18 Da (water) higher in mass with *m/z* 270 formed after turning on the collision gas (Ar at 103 kPa with collision voltage = 2 V). The effect is completely reversible, and the ratio of the $[Cp_2ZrO_2]^+$ and the $[Cp_2ZrO_2(H_2O)]^+$ ions was largely invariant with time.

Collins *et al.*, in earlier work, used helium as the collision gas to minimize this problem.[94] Still, this solution is limited in scope as any collisions are necessarily reduced in energy, which is a problem for ions resistant to fragmentation. The reduction of the Ar pressure from 103 to 20 kPa largely eliminates hydrolysis in the collision cell (compare Figure 4.8 a vs. 4.8 b and 4.8 c). Low argon pressures were used in all subsequent work for ions requiring MS/MS characterization. Evidently, the source of the water in these MS/MS experiments is either the 5.0 Ar gas in use ($\leq$ 3 ppm H_2O) or adsorbed water in the collision cell, which is dislodged from the inner surfaces during analysis. Since the He gas used earlier and the Ar gas used here were of similar purity, we suspect that it is adsorbed water in the collision cell responsible for these artifacts.

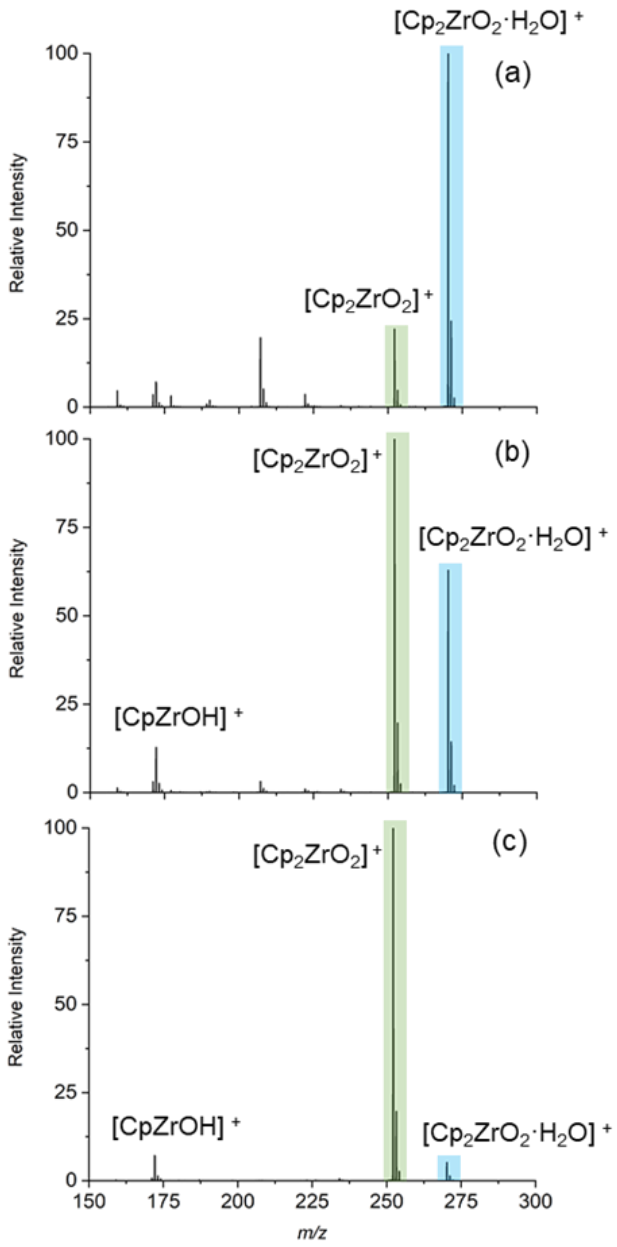

Figure 4.8 MS/MS of $[Cp_2ZrO_2]^+$ (*m/z* 252, green) species with argon collision gas at (a) high (b) medium and (c) low collision cell pressures to form $[Cp_2ZrO_2(H_2O)]^+$ (*m/z* 270, blue)

As $[Cp_2ZrMe]^+$ forms from $[Cp_2Zr(\mu\text{-}Me)_2AlMe_2]^+$ via CID and the oxidized product with *m/z* 252 is formed by way of a reaction of O_2 with $[Cp_2ZrMe]^+$, spectra were recorded at two different cone voltages (Figure 4.9).

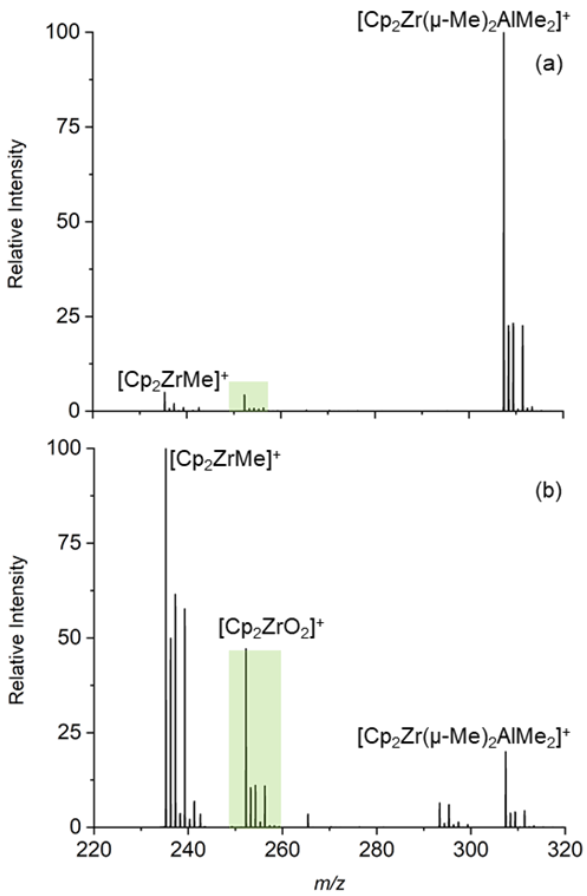

Figure 4.9 The $[Cp_2Zr(\mu\text{-}Me)_2AlMe_2]^+$ mass spectrum with N_2 supply from a generator at (a) 12 V and (b) 24 V cone voltage.

When the cone voltage is at 12 V the predominant species is $[Cp_2Zr(\mu\text{-}Me)_2AlMe_2]^+$ but when the cone voltage is increased to 24 V both $[Cp_2ZrMe]^+$ and $[Cp_2ZrO_2]^+$ increase in intensity. This increased reactivity is in response to high cone voltage causing Me_3Al loss, generating a vacant coordination site, and increasing the internal energy of the $[Cp_2ZrMe]^+$ ion.

In a separate experiment, cone voltage was ramped up to 100 V, and traces from individual ions were plotted vs. cone voltage (Figure 4.10). As the cone voltage increases, the $[Cp_2Zr(\mu\text{-}Me)_2AlMe_2]^+$ ion decreases in intensity and both $[Cp_2ZrMe]^+$ and $[Cp_2ZrO_2]^+$

ions form. The formation of $[Cp_2ZrO_2]^+$ largely parallels the behavior of $[Cp_2ZrMe]^+$, suggesting that the former is generated from the latter.

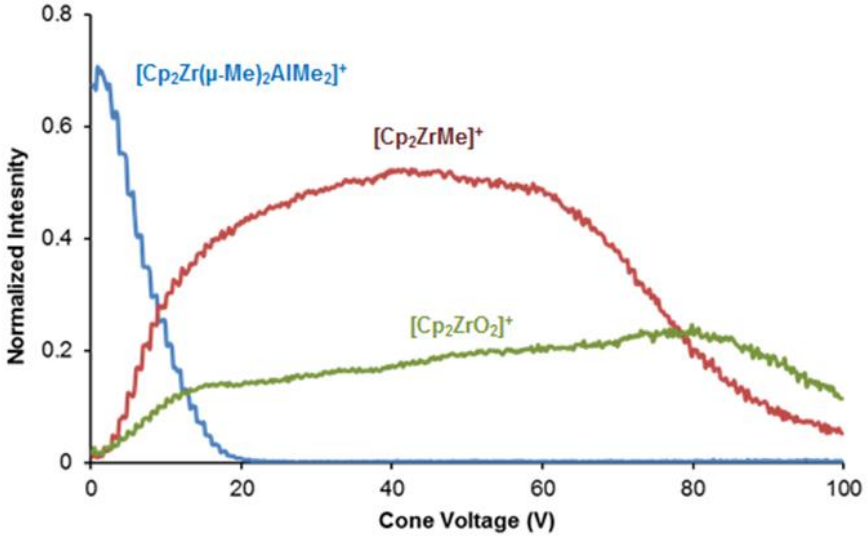

Figure 4.10 Normalized ion intensities for $[Cp_2Zr(\mu\text{-}Me)_2AlMe_2]^+$ (blue), $[Cp_2ZrMe]^+$ (red) and $[Cp_2ZrO_2]^+$ (green) using generator N_2 vs. cone voltage. The latter was systematically ramped from 0-100V using an AutoHotKey script.

The gas-phase reactivity of $[Cp_2ZrMe]^+$ is limited to the work published by Richardson *et al.*[221–223] and Chen.[224] Other than comments about the hydrolytic sensitivity in the experimental sections, there is no published work discussing the reaction with O_2. We decided to model the reaction of the formation of $[Cp_2ZrO_2]^+$ from $[Cp_2ZrMe]^+$ in the gas phase computationally.

4.6 Computational studies on the formation of $[Cp_2ZrO_2]^+$

Conversion from $[Cp_2ZrMe]^+$ to the oxidized species *via* a $[Cp_2Zr]^+$ intermediate is energetically prohibitive, so a concerted mechanism where O_2 replaces the methyl group was considered (Figure 4.11).

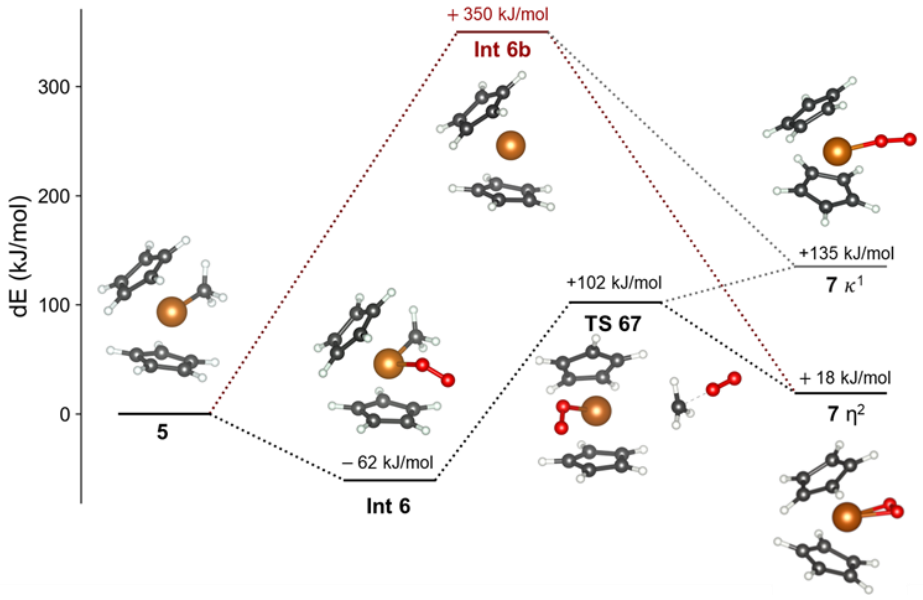

Figure 4.11 The $[Cp_2ZrMe]^+ + O_2$ reaction pathways calculated with SIESTA (UPBE-D2). The Zr ligand exchange is assisted by stabilizing the Me leaving group (TS 67). Calculations were done by Sofia Donnecke.

However, reaction coordinate analysis through linear transit scans at 0 K identified a stable intermediate where Zr is bound to both O_2 and Me (**Int 6** in Figure 4.11), which was not observed experimentally. The gas-phase calculations of the possible $[Cp_2ZrMe]^+ + O_2 \rightarrow [Cp_2ZrO_2]^+ + Me\cdot$ reaction via a concerted mechanism found that the methyl radical was too reactive to present as an independent leaving group. Instead, the metal center accommodated both ligands as $[Cp_2ZrMeO_2]^+$, an intermediate species not observed in the mass spectra. Instead, $[Cp_2ZrO_2]^+$ is observed directly in the experiment, suggesting that

the methyl group has to leave through a stabilized pathway, such as by attaching to a scavenging group. Gas-phase scavenging reactions have been observed in MS previously.[236,237] Ab initio molecular dynamics calculations of the reactions between $[Cp_2ZrMeO_2]^+$ and possible scavengers were carried out at the PBE-vdwTS/DZP level in SIESTA, at a temperature of 300 K, for 2 ps. Fluorobenzene (solvent), N_2, and O_2 (present in the desolvation gas) being the only species present in abundance during the transfer from the solution phase to the high vacuum of the mass spectrometer, were all considered as scavenger candidates. Fluorobenzene and N_2 are inert to the $[Cp_2Zr(O_2)Me]^+$ complex, but O_2 facilitates the removal of the methyl radical and formation of $[Cp_2ZrO_2]^+$.

4.7 Conclusions

For most applications in electrospray ionization mass spectrometry, nitrogen generators eliminate enough oxygen that spectra are indistinguishable from high purity sources of nitrogen. Only the most reactive ions generate byproduct ions attributable to gas-phase oxygenation. In the case of an indicator developed to detect O_2[226,227] the extent of oxidation is <4 % at the highest flow rate examined (see Figure 4.4). On the other hand, extremely reactive ions such as the 14 e $[Cp_2ZrMe]^+$ complex are much more reactive towards oxygen and water; using such ions as probes, the source of contamination within the spectrometer can be readily discovered and corrected for as in the present work. Computational work provided insight into how the observed oxidation chemistry proceeded in the absence of species intermediate between the species injected and observed, which in the case of the zirconocene species required the involvement of another oxygen molecule to mediate the removal of the methyl group. Calculations pointed to both the oxidized titanocene and zirconocene species having dioxygen coordinated in a side-on binding mode.

4.8 Experimental Section

All experiments were performed under an inert atmosphere using standard Schlenk and glovebox techniques. Acetonitrile and methanol (reagent grade, Fisher Chemical) were dried over CaH_2 and distilled before use. Fluorobenzene (Oakwood) was refluxed over CaH_2, distilled under N_2, and dried over molecular sieves inside a glovebox for at least three days prior to use. Me_3Al (2 M in toluene) was purchased from Sigma-Aldrich and used as received. Cp_2TiCl_2 (Sigma-Aldrich) and zinc dust (325 mesh, Anachemia) were used without further purification. Cp_2ZrMe_2 was purchased from Strem Chemicals and was used as received. $[Ph_3C][B(C_6F_5)_4]$ was donated by Nova Chemicals Ltd. and recrystallized before use. $[Ph_3PNPPh_3][PPh_2(m\text{-}C_6H_4SO_3)]$ was prepared using literature procedures.[22,238] Polypropylene syringe filters (0.45 μm, Whatman) were dried before use in a vacuum oven.

All mass spectra were collected on a Micromass Q-ToF Micro mass spectrometer in negative mode (for phosphines) and positive mode (for titanocene and zirconium), using electrospray ionization. The capillary voltage was set at 3000 V with source and desolvation gas temperature at 85 °C and 185 °C, respectively, with the desolvation gas flow at 400 L h^{-1}. MS/MS data were obtained as product ion spectra using 5.0-grade argon as the collision gas and a voltage range of 2–100 V.

Nitrogen for desolvation and cone gas was supplied from cylinders (4.0 and 5.0 grades were purchased from Praxair) or using a refurbished Genius 1053 nitrogen generator, purchased from Peak Scientific. The cylinder and the generator were connected to three different mass spectrometers via a common gas manifold with manual switching capability between the two sources using two ball valves. In experiments featuring variable N_2 flow

rates, constant desolvation and cone gas settings were established at the Q-ToF Micro instrument, while flow settings at another instrument were adjusted to increase total N_2 flow from the generator. The use of a brand-new Genius 1053 generator resulted in even lower levels of oxidation.

4.8.1 Analysis of Phosphine Oxidation using $[N(PPh_3)_2][PPh_2(m\text{-}C_6H_4SO_3)]$ and $Pd(PPh_3)_4$

$[Ph_3PNPPh_3][PPh_2(m\text{-}C_6H_4SO_3)]$ (0.0100 g, 11.2 μmol) was dissolved in methanol (7 mL) in a Schlenk flask under N_2. $Pd(PPh_3)_4$ (0.0052 g, 4.5 μmol; 40% loading) was suspended in methanol (3 mL) and added by syringe to the stirred phosphine solution. The resulting solution was injected from the glove box to the spectrometer via PTFE tubing (1/16″ o.d., 0.005″ i.d.).

4.8.2 Analysis of $[Cp_2Ti(NCCH_3)_2][ZnCl_3]$

Preparation of $[Cp_2Ti(NCCH_3)_2]^+$ was done using a previously published procedure.[226] Cp_2TiCl_2 (32 mg, 0.13 mmol) was dissolved in 60 mL acetonitrile. Zinc dust (2 g, 30.6 mmol) was added, and the solution stirred for two days. Filtration gave a blue solution of $[Cp_2Ti(NCCH_3)_2]^+$, which was injected from the glove box to the spectrometer via PTFE tubing (1/16″ o.d., 0.005″ i.d.) at a rate of 40 μL/min.

4.8.3 Analysis of $[Cp_2ZrMe_2AlMe_2][B(C_6F_5)_4]$

Trityl tetrakis(pentafluorophenyl)borate, $[Ph_3C][B(C_6F_5)_4]$ (36 mg, 39.0 μmol) was weighed out and dissolved in fluorobenzene (5 mL). In a separate vial, 10 mg of Cp_2ZrMe_2 (40 μmol) was dissolved in fluorobenzene (5 mL). To this 0.2 mL of 2.0 M $AlMe_3$ solution (10 equiv.) was added. Finally, 0.2 mL of the $[Ph_3C][B(C_6F_5)_4]$ stock solution was further diluted to 5 mL, and 0.2 mL of Cp_2ZrMe_2/Me_3Al solution was added dropwise by syringe

with stirring. The resulting colorless solution of $[Cp_2ZrMe_2AlMe_2][B(C_6F_5)_4]$ and excess Me_3Al was injected from the glove box to the spectrometer via PTFE tubing (1/16″ o.d., 0.005″ i.d.) at a rate of 40 μL/min. Once the total ion chronogram had stabilized, cone voltages were adjusted to generate the *m/z* 235 ion (and its hydrolysis or oxidation products) in the gas phase (cone voltage typically 16-24 V).

Chapter 5 Catalyst Deactivation Processes During 1-Hexene Polymerization

Portions from this chapter have been previously published and are reproduced with permission from "Catalyst Deactivation Processes During 1-Hexene Polymerization" A Joshi, H.S Zijlstra, S Collins, and J. S McIndoe, ACS Catalysis, 2020, 10, 7195–7206. Supplementary spectra from this chapter are presented in Appendix D.

5.1 Introduction

In situ monitoring of olefin polymerization,[239] mediated by a metallocene or other transition metal catalysts, has emerged as a powerful tool for detecting initiators, resting states, and deactivation reactions inherent to these complex catalyst systems.[108] A variety of spectroscopic techniques, including UV-Vis[240] and NMR spectroscopy,[241] have been applied to this problem. Impressive gains in sensitivity have been achieved using NMR and isotopically labelled[242] or hyper-polarized monomer,[243] combined with the specialized flow or stopped-flow reactors.[244] NMR spectroscopy remains the definitive method for structural characterization of reactive intermediates,[245] though model compounds are often employed to confirm *in situ* spectroscopic assignments.[246] Mass spectrometric methods have also been employed to study various catalytic processes[77,78] including olefin polymerization,[247] with ESI-MS emerging as a sensitive and potent method for both detecting and identifying catalyst intermediates in solution,[92,225,248] and for studying their reactivity in the gas phase.[249]

These studies have revealed a wealth of information – the nature of the catalyst resting states is dependent on catalyst structure, the method of activation, the nature of the counter-ion, and even monomer.[108] In the case of discrete metallocenium ions, generated *in situ* from metallocene dialkyls and activators such as $B(C_6F_5)_3$ or $[Ph_3C][B(C_6F_5)_4]$, dormant

states are π-allyl complexes formed *in situ* via C-H activation of α-olefins or unsaturated chain ends.[250] The extent to which these well-studied complexes are competent for further chain growth is the catalyst, counter-ion, and monomer dependent.[251,252] In other cases where the (unhindered) metallocene is prone to β-H elimination, dormant contact ion-pairs such as $Cp_2ZrR(\mu\text{-}HB(C_6F_5)_3)$ form using borane-activated catalysts[253] and these can be rather resistant to further insertion.[254] In MAO-activated metallocenes, where Me_3Al is inevitably present as a chain transfer agent, the π-allyl species are also detected,[255] though their concentration is lower than that of the main, chain-carrying $[Cp_2Zr(\mu\text{-}R)(\mu\text{-}Me)AlMe_2]^+$ complexes identified some time ago by Brintzinger and Babushkin.[242] Further, in MAO-activated systems, the π-allyls appear susceptible to chain transfer to Al, which provides another mechanism for catalyst reactivation.

In other work featuring the use of *i*-Bu_3Al as the alkylating agent/scavenger and $[Ph_3C][B(C_6F_5)_4]$ as an activator, π-allyl cations can form *in situ*.[256] However, the principal resting state during polymerization in the case of *i*-Bu_2AlH features $[Cp_2ZrR]$ cations, stabilized by coordination of *i*-Bu_2AlH forming trinuclear Zr, Al_2 complexes with strong Zr-H-Al bridging.[257] Given the presence of *i*-Bu_2AlH in *i*-Bu_3Al solutions, one suspects these intermediates may play a role in olefin polymerization in a catalyst system developed many years ago – *viz.* $Cp_2ZrCl_2/R_3Al/[Ph_3C][B(C_6F_5)_4]$[258] as an alternative to MAO-activated catalysts.[259] Hexene has often been employed as a model monomer in these studies as a surrogate for more reactive monomers such as propene or ethylene. The latter is difficult to study, depending on the activator, as mass transfer effects can dominate[164] while the tactic or crystalline polymers formed are generally insoluble and can complicate the kinetics.[260] Further, at least one study has established that the rates of hexene

polymerization are insensitive to the nature of the counter-ion, while propene shows much wider variations.[261]

Under typical conditions in hydrocarbon media, the recent work of Kissin and co-workers, where GC-MS was used to study the hexene oligomer distribution in the case of Cp_2ZrCl_2 and MAO activation, is instructive.[262] There was evidence for chain transfer to Me_3Al, β-H elimination, and minor secondary insertion under the conditions studied (neat hexene, 50-100 °C, hydrolytic vs. non-hydrolytic MAO). It should be noted that incomplete monomer conversion was observed (50-75% conversion at or below 80 °C), and though not commented upon, that behavior is consistent with catalyst deactivation.

In a very recent study employing UV-Vis spectroscopy, Brintzinger and co-workers studied hexene polymerization using $[(SBI)Zr(\mu\text{-}Me)_2AlMe_2][B(C_6F_5)_4]$ (SBI = *rac*-$Me_2Si(\eta^5\text{-indenyl})_2$) in benzene solution.[252] They concluded that the propagating species formed two kinds of π-allyl complexes. Those formed from direct C-H activation of terminal alkenes (including hexene) were unreactive towards further monomer insertion, while those formed from iso-alkenes, formed following β-H elimination, were sluggishly reactive. The latter type also underwent slow reactivation through chain transfer to excess Me_3Al.

Over the past several years, the McIndoe group has applied ESI-MS to the study of MAO-activation of metallocene complexes in fluorobenzene (PhF) solution where both cationic and anionic species can be readily detected and characterized.[93,96] The group has studied ion-speciation in the case of additives such as octamethyltrisiloxane (OMTS), which forms well-defined ion-pairs $[Me_2Al(OMTS)][(MeAlO)_{16}(Me_3Al)_6Me]$ through the process of $[Me_2Al]^+$ abstraction from the MAO.[3] This additive has proven useful in monitoring both

aging and oxidation of MAO,[4,118] features known to be important in affecting the efficacy of this elusive but important activator.[109,112,263] The McIndoe research group has also studied the reaction of MAO-activated Cp_2ZrMe_2 with ethylene in the toluene solution at low ethylene pressures.[140] In that case, a hitherto undetected, but long-suspected process for catalyst deactivation[264] was revealed by ESI-MS – formation of inactive, dinuclear Zr_2 complexes arising from the reaction of active species (i.e. $[Cp_2ZrR]^+$) with each other. The authors explored using *in situ* reaction monitoring via pressurized sample infusion (PSI)[87] to study ethylene polymerization in PhF solution using diluted monomer (99:1 ethane:ethylene mixture) as both reactant and pressure source. Considerable difficulty was encountered in pumping dilute MAO solutions via the PSI technique due to incipient clogging issues (i.e., the formation of boehmite gel at the spray tip or along the flow path, which included an in-line filter to remove solid PE). These features gave rise to both random and systematic variations in flow rate and spray instability arising from the latter. This has a negative effect on the appearance of the total ion chronogram (TIC), which renders the collection of reliable kinetic data problematic. This chapter is, therefore, focussed on 1-hexene polymerization using the MAO-free catalyst system, $Cp_2ZrMe_2/Me_3Al/ [Ph_3C][B(C_6F_5)_4$. Since ESI-MS (and PSI) requires a polar solvent, these studies have been conducted mainly in PhF. The McIndoe group has shown a strong analogy between these conditions when it comes to catalyst activation using MAO vs. other spectroscopic studies in the toluene solution.[93]

5.2 Catalyst activation

The synthesis of $[Cp_2Zr(\mu\text{-}Me)_2AlMe_2][B(C_6F_5)_4]$ (**1**) involves addition of excess Me_3Al to $[Cp_2ZrMe][B(C_6F_5)_4]$ (**2**) generated *in situ* from Cp_2ZrMe_2 and $[Ph_3C][B(C_6F_5)_4]$ at low

temperature.[233] High isolated yields are obtained upon subsequent crystallization. However, we attempted to monitor this activation process at room temperature in PhF solvent using ESI-MS. Aside from the use of PhF, this approach mimics what is typically done in olefin polymerization studies – i.e., *in situ* catalyst generation.

One basic approach involved simultaneous pumping of a solution of $[Ph_3C][B(C_6F_5)_4]$ in PhF and a separate solution of Cp_2ZrMe_2 and Me_3Al in PhF into a mixing tee inside a glove-box with a short length of PTFE tubing running from the tee to the source compartment of the mass spectrometer.[248] By varying the flow rate through the mixing tee, one obtains "snapshots" of the instantaneous product distribution at various time scales in a continuous process.

An example of the data obtained is shown in Figure 5.1. At a 2:1 Al:Zr stoichiometry, formation of $[Cp_2Zr(\mu\text{-}Me)_2AlMe_2]^+$ (**1** *m/z* 307) and the dinuclear complex $[(Cp_2ZrMe)_2(\mu\text{-}Me)]^+$ (**3** *m/z* 485) occur at competitive rates. At longer reaction times (i.e., slower mixing rates), the formation of **3** is suppressed as the Cp_2ZrMe_2 is consumed, and **2** is competitively trapped by Me_3Al forming **1**.

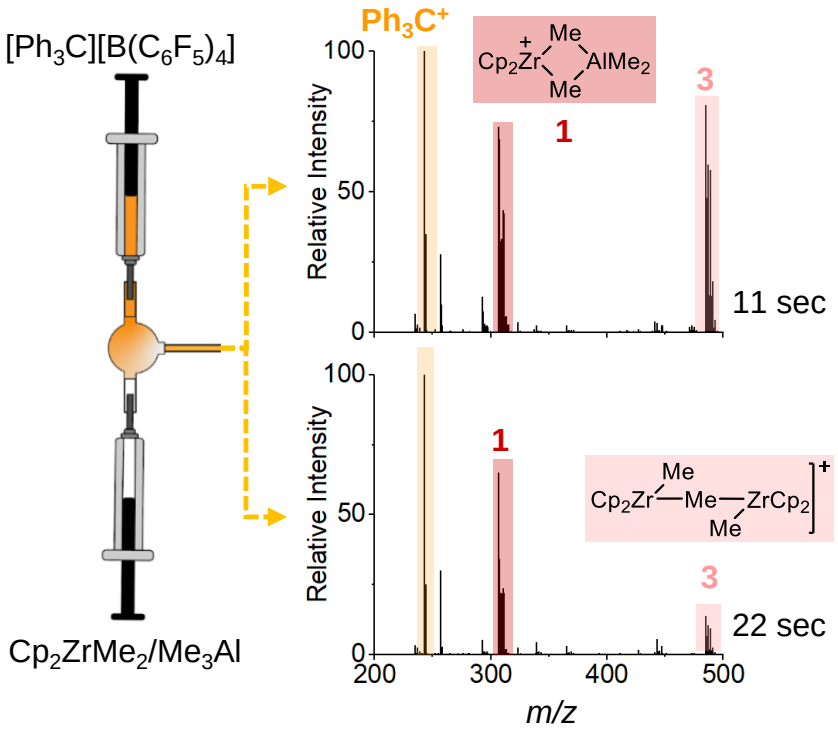

Figure 5.1 Monitoring of catalyst activation using $[Ph_3C][B(C_6F_5)_4]$ (0.31 mM), Cp_2ZrMe_2 (0.31 mM) and Me_3Al (0.61 mM). Representative mass spectra after 11 seconds and 22 seconds are shown.

Based on these results, slow addition of a 1:2 or 1:10 mixture of Cp_2ZrMe_2:$AlMe_3$ to a rapidly stirred solution of $[Ph_3C][B(C_6F_5)_4]$ in PhF (basically titration to a colorless endpoint) gave the cleanest formation of $[Cp_2Zr(\mu\text{-}Me)_2AlMe_2][B(C_6F_5)_4]$ (**1**). Hexene polymerization experiments were conducted with solutions dominated by **1**, but **3** also reacted with hexene, confirming that both **1**[233] and **3**[265] act as reservoirs of **2**. We attempted to generate **2** *in situ* by the addition of Cp_2ZrMe_2 to 1 equiv. of $[Ph_3C][B(C_6F_5)_4]$ in PhF. At [Zr] = 4.0 mM the reaction affords a mixture of **2** and **3**. The direct reaction between Cp_2ZrMe_2 and $[Ph_3C][B(C_6F_5)_4]$ is slower in comparison to reactions conducted in the presence of Me_3Al. It is known that competing formation of **3** impedes activation of Cp_2ZrMe_2.[233,265] Trace amounts of a fluorobenzene complex of **2** with *m/z* 331[92,266] were

also detected in this experiment (see Appendix D). Since the reaction was not clean, and it appears **2** is also unstable in PhF, decomposing to form $[(Cp_2ZrMe)_2(\mu\text{-}F)]^+$ (among other species) over 3 hours, we focused much of our subsequent efforts on the reactivity of **1**.

5.2.1 Catalyst speciation at steady state

Solutions of the activated catalyst [Zr] = 0.28 mM, and a solution of monomer 1-hexene (1000 equiv.) in PhF, each containing Me_3Al ([Al] = 2.8 mM), were simultaneously pumped into the mixing tee referred to earlier. Shown in Figure 5.2 are some representative mass spectra of product mixtures at different reaction times at a 1000:1 hexene:Zr ratio. Flow rate is a proxy for reaction time, with high flow rates corresponding to a short reaction time before the mixed solution emerges into the ESI-MS source.

With lag times of 4-16 seconds, we see a mixture of ions at *m/z* 279, 293, 311, 363, and 471. In the earlier work from the McIndoe group,[140] ions with *m/z* 279, 293, and 311 were also formed in PhF solution during PSI experiments involving diluted ethylene. The ion with *m/z* 279 was shown to be $[Cp_2Zr(\mu\text{-}H)_2AlMe_2]^+$ (hereinafter **6**) based on its MS/MS spectrum (Appendix D). The ion with *m/z* 293 is $[Cp_2Zr(\mu\text{-}H)(\mu\text{-}Me)AlMe_2]^+$ (hereinafter **7**) based on its MS/MS spectrum (Appendix D).

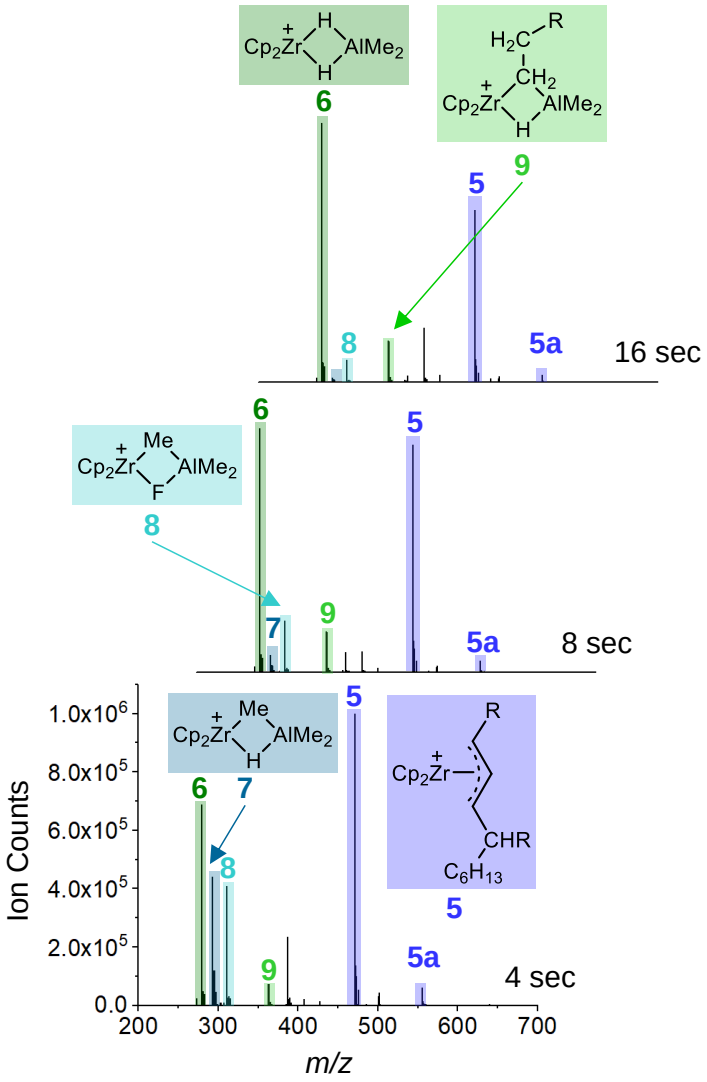

Figure 5.2 Positive ion ESI-MS of the product ions formed at different reaction times with hexene:Cp_2ZrMe_2 = 1000:1 in PhF ([Zr] = 0.31 mM). R = n-Bu

The ion with *m/z* 311, like complex **7**, is more prominent in the mixture at short reaction times. Since this ion was not observed in ethylene (or hexene) polymerization experiments conducted in toluene solution,[140] it was assigned to $[Cp_2Zr(\mu\text{-}F)(\mu\text{-}Me)AlMe_2]^+$ (**8**), ostensibly a product of C-F activation, a reaction that is known to be mediated by cationic zirconocene complexes in the presence of TiBAl.[267] The intensity of this ion was maximal upon initial pumping of solutions of ion-pair **1** and hexene. Prolonged pumping of these

solutions led to a pronounced decrease in the intensity of this ion relative to the others present (Figure 5.3). Subsequent pumping of a fresh solution of monomer and catalyst also exhibited low levels of **8,** suggesting this ion forms from a contaminant in the source compartment (rather than in solution), which is gradually depleted when pumping catalyst + monomer solutions.

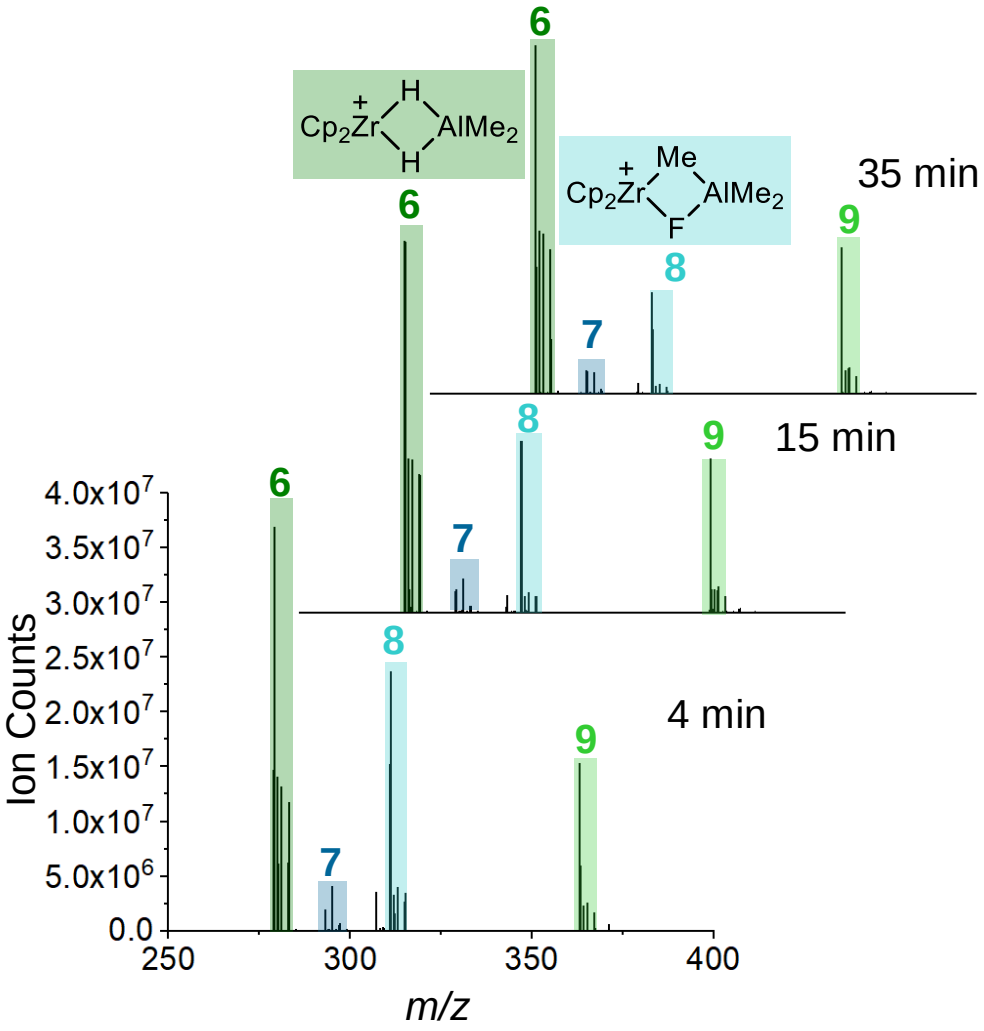

Figure 5.3 Mass spectra at various times following mixing of $[Cp_2ZrMe_2AlMe_2][B(C_6F_5)_4]$ (**1** [Zr] = 0.31 mM) and monomer with hexene:Zr = 10:1 in PhF**.**

The ion with *m/z* 363 fragments with initial loss of 84 Da (i.e. hexene), to form *m/z* 279, followed by a 58 Da loss (Me_2AlH) to form *m/z* 221 $[Cp_2ZrH]^+$ (Figure 5.4). It can thus be

formulated as $[Cp_2ZrH_2AlMe_2(hexene)]^+$ (**9**), though it could also correspond to the insertion product $[Cp_2Zr(\mu\text{-}H)(\mu\text{-}n\text{-}C_6H_{13})AlMe_2]^+$.

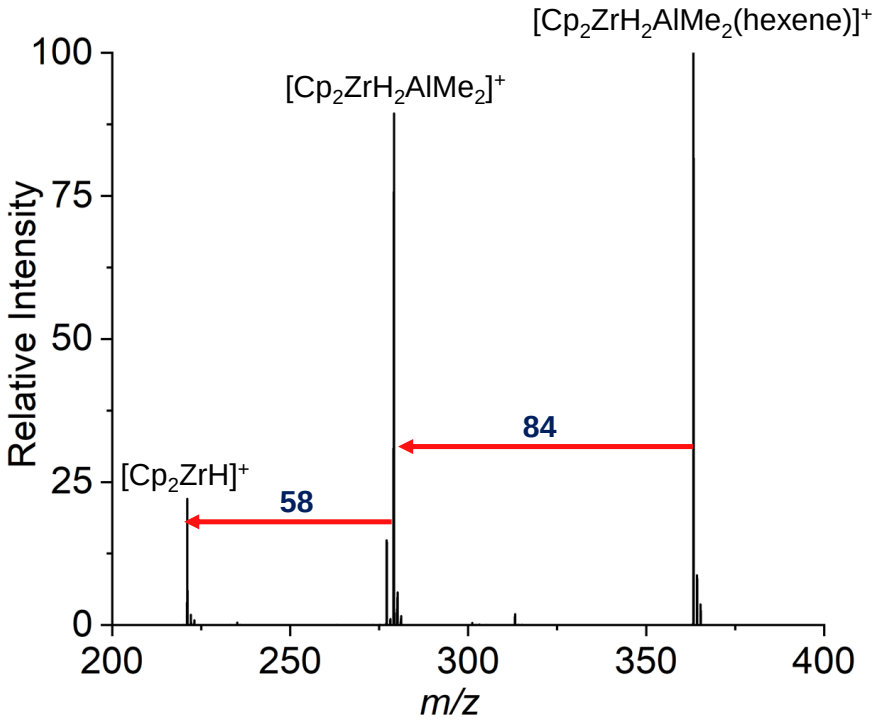

Figure 5.4 MS/MS of $[Cp_2ZrH_2AlMe_2(hexene)]^+$ (*m/z* 363).

The relative intensities of dimethylalane adducts **6** and **9** were highly variable in this work, and experiments at different cone voltages established that the loss of hexene from **9** occurs at low collision energies, during transit of ions from the source compartment to the high vacuum region of the spectrometer. Even subtle changes in the pressure (and presumably atmospheric composition[99]) within the source compartment had noticeable effects on the ratio of these two ions. Similar effects have been noted before in the case of ion $[Cp_2Zr(\mu\text{-}Me)_2AlMe_2]$ (**1**), which generates ion $[Cp_2ZrMe]^+$ (**2**) via CID within the source compartment of the mass spectrometer.[93,99] Indeed, in those experiments where ion dimethylalane complex **6** was prominent, the same was true of ion **2** - before introducing

hexene. When a solution containing **6** and **9** was treated with excess *i*-Bu_3Al, the substitution of the two Me groups for *i*Bu was observed (substitution of Me by *i*Bu leads to a mass difference of 42 Da), leading to the formation of ions with *m/z* 405 and 447 for species **9** (Figure 5.5).

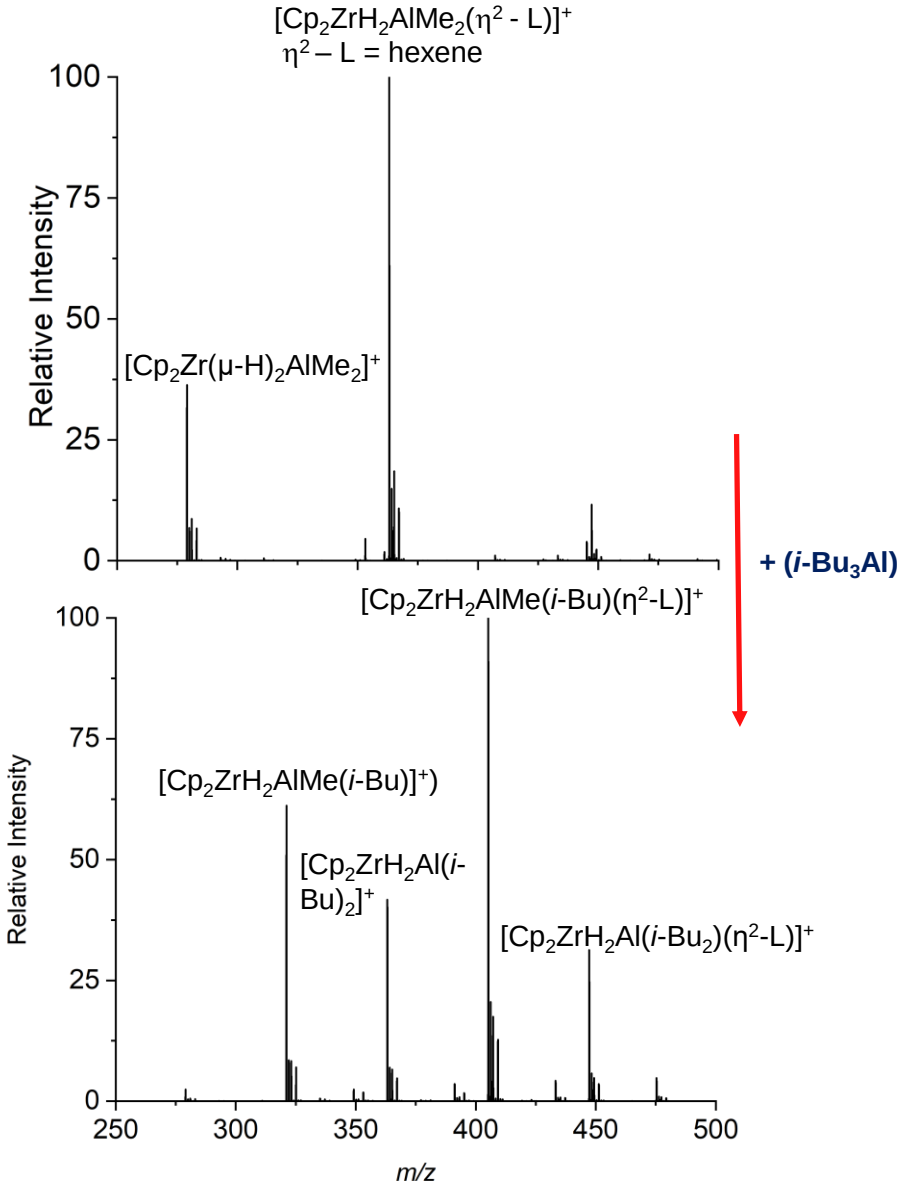

Figure 5.5 Mass spectra of a mixture of *m/z* 279 and 363 before (top) and after (bottom) after addition of *i*Bu_3Al showing the exchange of Al-Me groups by *i*Bu groups.

However, no ions corresponding to the substitution of a Zr- or Al-hexyl group were observed. One cannot exclude the possibility that **6** and **9** are in equilibrium with each other through the process of reversible binding of hexene, possibly coupled with reversible insertion (Scheme 5.1).

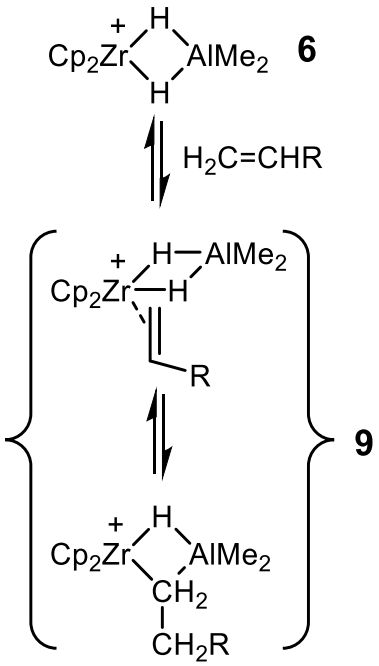

Scheme 5.1 Possible equilibria between ions 6 and 9. R = n-Bu.

The ion with *m/z* 471 was quite resistant to fragmentation by MS/MS. It successively loses 2 Da (i.e., H_2) over the range in collision energies investigated (2-100 V) forming *m/z* 469 and at higher energy *m/z* 467 (Figure 5.6). Its nominal mass is consistent with the formula $[Cp_2Zr(C_6H_{10})(C_6H_{12})_2H]^+$ and the fact that it is resistant to CID of neutral species is consistent with it being assigned as a π-allyl complex with a formula of $[Cp_2Zr(\eta^3\text{-}C_6H_{10})(C_6H_{12})_2H]^+$ (**5**). A related species with *m/z* 555 was also observed, which given its mass of 84 Da above that of π-allyl complex **5,** can be assigned as the allyl complex $[Cp_2Zr(\eta^3\text{-}C_6H_{10})(C_6H_{12})_3H]^+$ (**5a**).

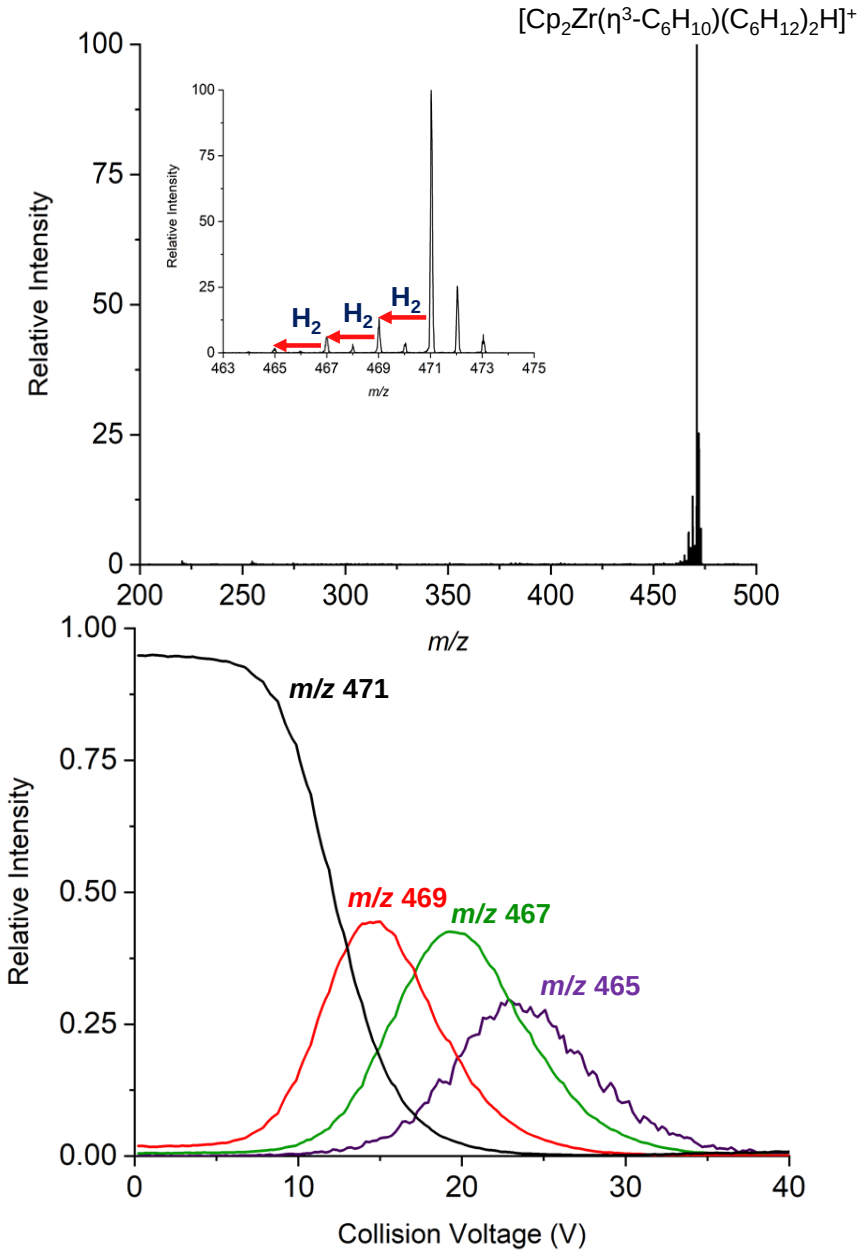

Figure 5.6 MS-MS of $[Cp_2Zr(\eta^3\text{-}C_6H_{10})(C_6H_{12})_2H]^+$ (*m/z* 471). Inset shows 3 consecutive losses of H_2 from the parent ion (Top). Breakdown curves for $[Cp_2Zr(\eta^3\text{-}C_6H_{10})(C_6H_{12})_2H]^+$ (*m/z* 471)

5.3 Catalyst Speciation during Slow Monomer Consumption

The study of basic kinetics in more detail requires batch reactions using either off-line or PSI techniques.[87,91,143] The advantages of the former are convenience and a consistent flow

rate (using a syringe pump) while PSI experiments are problematic to flow rate variations in reactions of this type (due to increasing viscosity of the medium and incipient clogging issues leading to variations in spray quality). On the other hand, PSI experiments feature lag times that are comparable to those just discussed and allow direct sampling from a reaction vessel.

5.3.1 Off-line Experiments – 10:1 Hexene:Zr

As illustrated in Figure 5.7 a, the mixture with 10 equiv. of hexene contains ions **6** - **9**. Also, an ion with *m/z* 445 (henceforth **10a**) was observed and was much more prominent in off-line experiments than the flow experiments discussed previously where it was not detected. Its MS/MS spectrum showed a low energy loss of 58 Da, followed by consecutive losses of 2 Da at higher collision energies (See Appendix D). Both lower (*m/z* 361, **10**) and higher homologs at *m/z* 529 (**10b**) and *m/z* 613 (**10c**) were also seen in these experiments, though with significantly diminished intensity. Collectively, the formation of these products was most noticeable at low monomer:catalyst ratios. Tentatively, these related ions are assigned σ-allyl dimethylalane adducts with a formula of $[Cp_2Zr\{\sigma\text{-}C_6H_{10}(C_6H_{12})_nH\}(\mu\text{-}HAlMe_2)]^+$ (**10**, n = 0; **10a**, *n* = 1; **10b**, *n* = 2; **10c**, *n* = 3) and will be discussed in greater detail later.

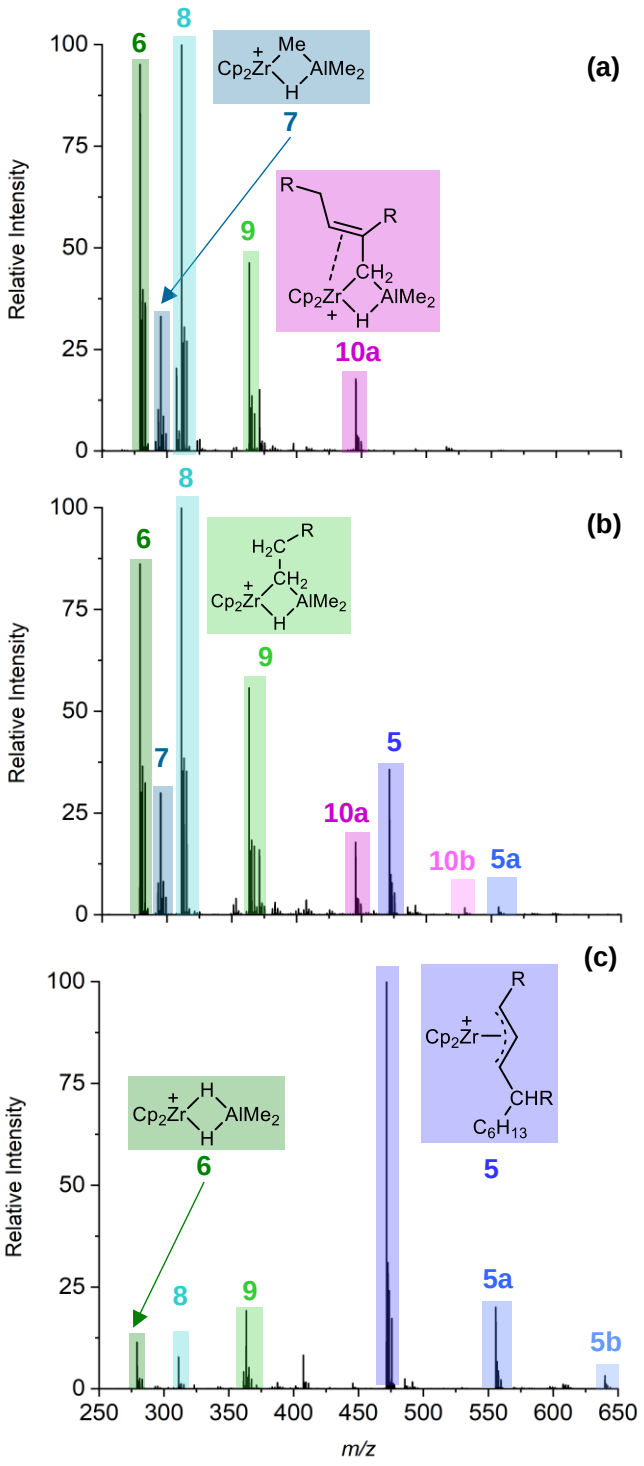

Figure 5.7 ESI-MS of reaction mixtures formed from 0.28 mM $[Cp_2ZrMe_2AlMe_2][B(C_6F_5)_4]$ and Me_3Al:Zr = 10:1 with a) 10 b) 100 and c) 1000 equiv. of hexene in PhF solution. Ions that are separated in mass by 84 Da (C_6H_{12}) are highlighted with different hues of the same color; R=n-Bu.

5.3.2 Off-line Experiments – 1000:1 Hexene:Zr

In experiments featuring a large excess of hexene (i.e., conditions corresponding to polymerization), off-line experiments show the predominant formation of π-allyl complex **5** and higher homologs separated in mass by 84 Da - i.e., **5a**, **5b,** etc. (see Figure 5.7 c). The other ions discussed above are also present but in significantly lower amounts (Figure 5.7 c), as might be anticipated from the flow experiment presented earlier. Though higher homologs of complex **5** were readily detected, lower MW species (i.e., *m/z* 387, 303) were present in essentially trace amounts in these experiments, suggesting the formation of π-allyl complex **5** is kinetically favored. In addition to this series of ions, ions differing in mass by +14 Da were seen with weaker and variable intensity (see Appendix D). These are assigned as analogous π-allyl complexes but involving chains that initiate with Zr-Me vs. Zr-H.

5.3.3 Off-line Experiments – Time-Dependent Behavior

While monitoring these off-line experiments as a function of time, it was observed that π-allyl complexes **5**, **5a**, **5b**... were unstable in solution, while ions σ-allyl ions **10**, **10a**, **10b**..., dimethylalane complex **6**, and hexene adduct **9** formed at their expense. Typical data are shown in Figure 5.8. Note that the rate of disappearance of **5**, **5a**, **5b**... is linear with time in this experiment (ca. 1.5 half-lives).

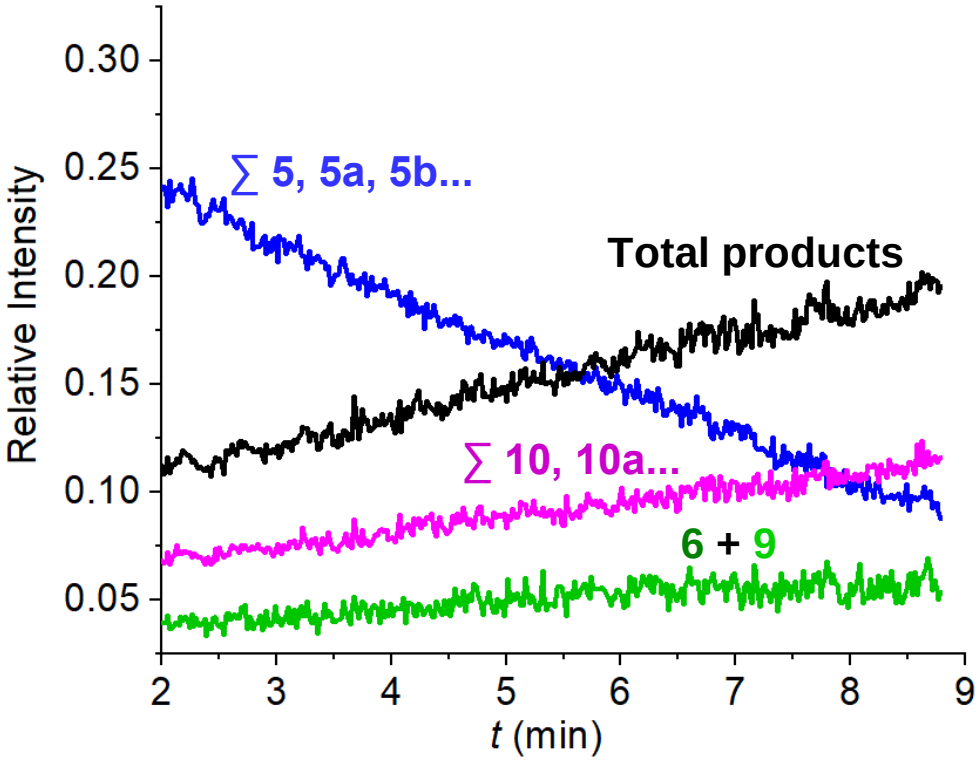

Figure 5.8 Sum of normalized ion intensities vs. time for reaction of $[Cp_2ZrMe_2AlMe_2][B(C_6F_5)_4]$ with 1000 equiv. of hexene in PhF.

5.3.4 Repetitive Monomer Addition Experiments

The reactivity of ions dimethylalane complex **6** and hexene adduct **9** towards monomer has not been demonstrated, and yet these ions are formed at the earliest stages of polymerization, at least under starved feed conditions. This was examined by looking at repetitive additions of hexene to a mixture of these ions using PSI techniques. As shown in Figure 5.9, the addition of 20 equiv. of hexene to a solution of **1** (0.25 mM) led to the rapid consumption of this ion with the formation of dimethylalane complex **6** and hexene adduct **9** as the principal products. Further additions of hexene did not lead to consumption (or further growth) of these products, even transiently.

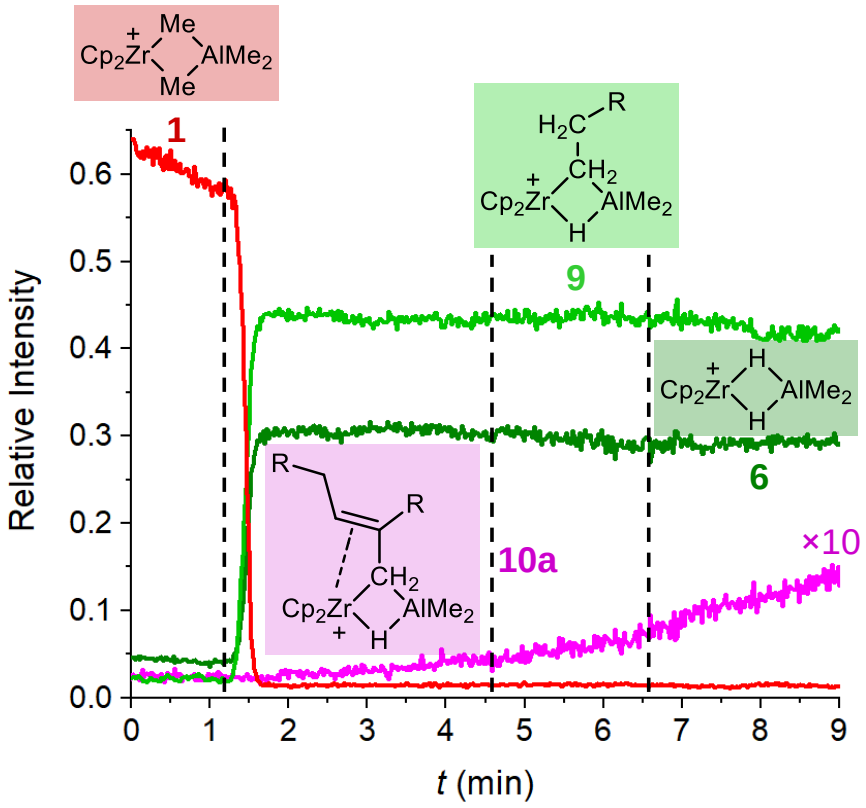

Figure 5.9 Normalized ion intensities vs. time for sequential additions of 20 equiv. of hexene to $[Cp_2ZrMe_2AlMe_2][B(C_6F_5)_4]$ (0.25 mM in PhF). Vertical dash lines indicate the additions of hexene, while the intensity of the ion 10a has been expanded 10-fold. R = n-Bu.

During these additions, slow growth of σ–allyl **10a** is seen, but as it is nearly continuous and unperturbed by the further additions of monomer, it is not obvious that either **6** or **9** are the precursors to this material. That monomer insertion is involved is evident from the higher MW of **10a** relative to either possible precursor. It may be a very unfavorable pre-equilibrium for dissociation of Me_2AlH from either **6** or **9** that is rate-determining in forming **10a.** Similar behavior is exhibited by $[L_2HfH_2Al^iBu_2][B(C_6F_5)_4]$ formed in situ from L_2HfCl_2, excess TiBAl and $[Ph_3C][B(C_6F_5)_4]$ (L_2 = 1,2-C_2H_4(Flu)(5,6-C_3H_6-2-MeInd) on addition of propene.[268] This experiment shows that the formation of dimethylalane complex **6** and hexene adduct **9** is accompanied by catalyst deactivation.

5.4 Pressurized Sample Infusion Experiments

Initial work of this type focused on the use of PhF as a solvent. However, considerable difficulty using this solvent and this technique, at least within the confines of a glove-box and using a simple apparatus such as that described in the literature.[87] However, better results were obtained using the more polar solvent *o*-difluorobenzene (ε = 13.4, *o*-$C_6H_4F_2$)[269], which is of similar volatility as PhF. Fortunately, the product distributions just discussed in detail were little perturbed by this solvent choice, while considerably more intense spectra were seen using this solvent. In Figure 5.10 are shown two experiments of this type at [Zr] = 0.28 mM with the addition of 10 or 1000 equiv. of monomer, with major ions illustrated.

Note that in Figure 5.10, a consumption of ion **1** is incomplete. This is expected as dissociation of Me_3Al from this ion is less favorable than for higher analogues[129] while ion-pairing in the resulting 14 e species is expected to be tighter as well, leading to the well-known phenomenon that the first insertion of monomer (with rate constant k_i) is generally quite a bit slower than subsequent insertions.[250,270] The initial appearance of ion **7** in Figure 5.10 a was observed. Both this ion (and ion **8**) appears at the earliest times in these PSI experiments, consistent with them forming most rapidly from starting material (see Figure 5.2). Under starved feed conditions, **7** is the primary product formed, while the formation of ions dimethylalane complex **6** and hexene adduct **9** involves additional steps. In particular, complex **7** might form directly from $[Cp_2Zr(\mu\text{-}R)(\mu\text{-}Me)AlMe_2]$ via β-H elimination, supposing that the propagating ions, in this case, are the same as those identified by NMR quite some time ago by Brintzinger and co-workers.[242]

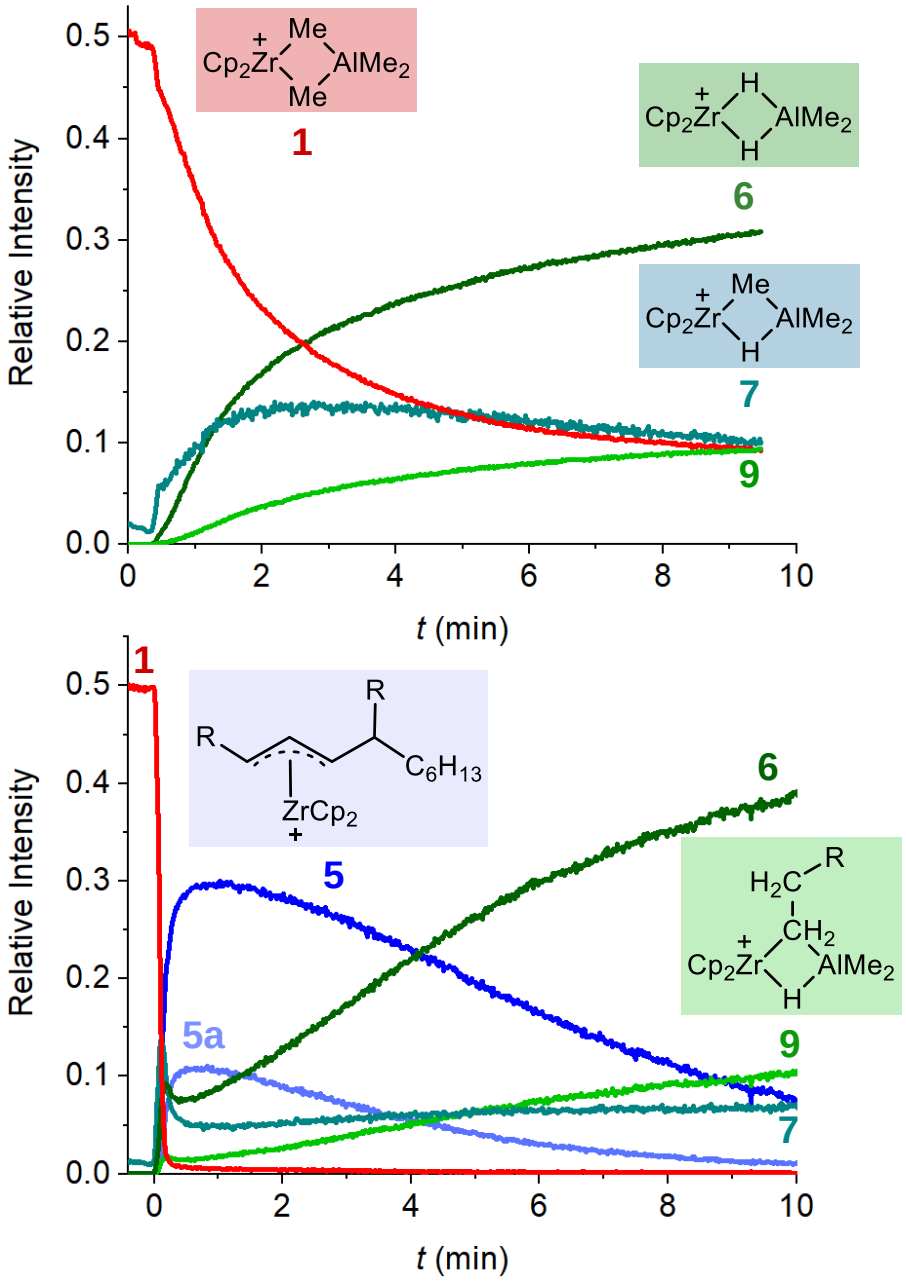

Figure 5.10 Normalized ion intensities vs. time for addition of a) 10 equiv. and b) 1000 equiv. of hexene to $[Cp_2ZrMe_2AlMe_2][B(C_6F_5)_4]$ in o-difluorobenzene with [Zr] = 0.28 mM. R = n-Bu

The second experiment at 1000:1 monomer to catalyst ratios exhibits a plethora of transient behavior at both short and long-time length scales, fully consistent with all prior experiments. The rapid formation of **7** (and **8**), subsequent formation of ions dimethylalane

complex **6** and hexene adduct **9**, concomitant formation, and subsequent disappearance of π-allyl complex **5** and homologs (**5a**, **5b,** etc.) are beautifully illustrated in this experiment. It is very clear from these two experiments that the π-allyl complexes **5** only forms in the presence of a large excess of hexene and at a time scale that is similar to the formation of **6** and **9** under these conditions. They clearly transform under longer time scales to **6** and **9** in this experiment where we have shown that these two ions are much less reactive towards monomer.

The kinetic behavior seen in this experiment is strongly reminiscent of that recently reported by Brintzinger and co-workers under similar conditions;[252] rapid consumption of the starting ion-pair with π-allyl intermediates detected at both short and long time scales by UV-Vis spectroscopy. Though we have not monitored these reactions by UV-Vis spectroscopy, there is an obvious color change (to pale orange-yellow) upon adding monomer to $[Cp_2ZrMe_2AlMe_2][B(C_6F_5)_4]$ (which is colorless), and though this color persists during the PSI experiment, the final solutions (which contain very little π-allyl complex **5**) are colorless. Their basic conclusion was that π-allyl complexes form at both time scales with some competent for further insertion vs. relatively unreactive. In their work, they also observed species at short time scales, which they assigned to the 14 e propagating alkyls $[(SBI)ZrR]^+$, though their presence was deduced from deconvolution of the observed spectra, rather than direct observation. In this work, we do not detect these species via ESI MS, and we believe that in the case of hexene, they are just too prone to β-H elimination (forming dimethylalane complex **7**) or reactive towards impurities (forming **8**) in the source compartment.

The formation of ions featuring coordinated Me_2AlH (i.e., **6**, **7**, **9**, and **10**, **10a,** and homologs) in these experiments and at the earliest stages of polymerization is without precedent as far as we are aware. That Me_2AlH would strongly bind to a 14 e metal alkyl or hydride is not surprising.[257,268] Given that ions such as dimethylalane complex **6** and **9** are resistant to further insertion, their predominant formation under starved feed conditions represents a hitherto unappreciated mechanism for catalyst deactivation or dormancy. To generate Me_2AlH in solution, a propagating intermediate would have to undergo β-H elimination, trapping of $[Cp_2ZrH]^+$ by Me_3Al to form ion **7,** which we do observe, and regeneration of $[Cp_2ZrMe]^+$ with the release of Me_2AlH, which we do not observe (Scheme 5.2). It is anticipated that the driving force for the formation of **6** vs. **7** from propagating intermediates $[Cp_2Zr(\mu\text{-}R)(\mu\text{-}Me)AlMe_2]$ is the stronger bridging for Al-H vs. Al-R bonds.

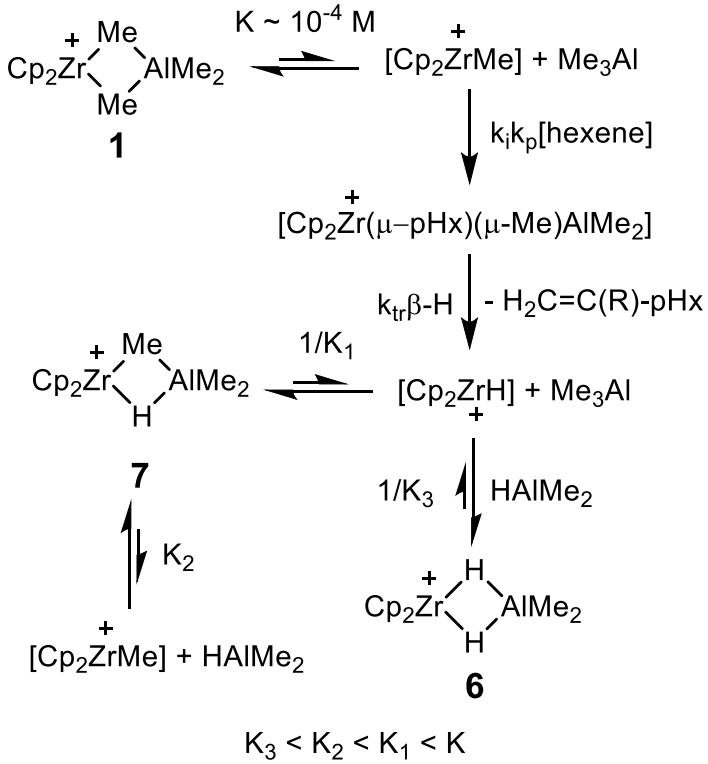

Scheme 5.2 Proposed formation of Me_2AlH and its complexes. pHx = poly(hexenyl) R = n-Bu

5.5 Conclusions

ESI-MS studies of hexene polymerization using $[Cp_2ZrMe_2AlMe_2][B(C_6F_5)_4]$ reveal unanticipated complexity and identification of a new pathway for catalyst deactivation – formation of dimethylalane stabilized complexes which are resistant to further insertion. Ironically, these complexes also form under starved feed conditions, or under any conditions that lead to this condition, such as poor mixing. On the other hand, π-allyl complexes dominate under other conditions, and our work suggests they have the more hindered structure and form following 2,1-insertion. We believe they are, in part, responsible for slow monomer consumption seen with this catalyst, and that eventually, all of the added catalyst pools in dormant or deactivated dimethylalane-stabilized complexes. Since these same catalysts are observed in the toluene solution, we conclude that the formation of dimethylalane-stabilized complexes may be a general phenomenon at least at lower temperatures.

Chapter 6 Miscellaneous and Future work

Portions from Section 6.1 have been previously published and are reproduced with permission from “Interaction of Neutral Donors with Methylalumoxane” H.S Zijlstra, A Joshi, M Linnolahti, S Collins, and J. S McIndoe, European Journal of Inorganic Chemistry, 2019, 2346–2355.

6.1 Interaction of neutral donors with methylalumoxane

Methylalumoxane (MAO) is a key activator for olefin polymerization catalysts, making its chemistry of ongoing interest. Strong and bidentate neutral donors such as 2,2’-bipyridine are effective abstractors of the dimethylaluminum cation, $[Me_2Al]^+$, from methylalumoxane (MAO), while monodentate, weaker donors such as THF and pyridine appear most prone to adduct formation with both free and bound trimethylaluminum. The ionization process can be readily investigated using electrospray ionization mass spectrometry (ESI-MS) in fluorobenzene (PhF) solution

6.1.1 Tetrahydrofuran

Tetrahydrofuran has long been recommended for the determination of the Me_3Al content of MAO using ^1H NMR spectroscopy. Typically, the addition of 10 molar equivalents with respect to Al (4:1 v:v equiv. for 30 wt. % MAO in toluene) has been recommended for this procedure; this leads to optimal separation of the sharp signal, due to Me_3Al-THF, from the main MAO resonances (Figure 6.1).[116]

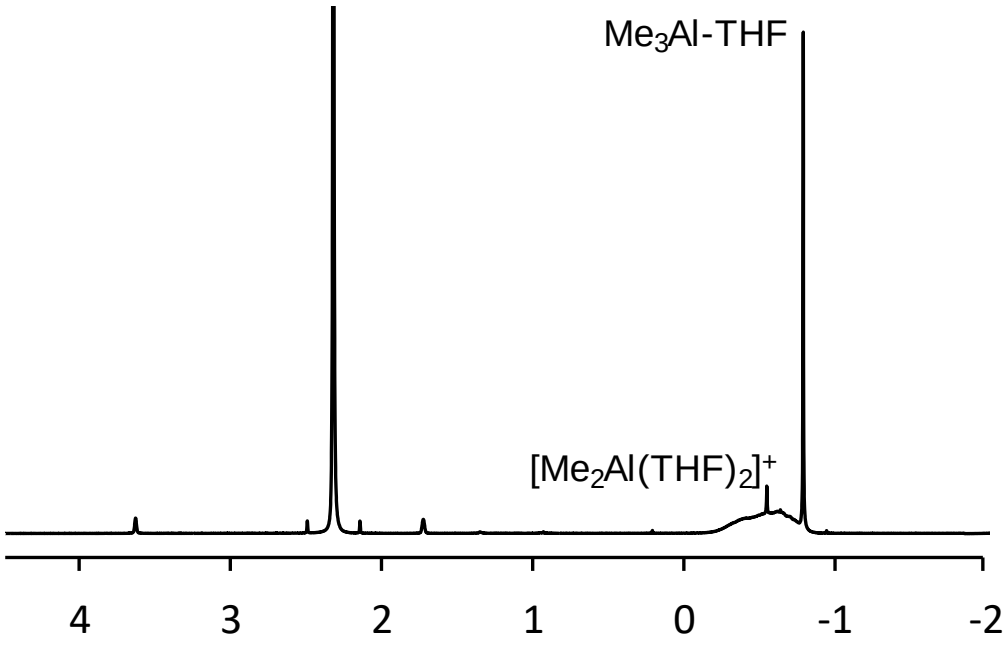

Figure 6.1 ^{1}H NMR spectrum of a commercial MAO (30 wt. % in toluene) containing 10 equiv. THF-d_8.

Though not recognized at the time of this first report, an additional sharp signal that is superimposed upon the main MAO resonance arises from the formation of $[Me_2Al(THF)_2]^+$, as shown by comparison to authentic samples of this cation partnered with, e.g., a $[B(C_6F_5)_4]^-$ anion,[141] an assignment subsequently confirmed by Bochmann and co-workers.[137] Typically, commercial samples of 30 wt. % MAO have Me_3Al content between 13-14 mol % using this technique while samples of MAO that have been shipped and stored cold have activator contents between 1-2 mol % when first analyzed by this method.

The positive and negative ion ESI-MS of 10 wt. % MAO + THF (10 mol %) are shown in Figures 6.2 a and 6.2 b, respectively. The positive ion spectrum is largely invariant to the

amount of THF added (between 1-40 mol % investigated) with the principle ions present being $[Me_2Al(THF)_2]^+$ and $[Me_2Al(THF)]^+$ with *m/z* 201 and 129, respectively. The relative intensity of these two ions is also largely insensitive to the amount of THF added at these levels. At sufficiently low cone voltage, only *m/z* 201 is observed.

The negative ion mass spectrum resembles that of MAO and other donor additives (*vide infra*), but at 1-40 mol %, THF the spectra are characterized by a low intensity per transient (<500 counts for the major ion present). The relative intensities of the anions present are insensitive to the amount of THF added, and the mass spectrum is largely dominated by the ion at *m/z* 1375, assigned by *m/z*, isotope pattern, and MS/MS behavior as [**16,6**]$^-$.

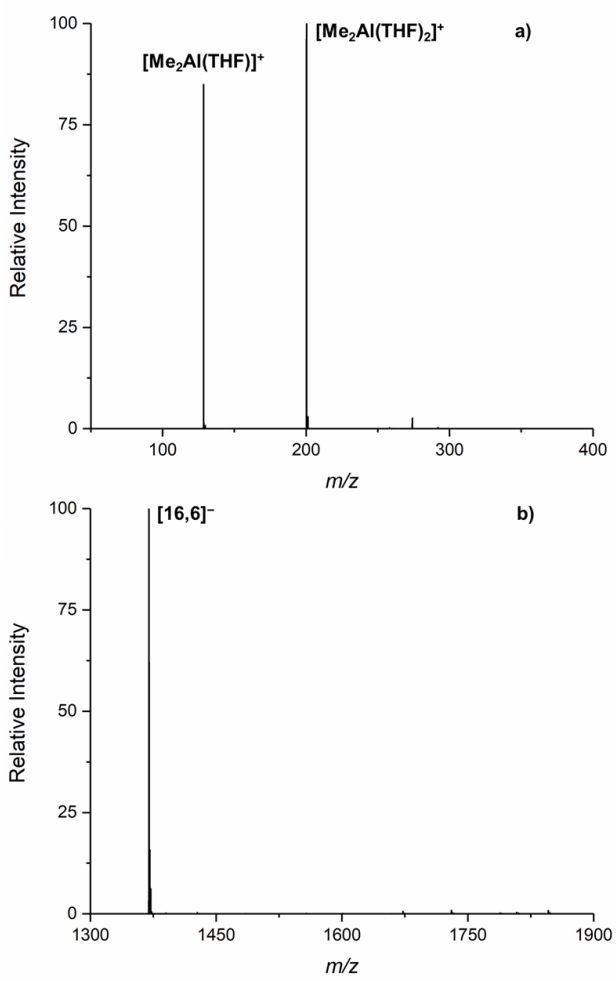

Figure 6.2 a) Positive and b) negative ion mass spectrum of a sample of commercial MAO (10 wt. % in toluene) containing 10 mol % THF in PhF solution ([Al] = 0.05 M). Cone voltage = 16 V.

6.1.2 Octamethyltrisiloxane (OMTS)

Disiloxanes and some cyclic siloxanes have been used as additives to furnish "stabilized MAO" formulations that are more resistant to gel formation while retaining their activation efficacy.[125] With linear, tri- or poly-siloxanes, including OMTS, and at higher concentrations in toluene solution, phase separation occurs to form an upper layer which is enriched in Me_3Al, and a lower layer that is an ionic liquid, swollen by an aromatic solvent[271] – first termed a liquid clathrate by Atwood and co-workers based on an ionic

host and aromatic guest formalism.[272] These liquid clathrates can be isolated in solid form by washing with hydrocarbon solvents, which remove Me_3Al and toluene.[271] ^{1}H, ^{27}Al and ^{29}Si NMR spectra of the solid formed from OMTS have been published in the patent literature in 1,3-dichlorobenzene, and the same reaction has been studied in PhF solution.[141] These studies strongly indicate that material with the composition $[Me_2Al(OMTS)]^+[MAO(Me)]^-$ is formed where the composition of the anion was not defined.

The negative ion ESI-MS spectra of MAO + OMTS are more intense at any given ratio than THF, and the signals due to higher MW anions are proportionately more intense compared to *m/z* 1375 (*cf*. Figure 6.3 with Figure 6.2 b). In earlier work, Zijlstra *et al.* showed that as the amount of OMTS was increased (from 1 to 100 mol %), the higher MW anions became increasingly accentuated relative to [**16,6**]$^-$.[3] This suggests that the corresponding neutral precursors are significantly less abundant in MAO than that due to [**16,6**]$^-$, or, more likely, are less reactive towards OMTS.

Evidently, a bidentate donor is more effective at abstracting $[Me_2Al]^+$ from the neutral MAO molecules than a mono-dentate donor of comparably basicity.[273] The corresponding positive ion spectrum showed the expected cation with *m/z* 293.[3]

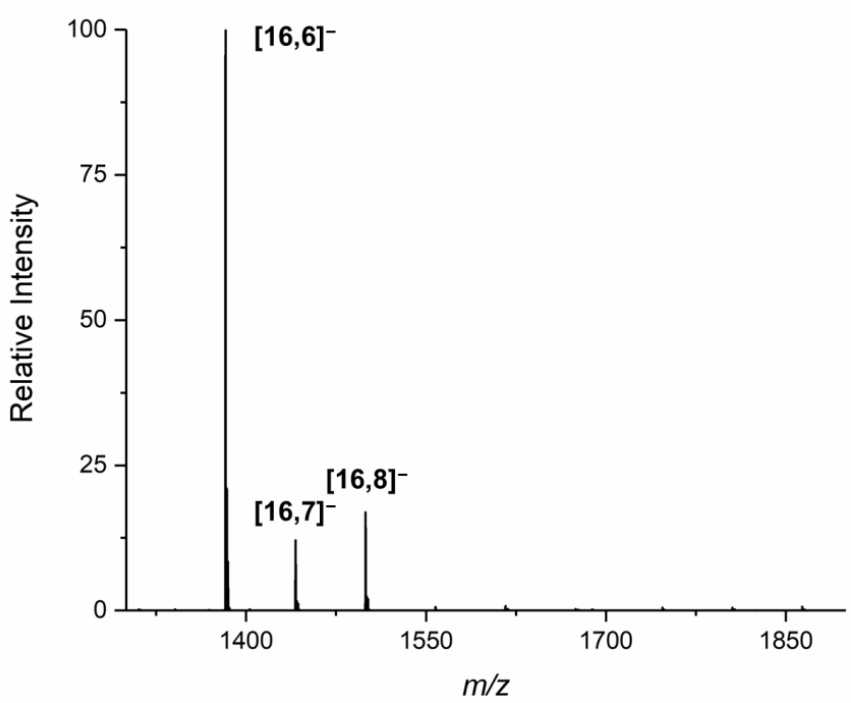

Figure 6.3 Negative ion mass spectrum of a sample of dried commercial MAO (30 wt. % in toluene) containing 2 mol % OMTS in PhF solution ([Al] = 0.05 M). Cone voltage = 16 V**.**

6.1.3 Pyridine and 2,2'-bipyridine

Pyridine was originally proposed for determining the Me_3Al content of MAO, but it has since been shown that excess pyridine (>5 equiv.) leads to degradation.[116,137,274] Pyridine disrupts dative Al---O bonding in tetra-t-butyldialuminoxane, which is dimeric in the solid-state and associated in solution, forming a structurally characterized, monomeric bis(pyridine) adduct (eqn. 6.1).[125] The mechanism for degradation of MAO by donors is unknown but likely involves similar reactions. We decided to investigate both pyridine and a chelating analog to compare with the oxygen-based donors already discussed.

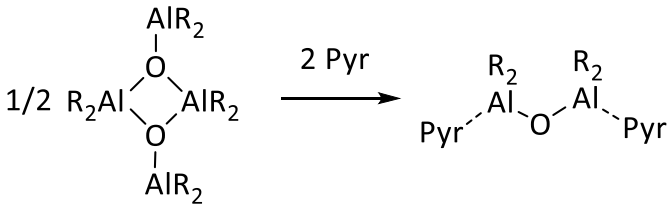

Equation 6.1 Formation of a monomeric bis(pyridine) adduct.

On the other hand, 2,2'-bipyridine (bipy), which gives well-defined chemistry at low levels with respect to MAO (i.e., < 10 mol % for the dried MAO). By ESI-MS, the clean formation of the $[Me_2Al(bipy)]^+[MAO\text{-}Me]^-$ ion-pair was observed. Positive and negative ion ESI-MS of MAO and bipy appear in Figure 6.4.

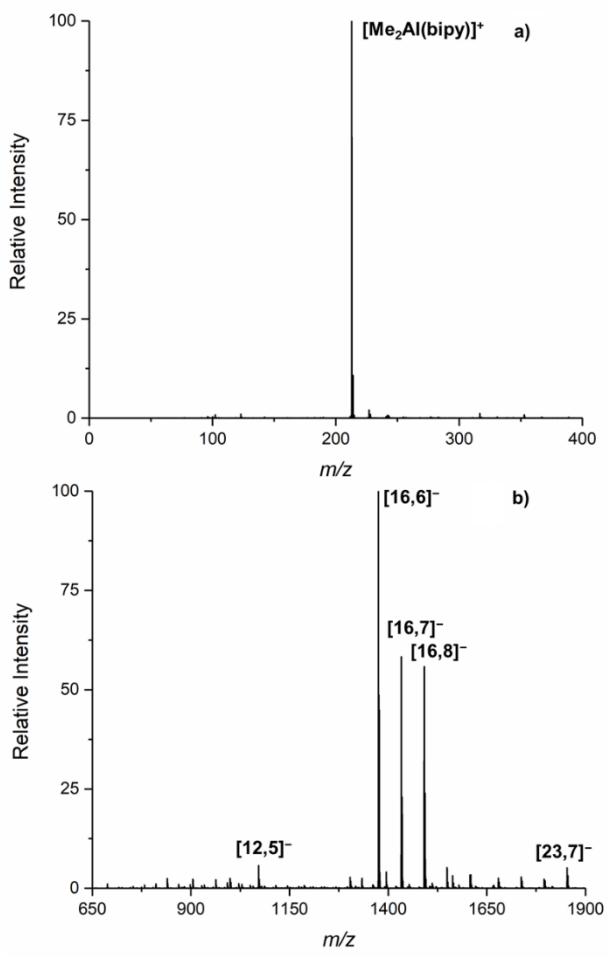

Figure 6.4 a) Positive and b) negative ion ESI-MS spectra of dried MAO + 4 mol % bipy in PhBr-d_5 diluted to [Al] = 0.02 M with PhF. Cone voltage = 16 V.

By comparing Figure 6.4 b with Figures 6.3 and 6.2 b, it can be seen that bipy is the most effective donor in forming ion-pairs with the largest range of neutral precursors, based on the relative intensity of the various anions present with respect to *m/z* 1375. It should be noted that the signal due to *m/z* 1375 in Figure 6.4 b has saturated the MCP detector (as is evident from the isotope pattern, which is distorted compared to the other anions present). The intensity of the other anions has been accentuated, relative to *m/z* 1375, by this artifact. Similar effects are also seen with excess OMTS.[3] Note that there are also anions lower in MW than *m/z* 1375 present at this level of bipy. As shown in Figure 6.5 at higher levels of bipy, only lower MW anions were detected in these mixtures so that high levels of bipy, like pyridine (or excess OMTS[3]) result in degradation of the MAO, presumably through adduct formation, which disrupts dative Al---O bonding as discussed earlier.

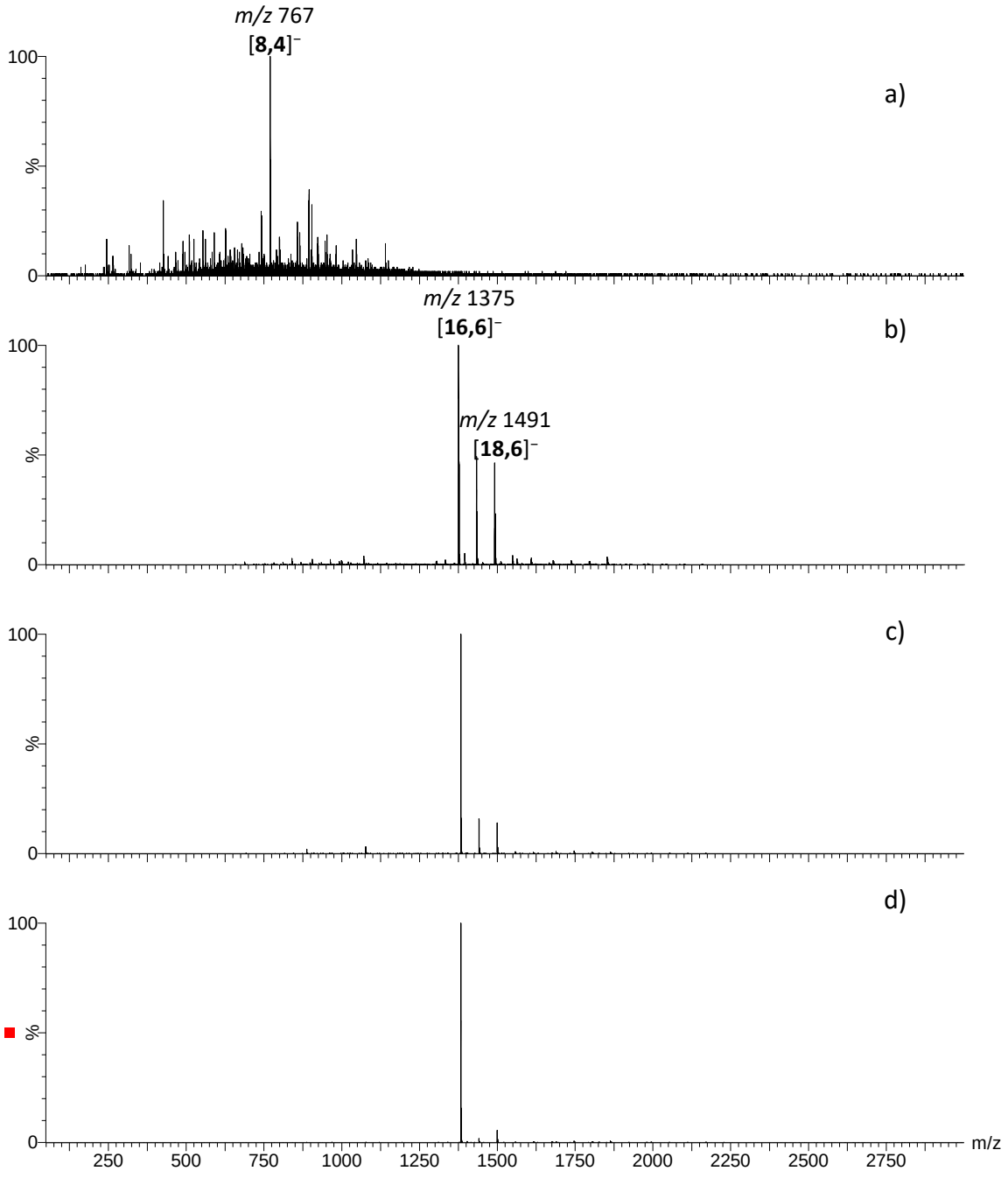

Figure 6.5 Negative ion ESI-MS of bipy + MAO in PhF under various conditions. a) 30 wt% MAO + >10 mol% bipy b) dried MAO + 4 mol% bipy c) 30 wt% MAO + 2 mol% bipy d) 30 wt% MAO + 1 mol% bipy.

The positive and negative ion ESI-MS of pyridine + MAO are shown in Figure 6.6. As with THF, the appearance of the positive ion MS in Figure 6.6 a is sensitive to cone voltage, suggesting the mono-pyridine complex with *m/z* 136 is derived from fragmentation of the *m/z* 215 ion. In comparing Figure 6.6 b with Figure 6.4 b, it is seen that only $[16,6]^-$ and $[16,7]^-$ are especially prominent, while lower MW anions are also present. Thus, the monodentate and strong donor pyridine shows different chemoselectivity towards ion-pair formation from MAO compared with bipy, though both additives form lower MW material at the same donor level.

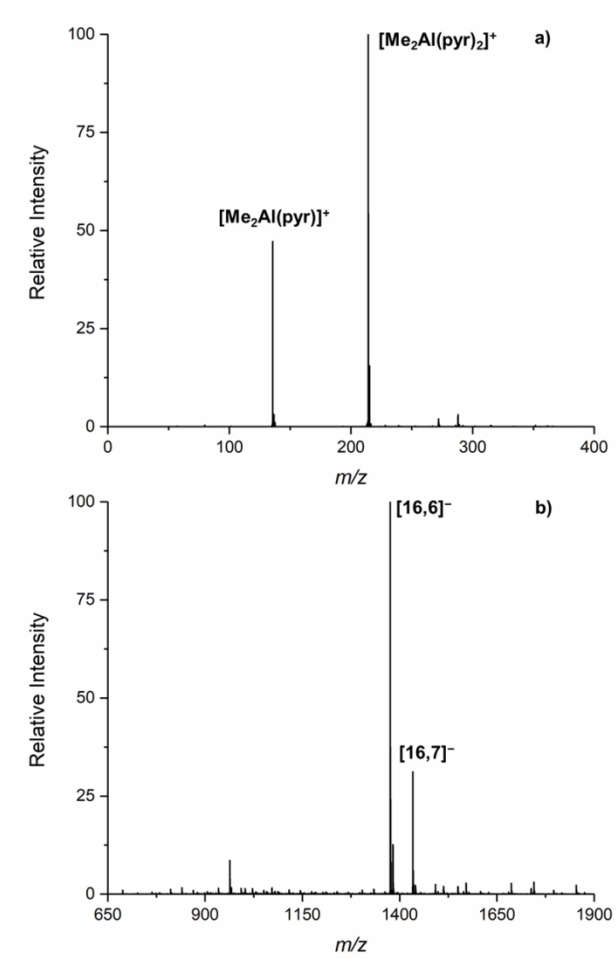

Figure 6.6 a) Positive and b) negative ion MS of dried MAO + 8 mol % pyridine in PhBr-d_5 diluted to [Al] = 0.02 M with PhF.

6.1.4 Experimental Section

Purification of Reagents. Pyridine (Sigma Aldrich), fluorobenzene (Oakwood), and bromobenzene (Sigma Aldrich) were all distilled from CaH_2 under N_2 and stored over activated 4Å molecular sieves (20% w:v) for several days prior to use. Tetrahydrofuran (Sigma Aldrich) was purified by passage through activated alumina under N_2 and stored over activated sieves for several days prior to use. 2,2'-Bipyridine (Sigma Aldrich) was used as received but stored in a glove-box as it is hygroscopic. Octamethyltrisiloxane (Sigma Aldrich) was used as received and stored in a glovebox prior to use.

ESI-MS Experiments. In a typical procedure, a stock solution (~3 mL) was prepared from MAO (0.75 mL of ~1.0 M), and the amount of a PhF solution of OMTS (0.5 mL of 0.015 M) needed to give an Al:OMTS ratio of ~100:1. After mixing, the stock solution was further diluted with PhF to provide a final solution ca. 1.5 mM in Al. The same procedure was used to obtain the THF, pyridine, and 2,2'-bipyridine mixture. This solution was analyzed using a Micromass QTOF *micro* mass spectrometer via pumping it at ca. 40 μL/min through PTFE tubing (1/16" o.d., 0.005" i.d.) to the ESI-MS probe and source using a syringe pump. The capillary voltage was set at 2700 V with source and desolvation gas temperature at 85 °C and 185 °C, respectively, with the desolvation gas flow at 400 L/hr. MS/MS data were obtained on product ion spectra using argon as the collision gas and a voltage range of 2-100 V.

Portions from this Section 6.2 have been previously published in "Strategies for avoiding saturation effects in ESI-MS" A.A.J Wei, A Joshi, Y Chen, and J. S McIndoe, International Journal of Mass Spectrometry, 450, 2020, 1163062.

6.2 Strategies for avoiding saturation effects in ESI-MS

All instruments with detectors are prone to saturation effects at high concentration, and mass spectrometers are no exception. The very high sensitivity of mass spectrometry makes the onset of saturation occur at lower concentrations than other methods, and in cases where the analyte of interest is very reactive, concentrations at which saturation can be problematic may be necessary to ensure decomposition is mitigated. A variety of detuning strategies can be employed to reduce saturation effects in the context of electrospray ionization mass spectrometry (ESI-MS), including lowering voltages on detector or capillary, increasing cone gas flow rates, or adjusting the probe position.[97] A combination of strategies generally allows researchers to make the best possible compromises when studying compounds at relatively high concentrations.

In this study, we primarily examined the trityl carbocation, $[Ph_3C]^+$, a reactive ionic compound used to abstract hydride or methide.[275] It is stable in the presence of a weakly coordinating anion (in this case, $[B(C_6F_5)_4]^-$), and as it is permanently positively charged, it is easy to detect using electrospray ionization mass spectrometry (ESI-MS). A common issue encountered for mass spectrometric analyses of highly reactive chemicals is sample decomposition at lower concentrations. As for trityl carbocation, data acquisition becomes challenging when the sample is at micromolar concentrations. An alternative solution is necessary when diluting the concentration is simply impractical. This section details how

the use of different diameter of cone sizes helps to detune the instrumental settings with a quadrupole time-of-flight (QTOF) mass spectrometer.

6.2.1 Cone size

The ion count, as seen on the spectrum, correlates to the number of ions entering from the sampling cone of the mass spectrometer. Tuning the number of incoming ions is an effective way to avoid saturation as it affects the ion transmission efficiency[276] and detunes the sensitivity of the instrument. Two cones, with diameters of 0.80 mm, the cone that is more commonly used for mass spectrometric experiments, and 0.36 mm, the less commonly used, were experimented with, and the effect of the cone size was investigated (Figure 6.7).

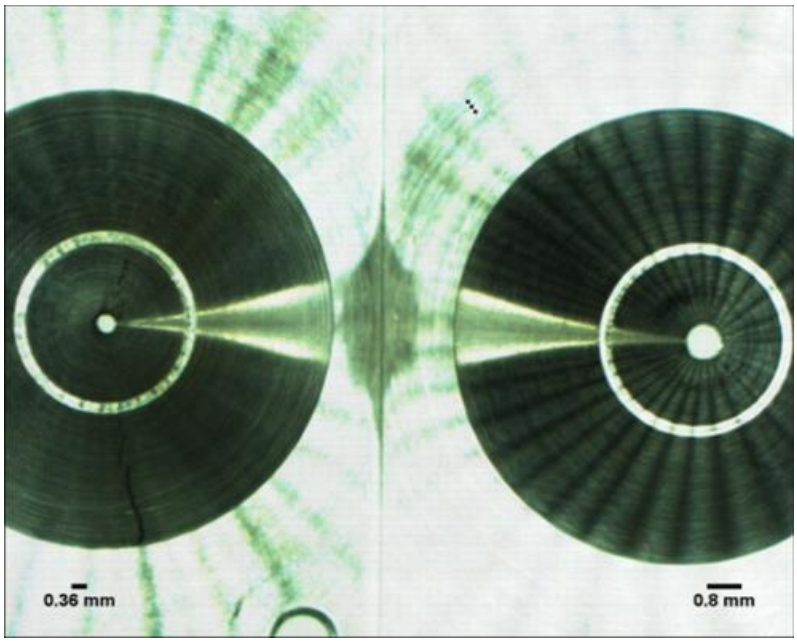

Figure 6.7 Two different cones used for the study.

Comparing the two cone sizes, experimental results showed the dramatic effect caused by the large difference in the number of ions entering the mass spectrometer (Figure 6.8). A

smaller cone size that effectively avoids the saturation issue is used for acquiring experimental results.

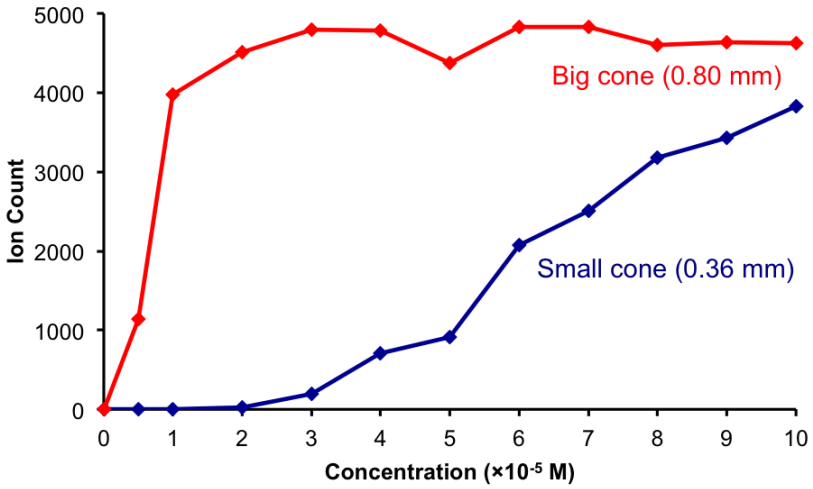

Figure 6.8 A graph where the calibration curves where the probe position the MCP detector voltage, the capillary voltage, and the cone gas flow all held constant and only the cone size changed.

6.2.2 Experimental

Experiments were performed with a Waters Micromass Q-ToF Micro Mass Spectrometer. Trityl tetrakis(pentafluorophenyl)borate, $[Ph_3C]^+[B(C_6F_5)_4]^-$, (1.0 mg, 1.0×10^{-4} mol) was weighed out and fluorobenzene (10 mL) was added to prepare a solution with a concentration of 100 μM (1.0×10^{-4} M). Fluorobenzene was dried with calcium hydride (CaH_2) overnight and distilled, kept over 4 Å activated molecular sieves prior to use to get rid of traces of moisture, and the sample was prepared in a glovebox under nitrogen atmosphere to avoid exposure to oxygen. Calibration curves were generated via the external calibration method. Twelve sample concentrations from 5 to 100 μM (5.0×10^{-6} to 1×10^{-4}) were prepared upon further dilution. Through a PTFE tubing that is connected directly from the glovebox into the mass spectrometer, sample was then injected via direct

sample infusion from the inside of the glovebox with a 1 mL syringe and a syringe pump set at a flow rate of 20 μL/min. For each parameter adjusted, a different ESI-MS(+) spectrum was acquired for one minute, where an average the total ion count at the ion peak *m/z* 243 Da was taken. A plot of ion intensity vs. concentration was generated.

Portions from Section 6.3 have been previously published in "Competitive Ligand Exchange and Dissociation in Ru Indenyl Complexes" R.G. Belli, Y Wu, H Ji, A Joshi, L.P.E. Yunker, J.S McIndoe and L Rosenberg, Inorganic Chemistry, 2019, 58, 747−755.

6.3 Competitive Ligand Exchange and Dissociation in Ru Indenyl Complexes

A ruthenium complex $[Ru(\eta^5\text{ -indenyl})(NCPh)(PPh_3)_2]^+$(**1**) that is used by Rosenberg group as a catalyst precursor for hydrophosphination was studied by ESI-MS.[5] Since the complex **1** is charged, the study of this complex via ESI-MS is straightforward. Using PSI-ESI-MS ligand substitution reactions were performed on **1** upon addition of a secondary phosphine PPh_2H at three different temperatures. The ligand substitution was over in 3 minutes at 60 °C (Figure 6.11) as compared to 60 mins at 30 °C (Figure 6.9).

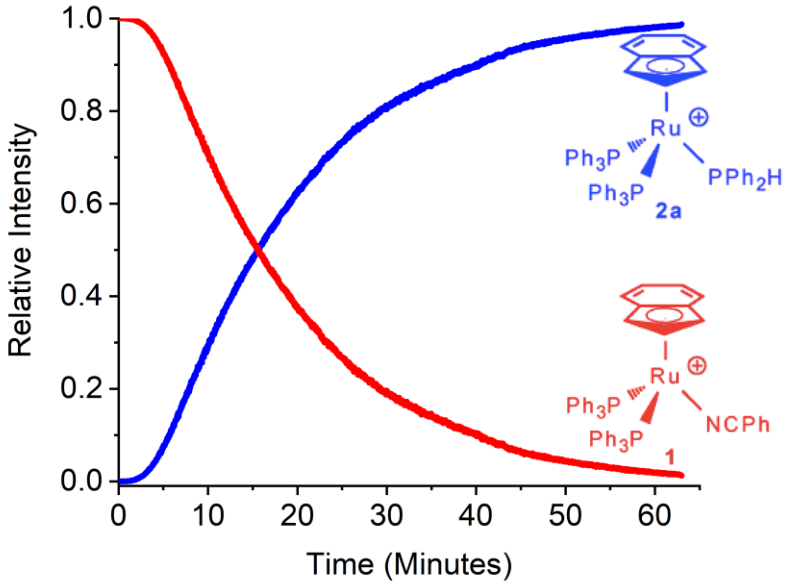

Figure 6.9 Experiment showing consumption of **1** in its reaction with 10 equiv. of PPh_2H at 30°C in PhF, as monitored by PSI-ESI-MS.

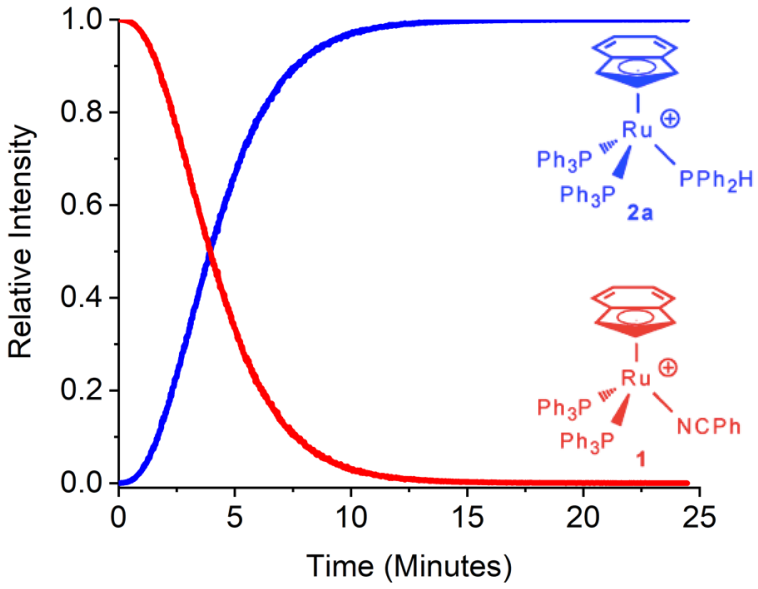

Figure 6.10 Experiment showing consumption of **1** in its reaction with 10 equiv. of PPh_2H at 45°C in PhF, as monitored by PSI-ESI-MS.

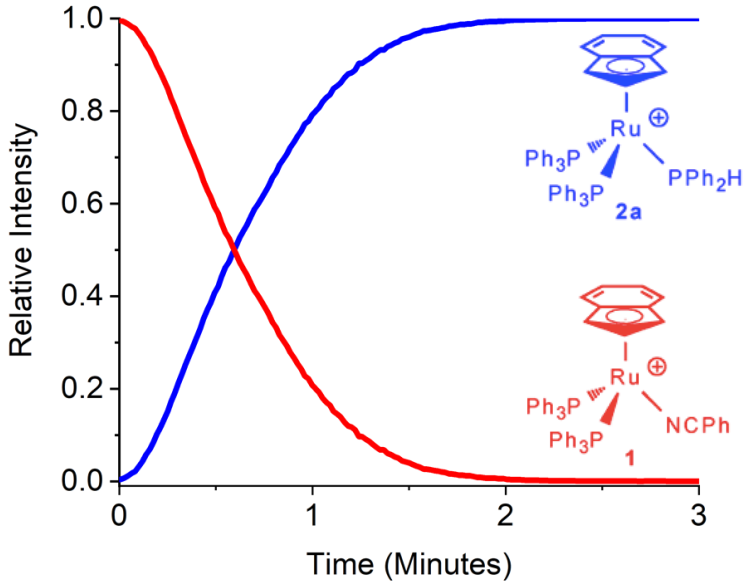

Figure 6.11 Experiment showing consumption of **1** in its reaction with 10 equiv. of PPh_2H at 60°C in PhF, as monitored by PSI-ESI-MS.

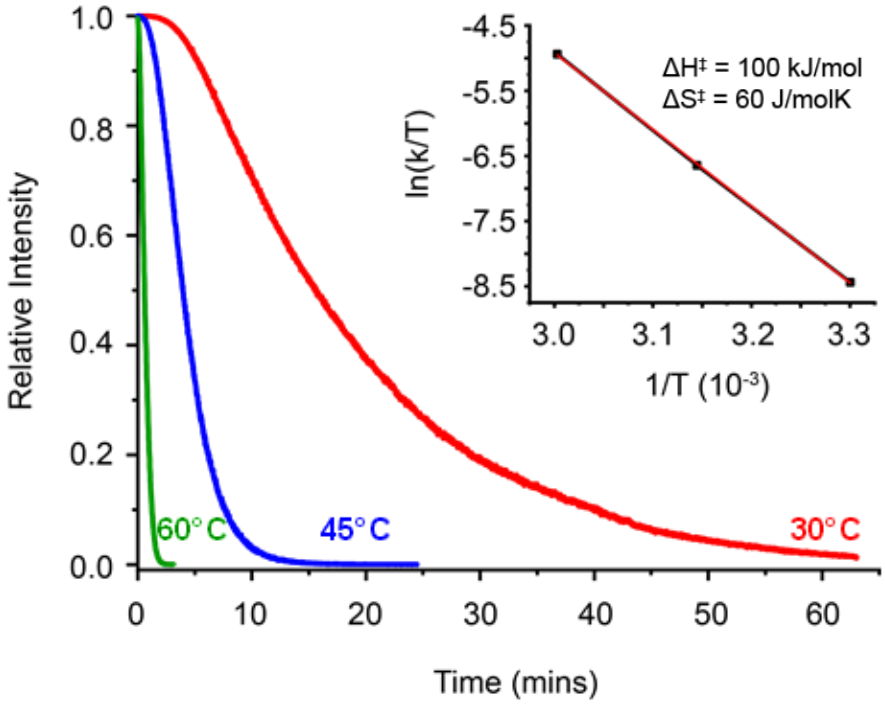

Figure 6.12 Preliminary experiments showing consumption of **1** in its reaction with 10 equiv. of PPh_2H at 30°C (red), 45°C (blue), and 60°C (green) in PhF, as monitored by PSI-ESI-MS.

In Figure 6.12, slight induction periods were observed for the 45°C and 30°C runs and are attributed to the delay between the addition of phosphine to the solution and the time it takes for the mixed solution to move into the mass spectrometer (about 10-20 s). Inset in Figure 6.12 shows an Eyring plot with calculated activation parameters; the large positive $\Delta S^{\ddagger}$ provides evidence for the dissociative substitution mechanism. The PSI-ESI-MS data also correlated very nicely to the $^{31}P\{^{1}H\}$ NMR experiments by the Rosenberg group. The two techniques require two different conditions, with sample concentration being the most striking difference as the NMR sample requires higher concentration than the ESI-MS sample. ESI-MS experiment also produces one spectrum per second, while the $^{31}P\{^{1}H\}$ NMR experiment gave one spectrum (128 scans) per 20 min. However, the kinetic profiles from both the techniques are almost identical, given the factor of three million between concentrations used for the MS and NMR experiments.

6.4 Current and Future work

Most of the experiments on MAO discussed in previous chapters are to be done in the ESI negative mode. That said, it bears mentioning that these negative ion species only account for active species in an MAO cluster, i.e., species that react with OMTS readily. The anion $[(MeAlO)_{16}(Me_3Al)_6Me]^-$ that is formed upon the addition of OMTS to MAO is not believed to be the only species present; there are likely neutrals in MAO which are not observed by our technique. These species remain undetected by ESI-MS as they do not lose the $[Me_2Al]^+$ unit. An important question that remains is whether the neutrals in MAO behave like MAO anions when it comes to processes such as aging and oxidation. It is a question worthy of future experimentation and one that will comprise the ongoing research

problem. The challenge that remains is to find a way in which we can observe these neutral MAO species via ESI-MS.

Though our group has a long history of using charged tags to investigate neutral species using ESI-MS[17,87,277] neutral MAO species have not been studied via charge tagging. Recently Zaccaria and co-workers reported phenol modified MAO by the addition of 2,6-di-tert-butyl-4-methylphenol (BHT).[172] As shown in Scheme 6.1, the BHT fragment after addition to MAO attaches to the MAO cluster, and this process occurs with the evolution of methane as a by-product.

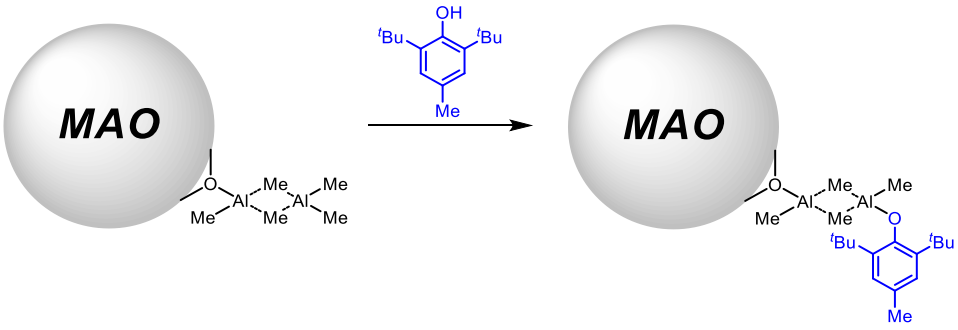

Scheme 6.1 Modifying MAO after addition of neutral BHT.

We hypothesize that if one can charge tag the BHT fragment, it would do the similar chemistry as the neutral BHT and lead to the analysis of the neutral MAO species.

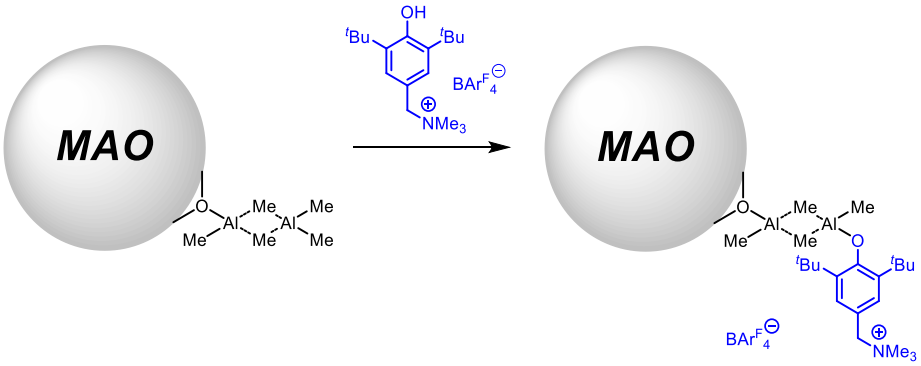

Scheme 6.2 Modifying MAO after addition of charge tagged BHT.

The synthesis of the charge tag involves the addition of methyl iodide to 2,6-di-tert-butyl-4-(dimethylaminomethyl)phenol followed by the exchange of the counter anion from iodide to a weakly coordinating anion such as BArF (Scheme 6.3).

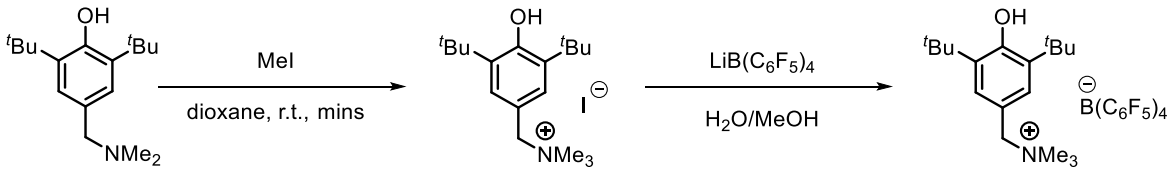

Scheme 6.3 Synthesis of charge tagged BHT.

The ESI-MS spectra confirm the formation of the charge tag at *m/z* 279 in positive mode and the counter anion $[B(C_6F_5)]^-$ at *m/z* 679.

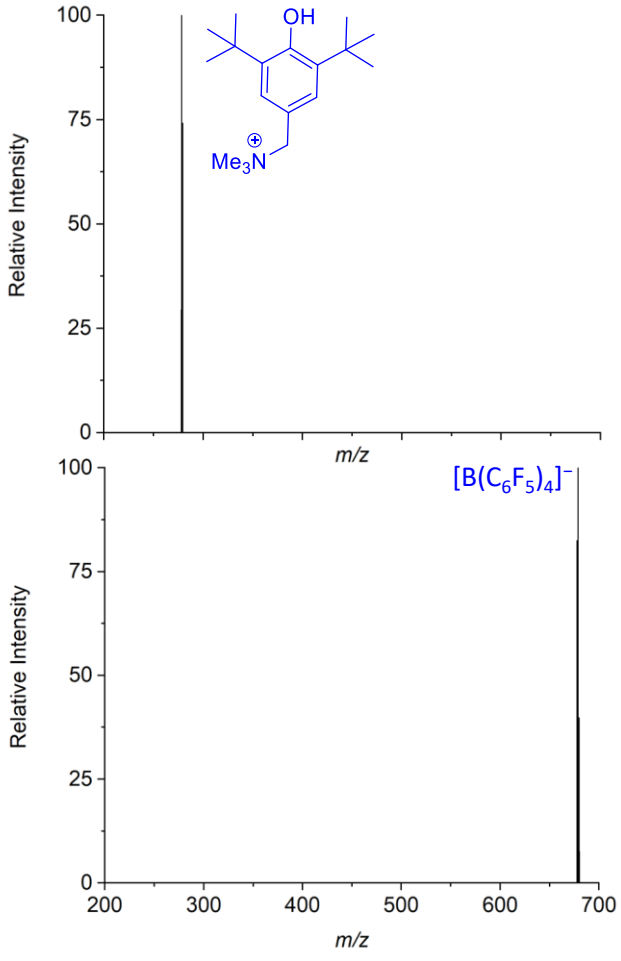

Figure 6.13 ESI-MS spectra in a) positive mode and b) negative mode of charged tag BHT.

The addition of Me_3Al to the charge tagged BHT leads to the formation of species with *m/z* 334, which could be assigned to $(CH_3)_3NCH_2C_6H_2[C(CH_3)_3]_2OAlMe_2$ (Figure 6.14).

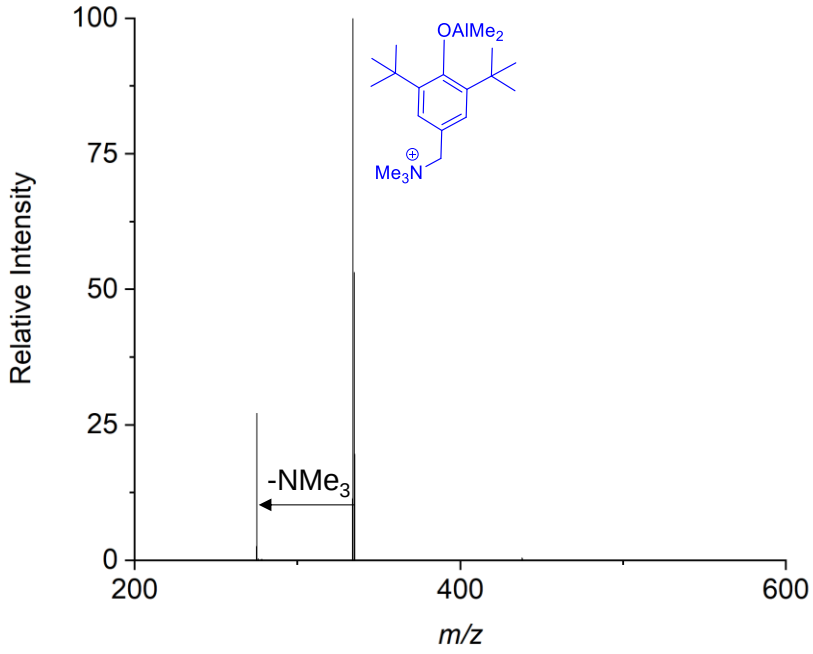

Figure 6.14 ESI-MS in positive mode after the addition of Me_3Al to charge tagged BHT

This charge tag would further be added to MAO such that the charge tagged unit exchanges with the Me group in an MAO cluster and result in the incorporation of a positive charge in an MAO cluster. So far, all the preliminary attempts to tag MAO using this charge tag have been unsuccessful. The instability of the current charge tag in the presence of R_3Al, where the loss of Me_3N occurs readily in the source, even at low cone voltages, is concerning. Future work could be focussed on adding a spacer in the current charge tag to avoid NMe_3 elimination.

Another way to incorporate a charge tag is via synthesis of Me_2AlR (where Me_2AlR = $[Me_2Al(CH_2)_nNR_3][B(Ar_F)_4]$ (where n is a large number to avoid both steric and inductive effects at Al as well as any possible intra-molecular, elimination, etc. reactions). This

material could be generated via hydroalumination of a charged tag alkene $[H_2C=CH(CH_2)_nNR_3][B(Ar_F)_4]$. The resulting charge tag could then incorporate a charge in MAO via alkyl exchange.[168] The choice of charge tag is very specific as the steric and electronic effects are crucial elements that need to be addressed in their design. As mentioned previously, charge tagging an MAO cluster would allow for a better estimation of the molecular mass.

Chapter 7 Conclusions

My work explored the use of electrospray ionization mass spectrometry (ESI-MS) to analyze air and moisture sensitive samples. Chapter 1 summarized the advances by the various groups made to analyze air and moisture sensitive samples without decomposition via mass spectrometry. From this, the biggest breakthrough in the field had a glovebox next to a mass spectrometer such that samples could be sampled directly from inside the glovebox to the mass spectrometer via PEEK or PTFE tubing. This setup was used in addition to an ESI source for all my work.

Chapter 2 summarized my work on the modification of MAO after the addition of R_3Al (R = Et, *i*Bu, Oct). In the case of *i*Bu_3Al addition, rapid reactivity followed by statistical equilibration was observed. The addition of Et_3Al resulted in the highest number of substitutions of the methyl group in MAO. The higher substitutions for the ethyl suggested that the exchange was facile not just for the most exposed methyl groups on the oligomer but possibly also for Me groups, which are less labile by incorporation into the aluminoxane structure. The Oct_3Al addition gave the least number of substitutions, and this result was unexpected as the octyl group is intermediate in steric hindrance (i.e., Et < *n*Oct < *i*Bu) and one would have expected more substitutions of octyl compared to isobutyl. Pressurized sample infusion was used to study the alkyl exchange process in real-time. These results are relevant to get insight into modified MAO (MMAO), which are routinely used as an alternative to MAO in polymerization studies.

Since its discovery in 1973 by Sinn and Kaminsky, the structure and composition of MAO has been a mystery. The synthesis of prominent activator MAO was tracked by ESI-MS in

real-time, and the results are summarized in Chapter 3. The reaction of water to TMA followed by ionization by OMTS produced a solution dominated by the same ion [**16**,**6**]$^-$ observed in commercial MAO samples, and this was remarkable considering the differences in reaction conditions between a small syringe and an industrial-scale reactor. Computationally, a new sheet structure was located for this ion. The approach and results in Chapter 3 are a revealing first step towards understanding and optimizing the formation of those components of MAO most capable of behaving as activators.

Nitrogen generators are gaining attention for use in mass spectrometry labs as they supply nitrogen on demand and save a significant amount of money. As summarized in Chapter 4, an N_2 generator was installed as a source of desolvation gas, and in the case of an indicator developed for detection of O_2, the extent of oxidation was <4 % at the highest flow rate examined. The extremely reactive ions such as the $[Cp_2ZrMe]^+$ complex was more reactive towards oxygen and water, and using such ions as probes, the source of contamination within the spectrometer was readily discovered. The reduction in the collision gas pressure largely eliminates hydrolysis in the collision cell, and reliable MS/MS was collected.

A study into hexene polymerization using $[Cp_2ZrMe_2AlMe_2][B(C_6F_5)_4]$ was initiated, and it revealed unanticipated complexity and identification of a new pathway for catalyst deactivation – formation of dimethylalane stabilized complexes which are resistant to further insertion.

In the future, studying MAO via charge tagging will be attempted as that could provide a more accurate estimation of the molecular mass of MAO. Overall, the work in this thesis demonstrates how to extract meaningful data on elusive and extremely reactive compounds

and will be of great interest to the catalysis and analysis communities looking to extract new information from complex and previously intractable systems.

Bibliography

(1) Trefz, T. K.; Henderson, M. A.; Wang, M. Y.; Collins, S.; McIndoe, J. S. Mass Spectrometric Characterization of Methylaluminoxane. *Organometallics* **2013**, *32* (11), 3149–3152.

(2) Trefz, T. K.; Henderson, M. A.; Linnolahti, M.; Collins, S.; McIndoe, J. S. Mass Spectrometric Characterization of Methylaluminoxane-Activated Metallocene Complexes. *Chem. - A Eur. J.* **2015**, *21* (7), 2980–2991.

(3) Zijlstra, H. S.; Linnolahti, M.; Collins, S.; McIndoe, J. S. Additive and Aging Effects on Methylalumoxane Oligomers. *Organometallics* **2017**, *36* (9), 1803–1809.

(4) Zijlstra, H. S.; Collins, S.; McIndoe, J. S. Oxidation of Methylalumoxane Oligomers. *Chem. - A Eur. J.* **2018**, *24* (21), 5506–5512.

(5) Belli, R. G.; Wu, Y.; Ji, H.; Joshi, A.; Yunker, L. P. E.; McIndoe, J. S.; Rosenberg, L. Competitive Ligand Exchange and Dissociation in Ru Indenyl Complexes. *Inorg. Chem.* **2019**, *58* (1).

(6) Zijlstra, H. S.; Joshi, A.; Linnolahti, M.; Collins, S.; McIndoe, J. S. Modifying Methylalumoxane via Alkyl Exchange. *Dalt. Trans.* **2018**, *47* (48).

(7) Joshi, A.; Donnecke, S.; Granot, O.; Shin, D.; Collins, S.; Paci, I.; Scott McIndoe, J. Reactive Metallocene Cations as Sensitive Indicators of Gas-Phase Oxygen and Water. *Dalt. Trans.* **2020**, *49* (21), 7028–7036.

(8) Joshi, A.; Zijlstra, H. S.; Collins, S.; McIndoe, J. S. Catalyst Deactivation Processes during 1-Hexene Polymerization. *ACS Catal.* **2020**, 7195–7206.

(9) Dole, M.; Mack, L. L.; Hines, R. L.; Mobley, R. C.; Ferguson, L. D.; Alice, M. B. Molecular Beams of Macroions. *J. Chem. Phys.* **1968**, *49* (5), 2240–2249.

(10) Yamashita, M.; Fenn, J. B. Electrospray Ion Source. Another Variation on the Free-Jet Theme. *J. Phys. Chem.* **1984**, *88* (20), 4451–4459.

(11) Yamashita, M.; Fenn, J. B. Negative Ion Production with the Electrospray Ion Source. *J. Phys. Chem.* **1984**, *88* (20), 4671–4675.

(12) Whitehouse, C. M.; Dreyer, R. N.; Yamashita, M.; Fenn, J. B. Electrospray Interface for Liquid Chromatographs and Mass Spectrometers. *Anal. Chem.* **1985**, *57* (3), 675–679.

(13) Fenn, J. B.; Mann, M.; Meng, C. K.; Wong, S. F.; Whitehouse, C. M. Electrospray Ionization for Mass Spectrometry of Large Biomolecules. *Science*. 1989.

(14) Iribarne, J. V; Thomson, B. A. On the Evaporation of Small Ions from Charged Droplets. *J. Chem. Phys.* **1976**, *64* (6), 2287–2294.

(15) Henderson, W.; McIndoe, J. S. *Mass Spectrometry of Inorganic, Coordination, and Organometallic Compounds: Tools- Techniques-Tips*; John Wiley & Sons., 2005.

(16) McQuinn, K.; Hof, F.; McIndoe, J. S. Direct Observation of Ion Evaporation from

a Triply Charged Nanodroplet. *Chem. Commun.* **2007**, No. 40, 4099–4101.

(17) Ahmadi, Z.; McIndoe, J. S. A Mechanistic Investigation of Hydrodehalogenation Using ESI-MS. *Chem. Commun.* **2013**, *49* (98), 11488–11490.

(18) Vikse, K. L.; Ahmadi, Z.; Manning, C. C.; Harrington, D. A.; McIndoe, J. S. Powerful Insight into Catalytic Mechanisms through Simultaneous Monitoring of Reactants, Products, and Intermediates. *Angew. Chemie Int. Ed.* **2011**, *50* (36), 8304–8306.

(19) Vikse, K.; Khairallah, G. N.; McIndoe, J. S.; O'Hair, R. A. J. Fixed-Charge Phosphine Ligands to Explore Gas-Phase Coinage Metal-Mediated Decarboxylation Reactions. *Dalt. Trans.* **2013**, *42* (18), 6440–6449.

(20) Thomas, G. T.; Janusson, E.; Zijlstra, H. S.; Mcindoe, J. S. Step-by-Step Real Time Monitoring of a Catalytic Amination Reaction †. *Chem. Commun* **2019**, *55*, 11727.

(21) Omari, I.; Zhu, H.; McGarvey, G. B.; McIndoe, J. S. Acid-Selective Mass Spectrometric Analysis of Petroleum Fractions. *Int. J. Mass Spectrom.* **2019**, *435*, 315–320.

(22) Vikse, K. L.; Henderson, M. A.; Oliver, A. G.; McIndoe, J. S. Direct Observation of Key Intermediates by Negative-Ion Electrospray Ionisation Mass Spectrometry in Palladium-Catalysed Cross-Coupling. *Chem. Commun.* **2010**, *46* (39), 7412–7414.

(23) Dawson, P. H. Quadrupole Mass Analyzers: Performance, Design and Some Recent Applications. *Mass Spectrom. Rev.* **1986**, *5* (1), 1–37.

(24) Guilhaus, M.; Selby, D.; Mlynski, V. Orthogonal Acceleration Time-of-Flight Mass Spectrometry. *Mass Spectrom. Rev.* **2000**, *19* (2), 65–107.

(25) Guilhaus, M.; Mlynski, V.; Selby, D. Perfect Timing: Time-of-Flight Mass Spectrometry†. *Rapid Commun. Mass Spectrom.* **1997**, *11* (9), 951–962.

(26) Standing, K. G. Timing the Flight of Biomolecules: A Personal Perspective. *Int. J. Mass Spectrom.* **2000**, *200* (1), 597–610.

(27) Dawson, J. H. J.; Guilhaus, M. Orthogonal-Acceleration Time-of-Flight Mass Spectrometer. *Rapid Commun. Mass Spectrom.* **1989**, *3* (5), 155–159.

(28) Chernushevich, I. V.; Ens, W.; Standing, K. G. Peer Reviewed: Orthogonal-Injection TOFMS for Analyzing Biomolecules. *Anal. Chem.* **1999**, *71* (13), 452A-461A.

(29) Wiza, J. L. *MICROCHANNEL PLATE DETECTORS*; 1979; Vol. 162.

(30) Chernushevich, I. V; Loboda, A. V; Thomson, B. A. An Introduction to Quadrupole–Time-of-Flight Mass Spectrometry. *J. Mass Spectrom.* **2001**, *36* (8), 849–865.

(31) McLafferty, F. W. Tandem Mass Spectrometry. *Science (80-.).* **1981**, *214* (4518), 280 LP – 287.

(32) Dempster, A. J. A New Method of Positive Ray Analysis. *Phys. Rev.* **1918**, *11* (4),

316–325.

(33) Vikse, K. L.; Scott McIndoe, J. Ionization Methods for the Mass Spectrometry of Organometallic Compounds. *J. Mass Spectrom.* **2018**, *53* (10), 1026–1034.

(34) Traeger, J. C. The Development of Electron Ionization. In *The Encyclopedia of Mass Spectrometry*; Gross, M. L., Caprioli, R. M., Eds.; Elsevier: Boston, 2016; pp 77–82.

(35) King, R. B. Mass Spectra of Organometallic Compounds. I. Metal Carbonyl Complexes of Tris(Dimethylamino)Phosphine. *J. Am. Chem. Soc.* **1968**, *90* (6), 1412–1417.

(36) Cloke, F. G. N.; Day, J. P.; Greenway, A. M.; Seddon, K. R.; Shimran, A. A.; Swain, A. C. Mass Spectrometric Studies of Some Bis(H5-Pentamethylcyclopentadienyl)Metal Derivatives, and Related Complexes. *J. Organomet. Chem.* **1989**, *372* (2), 231–249.

(37) Barfuss, S.; Emrich, K.-H.; Hirschwald, W.; Dowben, P. A.; Boag, N. M. A Mass Spectrometric Investigation of Chloro-, Bromo- and Methyl-Ferrocenes by Electron and Photon Impact Ionisation. *J. Organomet. Chem.* **1990**, *391* (2), 209–218.

(38) Zanello, P.; Opromolla, G.; Giorgi, G.; Sasso, G.; Togni, A. Redox Behaviour of Ferrocene Derivatives VIII. 1,1′-Bis(Diphenylphosphino)Ferrocenes. *J. Organomet. Chem.* **1996**, *506* (1), 61–65.

(39) Messerle, L.; Malus, L. M.; Hatch, P. J. An Inexpensive Sample Holder for Storage and Introduction of Air-Sensitive Organometallic Compounds into a Mass Spectrometer with Inert-Atmosphere Blanketing. *J. Chem. Educ.* **1989**, *66* (7), 618.

(40) Tse, R. S.; Wong, S. C. Mass Spectrometer Inlet Device for Highly Air-Sensitive Liquids and Solids. *Anal. Chem.* **1974**, *46* (7), 967–968.

(41) Liang, Z.; Marshall, A. G.; Marçalo, J.; Marques, N.; de Matos, A. P.; Santos, I.; Weil, D. A. Laser Desorption Fourier Transform Mass Spectrometric Analysis of Organoactinides: Uranium and Thorium Polypyrazolylborates. *Organometallics* **1991**, *10* (8), 2794–2797.

(42) Bjarnason, A.; Desenfants, R. E.; Barr, M. E.; Dahl, L. F. Fourier Transform Mass Spectrometry of Several Organometallic Complexes: Laser Desorption versus Electron Impact Ionization. *Organometallics* **1990**, *9* (3), 657–661.

(43) Yunker, L. P. E.; Stoddard, R. L.; McIndoe, J. S. Practical Approaches to the ESI-MS Analysis of Catalytic Reactions. *J. Mass Spectrom.* **2014**, *49* (1), 1–8.

(44) Penafiel, J.; Hesketh, A. V.; Granot, O.; Scott McIndoe, J. Electron Ionization Mass Spectrometric Analysis of Air- and Moisture-Sensitive Organometallic Compounds. *Dalt. Trans.* **2016**, *45* (39), 15552–15556.

(45) Zhang, Z.; Pawliszyn, J. Sampling Volatile Organic Compounds Using a Modified Solid Phase Microextraction Device. *J. High Resolut. Chromatogr.* **1996**, *19* (3), 155–160.

(46) Beceiro-González, E.; Guimaraes, A.; Alpendurada, M. F. Optimisation of a Headspace-Solid-Phase Micro-Extraction Method for Simultaneous Determination of Organometallic Compounds of Mercury, Lead and Tin in Water by Gas Chromatography-Tandem Mass Spectrometry. *J. Chromatogr. A* **2009**, *1216* (29), 5563–5569.

(47) Cody, R. B.; Laramée, J. A.; Durst, H. D. Versatile New Ion Source for the Analysis of Materials in Open Air under Ambient Conditions. *Anal. Chem.* **2005**, *77* (8), 2297–2302.

(48) Gross, J. H. Direct Analysis in Real Time-a Critical Review on DART-MS. *Anal. Bioanal. Chem.* **2014**, *406* (1), 63–80.

(49) Young, J. D.; Khan, M. A.; Powell, D. R.; Wehmschulte, R. J. M-Terphenylaluminum and -Gallium Compounds: Synthesis and Conversion into Low-Coordinate Organogallium Cations. *Eur. J. Inorg. Chem.* **2007**, *2007* (12), 1671–1681.

(50) Borges, D. L. G.; Sturgeon, R. E.; Welz, B.; Curtius, A. J.; Mester, Z. Ambient Mass Spectrometric Detection of Organometallic Compounds Using Direct Analysis in Real Time. *Anal. Chem.* **2009**, *81* (23), 9834–9839.

(51) Mazzotta, M. G.; Young, J. O. E.; Evans, J. W.; Dopierala, L. A.; Claytor, Z. A.; Smith, A. C.; Snyder, C.; Tice, N. C.; Smith, D. L. Direct Analysis in Real Time Mass Spectrometry of Fused Ring Heterocyclic Organometallic Compounds. *Anal. Methods* **2015**, *7* (9), 4003–4007.

(52) Beckey, H. D.; Schulten, H. -R. Field Desorption Mass Spectrometry. *Angew. Chemie Int. Ed. English* **1975**, *14* (6), 403–415.

(53) Games, D. E.; Jackson, A. H.; Kane-Maguire, L. A. P.; Taylor, K. Field Desorption Mass Spectrometry of Organometallic Complex Salts. *J. Organomet. Chem.* **1975**, *88* (3), 345–349.

(54) Games, D. E.; Kane-Maguire, L. A. P.; Sweigart, D. A. Field Desorption Mass Spectra of [M(CO)3(η-Arene)]X (M□Mn, Re; X□BF4, PF6) Salts. *J. Organomet. Chem.* **1982**, *234* (3), 323–327.

(55) McEwen, C. N.; Ittel, S. D. Field Desorption Mass Spectrometry of Air Sensitive Transition Metal Complexes. *Org. Mass Spectrom.* **1980**, *15* (1), 35–37.

(56) Schulten, H. R.; Monkhouse, P. B.; Müller, R. Laser-Assisted Field Desorption Mass Spectrometry of Inorganic and Organometallic Compounds. *Anal. Chem.* **1982**, *54* (4), 654–659.

(57) Beckey, H. D.; Heindrichs, A.; Winkler, H. U. Some New Field Desorption Techniques. *Int. J. Mass Spectrom. Ion Phys.* **1970**, *3* (6), A9–A11.

(58) Linden, H. B. Liquid Injection Field Desorption Ionization: A New Tool for Soft Ionization of Samples Including Air-Sensitive Catalysts and Non-Polar Hydrocarbons. *Eur. J. Mass Spectrom.* **2004**, *10* (4), 459–468.

(59) Belli, R. G.; Burton, K. M. E.; Rufh, S. A.; McDonald, R.; Rosenberg, L. Inner- and Outer-Sphere Roles of Ruthenium Phosphido Complexes in the

Hydrophosphination of Alkenes. *Organometallics* **2015**, *34* (23), 5637–5646.

(60) Gross, J. H.; Nieth, N.; Linden, H. B.; Blumbach, U.; Richter, F. J.; Tauchert, M. E.; Tompers, R.; Hofmann, P. Liquid Injection Field Desorption/Ionization of Reactive Transition Metal Complexes. *Anal. Bioanal. Chem.* **2006**, *386* (1), 52–58.

(61) Dransfield, T. A.; Nazir, R.; Perutz, R. N.; Whitwood, A. C. Liquid Injection Field Desorption/Ionization of Transition Metal Fluoride Complexes. *J. Fluor. Chem.* **2010**, *131* (11), 1213–1217.

(62) Chen, E. Y.-X.; Marks, T. J. Cocatalysts for Metal-Catalyzed Olefin Polymerization: Activators, Activation Processes, and Structure−Activity Relationships. *Chem. Rev.* **2000**, *100* (4), 1391–1434.

(63) Fagan, P. J.; Manriquez, J. M.; Maatta, E. A.; Seyam, A. M.; Marks, T. J. Synthesis and Properties of Bis(Pentamethylcyclopentadienyl) Actinide Hydrocarbyls and Hydrides. A New Class of Highly Reactive f-Element Organometallic Compounds. *J. Am. Chem. Soc.* **1981**, *103* (22), 6650–6667.

(64) Breunig, H. J.; Linden, H. B.; Moldovan, O. Liquid Injection Field Desorption Ionization Mass Spectrometry of Cyclic Metal Carbonyl Complexes with Tetra-Antimony Ligands. *J. Am. Soc. Mass Spectrom.* **2013**, *24* (1), 164–166.

(65) Linden CMS https://www.linden-cms.de/.

(66) Miller, J. M. Fast Atom Bombardment Mass Spectrometry (FAB MS) of Organometallic, Coordination, and Related Compounds. *Mass Spectrom. Rev.* **1990**, *9* (3), 319–347.

(67) Miller, J. M. Fast-Atom Bombardment Mass Spectrometry and Related Techniques. *Adv. Inorg. Chem.* **1984**, *28* (C), 1–27.

(68) Bruce, M. I.; Liddell, M. J. Applications of Fast Atom Bombardment Mass Spectrometry (FAB MS) to Organometallic and Coordination Chemistry. *Appl. Organomet. Chem.* **1987**, *1* (3), 191–226.

(69) Van Breemen, R. B.; Martin, L. B.; Schreiner, A. F. Comparison of Electron Impact, Desorption Chemical Ionization, Field Desorption, and Fast Atom Bombardment Mass Spectra of Nine Monosubstituted Group VI Metal Carbonyls. *Anal. Chem.* **1988**, *60* (13), 1314–1318.

(70) Stoll, R. G.; Harvan, D. J.; Hass, J. R. Liquid Secondary Ion Mass Spectrometry with a Focussed Primary Ion Source. *Int. J. Mass Spectrom. Ion Process.* **1984**, *61* (1), 71–79.

(71) Barber, M.; Bordoli, R. S.; Sedgwick, R. D.; Tyler, A. N. Fast Atom Bombardment of Solids as an Ion Source in Mass Spectrometry. *Nature* **1981**, *293* (5830), 270–275.

(72) Abdul-Sada, A. K.; Greenway, A. M.; Seddon, K. R. The Extent of Aggregation of Air-Sensitive Alkyllithium Compounds as Determined by Fast-Atom-Bombardment Mass Spectrometry. *J. Organomet. Chem.* **1989**, *375* (1), C17–C19.

(73) Guilhaus, M.; Brenton, A. G.; Beynon, J. H.; Theis, M.; Maercker, A. A

Technique for Introducing Air-Sensitive Compounds into a Mass Spectrometer and Its Application to the Study of Alkyllithium Compounds. *Org. Mass Spectrom.* **1985**, *20* (9), 592–594.

(74) Huang, M. W.; Chei, H. L.; Huang, J. P.; Shiea, J. Application of Organic Solvents as Matrixes to Detect Air-Sensitive and Less Polar Compounds Using Low-Temperature Secondary Ion Mass Spectrometry. *Anal. Chem.* **1999**, *71* (14), 2901–2907.

(75) Tanaka, K.; Waki, H.; Ido, Y.; Akita, S.; Yoshida, Y.; Yoshida, T.; Matsuo, T. Protein and Polymer Analyses up to m/z 100 000 by Laser Ionization Time-of-flight Mass Spectrometry. *Rapid Commun. Mass Spectrom.* **1988**, *2* (8), 151–153.

(76) Karas, M.; Bachmann, D.; Bahr, U.; Hillenkamp, F. Matrix-Assisted Ultraviolet Laser Desorption of Non-Volatile Compounds. *Int. J. Mass Spectrom. Ion Process.* **1987**, *78* (C), 53–68.

(77) Eelman, M. D.; Blacquiere, J. M.; Moriarty, M. M.; Fogg, D. E. Shining New Light on an Old Problem: Retooling MALDI Mass Spectrometry for Organotransition-Metal Catalysis. *Angew. Chemie Int. Ed.* **2008**, *47* (2), 303–306.

(78) Bailey, G. A.; Fogg, D. E. Confronting Neutrality: Maximizing Success in the Analysis of Transition-Metal Catalysts by MALDI Mass Spectrometry. *ACS Catal.* **2016**, *6* (8), 4962–4971.

(79) Bai, G.; Wei, P.; Stephan, D. W. Reductions of β-Diketiminato-Titanium (III) Complexes. *Organometallics* **2006**, *25* (10), 2649–2655.

(80) May, M. A.; Marshall, A. G. Inert Gas Purgebox for Fourier Transform Ion Cyclotron Resonance Mass Spectrometry of Air-Sensitive Solids. *Rev. Sci. Instrum.* **1994**, *65* (3), 612–616.

(81) Traeger, J. C. Electrospray Mass Spectrometry of Organometallic Compounds. *Int. J. Mass Spectrom.* **2000**, *200* (1), 387–401.

(82) Chen, P. Electrospray Ionization Tandem Mass Spectrometry in High-Throughput Screening of Homogeneous Catalysts. *Angew. Chemie - Int. Ed.* **2003**, *42* (25), 2832–2847.

(83) Jiráško, R.; Holčapek, M. Structural Analysis of Organometallic Compounds with Soft Ionization Mass Spectrometry. *Mass Spectrom. Rev.* **2011**, *30* (6), 1013–1036.

(84) Lipshutz, B. H.; Keith, J.; Buzard, D. J. An Electrospray Ionization Mass Spectrometry Study of the Aggregation States of Organocopper Complexes in Solution. *Organometallics* **1999**, *18* (9), 1571–1574.

(85) Schnegelsberg, C.; Bachmann, S.; Kolter, M.; Auth, T.; John, M.; Stalke, D.; Koszinowski, K. Association and Dissociation of Grignard Reagents RMgCl and Their Turbo Variant RMgCl·LiCl. *Chem. – A Eur. J.* **2016**, *22* (23), 7752–7762.

(86) Evans, W. J.; Johnston, M. A.; Greaves, J. Utility of Electrospray Mass Spectrometry for the Characterization of Air-Sensitive Organolanthanides and Related Species. *Organometallics* **2000**, *19* (21), 4258–4265.

(87) Vikse, K. L.; Woods, M. P.; McIndoe, J. S. Pressurized Sample Infusion for the Continuous Analysis of Air- And Moisture-Sensitive Reactions Using Electrospray Ionization Mass Spectrometry. *Organometallics* **2010**, *29* (23), 6615–6618.

(88) Lubben, A. T.; McIndoe, J. S.; Weller, A. S. Coupling an Electrospray Ionization Mass Spectrometer with a Glovebox: A Straightforward, Powerful, and Convenient Combination for Analysis of Air-Sensitive Organometallics. *Organometallics* **2008**, *27* (13), 3303–3306.

(89) Schade, M. A.; Fleckenstein, J. E.; Knochel, P.; Koszinowski, K. Charged Tags as Probes for Analyzing Organometallic Intermediates and Monitoring Cross-Coupling Reactions by Electrospray-Ionization Mass Spectrometry. *J. Org. Chem.* **2010**, *75* (20), 6848–6857.

(90) Thomas, G. T.; MacGillivray, L.; Dean, N. L.; Stoddard, R. L.; Yunker, L. P. E.; McIndoe, J. S. Confounding Contaminants in Mass Spectrometric Reaction Monitoring. *Int. J. Mass Spectrom.* **2019**, *441*, 14–18.

(91) Hesketh, A. V; Nowicki, S.; Baxter, K.; Stoddard, R. L.; McIndoe, J. S. Simplified Real-Time Mass Spectrometric Analysis of Reactions. *Organometallics* **2015**, *34* (15), 3816–3819.

(92) Jiang, J.; Zhang, H.; Li, M.; Dulay, M. T.; Ingram, A. J.; Li, N.; You, H.; Zare, R. N. Droplet Spray Ionization from a Glass Microscope Slide: Real-Time Monitoring of Ethylene Polymerization. *Anal. Chem.* **2015**, *87* (16), 8057–8062.

(93) Trefz, T. K.; Henderson, M. A.; Linnolahti, M.; Collins, S.; McIndoe, J. S. Mass Spectrometric Characterization of Methylaluminoxane-Activated Metallocene Complexes. *Chem. – A Eur. J.* **2015**, *21* (7), 2980–2991.

(94) Collins, S.; Linnolahti, M.; Zamora, M. G.; Zijlstra, H. S.; Rodríguez Hernández, M. T.; Perez-Camacho, O. Activation of Cp_2ZrX_2 (X = Me, Cl) by Methylaluminoxane As Studied by Electrospray Ionization Mass Spectrometry: Relationship to Polymerization Catalysis. *Macromolecules* **2017**, *50* (22), 8871–8884.

(95) Zijlstra, H. S.; Collins, S.; McIndoe, J. S. Oxidation of Methylalumoxane Oligomers. *Chem. - A Eur. J.* **2018**, *24* (21), 5506–5512.

(96) Trefz, T. K.; Henderson, M. A.; Wang, M. Y.; Collins, S.; McIndoe, J. S. Mass Spectrometric Characterization of Methylaluminoxane. *Organometallics* **2013**, *32* (11), 3149–3152.

(97) Wei, A. A. J.; Joshi, A.; Chen, Y.; McIndoe, J. S. Strategies for Avoiding Saturation Effects in ESI-MS. *Int. J. Mass Spectrom.* **2020**, *450*, 116306.

(98) Williams, D. B. G.; Lawton, M. Drying of Organic Solvents: Quantitative Evaluation of the Efficiency of Several Desiccants. *J. Org. Chem.* **2010**, *75* (24), 8351–8354.

(99) Joshi, A.; Donnecke, S.; Granot, O.; Shin, D.; Collins, S.; Paci, I.; Scott McIndoe, J. Reactive Metallocene Cations as Sensitive Indicators of Gas-Phase Oxygen and Water. *Dalt. Trans.* **2020**.

(100) O'Hair, R. A. J. The 3D Quadrupole Ion Trap Mass Spectrometer as a Complete Chemical Laboratory for Fundamental Gas-Phase Studies of Metal Mediated Chemistry. *Chem. Commun.* **2006**, No. 14, 1469–1481.

(101) Khairallah, G. N.; Meyer, M. M.; O'Hair, R. A. J.; Fattahi, A.; Schmidt, J.; Kass, S. R. Reactions of Doubly Deprotonated 2,6-Naphthalenedicarboxylic Acid with Alcohols: Proton Transfer versus Solvation. *Int. J. Mass Spectrom.* **2017**, *418*, 180–187.

(102) McEwen, C. N.; McKay, R. G.; Larsen, B. S. Analysis of Solids, Liquids, and Biological Tissues Using Solids Probe Introduction at Atmospheric Pressure on Commercial LC/MS Instruments. *Anal. Chem.* **2005**, *77* (23), 7826–7831.

(103) Naim, A.; Farenc, M.; Hubert-Roux, M.; Chavagnan, T.; Cirriez, V.; Welle, A.; Vantomme, A.; Kirillov, E.; Carpentier, J. F.; Afonso, C.; Giusti, P. Paraffin-Inert Atmospheric Solid Analysis Probe: A Fast and Easy Approach to Characterize Extremely Air-Sensitive Organometallic Complexes by Mass Spectrometry. *Anal. Chem.* **2020**, *92* (4), 2922–2925.

(104) Weis, P.; Schaub, A.; Krossing, I. Inert Atmospheric Solids Analysis Prove System. US 2017/0110308 A1, 2017.

(105) Mosely, J. A.; Stokes, P.; Parker, D.; Dyer, P. W.; Messinis, A. M. Analysis of Air-, Moisture- and Solvent-Sensitive Chemical Compounds by Mass Spectrometry Using an Inert Atmospheric Pressure Solids Analysis Probe. *Eur. J. Mass Spectrom.* **2018**, *24* (1), 74–80.

(106) Hiraoka, K.; Nishidate, K.; Mori, K.; Asakawa, D.; Suzuki, S. Development of Probe Electrospray Using a Solid Needle. *Rapid Commun. Mass Spectrom.* **2007**, *21* (18), 3139–3144.

(107) Liu, P.; Forni, A.; Chen, H. Development of Solvent-Free Ambient Mass Spectrometry for Green Chemistry Applications. *Anal. Chem.* **2014**, *86* (8), 4024–4032.

(108) Bochmann, M. The Chemistry of Catalyst Activation: The Case of Group 4 Polymerization Catalysts. *Organometallics* **2010**, *29* (21), 4711–4740.

(109) Zijlstra, H. S.; Harder, S. Methylalumoxane - History, Production, Properties, and Applications. *European Journal of Inorganic Chemistry*. Wiley-VCH Verlag January 1, 2015, pp 19–43.

(110) Kaminsky, W. Discovery of Methylaluminoxane as Cocatalyst for Olefin Polymerization. *Macromolecules* **2012**, *45* (8), 3289–3297.

(111) Pédeutour, J.-N.; Radhakrishnan, K.; Cramail, H.; Deffieux, A. Reactivity of Metallocene Catalysts for Olefin Polymerization: Influence of Activator Nature and Structure. *Macromol. Rapid Commun.* **2001**, *22* (14), 1095–1123.

(112) Z Velthoen, M. E.; Mun, A.; Bouhmadi, A.; Diefenbach, S.; Weckhuysen, B. M. The Multifaceted Role of Methylaluminoxane in Metallocene-Based Olefin Polymerization Catalysis The Influence of Supporting The. *Macromolecules* **2018**, *51*, 54.

(113) Tanaka, R.; Kawahara, T.; Shinto, Y.; Nakayama, Y.; Shiono, T. An Alternative Method for the Preparation of Trialkylaluminum-Depleted Modified Methylaluminoxane (DMMAO). *Macromolecules* **2017**, *50* (15), 5989–5993.

(114) Oliva, L.; Oliva, P.; Galdi, N.; Pellecchia, C.; Sian, L.; Macchioni, A.; Zuccaccia, C. Solution Structure and Reactivity with Metallocenes of AlMe2F: Mimicking Cation–Anion Interactions in Metallocenium–Methylalumoxane Inner-Sphere Ion Pairs. *Angew. Chemie Int. Ed.* **2017**, *56* (45), 14227–14231.

(115) Luo, L.; Jain, A.; J Harlan. Evidence of Coordinated Trimethylaluminum (TMA) in Methylaluminoxane (MAO) as the Major Active Site and Its Quantification. In *Abstract of papers, 253rd ACS National Meeting, 2017, INOR-1169; PMSE-126.*

(116) Imhoff, D. W.; Simeral, L. S.; Sangokoya, S. A.; Peel, J. H. Characterization of Methylaluminoxanes and Determination of Trimethylaluminum Using Proton NMR. *Organometallics* **1998**, *17* (10), 1941–1945.

(117) Rocchigiani, L.; Busico, V.; Pastore, A.; Macchioni, A. Probing the Interactions between All Components of the Catalytic Pool for Homogeneous Olefin Polymerisation by Diffusion NMR Spectroscopy. *Dalt. Trans.* **2013**, *42* (25), 9104–9111.

(118) Endres, E.; Zijlstra, H. S.; Collins, S.; McIndoe, J. S.; Linnolahti, M. Oxidation of Methylalumoxane Oligomers: A Theoretical Study Guided by Mass Spectrometry. *Organometallics* **2018**, *37* (21), 3936–3942.

(119) Linnolahti, M.; Collins, S. Formation, Structure, and Composition of Methylaluminoxane. *ChemPhysChem* **2017**, *18* (23), 3369–3374.

(120) Kuklin, M. S.; Hirvi, J. T.; Bochmann, M.; Linnolahti, M. Toward Controlling the Metallocene/Methylaluminoxane-Catalyzed Olefin Polymerization Process by a Computational Approach. *Organometallics* **2015**, *34* (14), 3586–3597.

(121) Linnolahti, M.; Laine, A.; Pakkanen, T. A. Screening the Thermodynamics of Trimethylaluminum-Hydrolysis Products and Their Co-Catalytic Performance in Olefin-Polymerization Catalysis. *Chem. - A Eur. J.* **2013**, *19* (22), 7133–7142.

(122) Zurek, E.; Ziegler, T. Theoretical Studies of the Structure and Function of MAO (Methylaluminoxane). *Prog. Polym. Sci.* **2004**, *29* (2), 107–148.

(123) Harlan, C. J.; Bott, S. G.; Barron, A. R. Three-Coordinate Aluminum Is Not a Prerequisite for Catalytic Activity in the Zirconocene-Alumoxane Polymerization of Ethylene. *J. Am. Chem. Soc.* **1995**, *117* (24), 6465–6474.

(124) Harlan, C. J.; Mason, M. R.; Barron, A. R. Tert-Butylaluminum Hydroxides and Oxides: Structural Relationship between Alkylalumoxanes and Alumina Gels. *Organometallics* **1994**, *13* (8), 2957–2969.

(125) Mason, M. R.; Smith, J. M.; Bott, S. G.; Barron, A. R. Hydrolysis of Tri-Tert-Butylaluminum: The First Structural Characterization of Alkylalumoxanes [(R2Al)2O]n and (RAlO)N. *J. Am. Chem. Soc.* **1993**, *115* (12), 4971–4984.

(126) Busico, V.; Cipullo, R.; Pellecchia, R.; Talarico, G.; Razavi, A. Hafnocenes and MAO: Beware of Trimethylaluminum! *Macromolecules* **2009**, *42* (6), 1789–1791.

(127) Busico, V.; Cipullo, R.; Cutillo, F.; Friederichs, N.; Ronca, S.; Wang, B. Improving the Performance of Methylalumoxane: A Facile and Efficient Method to Trap "Free" Trimethylaluminum. *J. Am. Chem. Soc.* **2003**, *125* (41), 12402–12403.

(128) Bochmann, M.; Lancaster, S. J. Monomer–Dimer Equilibria in Homo- and Heterodinuclear Cationic Alkylzirconium Complexes and Their Role in Polymerization Catalysis. *Angew. Chemie Int. Ed. English* **1994**, *33* (1516), 1634–1637.

(129) Camara, J. M.; Petros, R. A.; Norton, J. R. Zirconium-Catalyzed Carboalumination of α-Olefins and Chain Growth of Aluminum Alkyls: Kinetics and Mechanism. *J. Am. Chem. Soc.* **2011**, *133* (14), 5263–5273.

(130) Hoff, R.; Mathers, R. *Handbook of Transition Metal Polymerization Catalysts*; John Wiley & Sons, 2010.

(131) Kleinschmidt, R.; van der Leek, Y.; Reffke, M.; Fink, G. Kinetics and Mechanistic Insight into Propylene Polymerization with Different Metallocenes and Various Aluminium Alkyls as Cocatalysts. *J. Mol. Catal. A Chem.* **1999**, *148* (1), 29–41.

(132) Ghiotto, F.; Pateraki, C.; Severn, J. R.; Friederichs, N.; Bochmann, M. Rapid Evaluation of Catalysts and MAO Activators by Kinetics: What Controls Polymer Molecular Weight and Activity in Metallocene/MAO Catalysts? *Dalt. Trans.* **2013**, *42* (25), 9040–9048.

(133) Černý, Z.; Fusek, J.; Kříž, O.; Heřmánek, S.; Šolc, M.; Čásenský, B. 27Al NMR Study of the Trimethylaluminum Monomer-Dimer Equilibrium. *J. Organomet. Chem.* **1990**, *386* (2), 157–165.

(134) Watanabi, M.; McMahon, C. N.; Harlan, C. J.; Barron, A. R. Reaction of Trimethylaluminum with [(TBu)Al(M3-O)]6: Hybrid Tert-Butylmethylalumoxanes as Cocatalysts for Olefin Polymerization. *Organometallics* **2001**, *20* (3), 460–467.

(135) Tritto, I.; Sacchi, M. C.; Locatelli, P.; Li, S. X. Low-Temperature 1H and 13C NMR Investigation of Trimethylaluminium Contained in Methylaluminoxane Cocatalyst for Metallocene-Based Catalysts in Olefin Polymerization. *Macromol. Chem. Phys.* **1996**, *197* (4), 1537–1544.

(136) Siedle, A. R.; Newmark, R. A.; Lamanna, W. M.; Schroepfer, J. N. Exchange Reactions between Dialkylzirconocene and Alkylaluminium Compounds. *Polyhedron* **1990**, *9* (2), 301–308.

(137) Ghiotto, F.; Pateraki, C.; Tanskanen, J.; Severn, J. R.; Luehmann, N.; Kusmin, A.; Stellbrink, J.; Linnolahti, M.; Bochmann, M. Probing the Structure of Methylalumoxane (MAO) by a Combined Chemical, Spectroscopic, Neutron Scattering, and Computational Approach. *Organometallics* **2013**, *32* (11), 3354–3362.

(138) Henderson, M. A.; Trefz, T. K.; Collins, S.; Wang, M. Y.; McIndoe, J. S. Characterization of Isobutylaluminoxanes by Electrospray Ionization Mass Spectrometry. *Organometallics* **2013**, *32* (7), 2079–2083.

(139) Trefz, T. K.; Henderson, M. A.; Linnolahti, M.; Collins, S.; McIndoe, J. S. Mass Spectrometric Characterization of Methylaluminoxane-Activated Metallocene Complexes. *Chem. – A Eur. J.* **2015**, *21* (7), 2980–2991.

(140) Collins, S.; Linnolahti, M.; Zamora, M. G.; Zijlstra, H. S.; Rodríguez Hernández, M. T.; Perez-Camacho, O. Activation of Cp2ZrX2 (X = Me, Cl) by Methylaluminoxane As Studied by Electrospray Ionization Mass Spectrometry: Relationship to Polymerization Catalysis. *Macromolecules* **2017**, *50* (22), 8871–8884.

(141) Luo, L.; Sangokoya, S. A.; Xiao, W.; Diefenbach, S. P.; Kneale, B. Aluminoxane Catalyst Activators Derived From Dialkylaluminum Cation Precursor Agents, Processes For Making Same, And Use Thereof In Catalysts And Polymerization Of Olefins. 8354485 B2, January 15, 2009.

(142) Vikse, K. L.; Woods, M. P.; McIndoe, J. S. Pressurized Sample Infusion for the Continuous Analysis of Air- And Moisture-Sensitive Reactions Using Electrospray Ionization Mass Spectrometry. *Organometallics* **2010**, *29* (23), 6615–6618.

(143) Vikse, K. L.; Ahmadi, Z.; Luo, J.; van der Wal, N.; Daze, K.; Taylor, N.; McIndoe, J. S. Pressurized Sample Infusion: An Easily Calibrated, Low Volume Pumping System for ESI-MS Analysis of Reactions. *Int. J. Mass Spectrom.* **2012**, *323–324*, 8–13.

(144) Cartledge, F. K. Steric Effects on Reactivity in Silicon Chemistry. *Organometallics* **1983**, *2* (3), 425–430.

(145) Song, L. D.; Rosen, M. J. Surface Properties, Micellization, and Premicellar Aggregation of Gemini Surfactants with Rigid and Flexible Spacers. *Langmuir* **1996**, *12* (5), 1149–1153.

(146) Omari, I.; Randhawa, P.; Randhawa, J.; Yu, J.; Mcindoe, J. S. Structure, Anion, and Solvent Effects on Cation Response in ESI-MS. *J. Am. Soc. Mass Spectrom.* **2019**, 1750–1757.

(147) Smith, M. B. The Monomer-Dimer Equilibria of Liquid Aluminum Alkyls: II. Triisobutylaluminum. *J. Organomet. Chem.* **1970**, *22* (2), 273–281.

(148) Smith, M. B. The Monomer−dimer Equilibria of Liquid Aliminum Alkyls: III. Trimethylaluminum: The Monomer−dimer Equilibria of Liquid and Gaseous Trimethylaluminum and Triethylaluminum. *J. Organomet. Chem.* **1972**, *46* (1), 31–49.

(149) Smith, M. B. Monomer-Dimer Equilibria of Liquid Aluminum Alkyls. I. Triethylaluminum. *J. Phys. Chem.* **1967**, *71* (2), 364–370.

(150) Andresen, A.; Cordes, H.-G.; Herwig, J.; Kaminsky, W.; Merck, A.; Mottweiler, R.; Pein, J.; Sinn, H.; Vollmer, H.-J. Halogen-Free Soluble Ziegler Catalysts for the Polymerization of Ethylene. Control of Molecular Weight by Choice of Temperature. *Angew. Chemie Int. Ed. English* **1976**, *15* (10), 630–632.

(151) Sinn, H.; Kaminsky, W.; Vollmer, H.-J.; Woldt, R. "Living Polymers" on Polymerization with Extremely Productive Ziegler Catalysts. *Angew. Chemie Int.*

Ed. English **1980**, *19* (5), 390–392.

(152) Davis, R. L. Alkylaluminoxane Process. 4,968,827, November 6, 1990.

(153) Welborn, H. C.; Tornqvist, E. G. M. Process for the Preparation of Alumoxanes. 4,665,208, May 12, 1987.

(154) Bottelberghe, S. A. Aluminoxane Process. 4,908,463, March 13, 1990.

(155) Bottelberghe, S. A. Alkylaluminoxane Process. 4,924,018, May 8, 1990.

(156) Crapo, C. C.; Malpass, D. B. Synthesis of Methylaluminoxanes. 4,960,878, October 2, 1990.

(157) Zurek, E.; Ziegler, T. Toward the Identification of Dormant and Active Species in MAO (Methylaluminoxane)-Activated, Dimethylzirconocene-Catalyzed Olefin Polymerization. *Organometallics* **2002**, *21* (1), 83–92.

(158) Jongsomjit, B.; Kaewkrajang, P.; Shiono, T.; Praserthdam, P. Supporting Effects of Silica-Supported Methylaluminoxane (MAO) with Zirconocene Catalyst on Ethylene/1-Olefin Copolymerization Behaviors for Linear Low-Density Polyethylene (LLDPE) Production. *Ind. Eng. Chem. Res.* **2004**, *43* (24), 7959–7963.

(159) Beck, S.; Brintzinger, H. H. Alkyl Exchange between Aluminum Trialkyls and Zirconocene Dichloride Complexes - A Measure of Electron Densities at the Zr Center. *Inorganica Chim. Acta* **1998**, *270* (1–2), 376–381.

(160) Pédeutour, J.; Coevoet, D.; Cramail, H.; Deffieux, A. Activation of IPr(CpFluo)ZrCl2 by Methylaluminoxane, 4. UV/Visible Spectroscopic Study in Hydrocarbon and Chlorinated Media. *Macromol. Chem. Phys.* **1999**, *200* (5), 1215–1221.

(161) Hasan, T.; Ioku, A.; Nishii, K.; Shiono, T.; Ikeda, T. Syndiospecific Living Polymerization of Propene with [t-BuNSiMe2Flu]TiMe2 Using MAO as Cocatalyst. *Macromolecules* **2001**, *34* (10), 3142–3145.

(162) Zaccaria, F.; Zuccaccia, C.; Cipullo, R.; Budzelaar, P. H. M.; Macchioni, A.; Busico, V.; Ehm, C. BHT-Modified MAO: Cage Size Estimation, Chemical Counting of Strongly Acidic Al Sites, and Activation of a Ti-Phosphinimide Precatalyst. *ACS Catal.* **2019**, *9* (4), 2996–3010.

(163) Ghiotto, F.; Pateraki, C.; Severn, J. R.; Friederichs, N.; Bochmann, M. Rapid Evaluation of Catalysts and MAO Activators by Kinetics: What Controls Polymer Molecular Weight and Activity in Metallocene/MAO Catalysts? *Dalt. Trans.* **2013**, *42* (25), 9040–9048.

(164) Song, F.; Cannon, R. D.; Bochmann, M. Zirconocene-Catalyzed Propene Polymerization: A Quenched-Flow Kinetic Study. *J. Am. Chem. Soc.* **2003**, *125* (25), 7641–7653.

(165) Ehm, C.; Cipullo, R.; Budzelaar, P. H. M.; Busico, V. Role(s) of TMA in Polymerization. *Dalt. Trans.* **2016**, *45* (16), 6847–6855.

(166) Ehm, C.; Antinucci, G.; Budzelaar, P. H. M.; Busico, V. Catalyst Activation and

the Dimerization Energy of Alkylaluminium Compounds. *J. Organomet. Chem.* **2014**, *772*, 161–171.

(167) Cipullo, R.; Melone, P.; Yu, Y.; Iannone, D.; Busico, V. Olefin Polymerisation Catalysts: When Perfection Is Not Enough. *Dalt. Trans.* **2015**, *44* (27), 12304–12311.

(168) Zijlstra, H. S.; Joshi, A.; Linnolahti, M.; Collins, S.; McIndoe, J. S. Modifying Methylalumoxane via Alkyl Exchange. *Dalt. Trans.* **2018**, *47* (48), 17291–17298.

(169) Hirvi, J. T.; Bochmann, M.; Severn, J. R.; Linnolahti, M. Formation of Octameric Methylaluminoxanes by Hydrolysis of Trimethylaluminum and the Mechanisms of Catalyst Activation in Single-Site α-Olefin Polymerization Catalysis. *ChemPhysChem* **2014**, *15* (13), 2732–2742.

(170) Ghiotto, F.; Pateraki, C.; Tanskanen, J.; Severn, J. R.; Luehmann, N.; Andrékusmin, A.; Stellbrink, J.; Linnolahti, M.; Bochmann, M. Probing the Structure of Methylalumoxane (MAO) by a Combined Chemical, Spectroscopic, Neutron Scattering, and Computational Approach. *Organometallics* **2013**, *32*, 17.

(171) Zaccaria, F.; Budzelaar, P. H. M.; Cipullo, R.; Zuccaccia, C.; Macchioni, A.; Busico, V.; Ehm, C. Reactivity Trends of Lewis Acidic Sites in Methylaluminoxane and Some of Its Modifications. *Inorg. Chem.* **2020**, *59* (8), 5751–5759.

(172) Zaccaria, F.; Zuccaccia, C.; Cipullo, R.; Budzelaar, P. H. M.; Macchioni, A.; Busico, V.; Ehm, C. On the Nature of the Lewis Acidic Sites in "TMA-Free" Phenol-Modified Methylaluminoxane. *Eur. J. Inorg. Chem.* **2020**, *2020* (11–12), 1088–1095.

(173) Velthoen, M. E. Z.; Muñoz-Murillo, A.; Bouhmadi, A.; Cecius, M.; Diefenbach, S.; Weckhuysen, B. M. The Multifaceted Role of Methylaluminoxane in Metallocene-Based Olefin Polymerization Catalysis. *Macromolecules* **2018**, *51* (2), 343–355.

(174) Roberg, J. K.; Burt, E. A. HIGH YELD ALUMINOXANE SYNTHESIS PROCESS. 5663394, September 2, 1997.

(175) Kaminsky, W.; Hahnsen, H. Process for the Preparation of Oligomeric Aluminoxanes. 4,544,762, 1985.

(176) Sangokoya, S. A. PREPARATION OF ALUMNOXANES. 5041583, June 28, 1991.

(177) Winter, H.; Schnuchel, W.; Sinn, H. The Preparation of Aluminoxane from Trimethylaluminium at a Defined Surface of Deeply Cooled Ice. *Macromol. Symp.* **1995**, *97* (1), 119–125.

(178) Manyik, R. M.; Walker, W. E.; Wilson, T. P. Continuous Processes for the Production of Ethylene Polymers and Catalysts Suitable Therefor. United States Patent 3300458A, August 19, 1967.

(179) Schoenthal, G. W.; Slaugh, L. H. PROCESS FOR PREPARING ALUMNOXANES. United States Patent, US4730071A, March 8, 1988.

(180) Kissin, Y. V.; Brandolini, A. J. An Alternative Route to Methylalumoxane: Synthesis, Structure, and the Use of Model Methylalumoxanes as Cocatalysts for Transition Metal Complexes in Polymerization Reactions. *Macromolecules* **2003**, *36* (1), 18–26.

(181) Okajima, Y.; Nakayama, Y.; Shiono, T.; Tanaka, R. Preparation of Methylaluminoxane from CO 2 and Me 3 Al. *Eur. J. Inorg. Chem.* **2019**, *2019* (18), 2392–2395.

(182) Kilpatrick, A. F. R.; Buffet, J. C.; Nørby, P.; Rees, N. H.; Funnell, N. P.; Sripothongnak, S.; O'Hare, D. Synthesis and Characterization of Solid Polymethylaluminoxane: A Bifunctional Activator and Support for Slurry-Phase Ethylene Polymerization. *Chem. Mater.* **2016**, *28* (20), 7444–7450.

(183) Kroto, H. W.; Heath, J. R.; O'Brien, S. C.; Curl, R. F.; Smalley, R. E. C60: Buckminsterfullerene. *Nature* **1985**, *318* (6042), 162–163.

(184) Yang, X.; Castleman, A. W. Large Protonated Water Clusters H+(H2O)n ($1 \leq n > 60$): The Production and Reactivity of Clathrate-Like Structures Under Thermal Conditions. *J. Am. Chem. Soc.* **1989**, *111* (17), 6845–6846.

(185) Zijlstra, H. S.; Joshi, A.; Linnolahti, M.; Collins, S.; McIndoe, J. S. Interaction of Neutral Donors with Methylaluminoxane. *Eur. J. Inorg. Chem.* **2019**, *2019* (18), 2346–2355.

(186) Zijlstra, H. S.; Collins, S.; McIndoe, J. S. Oxidation of Methylalumoxane Oligomers. *Chem. - A Eur. J.* **2018**, *24* (21), 5506–5512.

(187) Glaser, R.; Sun, X. Thermochemistry of the Initial Steps of Methylaluminoxane Formation. Aluminoxanes and Cycloaluminoxanes by Methane Elimination from Dimethylaluminum Hydroxide and Its Dimeric Aggregates. *J. Am. Chem. Soc.* **2011**, *133* (34), 13323–13336.

(188) Kostiainen, R.; Bruins, A. P. Effect of Solvent on Dynamic Range and Sensitivity in Pneumatically-assisted Electrospray (Ion Spray) Mass Spectrometry. *Rapid Commun. Mass Spectrom.* **1996**, *10* (11), 1393–1399.

(189) Yakelis, N. A.; Bergman, R. G. Safe Preparation and Purification of Sodium Tetrakis[(3,5-Trifluoromethyl) Phenyl]Borate (NaBArF 24): Reliable and Sensitive Analysis of Water in Solutions of Fluorinated Tetraarylborates. *Organometallics* **2005**, *24* (14), 3579–3581.

(190) Sinn, H. Proposals for Structure and Effect of Methylalumoxane Based on Mass Balances and Phase Separation Experiments. *Macromol. Symp.* **1995**, *97* (1), 27–52.

(191) Boleslawski, M.; Serwatowski, J. Synthesis and Structure of Alkylaluminoxanes. *J. Organomet. Chem.* **1983**, *254* (2), 159–166.

(192) Kimura, Y.; Tanimoto, S.; Yamane, H.; Kitao, T. Coordination Structure of the Aluminium Atoms of Poly(Methylaloxane), Poly(Isopropoxylaloxane) and Poly[(Acyloxy)Aloxane]. *Polyhedron* **1990**, *9* (2–3), 371–376.

(193) Pasynkiewicz, S. Alumoxanes: Synthesis, Structures, Complexes and Reactions.

Polyhedron **1990**, *9* (2–3), 429–453.

(194) Falls, Z.; Tymińska, N.; Zurek, E. The Dynamic Equilibrium Between (AlOMe)n Cages and (AlOMe)N·(AlMe3)m Nanotubes in Methylaluminoxane (MAO): A First-Principles Investigation. *Macromolecules* **2014**, *47* (24), 8556–8569.

(195) Zurek, E.; Ziegler, T. A Combined Quantum Mechanical and Statistical Mechanical Study of the Equilibrium of Trimethylaluminum (TMA) and Oligomers of (AIOCH3)n Found in Methylaluminoxane (MAO) Solution. *Inorg. Chem.* **2001**, *40* (14), 3279–3292.

(196) Teixeira, V. E.; Livotto, P. R. The Mechanism of the Reaction between MAO and TMA: DFT Study of the Electronic Structure and Characterization of Transition States for [AlOMe]6, [AlOMe]9 and [AlOMe]16 Cages. *J. Mol. Graph. Model.* **2020**, *99*, 107626.

(197) Negureanu, L.; Hall, R. W.; Butler, L. G.; Simeral, L. A. Methyaluminoxane (MAO) Polymerization Mechanism and Kinetic Model from Ab Initio Molecular Dynamics and Electronic Structure Calculations. **2006**.

(198) Zijlstra, H. S.; Stuart, M. C. A.; Harder, S. Structural Investigation of Methylalumoxane Using Transmission Electron Microscopy. *Macromolecules* **2015**, *48* (15), 5116–5119.

(199) Frisch, M. J.; Trucks, G. W.; Schlegel, H. B.; Scuseria, G. E.; Robb, M. A.; Cheeseman, J. R.; Scalmani, G.; Barone, V.; Petersson, G. A.; Nakatsuji, H.; Li, X.; Caricato, M.; Marenich, a. V.; Bloino, J.; Janesko, B. G.; Gomperts, R.; Mennucci, B.; Hratchian, H. P.; Ortiz, J. V.; Izmaylov, a. F.; Sonnenberg, J. L.; Williams; Ding, F.; Lipparini, F.; Egidi, F.; Goings, J.; Peng, B.; Petrone, A.; Henderson, T.; Ranasinghe, D.; Zakrzewski, V. G.; Gao, J.; Rega, N.; Zheng, G.; Liang, W.; Hada, M.; Ehara, M.; Toyota, K.; Fukuda, R.; Hasegawa, J.; Ishida, M.; Nakajima, T.; Honda, Y.; Kitao, O.; Nakai, H.; Vreven, T.; Throssell, K.; Montgomery Jr., J. a.; Peralta, J. E.; Ogliaro, F.; Bearpark, M. J.; Heyd, J. J.; Brothers, E. N.; Kudin, K. N.; Staroverov, V. N.; Keith, T. a.; Kobayashi, R.; Normand, J.; Raghavachari, K.; Rendell, a. P.; Burant, J. C.; Iyengar, S. S.; Tomasi, J.; Cossi, M.; Millam, J. M.; Klene, M.; Adamo, C.; Cammi, R.; Ochterski, J. W.; Martin, R. L.; Morokuma, K.; Farkas, O.; Foresman, J. B.; Fox, D. J. Gausssian 16, Revision B.01. **2016**, Gaussian, Inc., Wallingford CT.

(200) Zhao, Y.; Truhlar, D. G.; Zhao, Y.; Truhlar, · D G. The M06 Suite of Density Functionals for Main Group Thermochemistry, Thermochemical Kinetics, Noncovalent Interactions, Excited States, and Transition Elements: Two New Functionals and Systematic Testing of Four M06-Class Functionals and 12 Other Functionals and Inorganometallic Chemistry and for Noncovalent Interactions. *Theor Chem Acc.* **2008**, *120*, 215–241.

(201) Schäfer, A.; Huber, C.; Ahlrichs, R. Fully Optimized Contracted Gaussian Basis Sets of Triple Zeta Valence Quality for Atoms Li to Kr. *J. Chem. Phys.* **1994**, *100* (8), 5829–5835.

(202) Tobisch, S.; Ziegler, T. Catalytic Oligomerization of Ethylene to Higher Linear α-Olefins Promoted by the Cationic Group 4 [(H5-Cp-(CMe2-Bridge)-

Ph)MII(Ethylene)2]+ (M = Ti, Zr, Hf) Active Catalysts: A Density Functional Investigation of the Influence of the Metal on the Catalyt. *J. Am. Chem. Soc.* **2004**, *126* (29), 9059–9071.

(203) Zaccaria, F.; Cipullo, R.; Budzelaar, P. H. M.; Busico, V.; Ehm, C. Backbone Rearrangement during Olefin Capture as the Rate Limiting Step in Molecular Olefin Polymerization Catalysis and Its Effect on Comonomer Affinity. *J. Polym. Sci. Part A Polym. Chem.* **2017**, *55* (17), 2807–2814.

(204) Zaccaria, F.; Ehm, C.; Budzelaar, P. H. M.; Busico, V. Accurate Prediction of Copolymerization Statistics in Molecular Olefin Polymerization Catalysis: The Role of Entropic, Electronic, and Steric Effects in Catalyst Comonomer Affinity. *ACS Catal.* **2017**, *7* (2), 1512–1519.

(205) Parchomyk, T.; Koszinowski, K. Iron-Catalyzed Cross-Coupling: Mechanistic Insight for Rational Applications in Synthesis. *Synthesis (Germany)*. Georg Thieme Verlag August 1, 2017, pp 3269–3280.

(206) O'Hair, R. A. J.; Rijs, N. J. Gas Phase Studies of the Pesci Decarboxylation Reaction: Synthesis, Structure, and Unimolecular and Bimolecular Reactivity of Organometallic Ions. *Acc. Chem. Res.* **2015**, *48* (2), 329–340.

(207) Limberger, J.; Leal, B. C.; Monteiro, A. L.; Dupont, J. Charge-Tagged Ligands: Useful Tools for Immobilising Complexes and Detecting Reaction Species during Catalysis. *Chem. Sci.* **2015**, *6* (1), 77–94.

(208) Vikse, K.; Chemistry, J. M. Mechanistic Insights from Mass Spectrometry: Examination of the Elementary Steps of Catalytic Reactions in the Gas Phase. *Pure Appl. Chem.* **2015**, *87*, 361–377.

(209) Santos, L. S. What Do We Know about Reaction Mechanism? The Electrospray Ionization Mass Spectrometry Approach. *J. Braz. Chem. Soc.* **2011**, *22* (10), 1827–1840.

(210) Wehrli, D.; Chen, P. Research Services for the Chemical Industries. How to Find the Needle in the Haystack and How to Find It FAST... *Chimia (Aarau).* **2003**, *57* (6), 354–357.

(211) Johnson J, B. F. G.; McIndoe, S. Spectroscopic and Mass Spectrometric Methods for the Characterisation of Metal Clusters. *Coordination Chemistry Reviews*. Elsevier May 1, 2000, pp 901–932.

(212) Badu-Tawiah, A. K.; Eberlin, L. S.; Ouyang, Z.; Cooks, R. G. Chemical Aspects of the Extractive Methods of Ambient Ionization Mass Spectrometry. *Annu. Rev. Phys. Chem.* **2013**, *64* (1), 481–505.

(213) Müller, T.; Badu-Tawiah, A.; Cooks, R. G. Accelerated Carbon-Carbon Bond-Forming Reactions in Preparative Electrospray. *Angew. Chemie - Int. Ed.* **2012**, *51* (47), 11832–11835.

(214) Lee, J. K.; Samanta, D.; Nam, H. G.; Zare, R. N. Micrometer-Sized Water Droplets Induce Spontaneous Reduction. *J. Am. Chem. Soc* **2019**, *141* (27), 59.

(215) Chisholm, D. M.; Oliver, A. G.; McIndoe, J. S. Mono-Alkylated Bisphosphines as

Dopants for ESI-MS Analysis of Catalytic Reactions. *Dalt. Trans.* **2010**, *39* (2), 364–373.

(216) Sen, A.; Halpern, J. Role of Transition Metal-Dioxygen Complexes in Catalytic Oxidation. Catalysis of the Oxidation of Phosphines by Dioxygen Adducts of Platinum. *J. Am. Chem. Soc.* **1977**, *99* (25), 8337–8339.

(217) V. Grushin, V. Synthesis of Hemilabile Phosphine−Phosphine Oxide Ligands via the Highly Selective Pd-Catalyzed Mono-Oxidation of Bidentate Phosphines: Scope, Limitations, and Mechanism. *Organometallics* **2001**, *20* (18), 3950–3961.

(218) Birk, J. P.; Halpern, J.; Pickard, A. L. Substitution and Oxidative Addition Reactions of Platinum(0) Complexes. Evidence for Coordinatively Unsaturated Species in Solution and as Reactive Intermediates. *J. Am. Chem. Soc.* **1968**, *90* (16), 4491–4492.

(219) Halpern, J.; Pickard, A. L. Mechansim of the Tris(Triphenylphosphine)Platinum(0)-Catalyzed Oxidation of Triphenylphosphine. *Inorg. Chem.* **1970**, *9* (12), 2798–2800.

(220) Henderson, M. A.; Trefz, T. K.; Collins, S.; Wang, M. Y.; McIndoe, J. S. Characterization of Isobutylaluminoxanes by Electrospray Ionization Mass Spectrometry. *Organometallics* **2013**, *32* (7), 2079–2083.

(221) Christ, C. S.; Eyler, J. R.; Richardson, D. E. Gas-Phase Reactions of Bis(.Eta.5-Cyclopentadienyl)Methylzirconium1+ with Dihydrogen, Ethylene, and Propylene. *J. Am. Chem. Soc.* **1988**, *110* (12), 4038–4039.

(222) Christ, C. S.; Eyler, J. R.; Richardson, D. E. Insertion and .Sigma.-Bond Metathesis Pathways in Gas-Phase Reactions of Bis(.Eta.5-Cyclopentadienyl)Methylzirconium(1+) with Dihydrogen and Unsaturated Hydrocarbons. *J. Am. Chem. Soc.* **1990**, *112* (2), 596–607.

(223) Christ, C. S.; Eyler, J. R.; Richardson, D. E. Insertion, Adduct Formation, and Elimination of Alkenes in Gas-Phase Reactions of Bis(.Eta.5-Cyclopentadienyl)Methylzirconium(1+) with Nitriles. *J. Am. Chem. Soc.* **1990**, *112* (12), 4778–4787.

(224) Feichtinger, D.; Plattner, D. A.; Chen, P. Ziegler-Natta-like Tiefin Oligomerization by Alkylzirconocene Cations in an Electrospray Ionization Tandem Mass Spectrometer [13]. *Journal of the American Chemical Society*. American Chemical Society July 22, 1998, pp 7125–7126.

(225) Vatamanu, M. Observation of Zirconium Allyl Species Formed during Zirconocene-Catalyzed Propene Polymerization and Mechanistic Insights. *J. Catal.* **2015**, *323*, 112–120.

(226) Burgmayer, S. J. N. Use of a Titanium Metallocene as a Colorimetric Indicator for Learning Inert Atmosphere Techniques. *J. Chem. Educ.* **1998**, *75* (4), 460.

(227) Yeung, D.; Penafiel, J.; Zijlstra, H. S.; McIndoe, J. S. Oxidation of Titanocene(III): The Deceptive Simplicity of a Color Change. *Inorg. Chem.* **2018**, *57* (1), 457–461.

(228) Guo, T.; Taylor, R. L.; Singh, R. J.; Soldin, S. J. Simultaneous Determination of

12 Steroids by Isotope Dilution Liquid Chromatography-Photospray Ionization Tandem Mass Spectrometry. *Clin. Chim. Acta* **2006**, *372* (1–2), 76–82.

(229) Shirley, A. I.; Lemcoff, N. O. High-Purity Nitrogen by Pressure-Swing Adsorption. *AIChE J.* **1997**, *43* (2), 419–424.

(230) Schulte-Schulze-Berndt, A.; Krabiell, K. Nitrogen Generation by Pressure Swing Adsorption Based on Carbon Molecular Sieves. *Gas Sep. Purif.* **1993**, *7* (4), 253–257.

(231) Genius 1053 - Nitrogen gas generator https://www.peakscientific.com/products/genius/genius-1053-nitrogen-generator (accessed Feb 9, 2020).

(232) Woo, T. K.; Margl, P. M.; Deng, L.; Cavallo, L.; Ziegler, T. Towards More Realistic Computational Modeling of Homogenous Catalysis by Density Functional Theory: Combined QM/MM and Ab Initio Molecular Dynamics. *Catal. Today* **1999**, *50* (3–4), 479–500.

(233) Bochmann, M.; Lancaster, S. J. Monomer–Dimer Equilibria in Homo- and Heterodinuclear Cationic Alkylzirconium Complexes and Their Role in Polymerization Catalysis. *Angew. Chemie Int. Ed. English* **1994**, *33* (1516), 1634–1637.

(234) Bochmann, M.; Jagger, A. J.; Nicholls, J. C. Base-Free Cationic 14-Electron Titanium and Zirconium Alkyls: In Situ Generation, Solution Structures, and Olefin Polymerization Activity. *Angew. Chemie Int. Ed. English* **1990**, *29* (7), 780–782.

(235) Labinger, J. A.; Hart, D. W.; Seibert, W. E.; Schwartz, J. Electrophilic Cleavage of the Carbon-Zirconium(IV) Bond. Comparison and Contrast with Other Transition Metal Alkyl Systems. *J. Am. Chem. Soc.* **1975**, *97* (13), 3851–3852.

(236) Barlow, C. K.; Wright, A.; Easton, C. J.; O'Hair, R. A. J. Gas-Phase Ion-Molecule Reactions Using Regioselectively Generated Radical Cations to Model Oxidative Damage and Probe Radical Sites in Peptides. *Org. Biomol. Chem.* **2011**, *9* (10), 3733–3745.

(237) Böge, O.; Mutzel, A.; Iinuma, Y.; Yli-Pirilä, P.; Kahnt, A.; Joutsensaari, J.; Herrmann, H. Gas-Phase Products and Secondary Organic Aerosol Formation from the Ozonolysis and Photooxidation of Myrcene. *Atmos. Environ.* **2013**, *79*, 553–560.

(238) Barton, M. R.; Zhang, Y.; Atwood, J. D. Mono-Sulfonated Derivatives of Triphenylphosphine (See Abstract). *J. Coord. Chem.* **2002**, *55* (8), 969–983.

(239) Haven, J. J.; Junkers, T. Online Monitoring of Polymerizations: Current Status. *European J. Org. Chem.* **2017**, *2017* (44), 6474–6482.

(240) Babushkin, D. E.; Panchenko, V. N.; Brintzinger, H.-H. Zirconium Allyl Complexes as Participants in Zirconocene-Catalyzed α-Olefin Polymerizations. *Angew. Chemie Int. Ed.* **2014**, *53* (36), 9645–9649.

(241) Christianson, M. D.; Landis, C. R. Generalized Treatment of NMR Spectra for

Rapid Chemical Reactions. *Concepts Magn. Reson. Part A* **2007**, *30A* (4), 165–183.

(242) Babushkin, D. E.; Brintzinger, H. H. Reactive Intermediates Formed During Olefin Polymerization by Methylalumoxane-Activated Ansa-Zirconocene Catalysts: Identification of a Chain-Carrying Intermediate by NMR Methods. *J. Am. Chem. Soc.* **2010**, *132* (2), 452–453.

(243) Chen, C.-H.; Shih, W.-C.; Hilty, C. In Situ Determination of Tacticity, Deactivation, and Kinetics in [Rac-(C2H4(1-Indenyl)2)ZrMe][B(C6F5)4] and [Cp2ZrMe][B(C6F5)4]-Catalyzed Polymerization of 1-Hexene Using 13C Hyperpolarized NMR. *J. Am. Chem. Soc.* **2015**, *137* (21), 6965–6971.

(244) Christianson, M. D.; Tan, E. H. P.; Landis, C. R. Stopped-Flow NMR: Determining the Kinetics of [Rac-(C2H4(1-Indenyl)2)ZrMe][MeB(C6F5)3]-Catalyzed Polymerization of 1-Hexene by Direct Observation. *J. Am. Chem. Soc.* **2010**, *132* (33), 11461–11463.

(245) Landis, C. R.; Christianson, M. D. Metallocene-Catalyzed Alkene Polymerization and the Observation of Zr-Allyls. *Proc. Natl. Acad. Sci.* **2006**, *103* (42), 15349–15354.

(246) Vatamanu, M.; Stojcevic, G.; Baird, M. C. Detection of an η-Alkene Intermediate of the Type [Cp2Zr(Me)(H1-Alkene)]+: The Role of Such Species in Metallocene Catalyst Deactivation to Allylic Species. *J. Am. Chem. Soc.* **2008**, *130* (2), 454–456.

(247) Gies, A. P.; Kuhlman, R. L.; Zuccaccia, C.; Macchioni, A.; Keaton, R. J. Mass Spectrometric Mechanistic Investigation of Ligand Modification in Hafnocene-Catalyzed Olefin Polymerization. *Organometallics* **2017**, *36* (18), 3443–3455.

(248) Santos, L. S.; Metzger, J. O. Study of Homogeneously Catalyzed Ziegler–Natta Polymerization of Ethene by ESI-MS. *Angew. Chemie Int. Ed.* **2006**, *45* (6), 977–981.

(249) Feichtinger, D.; Plattner, D. A.; Chen, P. Ziegler−Natta-like Olefin Oligomerization by Alkylzirconocene Cations in an Electrospray Ionization Tandem Mass Spectrometer. *J. Am. Chem. Soc.* **1998**, *120* (28), 7125–7126.

(250) Resconi, L.; Cavallo, L.; Fait, A.; Piemontesi, F. Selectivity in Propene Polymerization with Metallocene Catalysts. *Chem. Rev.* **2000**, *100* (4), 1253–1346.

(251) Lieber, S.; Prosenc, M.-H.; Brintzinger, H.-H. Zirconocene Allyl Complexes: Dynamics in Solution, Reaction with Aluminum Alkyls, B(C6F5)3-Induced Propene Insertion, and Density-Functional Calculations on Possible Formation and Reaction Pathways. *Organometallics* **2000**, *19* (4), 377–387.

(252) Panchenko, V. N.; Babushkin, D. E.; Bercaw, J. E.; Brintzinger, H. H. Catalyst Speciation during Ansa-Zirconocene-Catalyzed Polymerization of 1-Hexene Studied by UV-Vis Spectroscopy—Formation and Partial Re-Activation of Zr-Allyl Intermediates †. *Polymers (Basel).* **2019**, *11* (6), 936.

(253) Al-Humydi, A.; Garrison, J. C.; Mohammed, M.; Youngs, W. J.; Collins, S.

Propene Polymerization Using Ansa-Metallocenium Ions: Catalyst Deactivation Processes during Monomer Consumption and Molecular Structures of the Products Formed. *Polyhedron* **2005**, *24* (11), 1234–1249.

(254) Moscato, B. M.; Zhu, B.; Landis, C. R. Mechanistic Investigations into the Behavior of a Labeled Zirconocene Polymerization Catalyst. *Organometallics* **2012**, *31* (5), 2097–2107.

(255) Panchenko, V. N.; Babushkin, D. E.; Brintzinger, H. H. Zirconium-Allyl Complexes as Resting States in Zirconocene-Catalyzed α-Olefin Polymerization. *Macromol. Rapid Commun.* **2015**, *36* (2), 249–253.

(256) Bryliakov, K. P.; Talsi, E. P.; Semikolenova, N. V; Zakharov, V. A.; Brand, J.; Alonso-Moreno, C.; Bochmann, M. Formation and Structures of Cationic Zirconium Complexes in Ternary Systems Rac-(SBI)ZrX2/AlBu3i/[CPh3][B(C6F5)4] (X=Cl, Me). *J. Organomet. Chem.* **2007**, *692* (4), 859–868.

(257) Baldwin, S. M.; Bercaw, J. E.; Henling, L. M.; Day, M. W.; Brintzinger, H. H. Cationic Alkylaluminum-Complexed Zirconocene Hydrides: NMR-Spectroscopic Identification, Crystallographic Structure Determination, and Interconversion with Other Zirconocene Cations. *J. Am. Chem. Soc.* **2011**, *133* (6), 1805–1813.

(258) Ewen, J. A.; Elder, M. J. Syntheses and Models for Stereospecific Metallocenes. *Makromol. Chemie. Macromol. Symp.* **1993**, *66* (1), 179–190.

(259) Chien, J. C. W.; Tsai, W. M.; Rausch, M. D. Isospecific Polymerization of Propylene Catalyzed by Rac-Ethylenebis(Indenyl)Methylzirconium Cation. *J. Am. Chem. Soc.* **1991**, *113* (22), 8570–8571.

(260) Fisch, A. G.; dos Santos, J. H. Z.; Cardozo, N. S. M.; Secchi, A. R. Mass Transfer in Olefin Polymerization: Estimative of Macro- and Microscale Diffusion Coefficients through the Swollen Polymer. *Chem. Eng. Sci.* **2008**, *63* (14), 3727–3739.

(261) Song, F.; Cannon, R. D.; Bochmann, M. The Kinetics of Propene and Hexene Polymerisation with [(SBI)ZrR]+X−: Evidence for Monomer-Dependent Early or Late Transition States. *Chem. Commun.* **2004**, *4* (5), 542–543.

(262) Kissin, Y. V. Oligomerization Reactions of 1-Hexene with Metallocene Catalysts: Detailed Data on Reaction Chemistry and Kinetics. *Mol. Catal.* **2019**, *463*, 87–93.

(263) Kilpatrick, A. F. R.; Rees, N. H.; Sripothongnak, S.; Buffet, J. C.; O'Hare, D. Slurry-Phase Ethylene Polymerization Using Pentafluorophenyl- and Pentafluorophenoxy-Modified Solid Polymethylaluminoxanes. *Organometallics* **2018**, *37* (1), 156–164.

(264) Lancaster, S. J.; Robinson, O. B.; Bochmann, M.; Coles, S. J.; Hursthouse, M. B. Synthesis and Reactivity of New Mono(Cyclopentadienyl)Zirconium and -Hafnium Alkyl Complexes. Crystal and Molecular Structure of [{C5H3(SiMe3)2}HfMe2(.Eta.6-Toluene)][BMe(C6F5)3]. *Organometallics* **1995**, *14* (5), 2456–2462.

(265) Beck, S.; Prosenc, M.-H.; Brintzinger, H.-H.; Goretzki, R.; Herfert, N.; Fink, G. Binuclear Zirconocene Cations with μ-CH3-Bridges in Homogeneous Ziegler-Natta Catalyst Systems. *J. Mol. Catal. A Chem.* **1996**, *111* (1), 67–79.

(266) Wu, F.; Dash, A. K.; Jordan, R. F. Structures and Reactivity of Zr(IV) Chlorobenzene Complexes. *J. Am. Chem. Soc.* **2004**, *126* (47), 15360–15361.

(267) Lanzinger, D.; Höhlein, I. M.; Weiß, S. B.; Rieger, B. Catalytic C-F Activation via Cationic Group IV Metallocenes. *J. Organomet. Chem.* **2015**, *778*, 21–28.

(268) Bryliakov, K. P.; Talsi, E. P.; Voskoboynikov, A. Z.; Lancaster, S. J.; Bochmann, M. Formation and Structures of Hafnocene Complexes in MAO- and AlBui3/CPh3[B(C6F5)4]-Activated Systems. *Organometallics* **2008**, *27* (23), 6333–6342.

(269) Pike, S. D.; Crimmin, M. R.; Chaplin, A. B. Organometallic Chemistry Using Partially Fluorinated Benzenes. *Chem. Commun.* **2017**, *53* (26), 3615–3633.

(270) Brintzinger, H. H.; Fischer, D.; Mülhaupt, R.; Rieger, B.; Waymouth, R. M. Stereospecific Olefin Polymerization with Chiral Metallocene Catalysts. *Angew. Chemie Int. Ed. English* **1995**, *34* (11), 1143–1170.

(271) SANGOKOYA, S. A.; GOODALL, B. L.; SIMERAL, L. S. IONIC ALUMINOXANATE COMPOSITIONS AND THEIR USE IN CATALYSIS. Int. Pat WO/2003/082879, October 9, 2003.

(272) MacGillivray, L. R.; Atwood, J. L. Structural Classification and General Principles for the Design of Spherical Molecular Hosts. *Angewandte Chemie - International Edition*. Wiley-VCH Verlag April 19, 1999, pp 1018–1033.

(273) Shepherd, B. D. Siloxane Basicity toward Strong Acid in Nonpolar Solution. *J. Am. Chem. Soc.* **1991**, *113* (15), 5581–5583.

(274) Barron, A. R. New Method for the Determination of the Trialkylaluminum Content in Alumoxanes. *Organometallics* **1995**, *14* (7), 3581–3583.

(275) Bahr, S. R.; Boudjouk, P. Trityl Tetrakis(3,5-Bis(Trifluoromethyl)Phenyl)- Borate: A New Hydride Abstraction Reagent. *J. Org. Chem* **1992**, *57*, 5545–5547.

(276) Wilm, M.; Mann, M. Analytical Properties of the Nanoelectrospray Ion Source. *Anal. Chem.* **1996**, *68* (1), 1–8.

(277) Chisholm, D. M.; Scott McIndoe, J. Charged Ligands for Catalyst Immobilisation and Analysis. *Dalt. Trans.* **2008**, No. 30, 3933–3945.

Appendix A Modifying methylalumoxane via alkyl exchange.

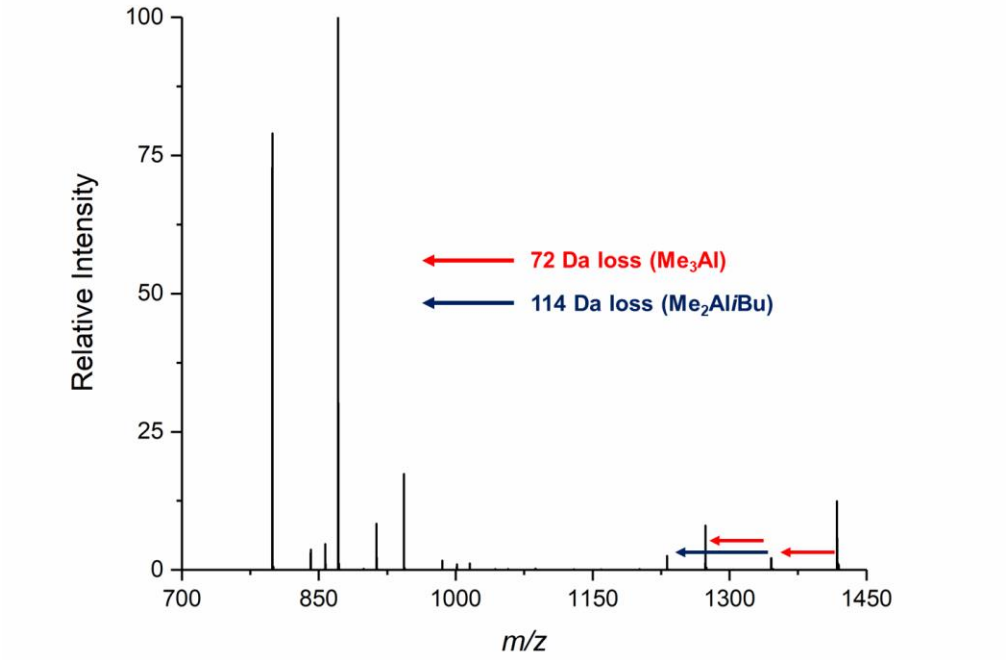

Figure A1. MS/MS spectrum of species containing one Me/*i*Bu substitution (*m/z* of 1417).

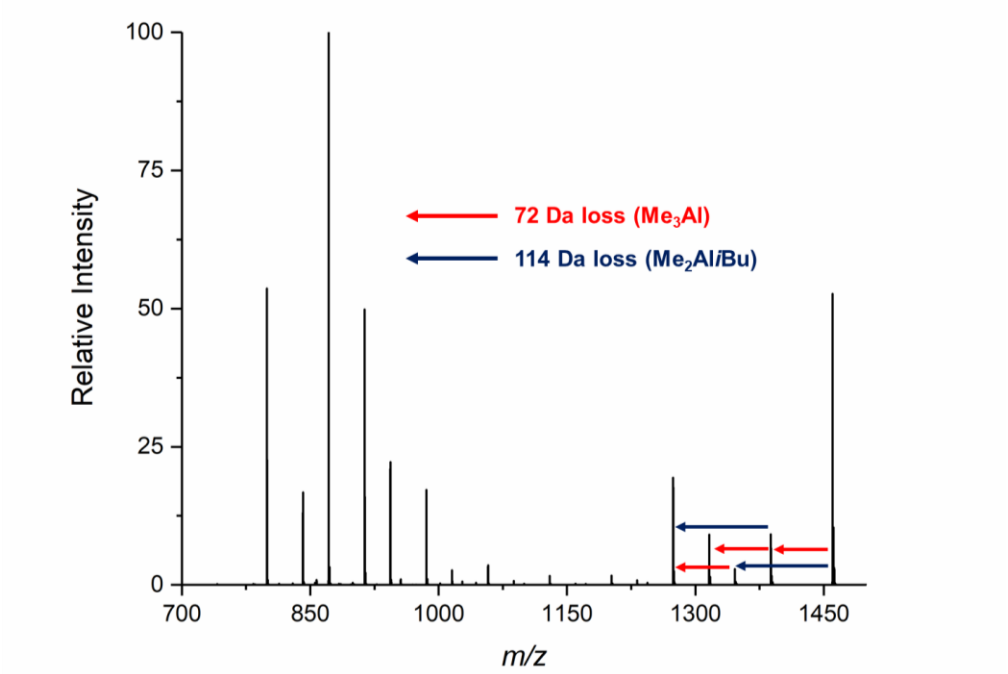

Figure A2. MS/MS spectrum of species containing two Me/*i*Bu substitutions (*m/z* of 1459).

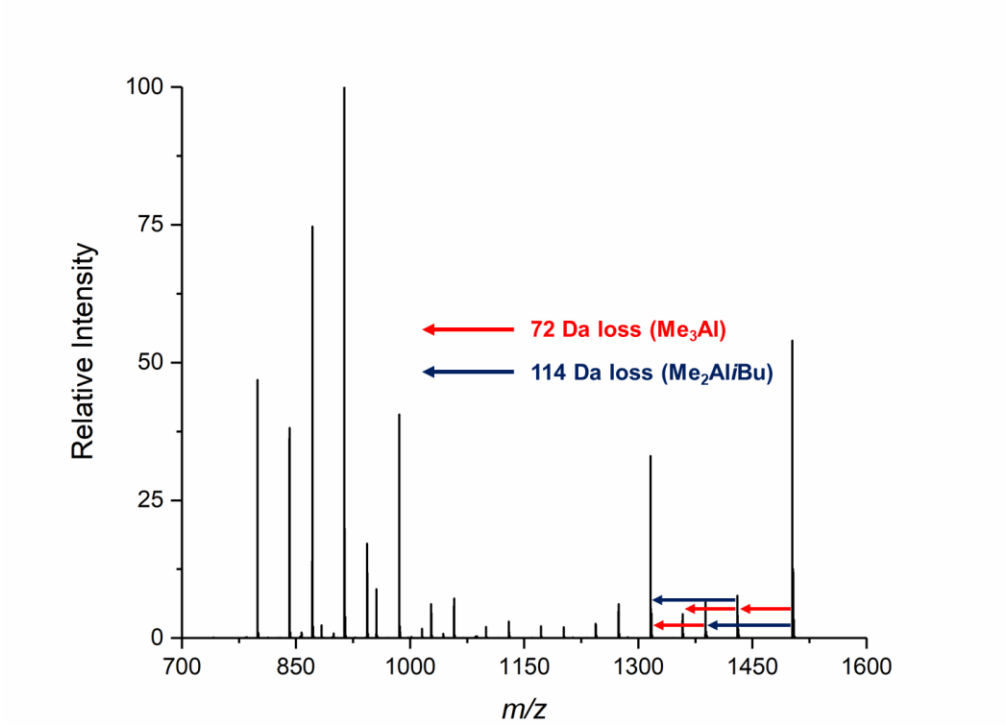

Figure A3. MS/MS spectrum of species containing three Me/*i*Bu substitutions (*m/z* of 1501).

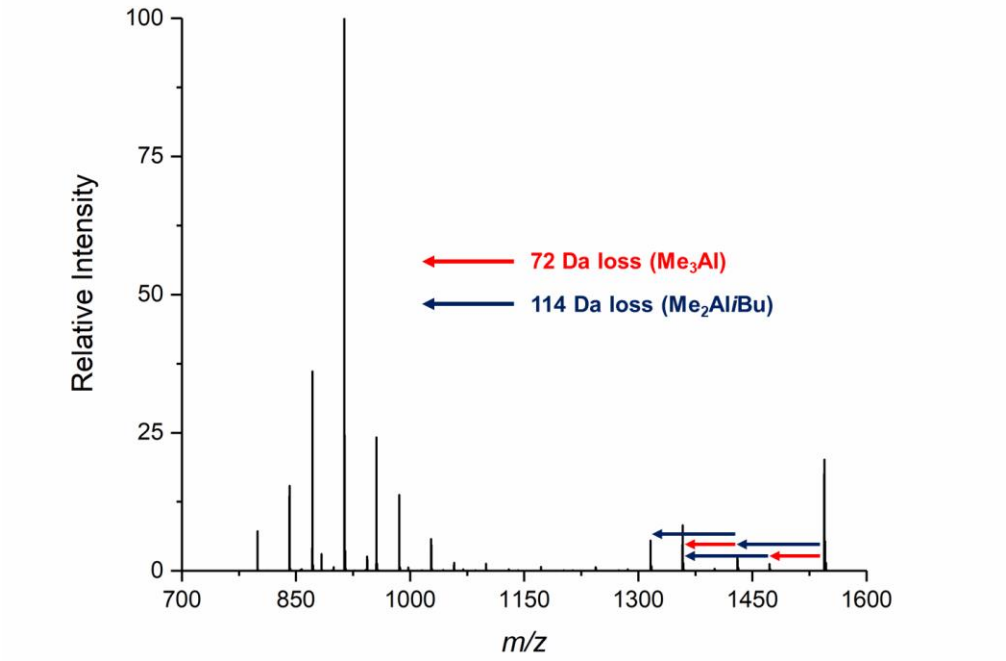

Figure A4. MS/MS spectrum of species containing four Me/*i*Bu substitutions (*m/z* of 1543).

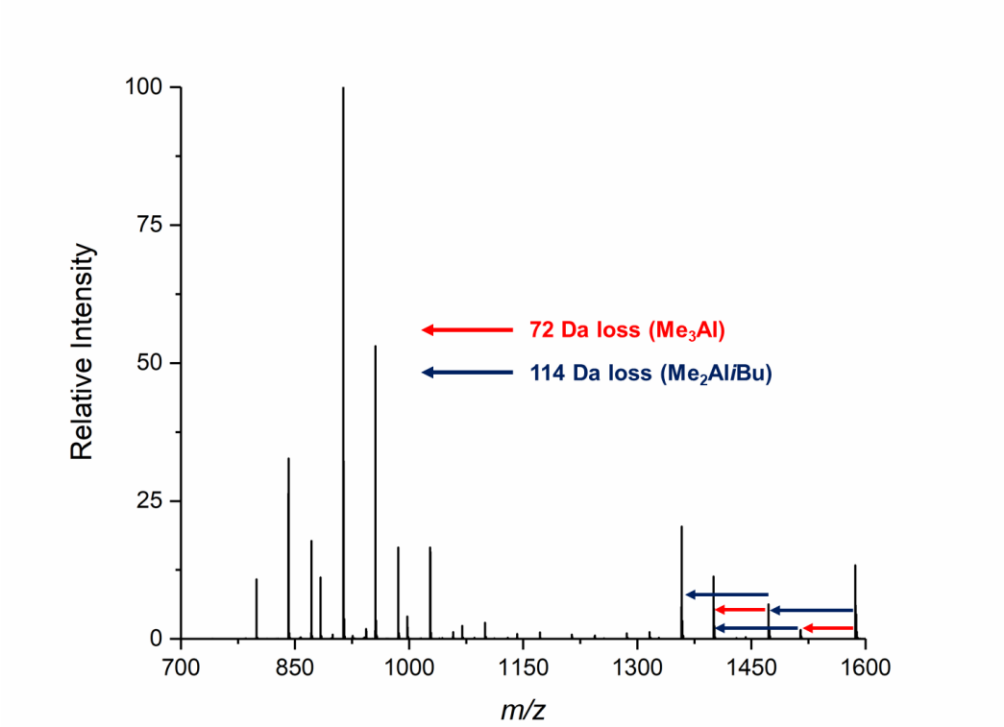

Figure A5. MS/MS spectrum of species containing five Me/*i*Bu substitutions (*m/z* of 1585).

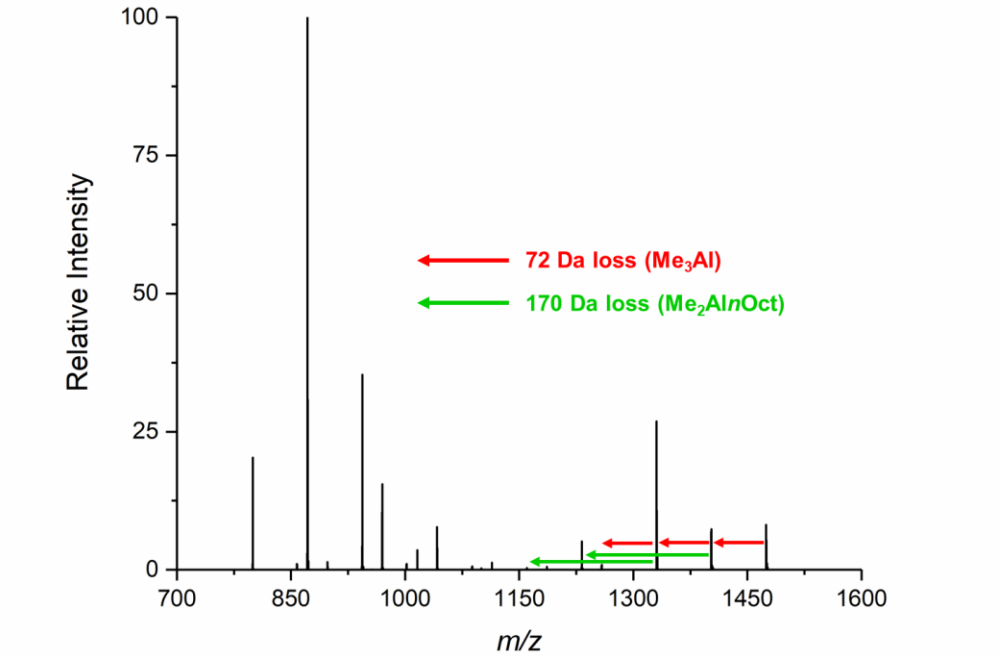

Figure A6. MS/MS spectrum of species containing one Me/*n*Oct substitution (*m/z* of 1473).

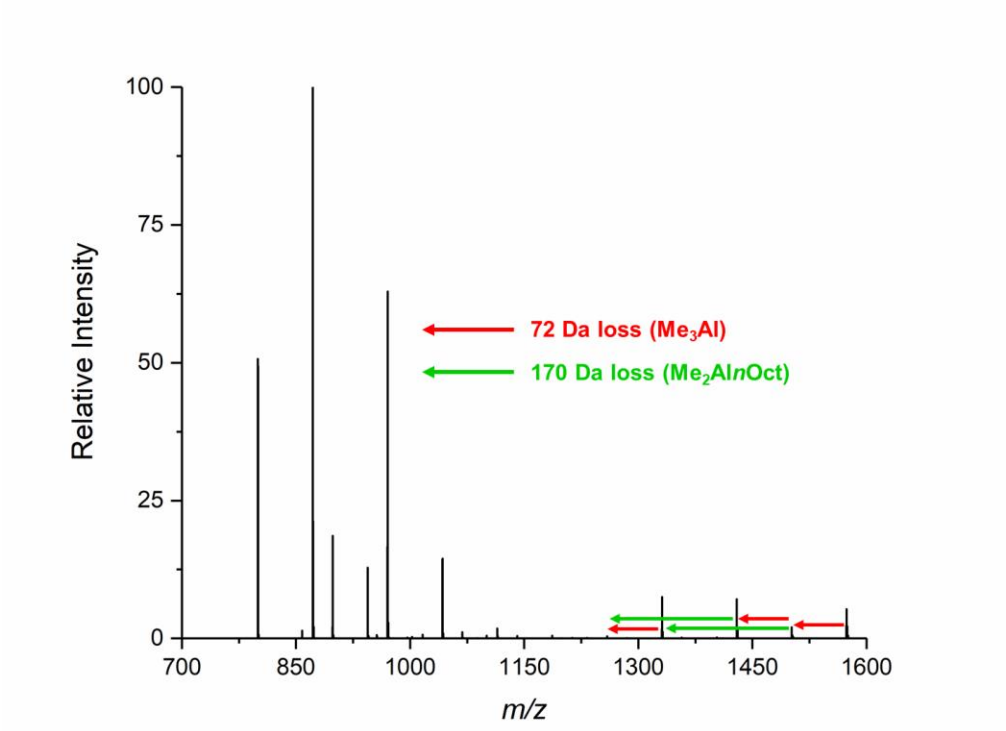

Figure A7. MS/MS spectrum of species containing two Me/*n*Oct substitutions (*m/z* of 1571).

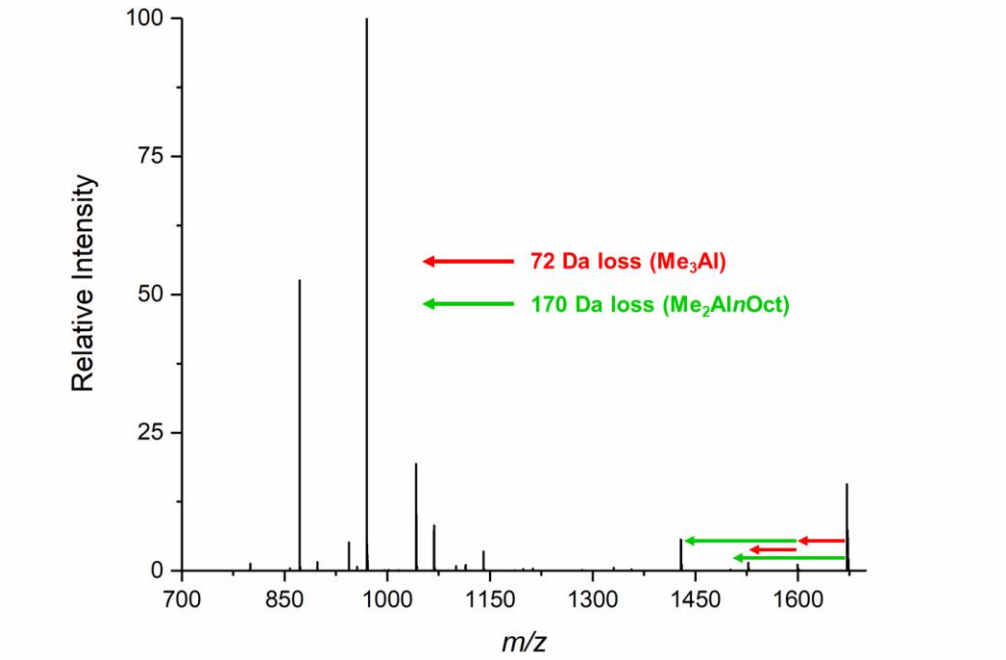

Figure A8. MS/MS spectrum of species containing three Me/*n*Oct substitutions (*m/z* of 1669).

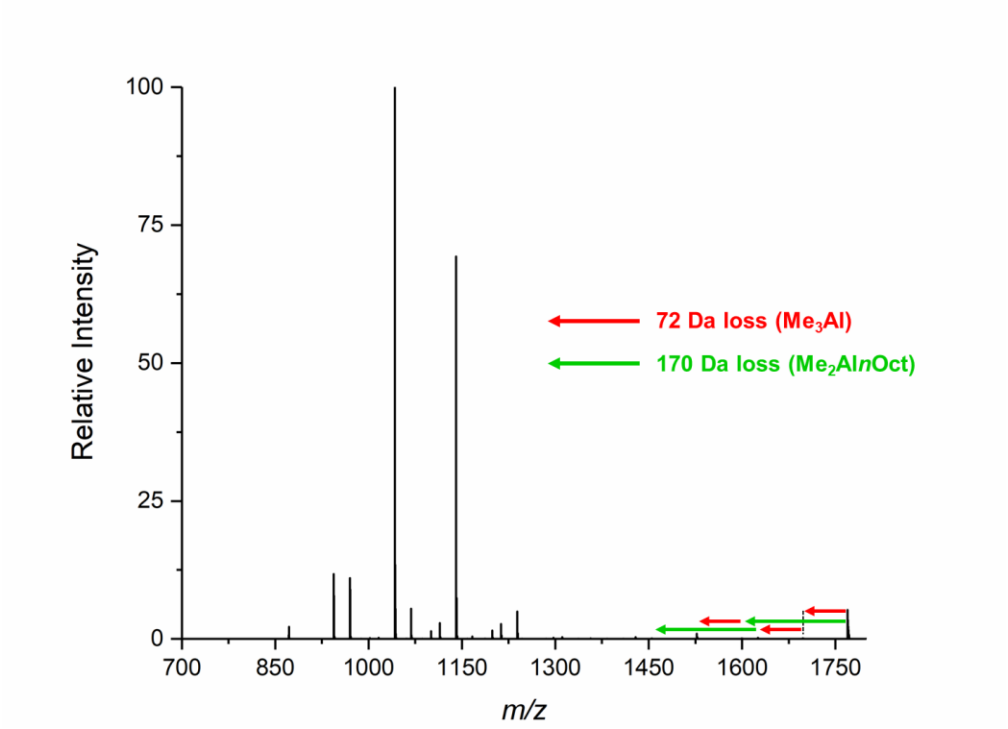

Figure A9. MS/MS spectrum of species containing four Me/*n*Oct substitutions (*m/z* of 1767).

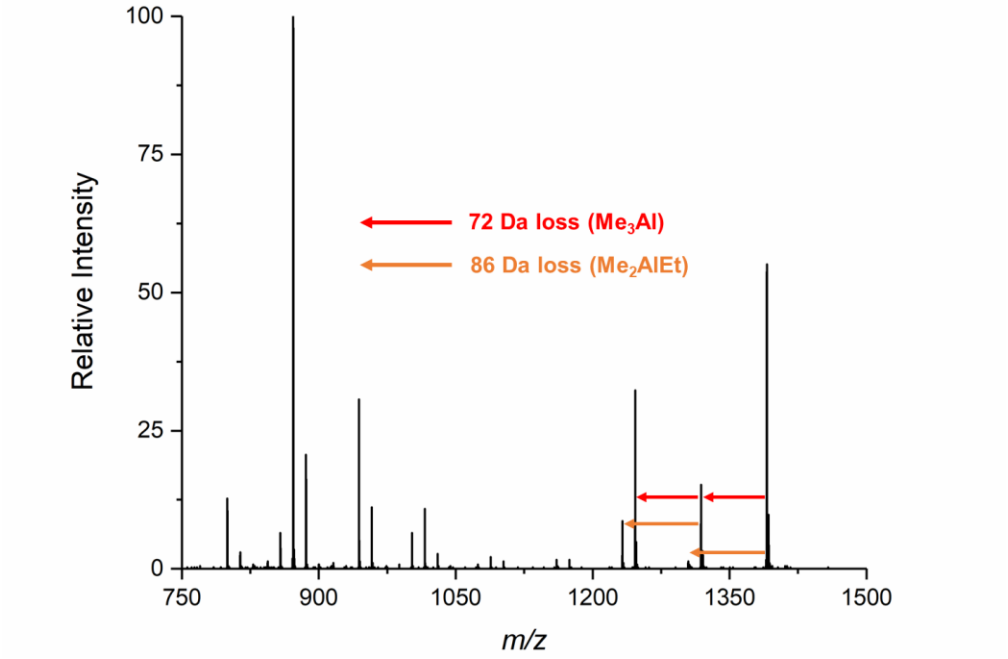

Figure A10. MS/MS spectrum of species containing one Me/Et substitution (*m/z* of 1389).

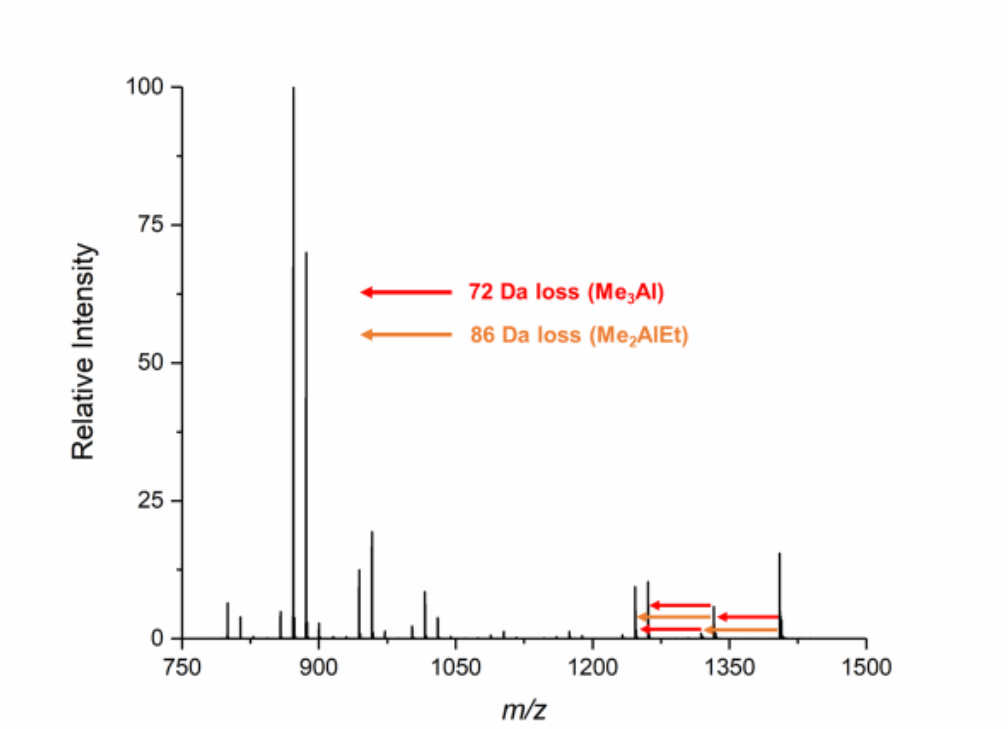

Figure A11. MS/MS spectrum of species containing two Me/Et substitutions (*m/z* of 1403).

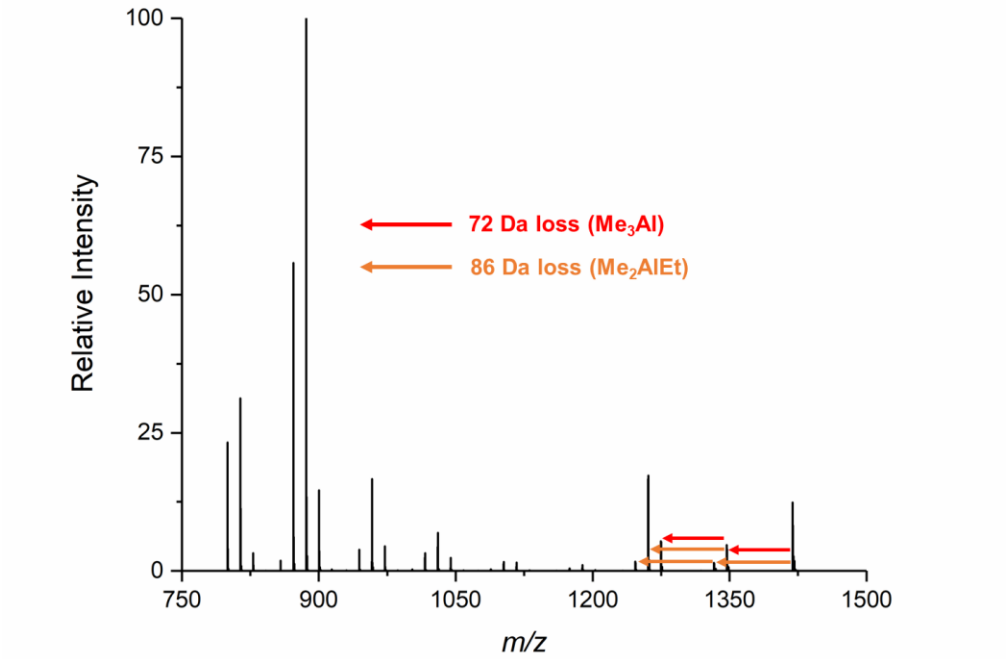

Figure A12. MS/MS spectrum of species containing three Me/Et substitutions (*m/z* of 1417).

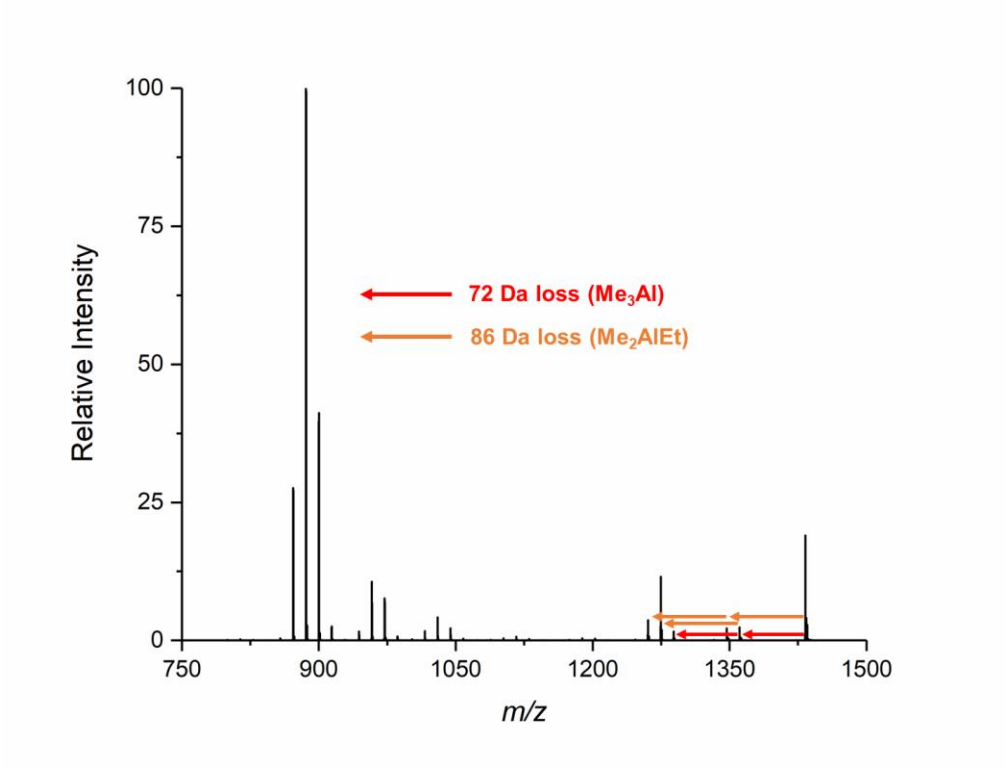

Figure A13. MS/MS spectrum of species containing four Me/Et substitutions (*m/z* of 1431).

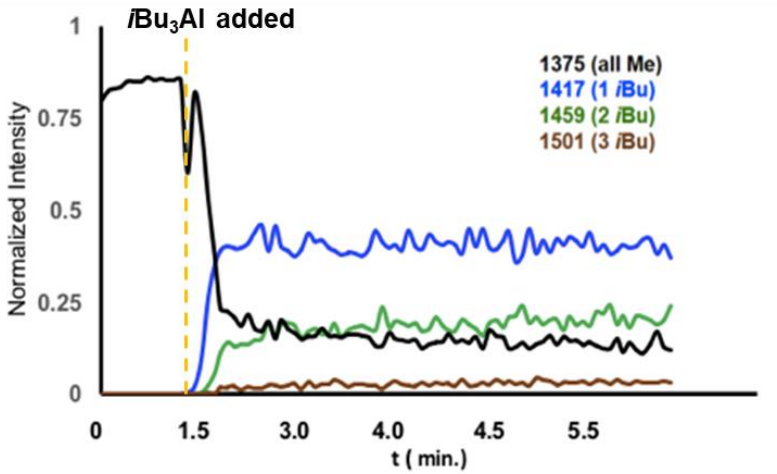

Figure A14. PSI of 1 mol % *i*Bu_3Al modified MAO/OMTS with Al:OMTS 100:1 in PhF.

Appendix B Real-time monitoring of methylalumoxane.

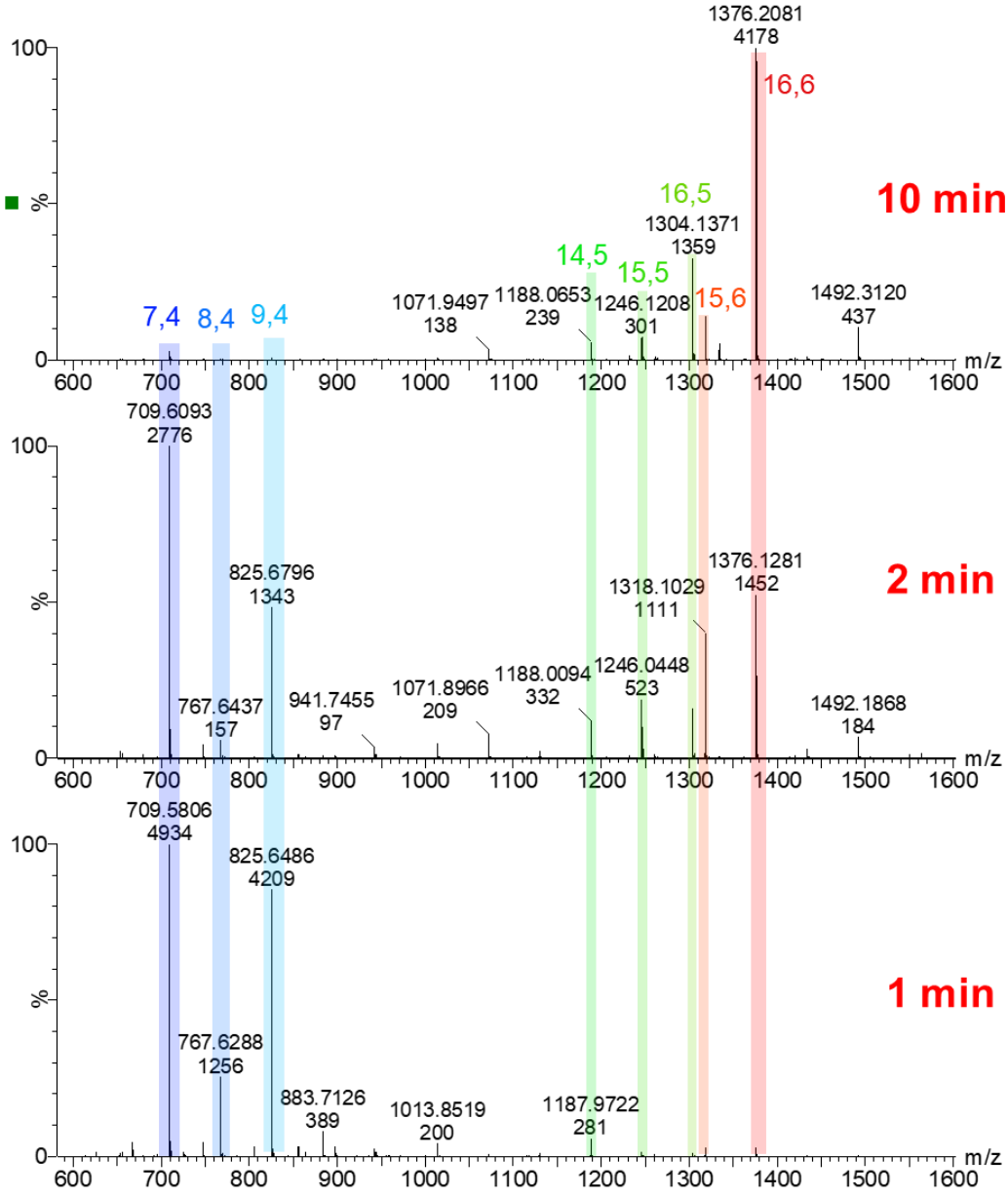

Figure B1. ESI-MS spectrum at 1, 2, and 10 minutes showing the change in the anion distribution during the synthesis of MAO in difluorobenzene with [H_2O] = 0.055 M. Run #1 of 7.

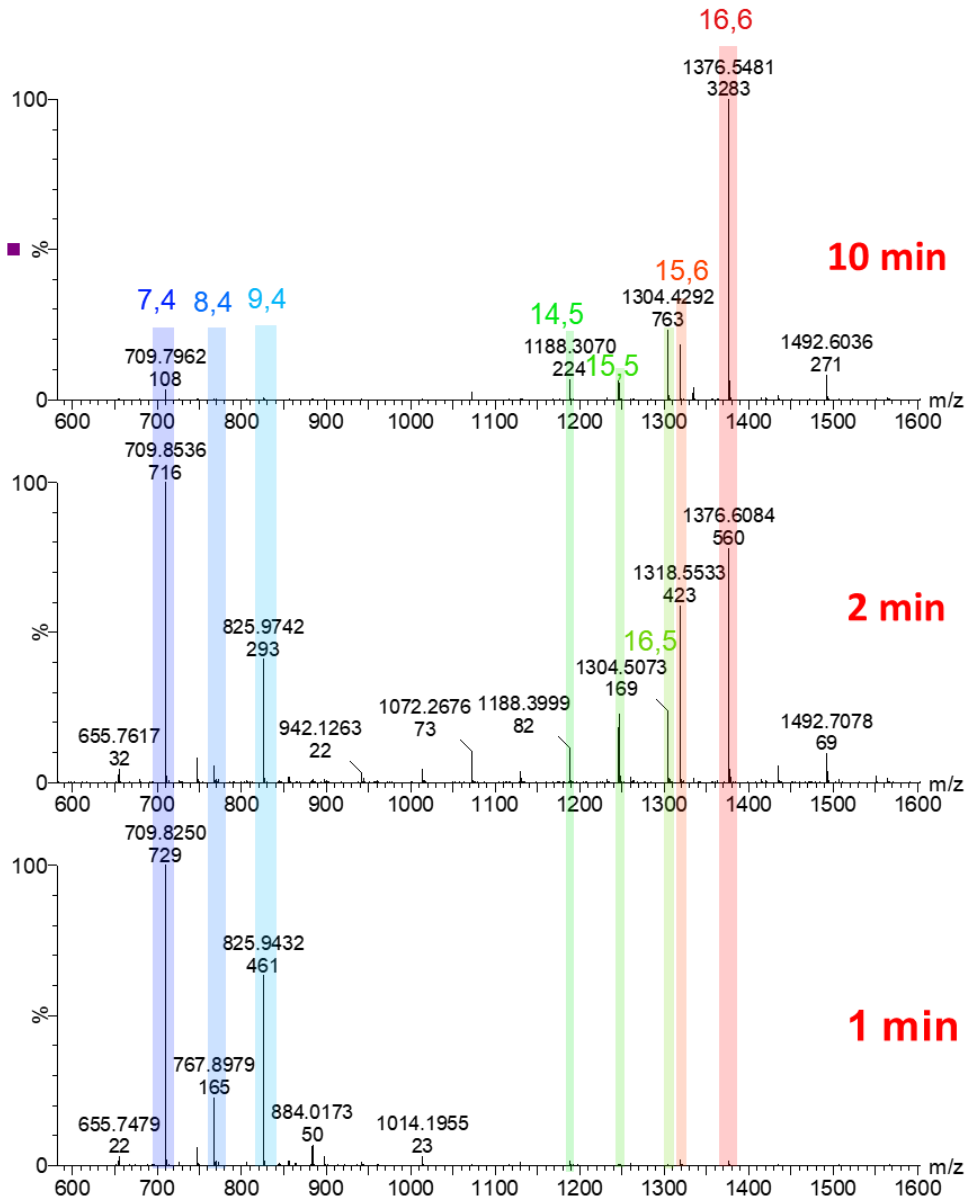

Figure B2. ESI-MS spectrum at 1, 2, and 10 minutes showing the change in the anion distribution during the synthesis of MAO in difluorobenzene with [H_2O] = 0.055 M. Run #2 of 7.

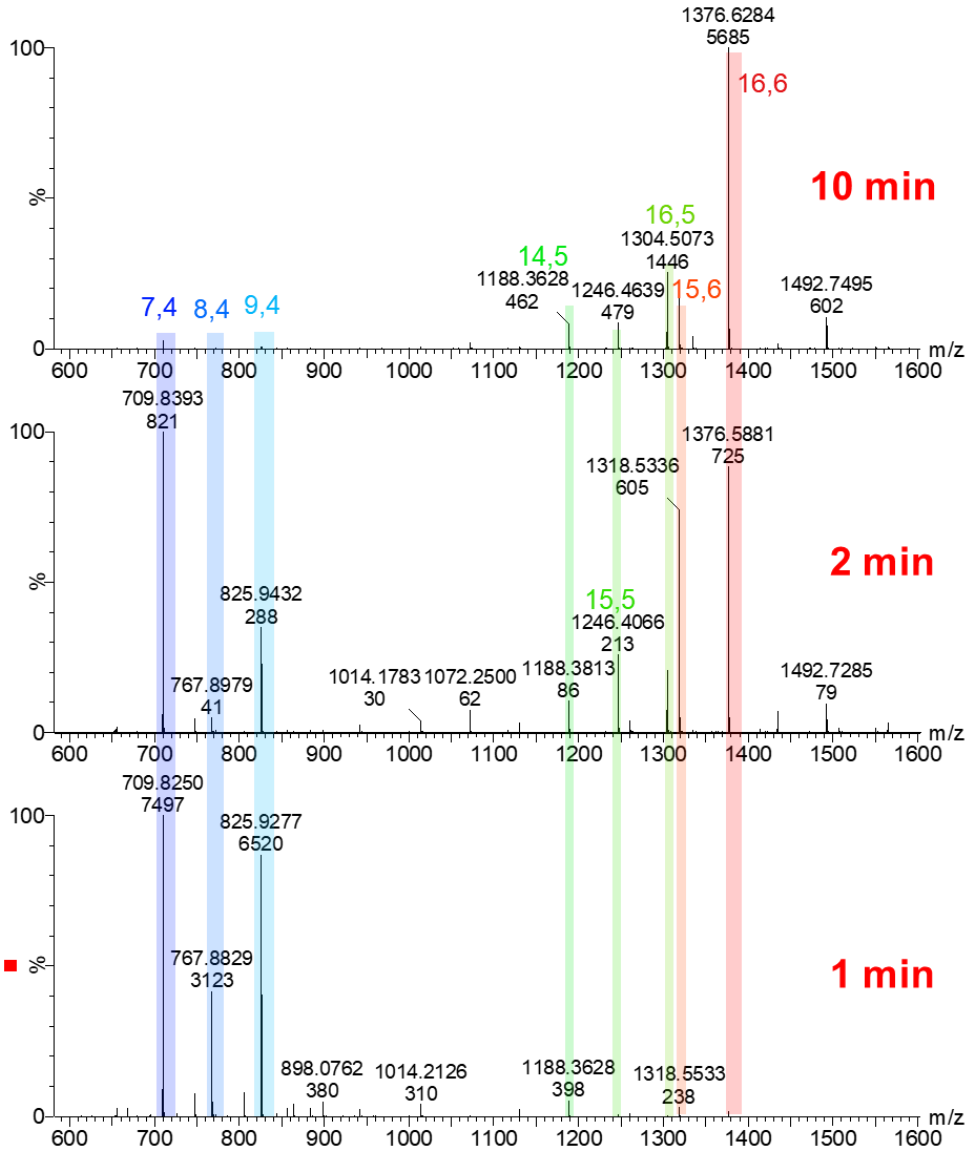

Figure B3. ESI-MS spectrum at 1, 2, and 10 minutes showing the change in the anion distribution during the synthesis of MAO in difluorobenzene with [H_2O] = 0.055 M. Run #3 of 7.

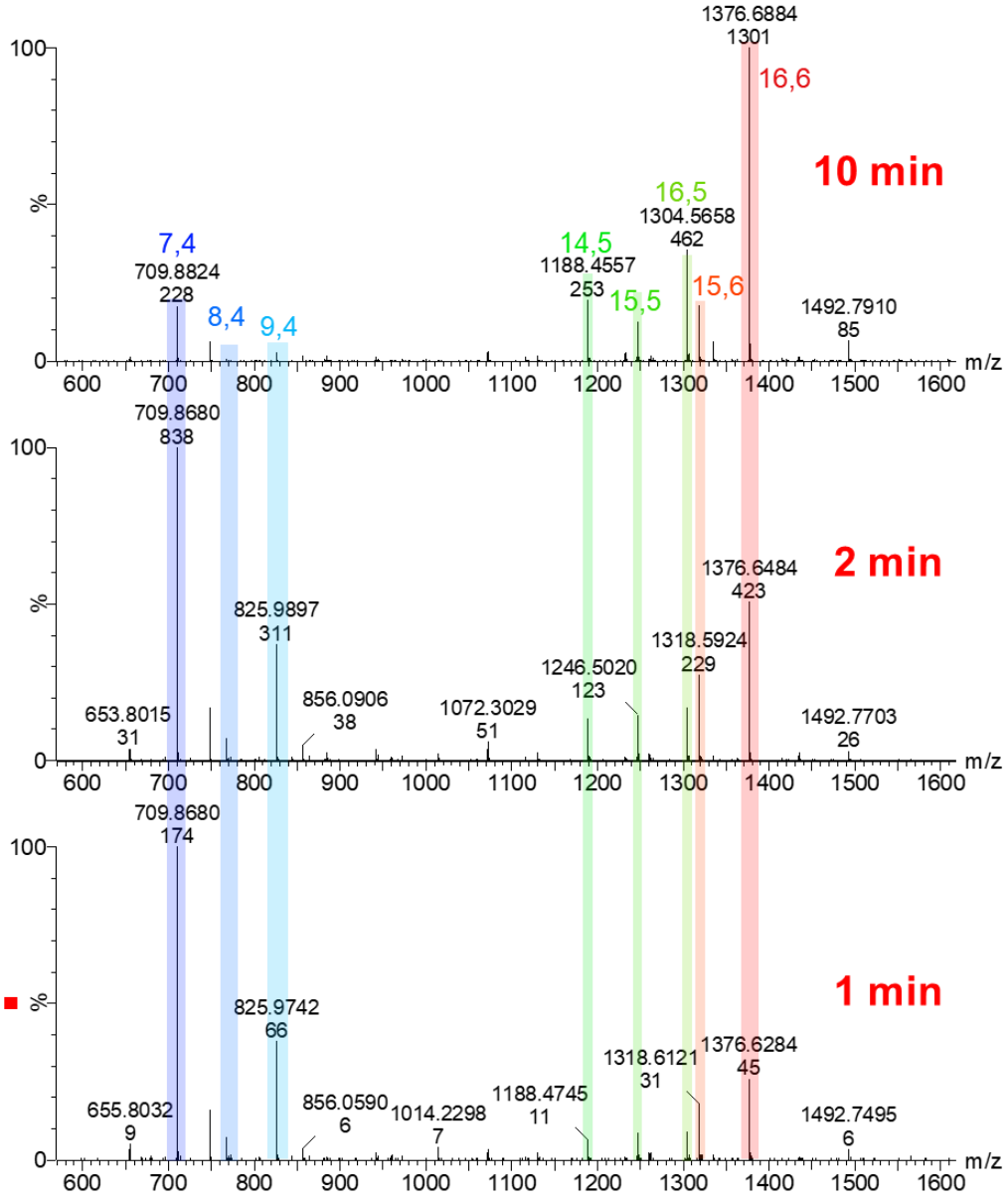

Figure B4. ESI-MS spectrum at 1, 2, and 10 minutes showing the change in the anion distribution during the synthesis of MAO in difluorobenzene with [H_2O] = 0.055 M. Run #4 of 7.

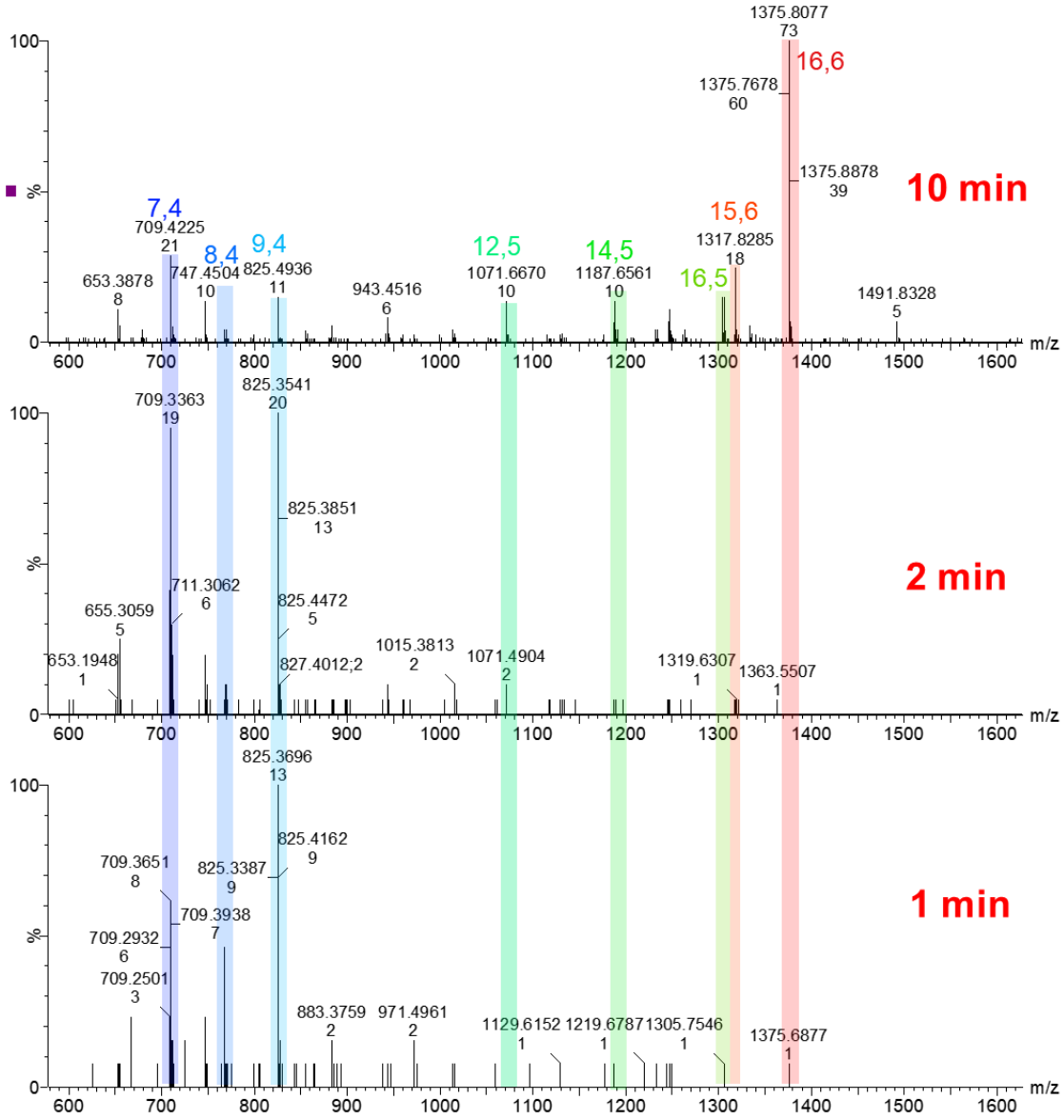

Figure B5. ESI-MS spectrum at 1, 2, and 10 minutes showing the change in the anion distribution during the synthesis of MAO in difluorobenzene with [H_2O] = 0.055 M. Run #5 of 7.

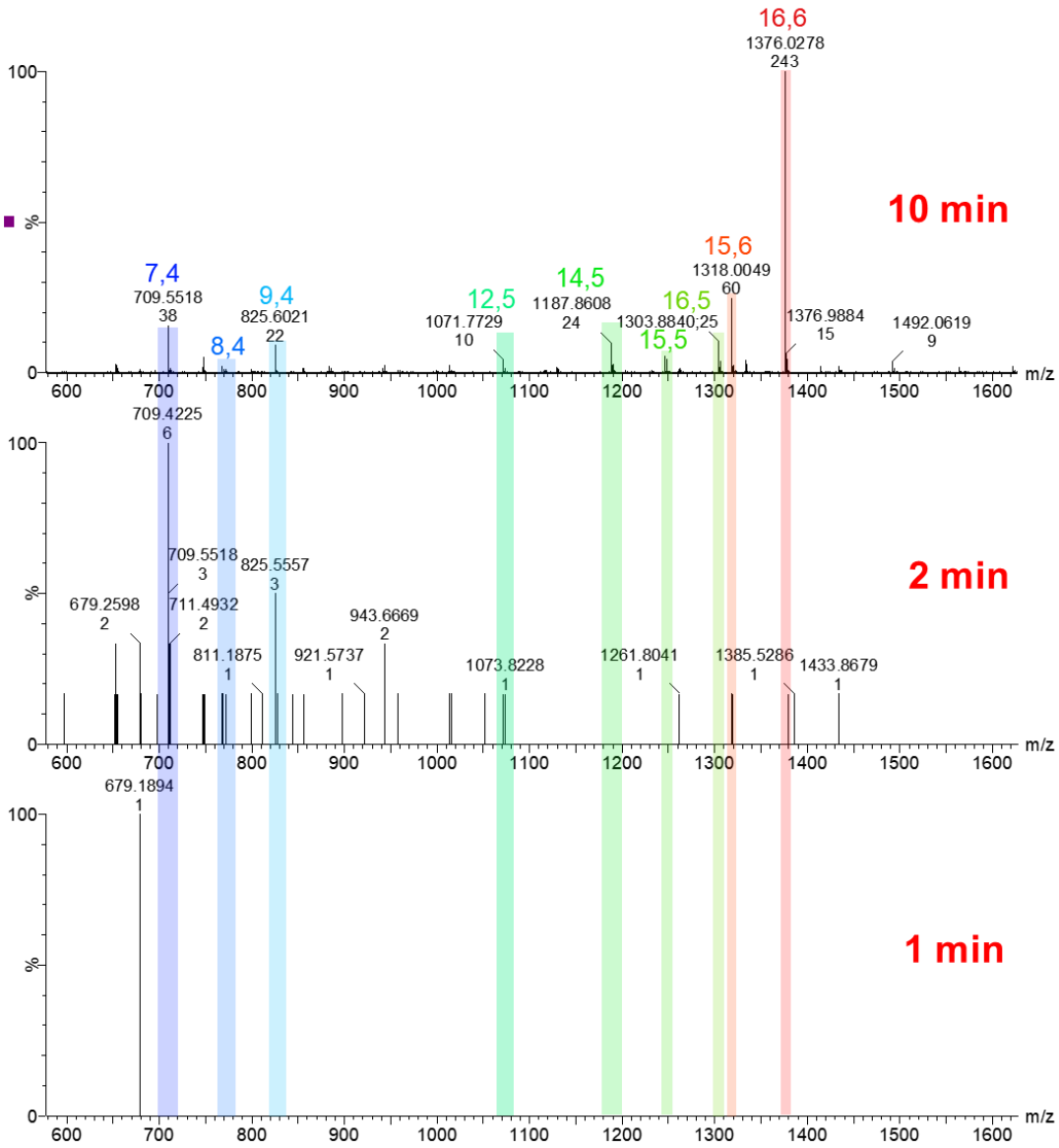

Figure B6. ESI-MS spectrum at 1, 2, and 10 minutes showing the change in the anion distribution during the synthesis of MAO in difluorobenzene with [H_2O] = 0.055 M. Run #6 of 7.

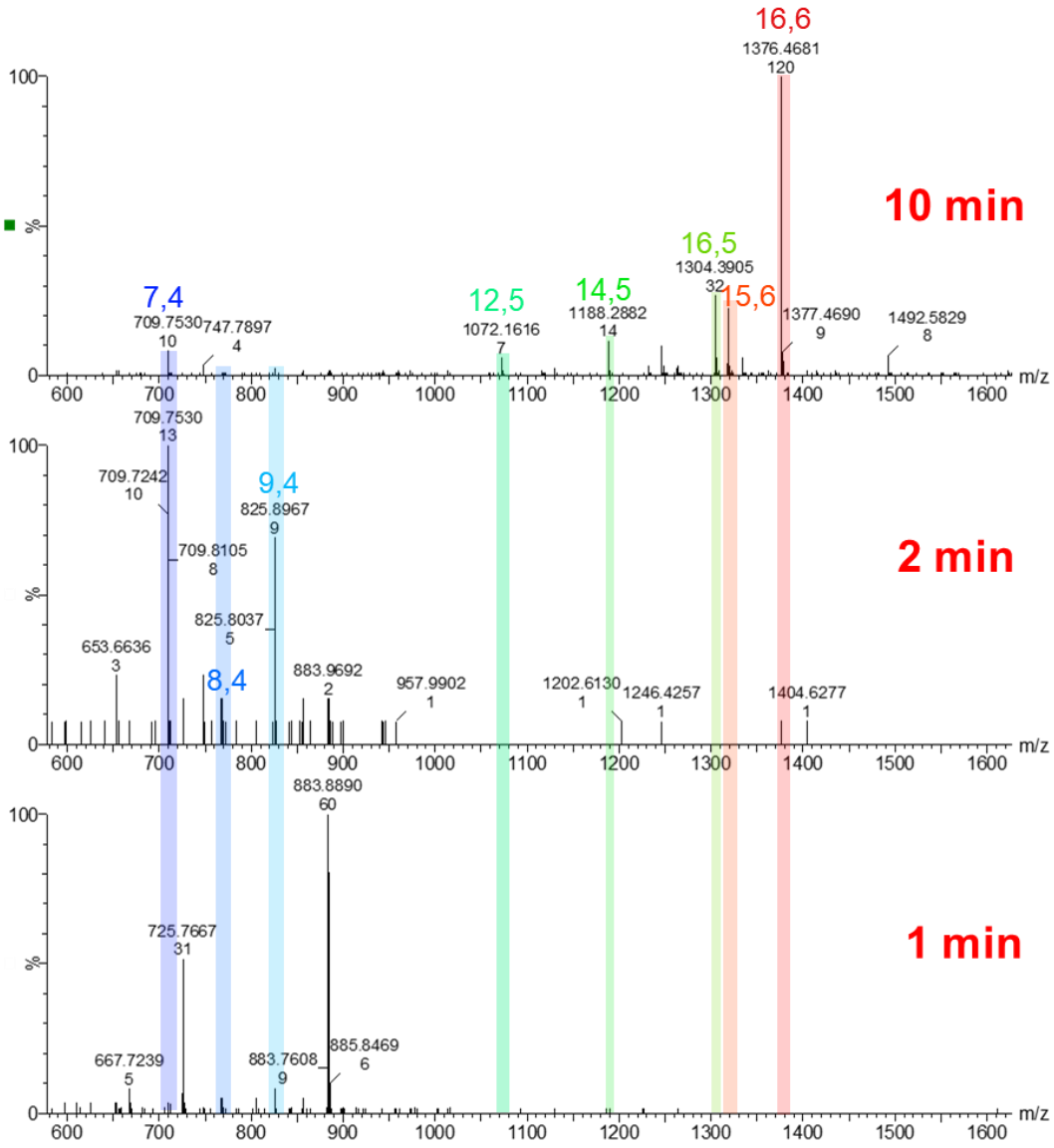

Figure B7. ESI-MS spectrum at 1, 2, and 10 minutes showing the change in the anion distribution during the synthesis of MAO in difluorobenzene with [H_2O] = 0.055 M. Run #7 of 7.

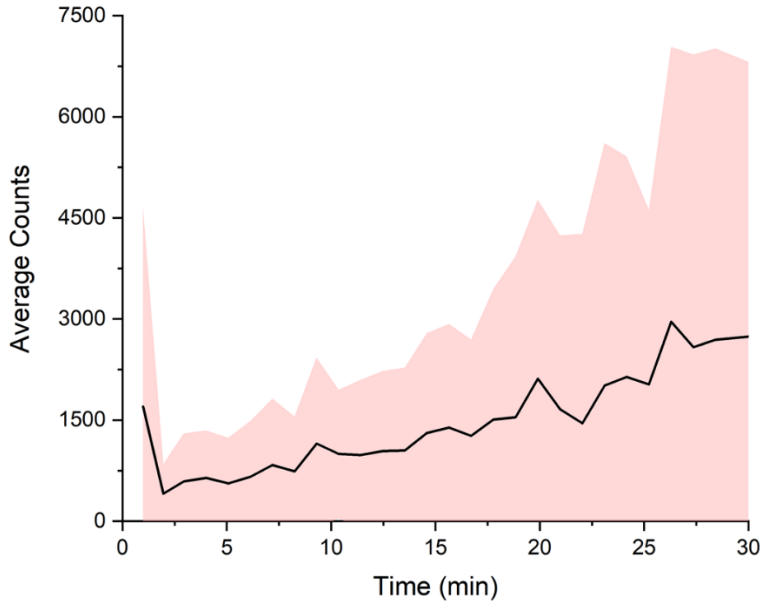

Figure B8. Error in the TIC for seven different experiments shown in red (standard deviation), and the average counts of all the experiments are shown by the black line.

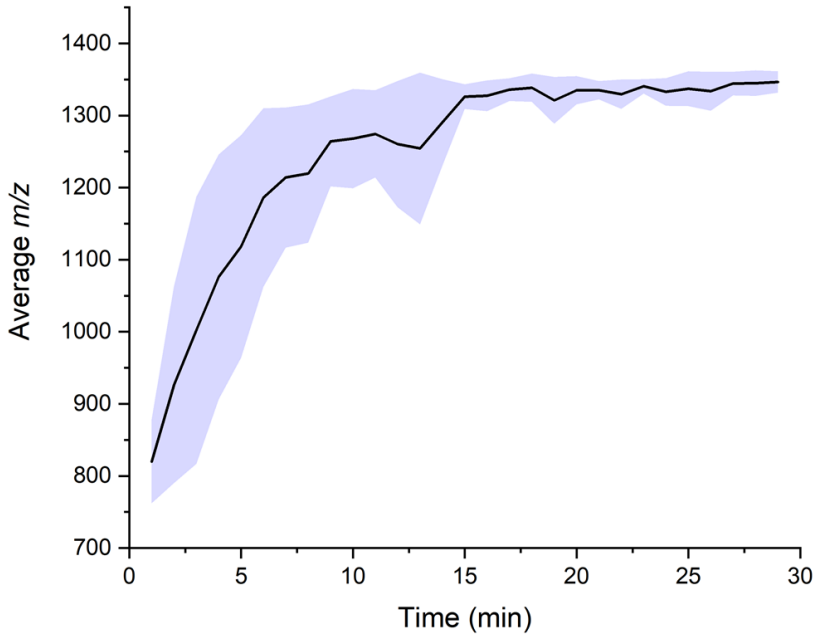

Figure B9. Error in the average molecular weight for MAO anions formed in different experiments in blue and the average *m/z* of all the experiments are shown by the black line.

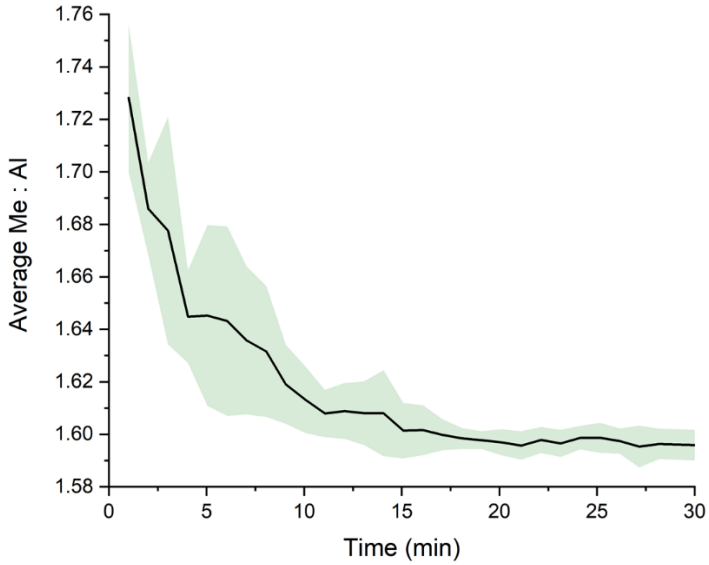

Figure B10. Error in the average Me:Al ratio for MAO anions formed in different experiments in green and the average Me:Al of all the experiments are shown by the black line.

MS/MS Spectra

The MS/MS product ion spectra show fragmentation exclusively through the loss of Me_3Al (-72 Da). The number of Me_3Al losses exceeds the y values for a given ion because, at high energies, the ion can rearrange to generate free Me_3Al via the process $3(MeAlO) \rightarrow Al_2O_3 + Me_3Al$.

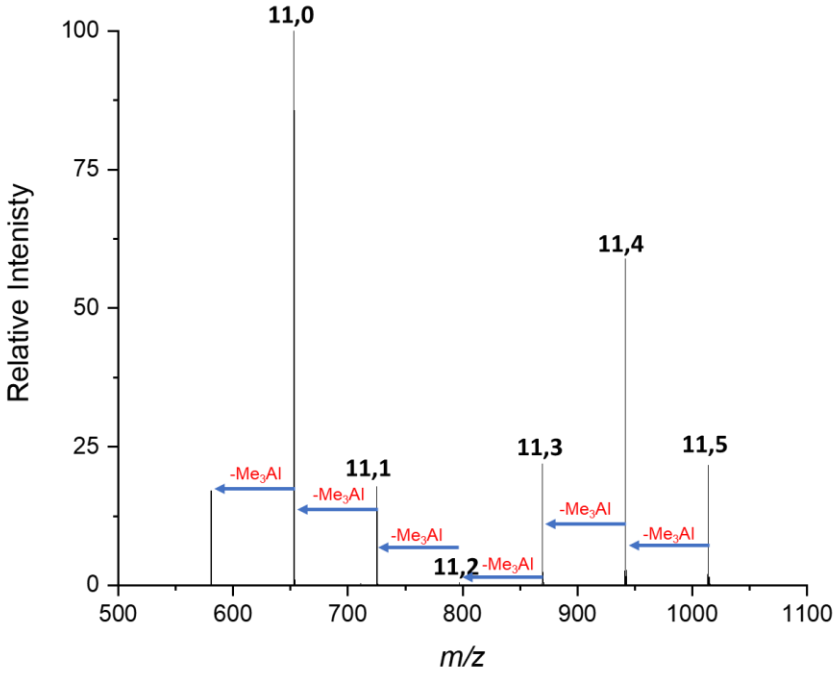

Figure B11. MS/MS spectrum of $[(MeAlO)_{11}(Me_3Al)_5Me]^-$.

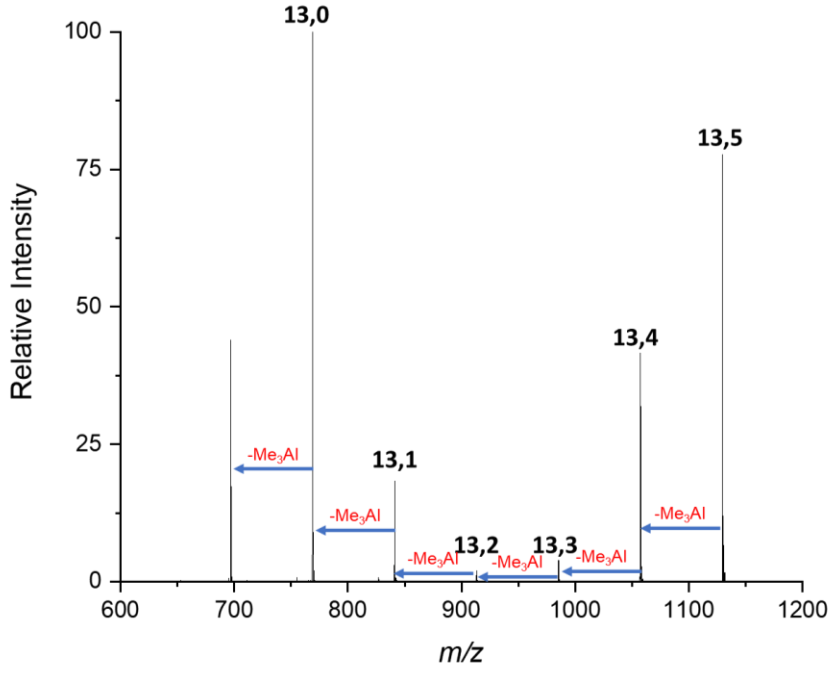

Figure B12. MS/MS spectrum of $[(MeAlO)_{13}(Me_3Al)_5Me]^-$.

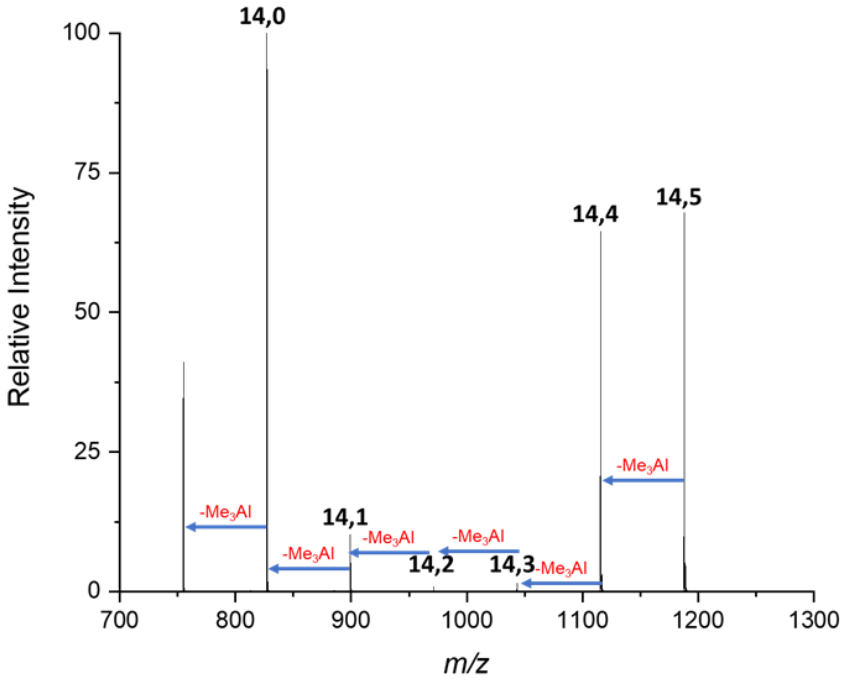

Figure B13. MS/MS spectrum of $[(MeAlO)_{14}(Me_3Al)_5Me]^-$.

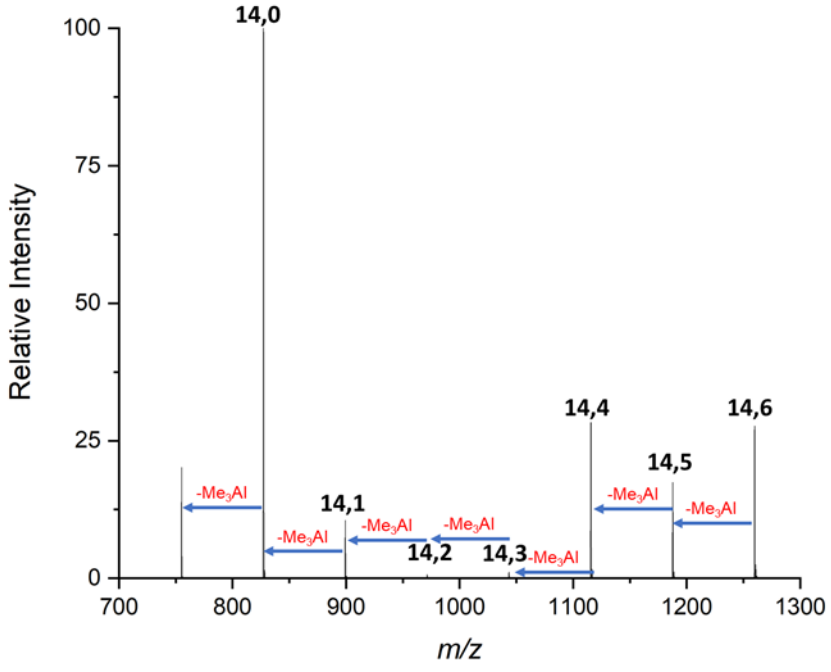

Figure B14. MS/MS spectrum of $[(MeAlO)_{14}(Me_3Al)_6Me]^-$.

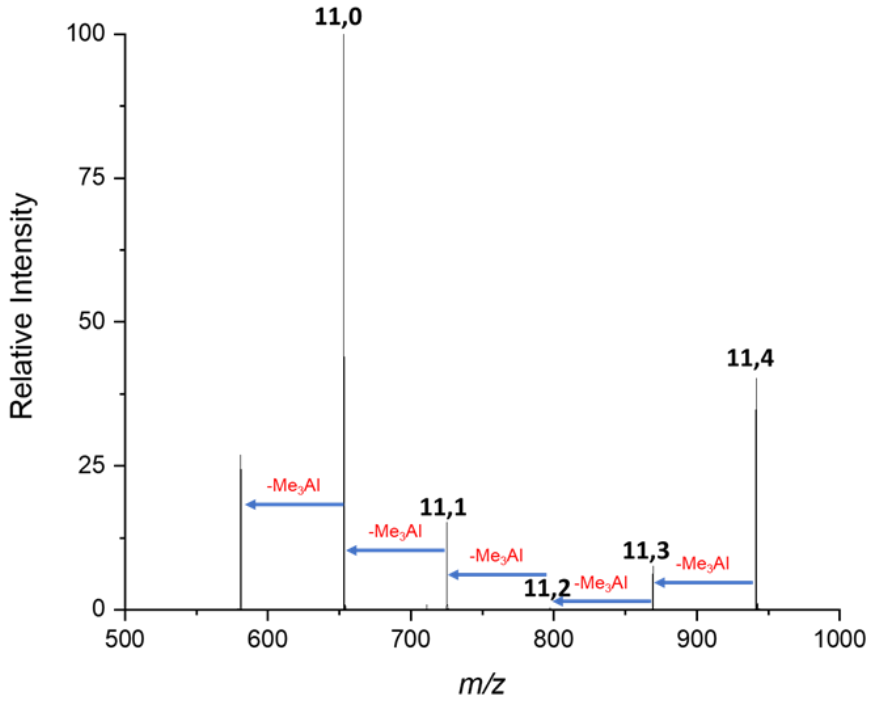

Figure B15. MS/MS spectrum of $[(MeAlO)_{11}(Me_3Al)_4Me]^-$.

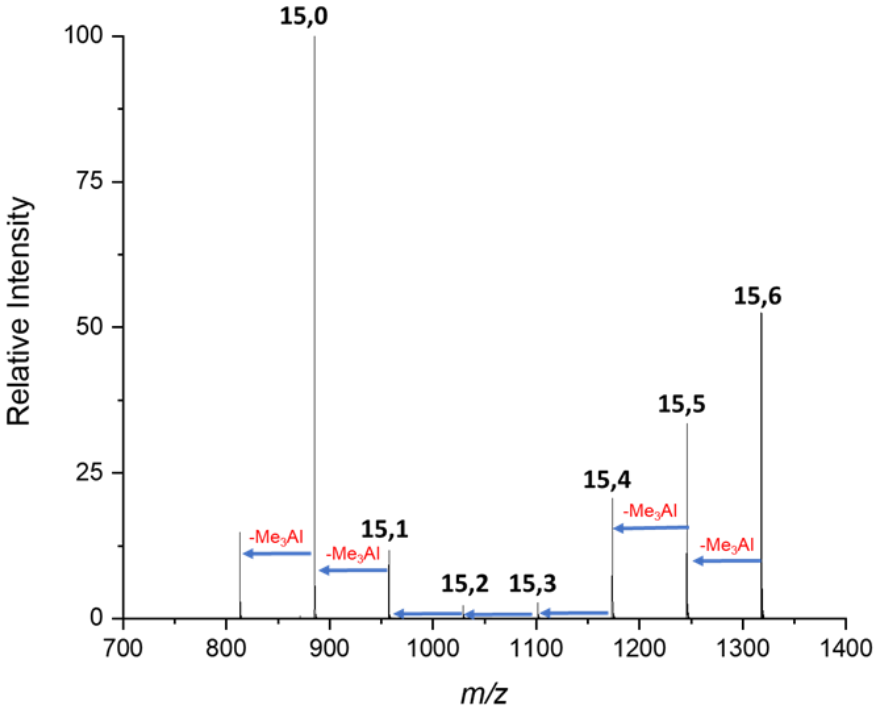

Figure B16. MS/MS spectrum of $[(MeAlO)_{15}(Me_3Al)_6Me]^-$.

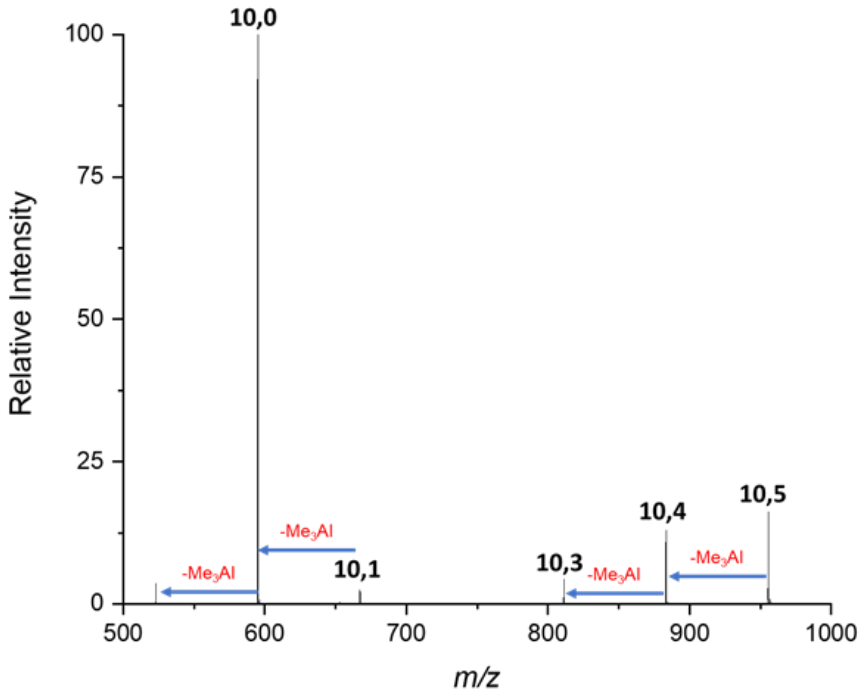

Figure B17. MS/MS spectrum of $[(MeAlO)_{10}(Me_3Al)_5Me]^-$.

Appendix C Reactive metallocene ions as sensitive indicators of gas-phase oxygen and water.

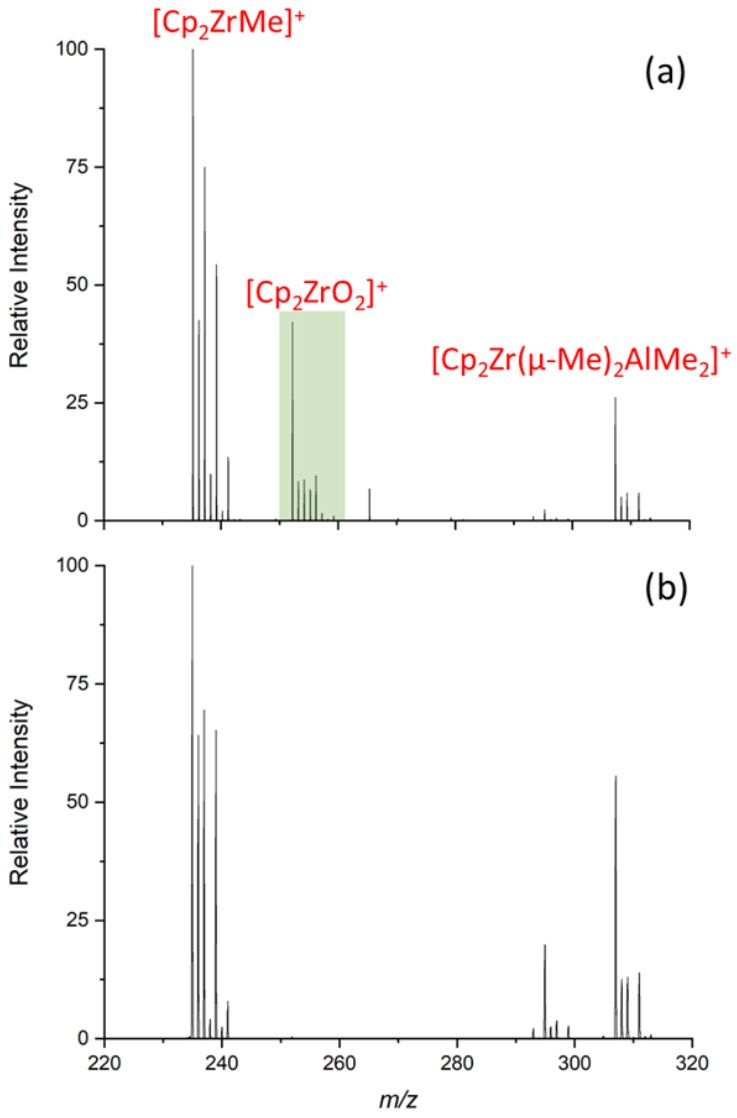

Figure C1. ESI-MS in positive mode of the ($[Cp_2Zr(\mu\text{-}Me)_2AlMe_2]^+$) system at a cone voltage of 24V with an N_2 supply from (a) factory refurbished N_2 generator and (b) brand new N_2 generator. The ion with *m/z* 252, i.e. ($[Cp_2ZrO_2]^+$), was not prominent while using the new generator.

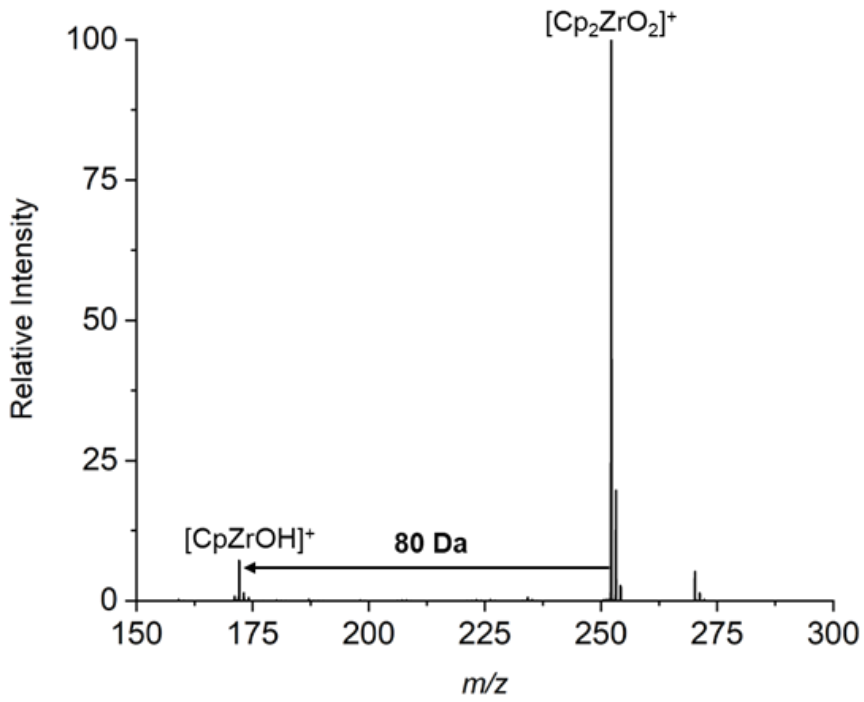

Figure C2. MS-MS of *m/z* 252 species showing no direct loss of O_2 but instead a rearrangement (shown below) to lose the fragment with *m/z* 80.

At low collision pressures, the lowest energy fragmentation of *m/z* 252 involves a loss of 80 Da. Neutral losses with this MW involving only C, H, and O could correspond to either C_5H_4O or C_6H_8. A logical fragment for the former is cyclopentadienone, while, e.g., methylcyclopentadiene does not make as much sense. We are not sure of the most stable structure for *m/z* 252, but if it adopts a metal-peroxo radical cation structure, as postulated by Schwartz and co-workers, one might explain the loss of 80 Da as shown in the Scheme below where rearrangement proceeds the loss. Note that *m/z* 252 could also have the structure shown on the right, which makes some sense for its strong tendency to bind water to form *m/z* 270.

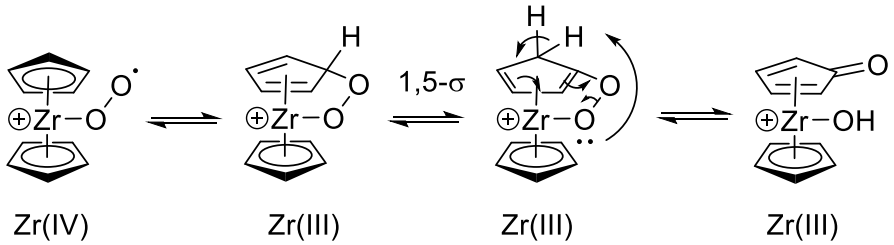

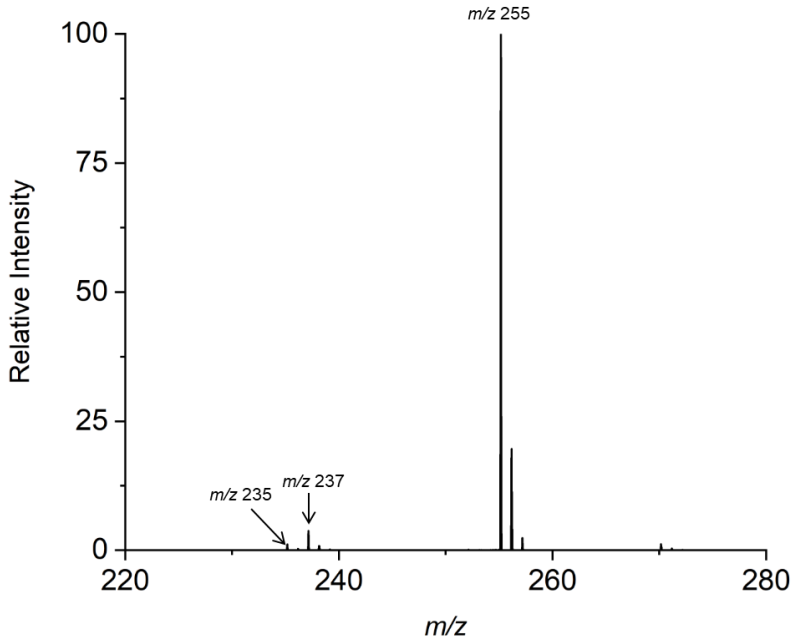

Figure C3. MS-MS of *m/z* 235 species showing hydrolysis at reduced collision energy. Due to water in the collision cell, we see *m/z* 237 [*m/z* 235 + 18 – 16 (CH_4) Da] and *m/z* 255, which is 18 Da higher in mass.

Appendix D Catalyst deactivation processes in 1-hexene polymerization

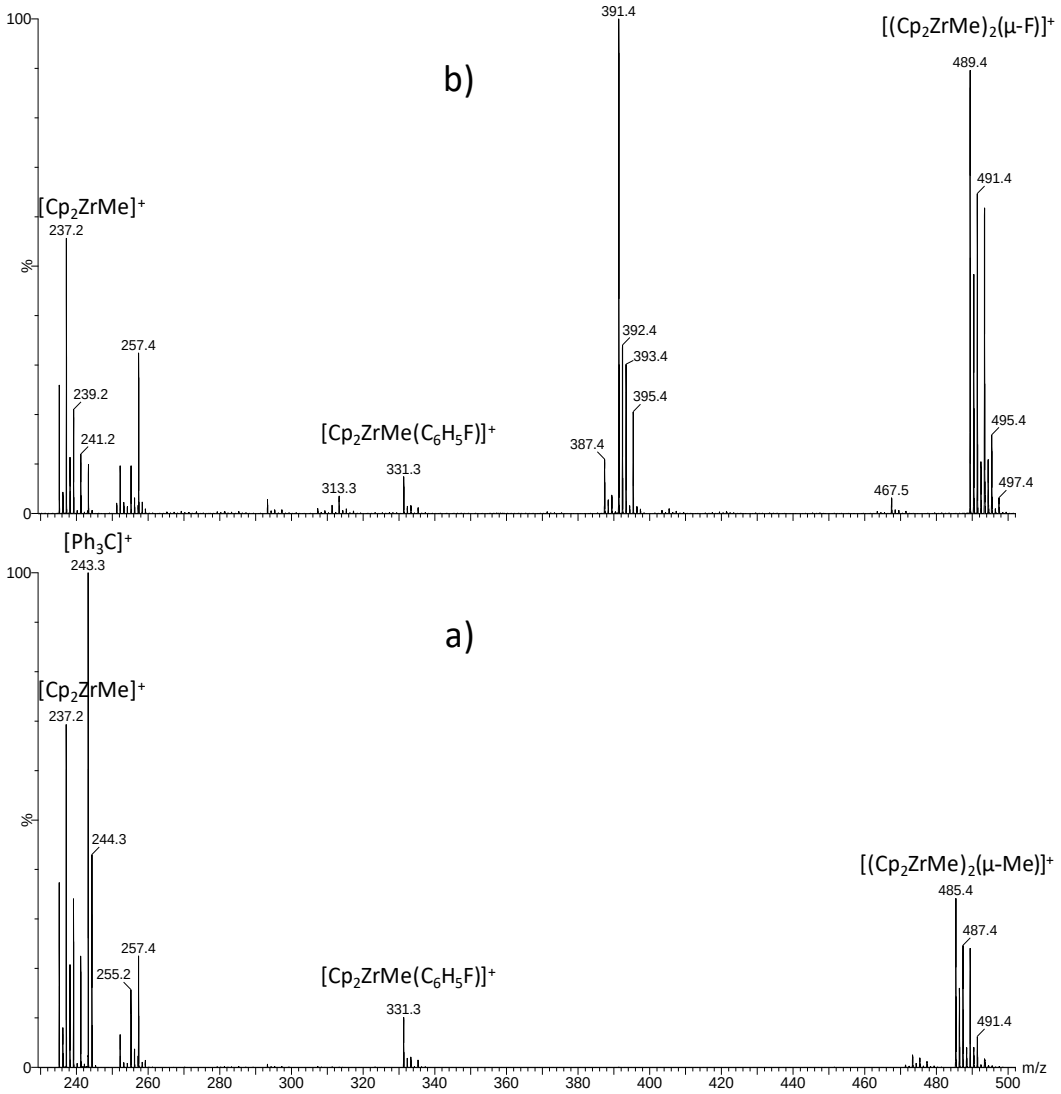

Figure D1 ESI-MS of a 1:1 mixture of Cp_2ZrMe_2 and $[Ph_3C][B(C_6F_5)_4]$ in PhF with [Zr] = 4.0 mM with assignments given. a) On mixing and b) after 3 hours at room temperature.

The M+2 isotopomer of *m/z* 235 is accentuated due to hydrolysis in the source compartment (cf. normal appearance of *m/z* 331). The identity of the ion with *m/z* 391 is unknown; its MS-MS is characterized by a single high energy loss of 152 Da forming

$[Cp_2ZrF]^+$. As 4-fluorobiphenyl is a minor contaminant of the fluorobenzene in use, it could be $[Cp_2Zr\text{-}(2\text{-}FC_6H_3)\text{-}4\text{-}C_6H_5]^+$.

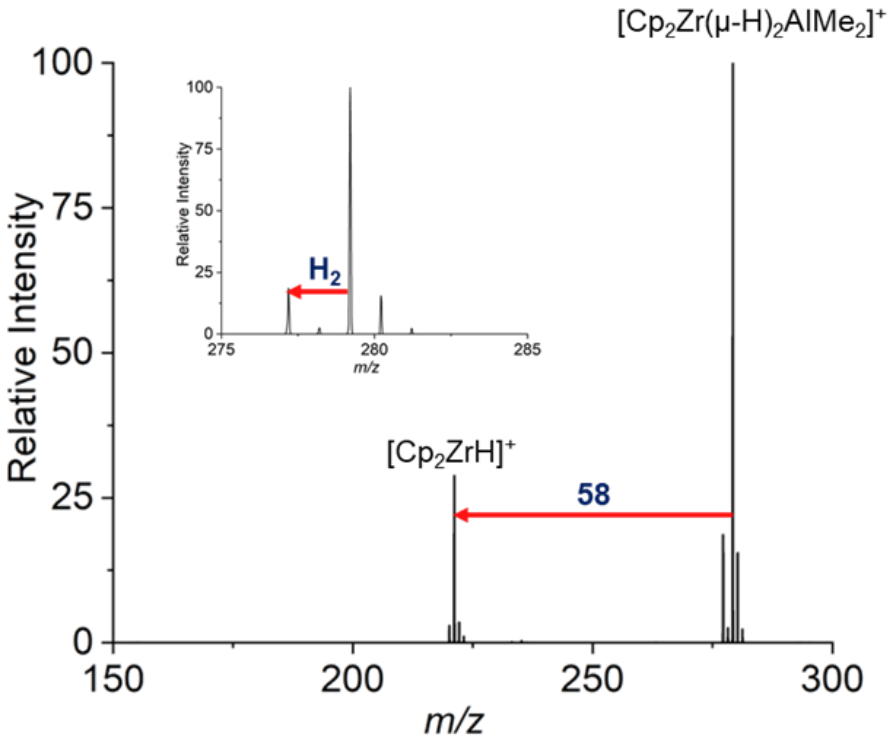

Figure D2. MS-MS of $[Cp_2Zr(\mu\text{-}H)_2AlMe_2]^+$ (*m/z* 279) species showing the loss of Me_2AlH (58 Da). Expansion shows the H_2 loss (2 Da).

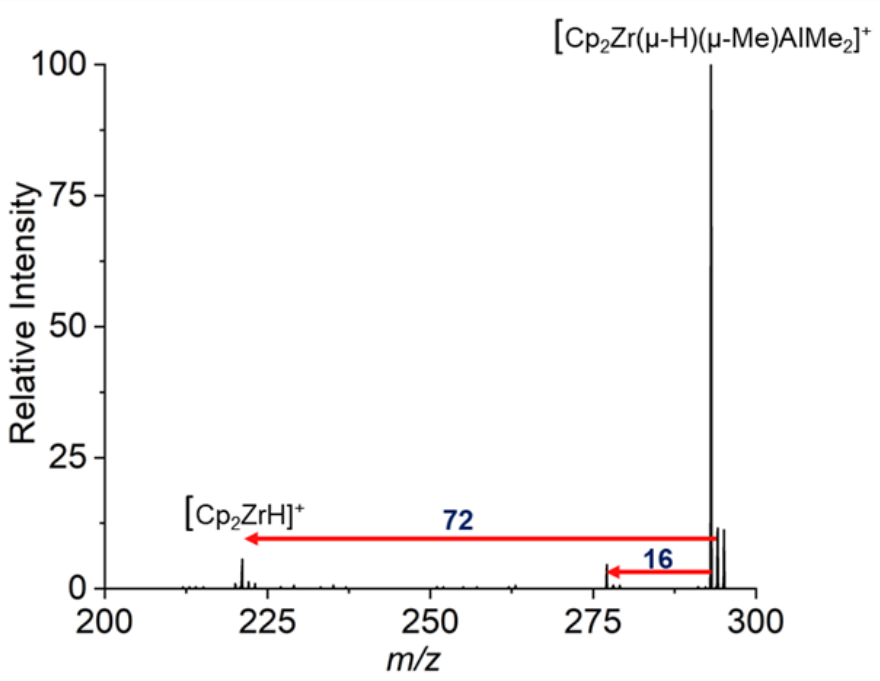

Figure D3. MS-MS of $[Cp_2Zr(\mu\text{-}H)(\mu\text{-}Me)AlMe_2]^+$ (*m/z* 293).

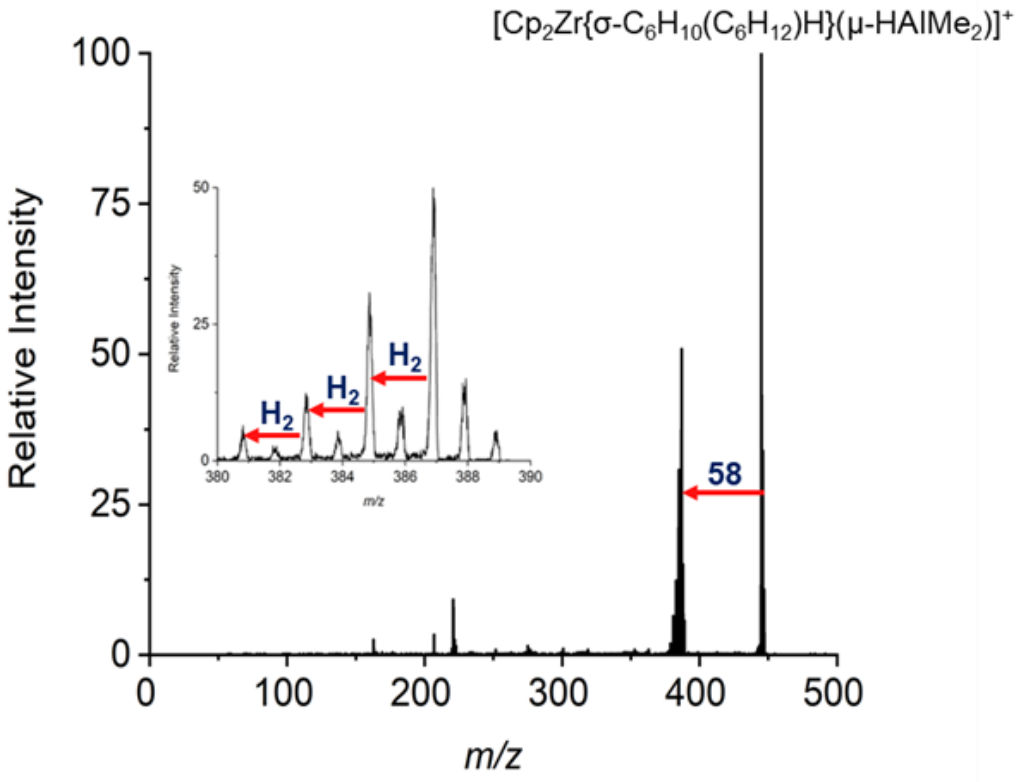

Figure D4. MS-MS of $[Cp_2Zr\{\sigma\text{-}C_6H_{10}(C_6H_{12})H\}(\mu\text{-}HAlMe_2)]^+$ (*m/z* 445). Inset shows 3 consecutive losses of H_2.

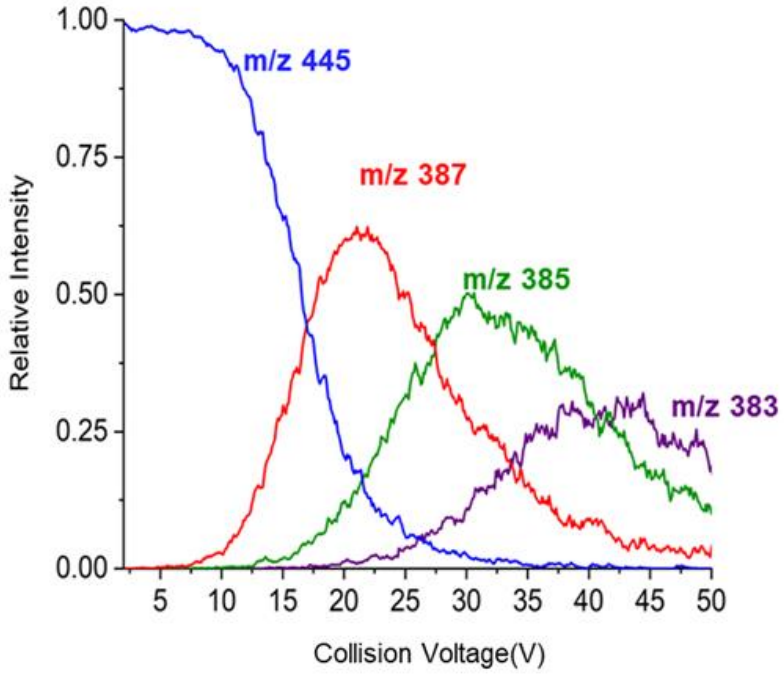

Figure D5. Breakdown curves for $[Cp_2Zr\{\sigma\text{-}C_6H_{10}(C_6H_{12})H\}(\mu\text{-}HAlMe_2)]^+$ (*m/z* 445).

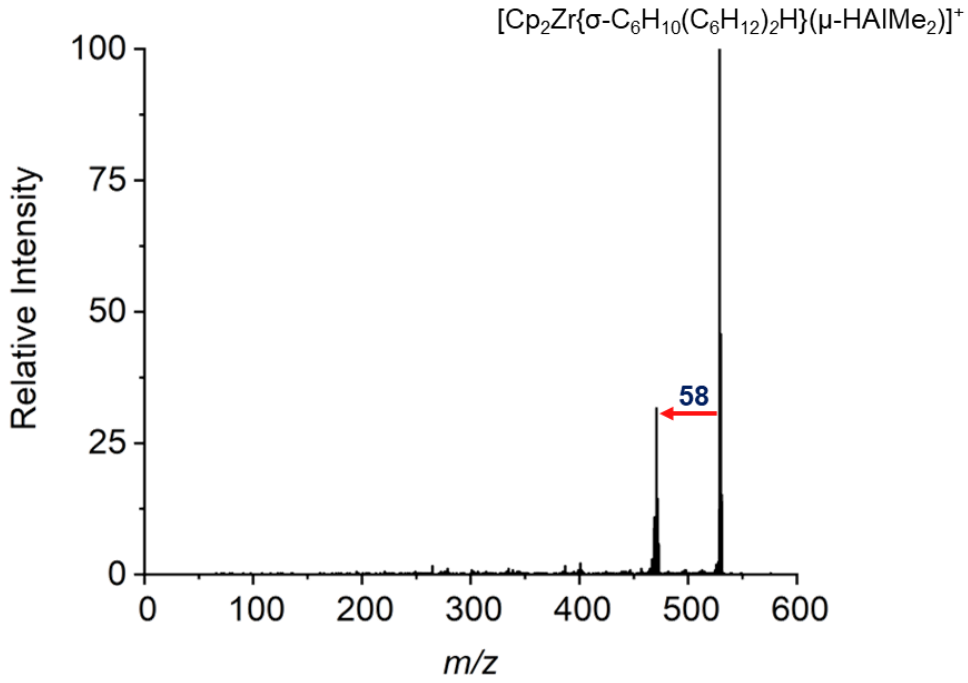

Figure D6. MS-MS of $[Cp_2Zr\{\sigma\text{-}C_6H_{10}(C_6H_{12})_2H\}(\mu\text{-}HAlMe_2)]^+$ (*m/z* 529).

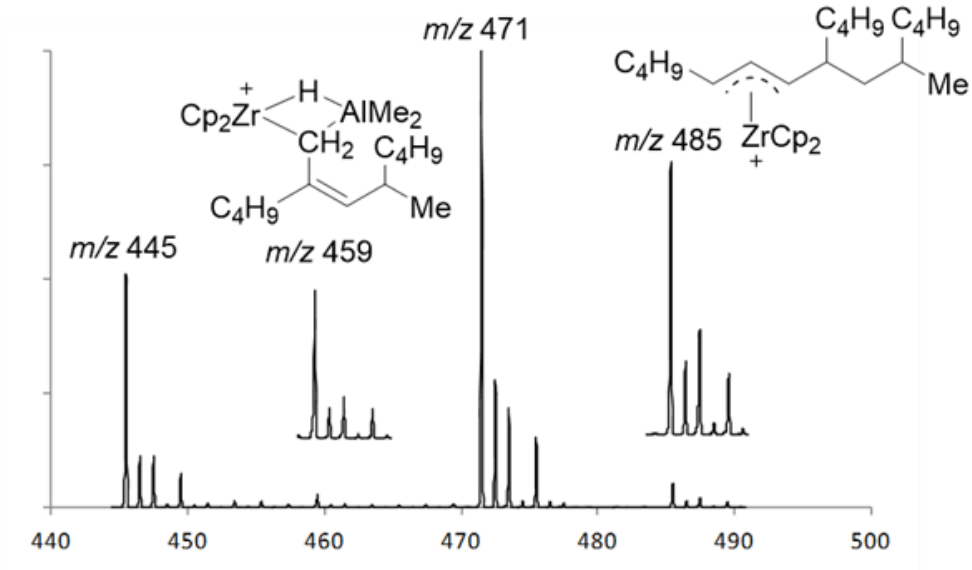

Figure D7 Expansion of an ESI-MS spectrum of hexene (100 equiv.) and $[Cp_2ZrMe_2AlMe_2][B(C_6F_5)_4]$ (0.28 mM) showing M+14 congeners of ions with *m/z* 445 and 471.